UNIVERSITY OF SOUTHAMPTON

Faculty of Natural and Environmental Sciences

School of Ocean and Earth Science

National Oceanography Centre, Southampton

THE TIMING AND FREQUENCY OF LARGE-VOLUME SUBMARINE LANDSLIDES AND TURBIDITY CURRENTS ALONG THE NORTH-EASTERN ATLANTIC MARGIN

by

Joshua Reg Allin

Thesis submitted for the degree of Doctor of Philosophy

October 2016

Graduate School of Ocean and Earth Sciences, National Oceanography Centre, Southampton

This Ph.D. dissertation by

Joshua Reg Allin

Has been produced under the supervision of the following persons:

Supervisors:

Prof. Peter J Talling

Dr. James E. Hunt

Chair of Advisory Panel:

Dr. Mark E. Vardy

ABSTRACT

UNIVERSITY OF SOUTHAMPTON
FACULTY OF NATURAL AND ENVIRONMENTAL SCIENCES
SCHOOL OF OCEAN AND EARTH SCIENCES

Doctor of Philosophy

THE TIMING AND FREQUENCY OF LARGE-VOLUME SUBMARINE LANDSLIDES AND TURBIDITY CURRENTS ALONG THE NORTH-EASTERN ATLANTIC MARGIN

By **Joshua Reg Allin**

Submarine landslides and turbidity currents are one of the most voluminous sediment transport mechanisms operating on our planet. Due to their potential size (>100 km^3) and speed (>20 m/s) they pose considerable risk to coastal settlements and strategic marine infrastructure. This thesis aims to investigate the processes that precondition and trigger submarine landslides and turbidity currents within submarine canyons and on open continental slopes. Sediment cores, age models, and statistical analyses are used initially to test the effects of eustatic sea level on the recurrence rates of turbidity currents that fill and flush the Nazaré Canyon. Recurrence rates of turbidity currents that fill the canyon are strongly influenced by eustatic sea level, while more infrequent flows that flush the canyon are only associated with shifts in eustatic sea level periodicity and amplitude. The form of the frequency distribution of canyon filling and flushing turbidity currents also differ markedly, suggesting they have different triggers.

This thesis also aims to understand the geohazard implications of large submarine landslides. The Trænadjupet Slide is a large (>400 km^3) submarine landslide that occurred approximately 4,000 years ago on the Norwegian Margin. Unlike some other large submarine landslides, the Trænadjupet Slide did not trigger a widespread tsunami based on available coastal studies. The age of the Trænadjupet Slide is refined here to between ~2,600 and ~3,400 cal BP. The absence of a widespread tsunami associated with the Trænadjupet Slide may be explained by its emplacement dynamics (e.g. speed, acceleration, or time gaps between stages of failure). These findings have importance for landslide geohazards in the North Atlantic, as they suggest that other similarly-sized slides on the Norwegian Margin or elsewhere may not have produced very damaging tsunamis.

Contents

List of Tables

List of Figures

List of Appendices

Declaration of Authorship

I, Joshua Reg Allin declare that this thesis entitled 'The timing and frequency of large volume submarine landslides and turbidity currents along the north-eastern Atlantic Margin', and the work presented in it are my own and has been generated by me as the result of my own original research.

I confirm that:

1. This work was done wholly or mainly while in candidature for a research degree at this University;

2. Where any part of this thesis has previously been submitted for a degree or any other qualification at this University or any other institution, this has been clearly stated;

3. Where I have consulted the published work of others, this is always clearly attributed;

4. Where I have quoted from the work of others, the source is always given. With the exception of such quotations, this thesis is entirely my own work;

5. I have acknowledged all main sources of help;

6. Where the thesis is based on work done by myself jointly with others, I have made clear exactly what was done by others and what I have contributed myself;

7. Parts of this work have been published as:

   Allin, J.R., Hunt, J.E., Talling, P.J., Clare, M.E., Pope, E., Masson, D.G., 2016. Different frequencies and triggers of canyon filling and flushing events in Nazaré Canyon, offshore Portugal. Marine Geology 371, 89-105.

8. Parts of this thesis have been submitted as:

   Allin, J.R., Hunt, J.E., Clare, M.E., Talling, P.J., *submitted*. Does eustatic sea level control the flushing of submarine canyons? Geological Society of America Bulletin.

   Mozzato, A., **Allin, J.R.**, Bondevik, S., Talling, P.J., Tappin, D.R., Haflidason, H., Hunt, J.E., Baeten, N., Pope, E., Cartigny, M.J.B., Watts, M.J., Long, D., Stanford, J.D., Dowdeswell, J.A., *in review*. Do large (>400-700 km3) submarine landslides always produce major tsunamis, and what is their relationship to glacial cycles? Earth and Planetary Science Letters.

9. Work during preparation of this thesis has contributed to:

Talling, P.J., **Allin, J.R.**, et al., 2015. Key future directions for research on turbidity currents and their deposits. Journal of Sedimentary Researc 85, 153-169.

Pope, E., Talling, P.J., Hunt, J.E., Dowdeswell, J.A., **Allin, J.R.**, Cartigny, M.J., Long, D., Mozzato, A., Stanford, J.D., Tappin, D.R., Watts, C.J., 2016. Long-term dynamics of the marine based Barents Sea Ice Sheet from a 140,000 year record. Quaternary Science Reviews 105, 55-66.

10. Work related to this thesis has been presented at the following conferences:

    Allin, J.R., Hunt, J.E., Talling, P.J., Clare, M.A., Pope, E.L., Masson, D.G., 2015. Variability in turbidity current frequency within a central Portuguese margin canyon. Geophysical Research Abstracts 17, 2298. European Geosciences Union 2015.

    Allin, J.R., Mozzato, A., Tappin, D., Talling, P.J., Hunt, J.E., 2016. Were the Trænadjupet and Nyk Slides tsunamigenic? Geophysical Research Abstracts 18, 2144. European Geosciences Union 2016.

11. I have also provided contributions to the following work presented at conferences:

    Mozzato, A., Tappin, D., Talling, P., Cartigny, M., Long, D., Hunt, J., Watts, C., Pope, E., **Allin, J.**, Stanford, J., Dowdeswell, J., 2015. Insights from new high-resolution data from the Traenadjupet Slide on the Norwegian margin. Geophysical Research Abstracts 17, 5455. European Geosciences Union 2015.

    Talling, P., Pope, E., Hunt, J., **Allin, J.**, Cartigny, M., Long, D., Mozzato, A., Stanford, J., Tappin, D., Watts, C., 2015. New insights into the timing, triggers and emplacement processes of prodigious submarine landslides in the Nordic Seas. Geophysical Research Abstracts 17, 2231. European Geosciences Union 2015.

    Watts, M., Hunt, J., Talling, P., **Allin, J.**, Pope, E., 2015. Geochemical insights into the provenance of large scale North Atlantic turbidites. Geophysical Research Abstracts 17, 8711. European Geosciences Union 2015.

Signed: .....

Date: .....

Acknowledgements

I would like to acknowledge my family, in particular my parents. Without their encouragement and support I would not have been able to make it to this point in my career. They always believed in me, no matter how badly I made a hash of things. Thanks Mum, Dad, and Meg. A big thanks to my sweetheart Lizzy, for being there during the latter and more challenging aspects of this thesis.

Secondly I would like to thank my supervisors, Peter Talling and James Hunt. Their expert guidance and advice throughout the last 3 years has been immeasurably important in the writing of this thesis, and in my own growth as a scientist. I will be forever grateful to them for giving me a chance to be a part of a very special group. Mike Clare also deserves a special thank you. Although not an official supervisor, his contributions have made this a better thesis, and have helped me immensely during the last 3 years. He also enabled me to grasp statistics; something I thought thoroughly impossible. Thanks are also due to Mark Vardy who acted as the panel chair for this thesis and provided useful comments and advice on structure and planning.

I would also like to thank my officemates in 786/23; Alessandro, Ed, Millie, Will, and Zoe. The rest of the sedimentology group should also receive a special mention; Mathieu, Esther, Frank, Age, Jamie, and Sophie. The fieldwork, conferences, research meetings and after-work drinks have made for some great laughs and valuable learning experiences.

There are several people at NOC who have helped me in non-supervisory capacities. Suzie MacLaughlin and Mike Edwards in BOSCORF have provided valuable assistance in core analysis and absolutely deserve a thank you for their help. I must also thank Jane Goswell for being willing to organise several trips and excursions for hapless sedimentologists.

Finally I would like to thank the 54 Padwell crew: Matt, Amy, Stu, Nico, James, and Sara. Many BBQs and sessions were had in that house, and I couldn't have asked for better friends to spend the last 3 years with. I'll never forget the craic and the banter.

Definitions, Abbreviations, and Symbols

^{14}C	Radiocarbon
ΔR	Reservoir correction value
AMS	Accelerator mass spectrometry
Cal BP	Calibrated years before present
K	Hurst exponent
Ka	Thousand years
Ma	Million years
N	Sample size
ODP	Ocean Drilling Program
PHM	Proportional hazards model
Q-Q	Quantile - quantlie
R^2	Correlatation coefficient
R_T	Normalised recurrence
TC	Turbidity current

Chapter 1: Introduction

Summary:

Submarine landslides and turbidity currents are important mechanisms for transporting sediment into the deep ocean. Their potential size (>100 km^3) and speed (>20 m/s) make them an important marine geohazard that can damage important subsea infrastructure and trigger tsunamis. Here the rationale for this thesis, its structure, and research aims are outlined. This thesis covers sediment transport processes in open continental slope, submarine canyon, and abyssal plain settings. As such the range of submarine mass movement types, their triggering mechanisms, preconditioning factors, and broader geohazard implications are discussed to provide sufficient context for the thesis.

1.1 Rationale

Submarine mass movements such as landslides and turbidity currents are some of the most volumetrically important sediment transport mechanisms on Earth. They dominate on continental slopes beyond the shelf break (Stow and Piper, 1984; Posamentier et al., 1991; Masson et al., 2006), but can also be observed in larger lakes (Schnellmann et al., 2005; Vardy et al., 2010), river deltas (Coleman et al., 1974), submarine canyons (Masson et al., 2011a), and fjords (Locat et al., 2003; Bellwald et al., 2016). Individual submarine landslides and turbidity currents can transport more than 100 km^3 of sediment, exceed speeds of 10 m/s, and can travel for hundreds of kilometres over exceptionally low gradients (<1º) (Piper et al., 1999; Haflidason et al., 2004; Masson et al., 2006; Talling et al., 2007a). Their potential speed and volume makes them a potential hazard to coastal settlements through the generation of tsunamis, as well as offshore hydrocarbon infrastructure and submarine telecommunication networks (Bryn et al., 2005; Carter et al., 2012; Harbitz et al., 2014). To properly assess the risks that these landslides and turbidity currents pose a better understanding of their triggers, preconditioning factors, dynamics, and frequency is required.

Canyon systems represent ideal locations to evaluate the behaviour and frequency of mass movements as they act as conduits for sediment transport between the shelf edge and the deep

ocean (Stow and Piper, 1984; Posamentier et al., 1991; Covault and Graham, 2010). The Iberian Abyssal Plain is located offshore Portugal and is fed with sediment by a number of submarine canyon systems; the largest of which is the Nazaré Canyon. The long-term tectonic evolution and modern-day sediment transport processes in these canyons has been the focus of previous work (Vanney and Mougenot, 1990; Milkert et al., 1996a; 1996b; Whitmarsh and Sawyer, 1996; de Stigter et al., 2007; Guerreiro et al., 2009; Masson et al., 2011a; Martin et al., 2011). However, little is known about the long-term history of sediment transport in the form of landslides and turbidity currents that slowly fill the canyon over geological time scales (Arzola et al., 2008). Even less is known about the frequency of large mass movements such as canyon flushing events that reach the Iberian Abyssal Plain. Previous work has shown variable mass movement frequency and transport distance within Nazaré Canyon, but focussed largely on the upper reaches at less than 3,000 m water depth (de Stigter et al., 2007; Martin et al., 2011). Longer and well-dated records of mass transport frequency within the Nazaré Canyon and the Iberian Abyssal Plain have to date not been properly evaluated for triggers and preconditioning factors. The frequency of mass movements within canyons world-wide is often poorly constrained due to the difficulty in direct monitoring. This limits our understanding of the tempo of sediment transport and the associated geohazards (Parker, 1982; Paull et al., 2005; Talling, 2014).

The role of large (>1 km^3) submarine mass movements, particularly landslides, in generating damaging tsunamis is well known (Heezen and Ewing, 1952; Dawson et al., 1994; Tappin et al., 2001). However, it is not clear whether all of even the largest (>100 km^3) submarine landslides are capable of generating tsunamis (Mozzato et al., in review). The tsunamigenic potential of a submarine slide is dependent on its initial volume and acceleration, and particularly whether or not it occurred as a single block failure, or in multiple disparate stages (Harbitz et al., 1992; Masson et al., 2002; Bryn et al., 2005; Haughen et al., 2005; Hunt et al., 2013a; Løvholt et al., 2014). Currently, there is limited geological evidence of tsunamis associated with most large submarine landslides that are mapped worldwide. This is because most very large landslides identified are tens or hundreds of thousands of years old (Rothwell et al., 1998; Lindberg et al., 2004; Løvholt et al., 2013; Hjelstuen and Andreassen et al., 2015). Any terrestrial tsunami deposits from these

landslides are likely buried, submerged by sea level, or have been removed by glaciers, eolian, or human processes (Dawson and Shi, 2000; Weiss and Bahlburg, 2006; Spiske et al., 2013). One of the most recent very large landslides, the Trænadjupet Slide, occurred on the Norwegian Margin between 3,000 - 5,000 years ago and involved an estimated 400 km^3 of sediment (Laberg and Vorren, 2000a; Laberg et al., 2002; 2006). Despite the large volume of sediment mobilised it does not appear to have triggered a widespread tsunami (Mozzato et al., in review). Regional geohazard assessment concerning submarine mass movements relies on understanding which slides will generate tsunamis, but also the properties of those that do not.

1.2 Research questions and thesis structure

The aims of this PhD thesis can be divided into two parts. First it aims to better understand the timing, controls, and triggers of turbidity currents in the Nazaré Canyon, offshore Portugal. Piston cores from the Nazaré Canyon and Iberian Abyssal Plain provide records of turbidity currents occurring over the last ~80,000 years. These records are analysed using statistical methods to evaluate any effect of sea level change on turbidity current frequency. A longer ODP record from the Iberian Abyssal Plain extends the length of the record and determines whether the frequency of canyon-flushing turbidity currents changes in response to sea level variability across multiple glacial cycles. The research questions this work aims to address are summarised as follows:

1. What is the frequency of turbidity currents within the Nazaré Canyon? (Chapter. 3)
2. Does the frequency of turbidity currents vary throughout the canyon? (Chapter. 3)
3. Is the frequency of canyon-filling turbidity currents affected by sea level? (Chapter. 3)
4. What is the frequency of much larger, poorly documented canyon-flushing events that reach the Iberian Abyssal Plain? (Chapters. 3 and 4)
5. What processes trigger canyon-flushing, and is there a relationship with sea level? (Chapters. 3 and 4)

Second, this thesis aims to better understand the timing and emplacement dynamics of much larger (>100 km^3) submarine slides on the Norwegian Margin. This will be done using a suite of newly acquired piston and multi- sediment cores from the deposits of the Trænadjupet Slide and Nyk Slides. The analysis of these cores will help characterise the deposits and sedimentology of these submarine slides, and in particular why the Trænadjupet Slide did not trigger a widespread tsunami. New AMS radiocarbon dates will also be used to provide better age constraint on the deposits and determine if the Trænadjupet Slide occurred in multiple disparate stages. The research aims for this section of the thesis are as follows:

1. To describe the sedimentology of the Trænadjupet and Nyk Slides in order to understand the distribution of deposit facies. (Chapter. 5)

2. To reduce the uncertainties on the age of the Trænadjupet and Nyk Slides. (Chapter. 5)

3. To account for the absence of Trænadjupet tsunami deposits on proximal coastlines. (Chapter. 5)

4. To test the hypothesis that the Trænadjupet and Nyk Slides occurred in multiple disparate stages. (Chapter. 5)

This thesis is divided into six chapters.

Chapter 2 provides a detailed breakdown of the methods used in all of the subsequent chapters. This includes sedimentology, geophysics, and statistics. Although many of the methods used in each chapter are discussed therein, much of the theoretical background is excluded for the sake of brevity. This is particularly true of many of the statistical analyses used, and so a more comprehensive overview of the methods is given.

Chapter 3 uses existing piston cores and new AMS radiocarbon dates, along with statistical analyses to evaluate the timing and controls of turbidity currents within the Nazaré Canyon and in the Iberian Abyssal Plain over the last 80,000 years. This chapter has been published as:

- Allin, J.R., Hunt, J.E., Talling, P.J., Clare, M.E., Pope, E., Masson, D.G., 2016. Different frequencies and triggers of canyon filling and flushing events in Nazaré Canyon, offshore Portugal. Marine Geology 371, 89-105.

Chapter 4 uses an existing ODP core from the Iberian Abyssal Plain to extend the record of large canyon-flushing turbidity currents back to 1.8 Ma. With this longer record it is possible to test the role of sea level in canyon-flushing events over more than one complete glacial cycle. This chapter has been submitted to the Geological Society of America Bulletin as:

- **Allin, J.R.**, Hunt, J.E., Clare, M.E., Talling, P.J.. Does eustatic sea level control the flushing of submarine canyons?

Chapter 5 focusses on refining the age and emplacement dynamics of the Trænadjupet and Nyk Slides, and to understand why the Trænadjupet Slide did not generate a tsunami. Minor elements during the development of this chapter have contributed to a submission to Earth and Planetary Science Letters as:

- Mozzato, A., **Allin, J.R.**, et al. Do large (>400-700 km3) submarine landslides always produce major tsunamis, and what is their relationship to glacial cycles?

The chapter as a whole will be submitted to Quaternary Science Reviews as:

- Allin, J.R., Mozzato, A., Talling, P.J., Hunt, J.E., Tappin, D., Haflidason, H., Baeten, N. A new view of very large (>400 km^3) and progressive multi-staged submarine landslides and their tsunamigenic potential

Chapter 6 provides some concluding remarks and some suggestions for future work.

1.3 Regional setting

1.3.1 Nazaré Canyon

Nazaré Canyon occurs in the Central-west Iberian Margin, and extends from ~1 km offshore from the coastline and into the Iberian Abyssal Plain (Fig. 1.1). The location of Nazaré Canyon on the

continental shelf and slope coincides with the presence of the Nazaré Fault, which runs ENE-WSW and extends across the margin. The Nazaré Canyon system is not directly fed by major rivers at present. Instead, Nazaré Canyon is fed largely by littoral drift sediment from smaller river systems to the north, and nepheloid transport of material to deeper sections of the canyon (van Weering et al., 2002; Oliveira et al., 2007; de Stigter et al., 2007).

The canyon itself can be divided into three sections; the upper section that extends from the canyon head to 2,000 m water depth; the middle section that spans between 2,000 and 4,000 m; and the lower section that lies below 4,000 m (Vanney and Mougenot, 1990; van Weering et al., 2002). The upper and middle sections have a steep v-shaped profile and are incised deeply into the continental shelf (200 - 2,500 m water depth), with a channel thalweg that is <100 m wide. Below 4,000 m water depth the canyon broadens to a width of 8 – 10 km and is markedly less incised into the substrate. Below 4,500 m water depth the canyon is less incised, and large levee structures have developed to the north and south of the canyon axis. These levees are between 100 and 200 m in height and taper distally into the Iberian Abyssal Plain, where they terminate at 5,300 m water depth (Arzola et al., 2008; Lastras et al., 2009).

1.3.2 Iberian Abyssal Plain

The Iberian Abyssal Plain is located 200 km off the western coast of Portugal between 40^{o} N and 43^{o} N and extends approximately 700 km to the northwest (Fig. 1.1). The abyssal plain has an average water depth of ~5,300 m but can be as deep as 5,400 m. The basin is bounded by the Galicia Bank to the northeast, the Estremadura Spur to the south, and by a series of seamounts along its western margin. The total area of the basin covers approximately 107,000 km^{2}. Previous work from ODP leg 149 has detailed the long-term basin infill record extending back to the Lower Cretaceous (140 Ma) (Milkert et al., 1996a; 1996b). This work demonstrated an onset of, terrestrial-derived mass movement deposition in the Iberian Abyssal Plain between 2.2 and 2.6 Ma, which continued into the late Pleistocene. Despite the extensive record from ODP drilling legs in the Iberian Abyssal Plain, very little of the recent (<100 ka) sedimentary architecture has been evaluated in detail. As a result, little is currently known about the frequency of large volume mass movements in the basin through the late Pleistocene.

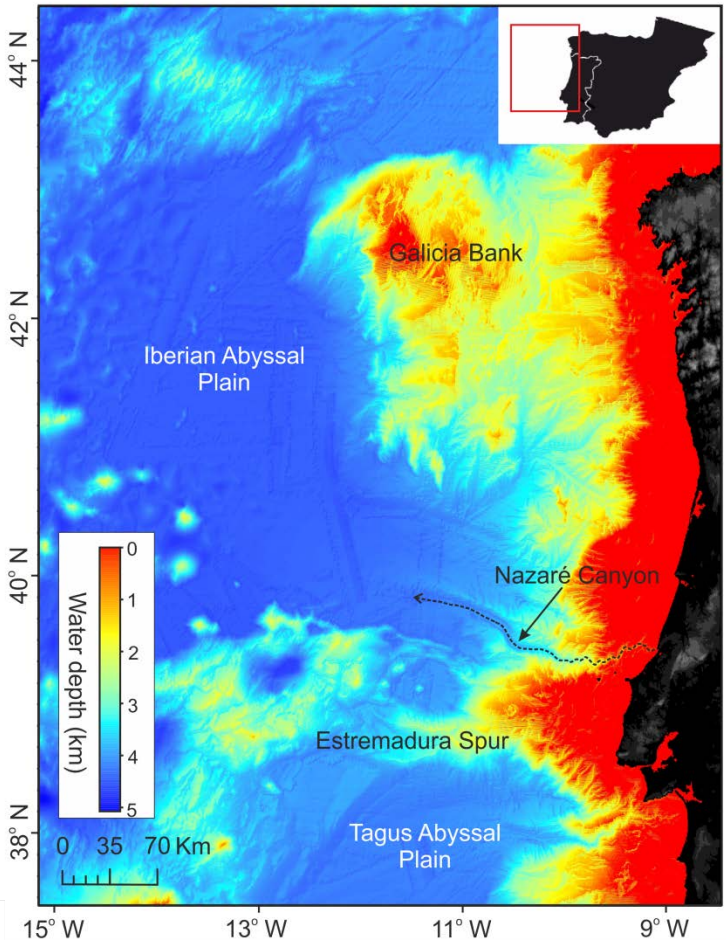

Figure 1.1: Map showing the locations of the Iberian Abyssal Plain and Nazaré Canyon.

1.3.3 Trænadjupet Slide

The Trænadjupet Slide is located on the north-east side of the Vøring Plateau on the Norwegian continental margin and extends from 300 to 3,200 m water depth in the Lofoten Basin. The headwall of the slide complex is located at the mouth of the Traenadjupet Cross-shelf Trough (Fig. 1.2). During Plio-/Pleistocene glaciations this trough was repeatedly filled by ice streams from continental ice sheets (Henriksen and Vorren, 1996; Laberg et al., 2002a; Dowdeswell et al., 2006). Sediment deposition from these ice streams during glacial periods resulted in very thick and rapid accumulations of glacigenic debris and stratified glacimarine sediments within the Trænadjupet Trough and on the Norwegian continental slope (Dahlgren and Vorren, 2003; Dowdeswell et al., 2006).

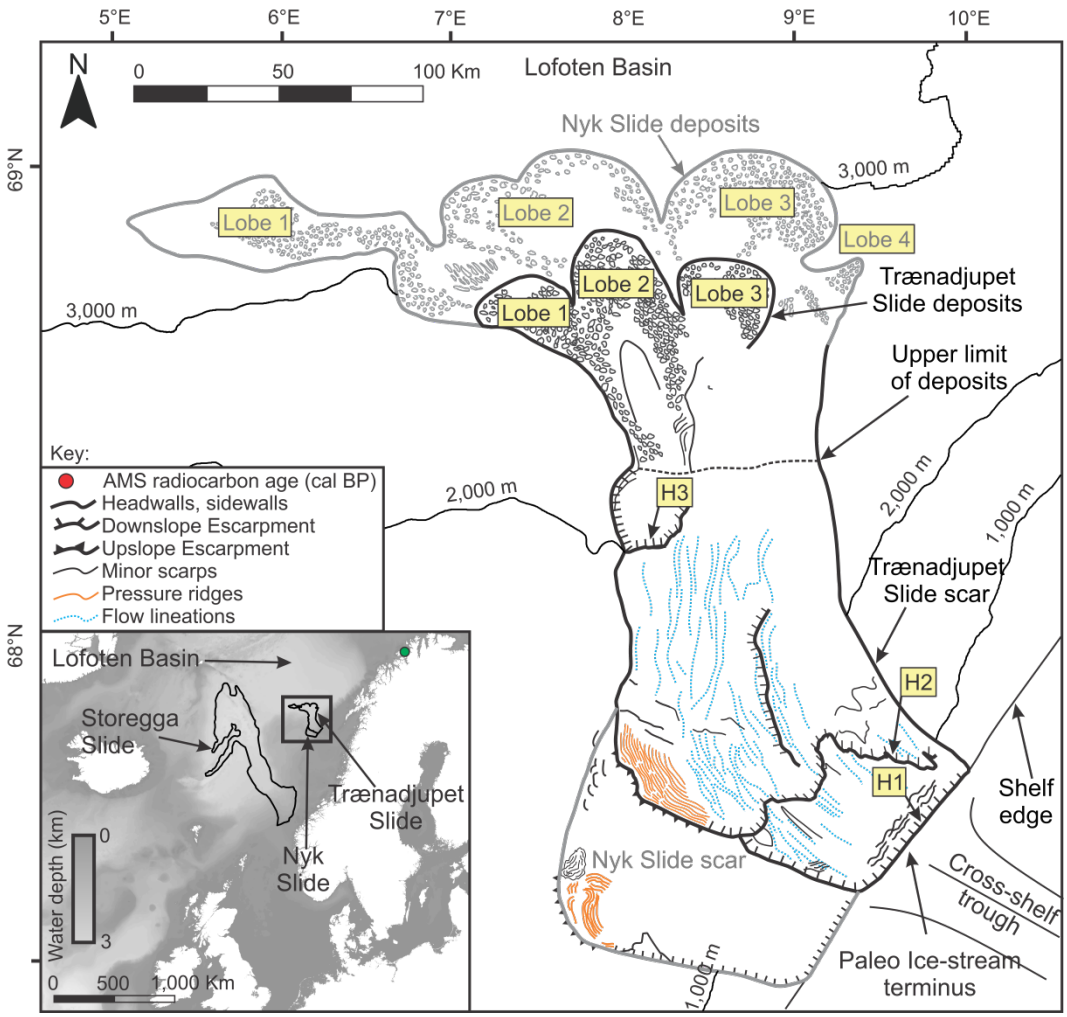

Figure 1.2: Map detailing the location and morphology of the Trænadjupet and Nyk Slides determined from bathymetry data from Mozzato et al. (in review) and TOBI data (Laberg and Vorren, 2000a; Laberg et al., 2002a). The Trænadjupet Slide is outlined in black, while the Nyk Slide is outlined in grey. Inset: location map showing the Trænadjupet Slide, and its position and scale relative to the Storegga Slide. Figure is adapted from Mozzato et al. (in review). Contours and inset bathymetry data from IBCAO Ver. 3 (Jakobsson et al., 2012).

The total area affected by landsliding is approximately 14,000 km^2, including slide scars and associated deposits (Laberg and Vorren, 2000a). There are two primary slide scars documented within the slide area (Fig. 1.2). The younger of these is the Trænadjupet Slide scar that extends from 400 m down to 2,200 m water depth (Laberg and Vorren, 2000a; Laberg et al., 2002a; Mozzato et al., in review). This Trænadjupet Slide scar covers an area of between 4,000 - 5,000 km^2 and has a headwall height of 100 - 120 m (Laberg and Vorren, 2000a). The trigger of the Trænadjupet Slide is not known, but seismicity due to isostatic rebound has been proposed (Laberg et al., 2002a). Southwest of the Trænadjupet Slide is the slide scar of an older slide known as the

Nyk Slide (Fig. 1.2). The Nyk slide scar extends from 400 m down to 1500 m water depth but is largely obscured by the presence of the more recent Trænadjupet scar, making its area and full depth range difficult to estimate (Lindberg et al., 2004). As with the Trænadjupet Slide, the trigger of the Nyk Slide is not well known, although high glacial sedimentation rates and the presence of weak, contouritic sediments are thought to have contributed (Lindberg et al., 2004).

1.4 Classification of subaqueous mass movements and their deposits

It is useful to define initially the terms used in the thesis. Subaqueous mass transport processes are the principal mechanisms by which sediment is transported into the deep ocean. However, due to the scarcity of direct in-situ observations, different mass transport processes have largely been inferred through the analysis of their deposits. Therefore, proper identification of deposit types is vital for characterising the type and frequency of mass transport occurring in modern and ancient depositional systems. Information regarding the frequency is of particular significance when the hazards posed by larger and more damaging mass transport processes are considered (Piper et al., 1999; Bondevik et al., 2005; Tappin et al., 2001).

There are many classification systems for subaqueous mass movements and sediment gravity flows (e.g. Mulder and Cochonat, 1996; Mulder and Alexander, 2001). For simplicity, subaqueous mass transport processes are often broken down into two broad types: coherent and incoherent. This section will outline the various different types of subaqueous mass transport that fall within these two broad groups. Before they are described, it is worth mentioning that these processes do not always exist in isolation, and coherent (high concentration) mass transport processes may evolve downslope into less coherent (low concentration) types (Fig. 1.1).

1.4.1 Coherent or elastic mass transport

Coherent or elastic mass transport processes involve the movement of large consolidated blocks or sheets of previously deposited sediment. These processes differ from incoherent processes by virtue of the sediment remaining largely consolidated and retaining internal bedding and structures. This is either due to the slow moving nature of the transport or the lithification (compaction) of the sediment prior to failure.

1.4.1.1 Submarine slides

While the term ‘landslide’ can be broadly used to define many types of mass movement, either subaerial or sub-aqueous, a ‘submarine slide’ has a more specific definition; although variations on this definition exist. Mulder and Cochonat (1996) define slides as ‘downslope displacements of coherent masses of sediments scarcely disturbed during the movement, which is limited, and bounded by distinct failure planes usually parallel to the stratification, except for the headwall region’. Masson et al. (2006) more broadly define a slide as ‘a coherent mass of sediment bounded by distinct failure planes’. This failure plane, often referred to as the glide plane, is a basal layer of high shear along which most of the movement occurs. If the failure plane is slope-parallel the slide is considered to be translational (Stow et al., 1996, Fig. 1.1). Slope-parallel failure planes that facilitate translational slides can consist of over-pressured mud, sand, or clathrate deposits, all of which act as weak layers. Translational slides typically involve brittle deformation of lithified or semi-lithified sediment, and undergo extensive basal shearing.

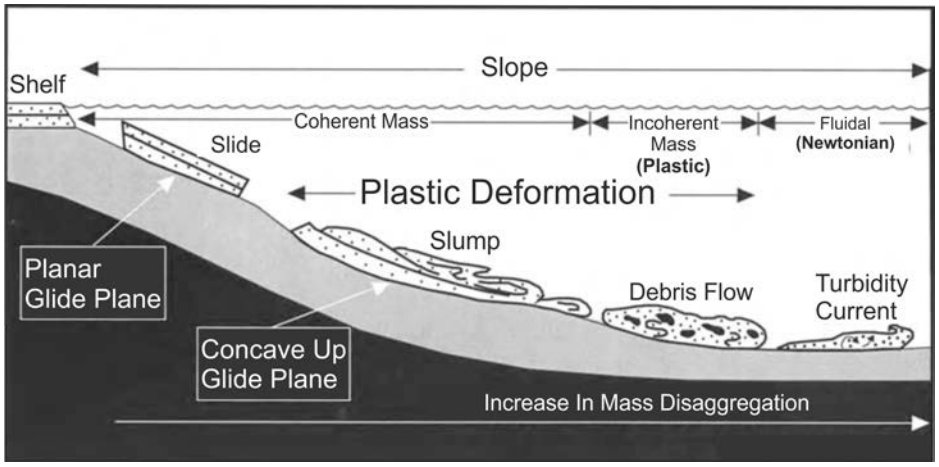

Figure 1.3: Schematic diagram of the continental slope showing the common types of mass transport processes that move sediment into the deep ocean. Translational slides with intact morphology may evolve into slumps with increasing internal deformation. If slumps incorporate fluid during transport they may evolve into a debris flow. If even more fluid is incorporated the debris flow can transition into a fluidal flow called a turbidity current. (Shanmugam et al.,1994).

In addition to translational slope-parallel movement, slides can also occur with a listric, or rotational morphology in which the glide plane is concave-up, and not always aligned with bedding

or slope (Fig. 1.3). These types of slides are sometime referred tom as ‘slumps’ so as to distinguish them from translational slides. The amount of deformation observed in slumps is much greater than in translational slides, where deformation can be minimal. This is due to both brittle and plastic deformation in the form of thrusting and folding in the body and toe of the sediment. While the morphology of slides and slumps may differ, the process of shear failure along a defined surface is common to both and we can refer to both as a ‘slide’ (Stow et al., 1996). Simple slides consist of only one failure along a single glide plane, while complex progressive or retrogressive slides may involve more than one failure, which can be disparate in time, termed multi-staged failure (Fig. 1.3). Progression or retrogression of slides can occur in the existing glide plane or scar via overburden release, or in neighbouring sediments (Mulder and Cochonat, 1996).

1.4.1.2 Debris avalanches and rockfalls

Debris avalanches are catastrophic, fast movements of cohesionless lithified rock fragments that occur on cliffs or steep slopes (Mulder and Cochonat, 1996). They are more commonly found on oceanic islands where steep flanks combined with volcanic hazards can result in precipitous releases of rock and sediment (Siebert, 1984; Chiocci and Alterils, 2003; Hunt et al., 2013a). Debris avalanches are characterised by a chaotic mixture of different sized fragments that interact in a high-energy manner, encouraging further disintegration (Bates and Jackson, 1987). Transported blocks of sediment may be anywhere in the region of tens to hundreds of meters in diameter. This type of transport mechanism can deposit material many kilometres from source (Masson et al., 2002).

Rockfalls are a similar process to debris avalanches and are defined as a ‘relatively free falling or precipitous movement of a newly detached segment of bedrock of any size from a cliff or a steep slope’ (Canals et al., 2004). Rockfalls are distinguished from debris avalanches primarily on the basis of volume and distance of transport. Rockfalls are thought to be a far more regular and short-lived occurrence as a result small-scale slope instabilities. A lack of confinement and limited clast interaction also distinguish rockfalls from debris avalanches (Stow et al., 1996).

1.4.1.3 Creep

Creep as a mass transport process has not been reported in the geographical areas covered in this thesis. However it is a common process affecting both subaerial and subaqueous slopes and so will be described. It is defined as 'the slow, gradual, more or less continuous, non-recoverable deformation sustained by ice, soil and rock materials under gravitational body stresses' (Canals et al., 2004). A definition more applicable to marine sediments is given by Mulder and Cochonat (1996): 'creep is the elastic deformation of sediment, usually clay, under constant load and very low deformation rate'. Importantly, sediment creep may evolve into a slide or slump if the yield strength of the sediment is overcome (creep rupture). It may be that creep plays a precursor role in the failure of large submarine landslides observed on the Norwegian Margin. Sediment cracks have been observed upslope of the Storegga submarine landslide scarp, and may indicate that slow creep is an ongoing process (Mienert et al., 2010).

1.4.2 Incoherent mass transport

Mass transport of largely disaggregated material consisting of individual grains or clasts is referred to as incoherent. Incoherent mass transport processes can result from the disaggregation of coherent blocks of material within slides, debris avalanches or rockfalls. However, they may also originate from sediment-dense fluvial input (Kriphounoff et al., 2009), sub-glacial discharge (Laberg and Vorren, 2000b), or tidal and storm resuspension (de Stigter et al., 2007). These types of mass transport have been broadly referred to as 'sediment-gravity flows', and a number of different criteria have been used to classify them including flow state (i.e. turbulent or laminar; Shanmugam, 2002), mechanism of sediment support (Mulder and Alexander, 2001), and flow rheology (i.e. yield strength). Talling et al. (2012) have argued for a deposit-based classification in cases where no direct measurements of flows exist; as in the case for this thesis. This leads to a somewhat simpler classification scheme that is comprised of two main types: en-masse and incremental settling. En-masse settling is considered to occur largely in debris flows and grain flows, while incremental settling is more characteristic of turbidity currents. This section will discuss these types of mass transport.

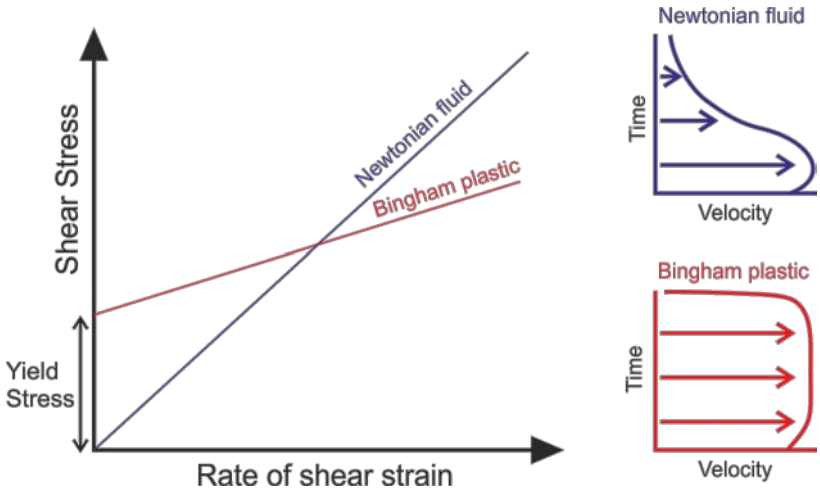

Figure 1.4: Conceptual diagram illustrating the difference between the flow characteristics of Newtonian and Bingham fluids. Flow rheology as a classification method is based on the relationship between applied stress acting on the fluid and the rate of strain. Newtonian fluids like dilute turbidity currents have no inherent strength and will begin to deform at the moment of applied stress. Bingham plastics like debris flows have inherent strength and will only deform once a given yield stress is overcome. Also shown are generalised schematics of the different velocity profiles associated with each type of flow.

1.4.2.1 Debris and grain flows

Debris flows are flows of granular material in which the principal support mechanism is matrix strength and the flow is largely laminar rather than turbulent (Bates and Jackson, 1987; Canals et al., 2004). In these flows the grains are well mixed with the interstitial fluid, and can range from clay to gravel in size (Shanmugam et al., 2006). Rheologically, debris flows can be described as viscoplastic Bingham fluids, whereby there is some initial yield strength that must be overcome before deformation and flow can take place (Mulder and Alexander, 2001, Fig. 1.4). It has been observed that debris flows can be subdivided into two categories: cohesive and in-cohesive (Stow et al., 1996; Talling et al., 2012). In strictest sense debris flows are only considered to be cohesive, while in-cohesive debris flows are sometimes referred to as grain flows or poorly cohesive debris flows.

Cohesive debris flows feature an interstitial mud and water matrix that has sufficient cohesive strength to support grains larger than sand during flow (Middleton and Hampton, 1973; Mulder and Alexander, 2001). An interstitial mud/water matrix of as low as 5% may be enough to facilitate grain suspension and flow. These cohesive debris flows can travel on relatively low-gradient slopes

and over long distances if the mad/water matrix has a high cohesive strength and high percentage volume (Stow et al., 1996; Dasgupta, 2003). The long run-outs are attributed to hydroplaning, whereby a thin film of water penetrates the base of the flow and decouples the sediment from the bed, reducing basal shear stress (Mohrig et al., 1998; Harbitz et al., 2003).

In-cohesive debris flows are something of a misnomer, as grain interactions and interstitial fluid provide the support for flow rather than a matrix (Lowe, 1976). Instead, in-cohesive debris flows are often referred to as grain flows, although a continuum likely exists between these two flow types (Parsons et al., 2001; Shanmugan, 2006; Talling et al., 2012). The deposits of both cohesive and in-cohesive debris flows are broadly referred to as debrites and result from en-masse freezing of the flow due to the gravity force decreasing below the yield strength of the flow (Fig. 1.2). The en-masse freezing can result in deposits that are poorly sorted, ungraded, and structure-less; although some grading and structure is evident in deposits that demonstrate characteristics of more than one process (e.g. linked debrites; Haughton et al., 2003).

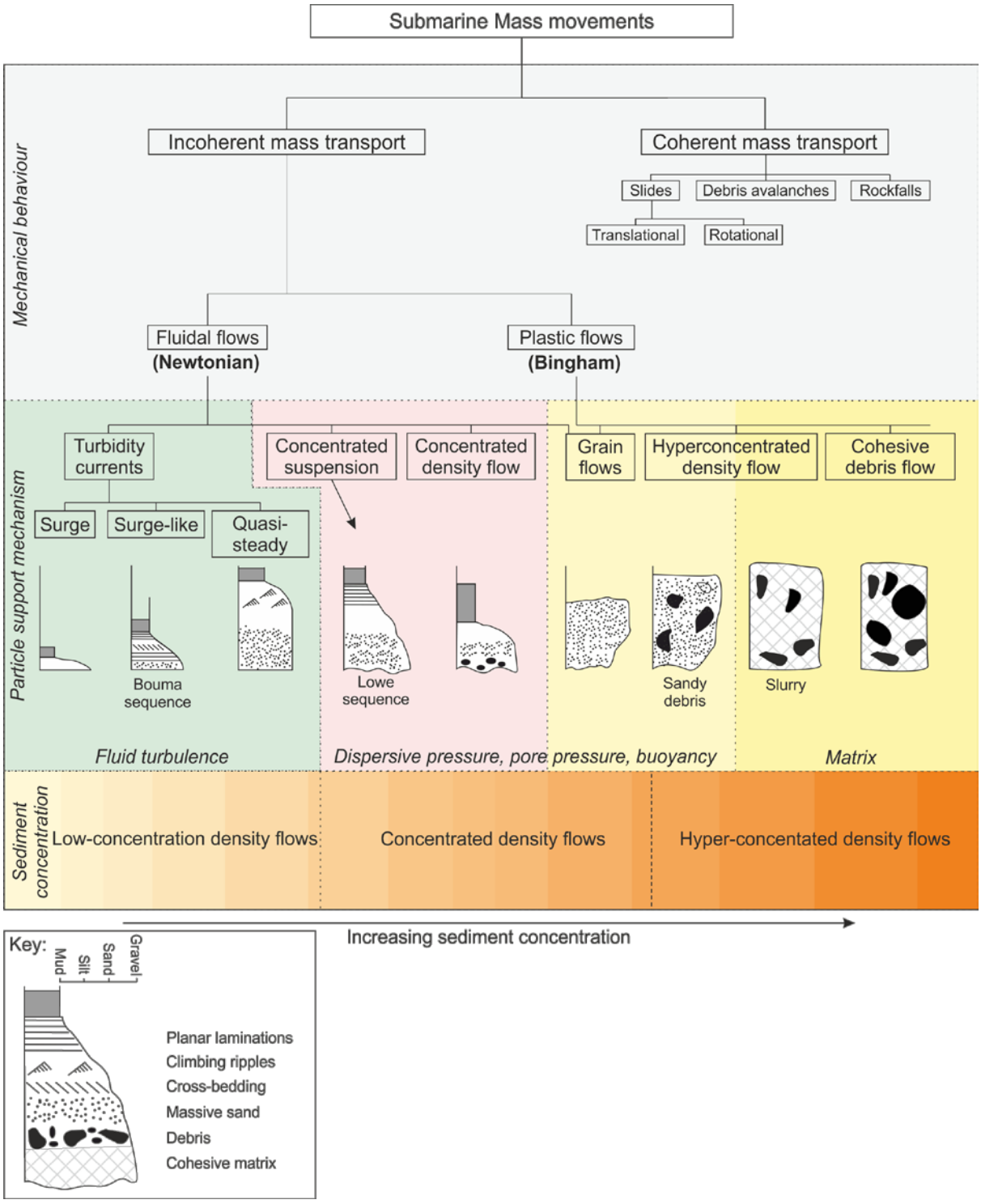

Figure 1.5: Schematic showing the different classification methods of in-coherent mass transport, including mechanical behaviour, particle support mechanism, and sediment concentration (Lowe, 1976; Lowe, 1982; Mulder and Cochonat, 1996; Stow et al., 1996; Mulder and Alexander, 2001; Dasgupta, 2003; Canals et al., 2004; Shanmugam, 2006; Adapted from Georgiopoulou, 2006).

1.4.2.2 Turbidity currents

Turbidity currents are defined as Newtonian fluids where sediment is kept in suspension primarily through fluid turbulence; although hindered settling and grain interaction may also contribute (Fig. 1.4; Bouma, 1962; Middleton and Hampton, 1973; Kneller and Buckee, 2000). Turbidity currents have a Newtonian rheology, which is distinct from the plastic (Bingham) rheology often observed in slides and debris flows. Newtonian fluids begin to deform and flow upon the initial application of shear stress, rather than having a yield stress that must be overcome before flow and deformation take place (Fig. 1.3). Sediment concentrations within turbidity currents can range from as low as 0.1% and up to 9%, beyond which fluid turbulence alone can no longer maintain particle suspension (Bagnold, 1962).

Classification systems for turbidity currents are numerous, but there are two in particular that are useful. The first is the horizontal approach of Mulder and Alexander (2001) that uses flow duration and the nature of the deposits to classify turbidity currents into 1) surging, 2) surge-like, and 3) quasi-steady (Fig. 1.5). Surging and surge-like turbidity currents are considered to be much smaller and consist of an initial pulse of sediment with a potential tail of slower moving material. These are thought to result via flow transformation from more concentrated flow types like grain flows (Mulder and Alexander, 2001). Quasi-steady flows result from a more continuous input of sediment rather than a near-instantaneous event like a landslide or nepheloid plunging. This can occur where river mouths discharge sediment laden water that descends due to its excess density compared with the ambient water. These types of flows are referred to as hyperpycnal flows.

Turbidity currents can also be classified into low- and high-density, where sediment concentration is the determinant factor in the classification (Lowe, 1982, Fig. 1.5). Mulder and Alexander (2001) have argued against this type of classification, claiming that the deposits of ‘high-density’ turbidity currents cannot have arisen from flows that are dominantly maintained by fluid turbulence. They instead argue for ‘concentrated’ and ‘hyper-concentrated’ density flows that refer to intermediates between debris flows and turbidity currents (Fig. 1.5). Low-density turbidity currents usually deposit through slow settling of suspended material. Basal traction is capable of creating small-scale ripples and laminated silts (Bouma, 1962; Stow et al., 1996; Mulder and Alexander, 2001).

More concentrated density flows deposit through a combination of fallout, aggradation, although traction at the dense near-bed layers may cause grain-flow conditions to prevail. If the density of a turbidity current exceeds a critical point, suspension of sediment is no longer possible, and transformation into debris flow-like conditions may deposit hybrid beds (Haughton et al., 2003; Talling et al., 2007b).

1.5 Triggers and preconditioning factors of subaqueous mass movements

Before a discussion on the different processes that cause submarine mass movements, it is important to highlight the distinction between a trigger and a preconditioning factor. Triggers of submarine mass movements can be thought of as near-instantaneous processes that directly result in movement of sediment downslope (e.g. earthquakes). This movement of sediment may be either coherent or in-coherent. Preconditioning factors refer to longer term processes (e.g. sedimentation rate) that render slopes more likely to fail in the event of triggering processes occurring. This distinction is valuable because while instantaneous triggers like earthquakes might have a measure of predictability, the preconditioning of slopes over time makes the likelihood of a failure occurring more difficult to predict.

1.5.1 Triggers of subaqueous mass movements

The term ‘trigger’ in this thesis refers to processes that happen near-instantaneously to cause a submarine mass movement. These processes can initiate coherent mass movements such as slides and slumps that may evolve down-slope into debris flows and turbidity currents (Fig. 1.1). Equally, some triggering processes may directly initiate in-coherent mass movements such as dilute turbidity currents. Here these different triggering processes will be discribed.

1.5.1.1 Earthquakes

Earthquakes have been recognised as a trigger of large submarine mass movements since the discovery of broken telecommunication cables associated with the Grand Banks earthquake of 1929 (Heezen and Ewing, 1952). Earthquakes can trigger sediment failure by destabilising in-situ

sediments via ground shaking. In submarine settings the shear strength of sediments may be considerably lower than on land due to a lack of consolidation and the presence of excess pore pressure. The cyclic loading of earthquake activity can also generate further excess pore pressure and eventually failure of the sediment (Lee et al., 2007). This typically results in coherent mass movements such as slumps and slides (Piper et al., 1999; Normark and Piper, 2009); although seismic shaking can directly trigger in-coherent density flows through liquefaction of sediments (Field, 1993; Papatheodorou and Ferentinos, 1997). Earthquake-triggered coherent mass movements can subsequently transform downslope into in-coherent debris flows and turbidity currents (Hampton et al., 1996; Piper et al., 1999; Bryn et al., 2005; Shanmugam, 2006). Earthquakes are thought to trigger large turbidity currents that periodically flush large volumes of sediment out of submarine canyons and into the deep ocean (Paull et al., 2005; Arzola et al., 2008; Talling, 2014), as well as several large (>100 km^3) open continental slope failures (Laberg et al., 2002; 2006; Bryn et al., 2005).

There has been a significant amount of research in the last three decades on the use of turbidites as a record of past earthquakes, known as turbidite paleoseismology (Adams, 1990; Sumner et al., 2013; Atwater et al., 2014). However, the use of these turbidite records as indicators of earthquake activity is complicated by the observation that not all large earthquakes trigger mass movements (Sumner et al., 2013; Pope et al., 2016). The absence of a mass movement associated with an earthquake may be due to distance of the slope from the earthquake epicentre, lack of sufficient ground shaking due to a low or insufficient magnitude, or a lack unstable sediment (Hampton et al., 1996; Lee et al., 2007; ten Brink et al., 2009). Recent work using cable-break datasets has shown that even large magnitude earthquakes in multiple settings may not always generate significant submarine mass movements (Pope et al., 2016). This draws into question one of the key assumptions of turbidite paleoseismology: that all or most earthquakes are recorded by a turbidite. Furthermore, geotechnical work has shown that seismic activity may actually increase slope stability through pore water expulsion and consolidation (Lee et al., 2004). Irrespective of the limited number of earthquakes that are independently known to have caused a mass movement, they are recognised as triggers of large-volume sediment transport (Piper and Normark, 2009).

Despite the limitations of turbidite paleoseismology it has been applied in several settings to determine a first-order estimate of the recurrence rate of large-magnitude earthquakes (Goldfinger et al., 2007; Gracia et al., 2010; Masson et al., 2011b; Moernaut et al., 2014).

In order to apply turbidite paleoseismology turbidites triggered by earthquakes must be distinguished from those caused by different triggering mechanisms. Currently there is no agreed upon sedimentological criteria for distinguishing earthquake-triggered turbidites (Sumner et al., 2013; Talling, 2014 and references therein). Turbidites deposited synchronously in different basins have been used to infer a regional seismic trigger (e.g. Gracia et al., 2010); although uncertainties in the AMS dating of turbidites may cast doubt on whether turbidites are truly synchronous (Urlaub et al., 2013; Pope et al., 2015). The confluence test of Adams (1990) has been applied to the convergence of submarine channels; the inference being that seismic shaking will trigger turbidites in more than one channel tributary. This triggering of turbidity currents in multiple channel tributaries will then produce a stacked turbidite sequence below a channel confluence. This test fails to account for the possibility of turbidity currents in multiple canyon tributaries being triggered by other mechanisms such as large storms (Shanmugam, 2008). Turbidity currents triggered in canyon tributaries may also fail to reach the canyon confluence, may cannibalise deposits from other tributaries, or may bypass the confluence entirely; all of which imply that an earthquake may not be recorded (Atwater et al., 2014). Turbidite paleoseismology remains problematic in settings where multiple triggers and disparate sources or turbidites, variable transport distance, and uncertainties in age determination exist.

1.5.1.2 Wave and storm resuspension

The triggering of submarine mass movements by the action of waves and storms has been well documented, particularly in canyon systems where their heads partially or fully cross the shelf (Puig et al., 2014, and references therein). Storm and wave activity are capable of suspending large volumes of shelf sediment, which can advect seaward as dilute or thin and dense turbidity currents through canyons or across narrow shelves (Traykovski et al., 2000; de Stigter et al., 2007; Masson et al., 2011a). These dilute flows can become erosive and travel into deeper water provided sufficient density and sediment availability (Piper, 1970; Parker, 1982; Fukushima, 1985; Piper and

Normark, 2009; Talling et al., 2013). However, most of these flows terminate within canyons and do not reach slope fans or distal basin settings (Paull et al., 2005; de Stigter et al., 2007; Masson et al., 2011a; Xu, 2011; Allin et al., 2016). Turbidites deposited from wave or storm-triggered flows are often thin, but can be thicker and mud-dominated due to persistent storms, particularly in canyons with higher volumes of available sediment (de Stigter et al., 2007; Arzola et al., 2008; Masson et al., 2011a). It has been proposed that storm and wave action can directly trigger slope failures through stress change associated with breaking waves (Dengler et al., 1984). However, there is little evidence that wave activity can influence slope stability below 100 m water depth (Lee and Edwards, 1986).

Sediment remobilised on continental shelves by storms can cascade off the shelf edge rather than directly into submarine canyons and channels. This cascading is an important mechanism by which sediment is moved from the shelf to the shelf edge and slope (Traykovski et al., 2000; Wright and Friedrichs, 2006). However, this process is not considered to be a significant hazard, as flows are typically slow (< 1 m/s) and their sediment concentration is low (0.001 vol.%; Canals et al., 2006; Puig et al., 2008). The deposits of these dilute turbidity currents are generally thin and fine grained (Palanques et al., 2009).

1.5.1.3 Hyperpycnal discharge

River discharge can carry large volumes of sediment in suspension, particularly during floods. The suspended sediment results in excess density (hyperpycnal) that causes plunging of river discharge below the ambient sea water (Normark and Piper, 1991; Mulder and Syvitski, 1995; Mulder et al., 2001). Hyperpycnal flows have been frequently observed where submarine canyons that incise the shelf are fed by river systems, such as the Var and Gaoping Canyons (Kriphounoff et al., 2009; 2012; Liu et al., 2012; Mas et al., 2010). These plunging flows can be erosive, although they typically are not and terminate before reaching canyon fans (Mulder et al., 1998; Carter et al., 2012b; Liu et al., 2012). While the volumes transported by hyperpycnal flows are thought to be small compared with other mass transport processes, some much larger flows proposed to be hyperpycnal have been shown to transport 0.06 km^3 of sediment (Liu et al., 2012). However, as is

noted in Talling et al. (2013) the deposits of hyperpycnal flows are difficult to distinguish from those deposited by turbidity currents generated via other processes.

1.5.1.4 Volcanic eruptions and flank collapses

Submarine mass movements such as debris flows and turbidity currents may occur as a continuation of subaerial volcanic mass transport events. These subaerial mass movements can originate from volcanic island flank collapses caused by over-steepening or volcanic eruption, by pyroclastic avalanches becoming submarine, or by the submarine emplacement of volcanic debris (Masson et al., 2002; Watt et al., 2012; Trofimovs et al., 2013; Le Friant et al., 2015). These subaerial slope failures can contain up to 100 km^3 of material and deposit over thousands of square kilometres of ocean floor (Watt et al., 2012; Hunt et al., 2014). It should be noted that submarine mass transport events may also be a continuation of, or triggered by subaerial failures that are unrelated to volcanic flanks, such as those observed on steep coastal cliffs (Graziani et al., 2006) or in mountainous regions (Kremer et al., 2012).

1.5.1.5 Gas hydrate dissociation and migration

Gas (methane) hydrate is a form of clathrate, combining methane gas and water into a frozen solid that occurs at specific temperatures and pressures within marine sediments, as well as some terrestrial settings (Kvenvolden and McMenamin, 1980). Generally speaking, its occurrence is limited to <700 m water depth (Sultan et al., 2004). Interest in gas hydrate-bearing sediment grew as it became apparent that the volume of methane stored could potentially affect the global climate if liberated by large mass movements (Paull et al., 2003; Maslin et al., 2004). Conversely, the volume of gas hydrates stored in the pore spaces of sea floor sediments suggested that their dissolution or migration as a result of changing pressure or temperature conditions might have a role in generating large mass transport events (Paull et al., 1996; Sultan et al., 2004; Hornbach et al., 2007; Owen et al., 2007). Masson et al. (2010) noted that the evidence for gas hydrates as a trigger of mass transport events is not substantive. Several large landslides that were proposed to have a gas hydrate involvement were shown to have been initiated below the gas hydrate stability zone (Bryn et al., 2005; Reagan and Moridis, 2008; Twichell et al., 2009). However, several recent

papers have again suggested a hydrate influence on slope stability (Riboulout et al., 2013; Crutchley et al., 2016); although this evidence is arguably still not conclusive of hydrate triggering (e.g. Elger et al., 2015).

1.5.1.6 Other triggers

There are several less significant processes that can trigger mass movements such as turbidity currents. Bottom trawling has been observed to trigger dilute turbidity currents in the heads of submarine canyons (Palanques et al., 2005; Martin et al., 2006). The discharge of mine tailing has also been observed to generate dilute turbidity currents (Hay et al, 1982). However, more damaging mass movements have been produced by construction activities (Gennesseaux et al., 1980), or by subaerial rockfalls (Kremer et al., 2012).

1.5.2 Factors that precondition slopes

Preconditioning factors are processes that affect slopes over years to millennia that do not directly initiate mass movements, but instead make failures more likely in the event of direct triggering processes occurring. These preconditions can include sedimentation rate, properties of the sediment inherited or acquired during or after deposition, as well as slope angle and pore pressure. There are uncertainties as to whether some of these preconditioning factors can instead be considered triggers, and these will be addressed in the following sections.

1.5.2.1 Sedimentation rate

Sedimentation rate on continental shelves and slopes is governed by a number of different processes, including sea level, glacial cyclicity, primary productivity, littoral transport, proximity to sediment conduits, and coastal erosion, among others. It might be argued that one of the most important determinants of sedimentation rate is latitude. Continental margins in high latitude regions receive significantly higher (>10 m/ka) sedimentation rates than those in mid-to low latitudes due to the presence of large ice sheets during glacial periods. In contrast, sedimentation rates on mid to low latitudes are lower and more stable. Notable exceptions to this are large river

fed fan systems such as the Amazon and Indus Fans that receive significant volumes of sediment from glaciated mountain ranges in continental interiors (Maslin et al., 1998; Clift et al., 2001).

Large increases in sedimentation rate cause the development of excess pore pressures that can lead to failure of sediment. Excess pore pressure within a soil occurs when the sedimentation rate exceeds the rate at which the interstitial fluid is expelled through compaction (Gibson, 1958; Green and Wang, 1986; Strout and Tjelta, 2005; Stigall and Dugan, 2010). The presence of layers of impermeable sediment may further limit the ability of fluid to escape and preserve the high excess pore pressure at depth. This over-pressuring of the sediment and pore fluid affects its shear strength and thus its resistance to downslope gravity forces. When gravitational loading exceeds the shear strength of the sediment failure occurs (Morgenstern, 1967; Lambe and Whitman, 1979; Mellow and Pratson, 1999). Seismic loading (ground acceleration) may also exceed the shear strength of slope sediment and cause failure (Kvalstad et al., 2005a).

1.5.2.2 Development of weak layers

A concise definition of a weak layer is given by Locat et al. (2014): ‘a layer (or band) consisting of sediment or rock that has strength potentially or actually sufficiently lower than that of adjacent units (strength contrast) to provide a potential focus for the development of a surface of rupture’. Weak layers have been suggested as contributory factors in a number of submarine landslides that have bedding-parallel glide planes (Kvalstad et al., 2005b; L’Hereaux et al., 2010). The exact properties and compositions of weak layers are not clear as it is likely they are removed during the landslide evacuation (Masson et al., 2010). However, it is thought that they correspond to specific sedimentological horizons (Haflidason et al. 2003; Krastel et al. 2006). The development of weak layers may result from the focussing of excess pore pressures in sandy horizons with greater porosity, and thus it is a combination of sedimentological and geotechnical factors that reduce shear strength (Masson et al., 2010). The failure of these weak layers due to gravitational force rather than an external factor might itself be considered a trigger resulting from the preconditioning of the sediment by overburden and excess pore pressure generation. On the other hand, failure of these week layers due to seismic shaking from earthquakes might classify their development as a preconditioning factor.

1.5.2.3 Sea level

For the past several decades it has been widely accepted that changes in sea level affect sediment delivery to the continental slopes, and thus affects the rate at which sediment is transported into the deep ocean by mass transport processes (Vail et al., 1977; Shanmugam and Moiola, 1982; Posamentier et al., 1991; Piper and Savoye, 1993; Lebreiro et al., 1997 Clark and Mix, 2000; Ducassou et al., 2009; Lebreiro et al., 2009; Covault and Graham, 2010). During times of glacial sea level lowstand when sea level exposes much of the continental shelf, sediment accommodation moves towards the continental slopes and basin. With the exposed shelf, rivers deposit sediment directly into canyons that do not cross the continental shelf, whereby it is transported by gravity flow processes into the deep ocean.

The role of sea level in submarine mass movements is somewhat complex. It had previously been proposed that sea level change could alter the stress conditions within the sediment and facilitate failure by either gas hydrate dissociation or the development of excess pore pressure (Lee et al., 1996; Maslin et al., 1998). However, geotechnical work has suggested that sea level change on glacial time-scales is not likely to influence slope stability in a significant way (Liu and Flemings, 2009). Sea level lowstands instead act as a mechanism through which sediment is delivered closer to the continental slope, thus increasing slope instability (Lebreiro et al., 2009; Covault and Graham, 2010). Sea level as a preconditioning factor for large submarine mass movements has been inferred by many authors (Maslin et al., 2004; Owen et al., 2007; Lee, 2009; Smith et al., 2013). Despite this, very little statistical evidence exists to support sea level as broad control, particularly on the largest submarine mass movements that reach deep ocean basins (Urlaub et al., 2013; Clare et al., 2015; Allin et al., 2016).

1.5.2.4 Oversteepening

Oversteepening of the continental shelf and slopes has been proposed as a preconditioning factor for large submarine mass movements (Schwab et al., 1991; Collot et al., 2001; Ratzov et al., 2007). Submarine slopes can become oversteepened by tectonic processes such as fault movement, salt diaperism, and plate subsidence (Tripsanas et al., 2004; Ratzov et al., 2007; Strasser et al., 2011).

Oversteepening or undercutting of marine slopes can also occur through erosion by bottom water currents (Hampton et al., 1996). Invoking tectonic oversteepening as a preconditioning factor of large slides is complicated by the possibility that landslides were preconditioned by sedimentological or geotechnical factors rather than slope changes. Along margins with complex sedimentary and tectonic regimes, identifying the principal preconditioning mechanisms is notably more difficult (Ross et al., 1994; Milia, 2000; Strasser et al., 2011).

1.6 Geohazards implications of subaqueous mass movements

Subaqueous mass movements have well recognised geohazard implications. These geohazards require a better understanding of the triggers and recurrence rates of subaqueous mass movements, particularly submarine landslides and turbidity currents. Here the different geohazards and their implications for coastal settlement and infrastructure will be discussed.

1.6.1 Catastrophic tsunami generation

Submarine mass movements, in particular landslides, can involve large volumes of sediment (>100 km^3), can move rapidly (>20 m/s), and can generate damaging tsunamis through displacement of the water column (Tappin et al., 2001; Bryn et al., 2005). Two tsunamis have been generated by submarine slides during historical times, including Papua New Guinea (1998; Tappin et al., 2001; 2008) and Grand Banks, Canada (1929, Heezen and Ewing, 1952). Both of these tsunamis caused significant damage, while the Papua New Guinea event resulted in significant loss of life. Slide-generated tsunamis with the potential for much greater damage and loss of life have been observed in the geological past. The Storegga Slide at ~8,200 years ago on the Norwegian continental margin generated a tsunami that reached onshore run-up heights of 20 m above sea level, and travelled as far as the Western European coastline and Greenland (Dawson et al., 1993; Bondevik et al., 2003; Bryn et al., 2005). The BIG'95 Slide in the Western Mediterranean may have generated tsunami waves that reached heights of 2 m on the south-eastern French and Spanish coastlines (Løvholt et al., 2013). Other very large submarine mass movements are evident from exceptionally large sedimentary deposits in deep ocean basins (Rothwell et al., 1998; Wynn et al., 2002; Hjelstuen and Andreassen et al., 2015). However, the failure dynamics of these landslides are

not well understood, and therefore it is not clear whether they triggered tsunamis (Harbitz et al., 2013; Løvholt et al., 2013).

1.6.2 Rupturing of undersea cables

Over 95% of all data traffic between continents is done through undersea optic-fibre cables, and includes private internet, financial services, and global telecommunications (Carter et al., 2009). The ability of submarine mass movements, such as fast-moving (>10 m/s) turbidity currents, to break undersea cables is well documented (Heezen and Ewing, 1952; Gennesseaux et al., 1980; Piper et al., 1999; Carter et al., 2014; Pope et al., 2016). Cable-breaks are typically very expensive to repair, and the breaking of numerous cables by long run-out mass movements makes the re-routing of data problematic (Carter et al., 2014). The threat posed by mass movements to vital undersea cables makes understanding their recurrence rates and magnitudes important for regional geohazard assessment.

1.6.3 Damage to oil and gas infrastructure

Offshore oil and gas infrastructure is often located proximal to where submarine mass movements occur, notably canyons, deltas, and slope fans (Redin et al., 1991; Clark and Pickering, 1996; Abdel Aal et al., 2000). Deep-water settings in particular are challenging environments in which to perform repairs or re-routing in the event of rupture due to submarine mass movements (Thomas et al., 2010). In addition to the great expense and difficult logistics of repairing oil and gas infrastructure, the environmental degradation associated with rupture can be severe (Camilli et al., 2010; Skogdalen and Vinnem, 2012). The risk to oil and gas infrastructure posed by submarine mass movements makes understanding their triggers and frequency even more important.

The largest and most hazardous landslides occur on time scales of thousands or tens of thousands of years (Laberg et al., 2006; Hunt et al., 2013b). However, smaller and more frequent landslides and turbidity currents arguably pose a greater risk to subsea infrastructure. These smaller slides and turbidity currents occur during all sea level states on active and passive margins, and in submarine canyons (Masson et al., 2011a; Baeten et al., 2014; Li et al., in press). While these smaller slides and turbidity currents are hard to predict they need to be considered in geohazard assessment.

Chapter 2: Methods

2.1 Introduction

The publication or intended publication of chapters 3 - 5 of this thesis limits the space for detailed description of the methodologies; in particular the statistical analyses. This chapter provides a more thorough explanation of the methods used in this thesis.

2.2 Sedimentology

2.2.1 Piston and multi- coring

The piston and multi cores used in this thesis were collected during four different research cruises. Cores from the Nazaré Canyon were collected during research cruises JC027 and CD157. Cores from the Trænadjupet area off the Norwegian Margin were collected during research cruise 64PE391. The ODP 898A core from the Iberian Abyssal Plain was retrieved during ODP leg 149.

2.2.2 Core logging

Logging of the >30 sediment cores used in this thesis consisted of identifying colour, classifying different sedimentary facies, and visually estimating the grain size using a grain size comparator. Photographic imagery was also collected using a Geotek^{TM} photographic scanner for use in core log figures.

2.3 Geophysical analysis

2.3.1 Magnetic Susceptibility

Magnetic susceptibility records positive excursions in the presence of magnetic sediment grains. This property is particularly useful in the identification of glacial-interglacial transitions, ice-rafted detritus, and volcanic tephra, all of which have been used in building core chronostratigraphies. It can also be used in the identification of turbidite sands that contain a higher proportion of magnetic grains. Magnetic susceptibility profiles were obtained for split sediment core sections using a

Geotek™ XYZ core scanner that uses a Barrington point sensor. This sensor works by detecting the degree of increased magnetic field strengthening in the presence of magnetic material.

2.3.2 Gamma-ray density

Different sediment types (i.e. turbidite sand, hemipelagite) can have different densities due to distinct grain size characteristics. Given this, the density of sediment can be used to support the interpretation of lithological boundaries made by visual logging. A Geotek™ multi-sensor core logger (MSCL) was used to obtain gamma-ray density profiles on split core sections. The MSCL uses a Caesium-137 source to emit a narrow beam of gamma rays with energies of 0.662 MeV, and the amount of scattering (attenuation) is measured by a detector. The degree of gamma ray beam attenuation is then used as a proxy for the density of the sediment.

2.3.3 Photospectrometry

Lithological boundaries such as turbidite-hemipelagite boundaries and glacial-interglacial transitions can be recorded by changes in sediment colour. Quantitative measures of sediment colour can thus aid in identifying these boundaries and for correlating between core sections. Photospectrometry data was obtained using a Konica Minolta™ colour photospectrometer attached to the Geotek™ XYZ scanner. The output data is divided into 10 nm bins of the colour spectrum between 360-740 nm, but for simplicity a Munsell colour value is also given.

2.3.4 ITRAX-μXRF

Turbidite-hemipelagite boundaries and glacial-interglacial transitions can also be recorded by changes in sediment chemistry. ITRAX-μXRF geochemical data was collected using a kWMo-tube X-ray source and XRF Si-drift chamber detector. The instrument operated at 60 kV and 45 mA, with a dwell time of 800 ms and a resolution of 500 μm. The K-shell peak areas are automatically measured and converted to intensity (counts) for a designated element (Croudace et al., 2006).

2.4 Identification of turbidites and mass transport deposits

In order to build age models used in determining recurrence intervals, turbidites and mass transport deposits must be differentiated from hemipelagic sediment deposited out of the water column. The turbidites and mass transport deposits analysed in this thesis originate from different geological settings and exhibit a range of different deposit types. Generally, turbidites can be identified by the presence of a sharp basal contact and a normally-graded profile; although many different depositional types have been identified (Bouma, 1962; Stow and Piper, 1984; Talling et al., 2012). Debrites are typically coarser grained, and depending on the amount of disintegration, can consist of very large (>1 m) clasts (Georgiopoulou et al., 2009). They can exhibit normal grading, but may also be inversely graded or weakly normally graded (Naylor, 1980; Talling et al., 2004; Talling et al., 2012).

2.5 Identification of hemipelagic sediments

There are a number of different classifications for proximal and distal abyssal plain sedimentary deposits that settle from the water column and that are not the result of mass transport processes like turbidity currents or submarine landslides. These include pelagite, marls, oozes, and hemipelagite, all of which are defined based on differing biogenic, terrestrial, and grain size characteristics (Stow and Tabrez, 1998). Due to the different depositional settings and sediment types covered in this thesis, distinct classifications of these slow-settling deposits are avoided. Instead sedimentary deposits derived via slow settling from the water column are grouped under the umbrella term ‘hemipelagite’. Hemipelagic sediment can be defined as being derived from the overlying water column, often consisting of calcareous and siliceous micro fossils such as foraminifera, coccolithophores, and diatoms, and containing minor terrigenous input via suspension, ice-rafting, aeolian deposition, and volcanic fallout. It should be noted that hemipelagite can be purely devoid of calcareous material due to the position of the carbonate compensation depth (CCD). Below the CCD calcium carbonate will not be preserved and hemipelagite will consist almost entirely of terrigenous and siliceous biogenic components (Hoogakker et al., 2004).

Hemipelagic sediment can be distinguished from mass transport deposits on the basis of colour, grain size, sorting, bioturbation, and degree of deformation. Due to the higher proportion of calcareous micro fossils, hemipelagite typically exhibits lighter colours that can be quantified using photospectrometry (Balsam et al., 1999). Notable exceptions to this are mass transport deposits derived from the failure of thick hemipelagic accumulations on sediment-starved continental slopes, or from the flanks of seamounts and ridges. These 'hemipelagic turbidites' can have a similar colour as well as high carbonate content (Alonso et al., 2008). Unlike most deposits related to mass transport processes, hemipelagic sediments do not have any grading (patterns) or internal sedimentary architecture. Hemipelagic sediments in distal settings are also rich in biogenic material such as foraminifera, coccolithophores, and diatoms; components that are much less abundant in terrestrially-derived mass transport deposits (Stow and Piper, 1984; Stow and Tabrez, 1998). The presence of larger biogenic components such as foraminifera also gives the sediment a pitted texture following the splitting of multi- and piston cores. Given the slow rate of accumulation in many areas, hemipelagic sediments are often heavily bioturbated. While this bioturbation is often observed in the upper 5 - 15 cm of some mass transport deposits, it not typically observed deeper; escape burrows being one notable exception. The mixing by bioturbation of hemipelagic sediment and mass transport deposits makes identifying a distinct boundary between the two sediment types difficult. In this thesis the boundary is defined where the two sediment types exist in equal proportions (Fig. 2.1)

2.6 Age model development

2.6.1 AMS radiocarbon dating

In order to separate sediment into distinct grain sizes, and to separate out foraminifera for picking, 2 - 10 cm^3 of sediment was wet-sieved through sieves of 3 different sizes. Foraminifera from the >250 μm fraction were preferentially picked due to their size and increased resistance to fragmentation. In cases where foraminifera were sparse the 125 - 250 μm fraction was also picked. The <125 μm fraction was typically discarded due the difficulty in handling grains and foraminifera of that size.

Sampling of foraminifera for radiocarbon analysis was done using a binocular microscope and a sable paintbrush. The recommended weight of foraminiferal material required by most AMS radiocarbon laboratories is 8 - 10 mg, and this weight was collected where possible. This typically amounts to between 500 and 1,000 individual foraminifera depending on their size. For several samples much less material was available, and in some cases only ~3 mg could be collected. While this weight is low, it is still within the range of detectability and can still produce meaningful AMS radiocarbon ages.

2.6.2 Estimation of turbidite age and recurrence interval

The statistical analysis of turbidite frequency and recurrence relies on obtaining either radiometric determinations or other chronostratigraphic estimates of their ages. Since acquiring radiometric determinations of the ages of all turbidites is not realistic, in this thesis hemipelagic age models are used to estimate the ages for use in the statistical analyses. AMS radiocarbon is used to provide datums in recent (<43,500 BP) sedimentary sequences. For older deposits published biostratigraphic datums were used. With these datums, and the thicknesses of hemipelagic sediment between them, sedimentation rates were calculated. The thicknesses of hemipelagic sediment were then divided by the sedimentation rates to convert them into time intervals, or slices; otherwise known as linear interpolation (Thompson and Weaver, 1994; Wynn et al., 2002; Grácia et al., 2010; Clare et al., 2014). From these time intervals the ages of individual turbidites can be estimated (Fig. 2.1). The use of hemipelagic age models in determining the age of turbidites relies on the assumption that there is minimal fluctuation in the rate of hemipelagic sediment accumulation through time (Milkert et al., 1996a; Lebreiro et al., 2009; Clare et al., 2015; Allin et al., 2016). It also relies on the assumption that subsequent turbidity currents do not significantly erode the sea floor (Weaver and Thomson, 1993; Thomson and Weaver, 1994; Weaver, 1994; Wynn et al., 2002; Gutiérrez-Pastor et al., 2009; Grácia et al., 2010).

Using the age model to estimate the emplacement age of each turbidite allows us to calculate individual recurrence intervals. Here we define the recurrence interval of a turbidite as the length of time since the turbidite that preceded it (Clare et al., 2014, 2015; Pope et al., 2015). Where hemipelagic age models cannot be constructed, we calculate recurrence interval by diving the

length of time between individual age datums by the number of turbidites to get an ‘average recurrence interval’.

2.7 Statistical analyses

2.7.1 Testing the distribution of turbidite recurrence intervals

Statistically analysing frequency and recurrence data of natural hazards and processes can provide useful information on the relationships to other environmental factors. In many cases, the frequency distribution of a given dataset will determine the range of statistical tests that are applicable (Limpert et al., 2003.). Thus, one of the first assessments of a recurrence dataset should be to determine its frequency distribution. Aside from providing information on suitable analysis types, the shape of data distribution forms can yield information about the dynamics governing the system that gave rise to it (van Rooij et al., 2013). It has been demonstrated that certain statistical distributions of recurrence intervals are indicative of time-dependent behaviour (Van daele et al., 2014). These statistical distributions may indicate that additive process (e.g. normal) or multiplicative processes (e.g. lognormal) are exerting control on a system (van Rooij et al., 2013; Clare et al., 2016). Equally, distributions may indicate a lack of memory, or additive interactions between distinct components (e.g. exponential; Clare et al., 2014). For these reasons, determining the statistical distribution of recurrence data is important. Here the different methods for assessing the frequency distribution of a given dataset are outlined.

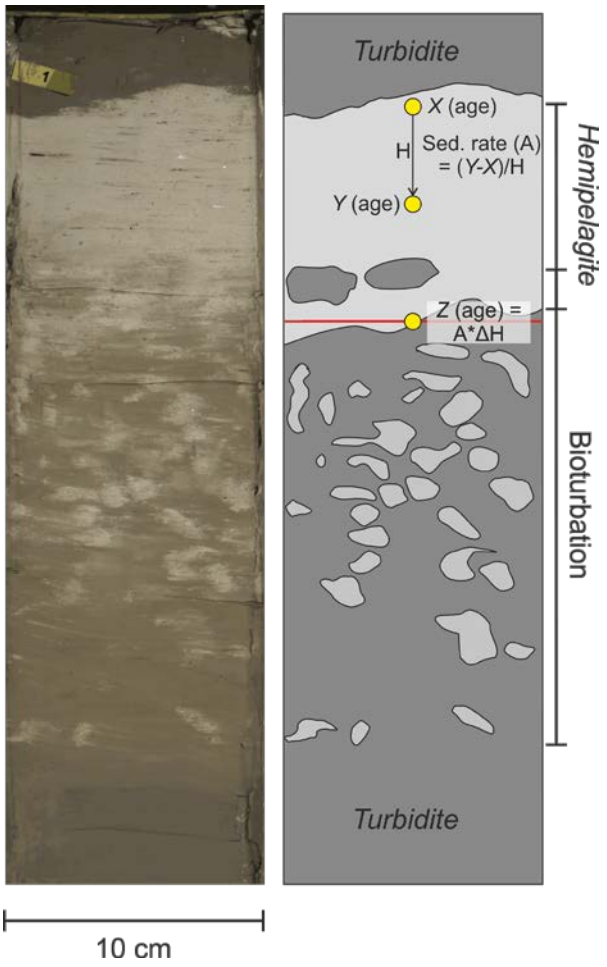

Figure 2.1: A photograph and schematic of a typical boundary between a turbidite deposit and overlying hemipelagic sedimentation. Bioturbation has caused mixing between the two sediment types making determining a definitive boundary difficult. Here we take the point at which both sediment types are in equal proportion, indicated by the red line. Estimation of turbidite ages is done through linear interpolation or extrapolation from known-age datums (X and Y) using sedimentations rate(s) (A) and thicknesses of hemipelagite (H).

2.7.1.1 Exceedance plots

Exceedance plots serve as a graphical method for determining the organisation of recurrence data. Different statistical distributions will have a different form when viewed on exceedance plots (Clare et al., 2014; Van Daele et al., 2014). Three main forms are considered and are thought to encompass the majority of common statistical distributions (van Rooij et al., 2013), and broad end-member scenarios in environmental systems (Hunt et al., 2013b; Clare et al., 2014; 2015; Allin et al., 2016). These three distribution forms are normal (Gaussian), lognormal, and exponential (Poisson; Fig. 2.2).

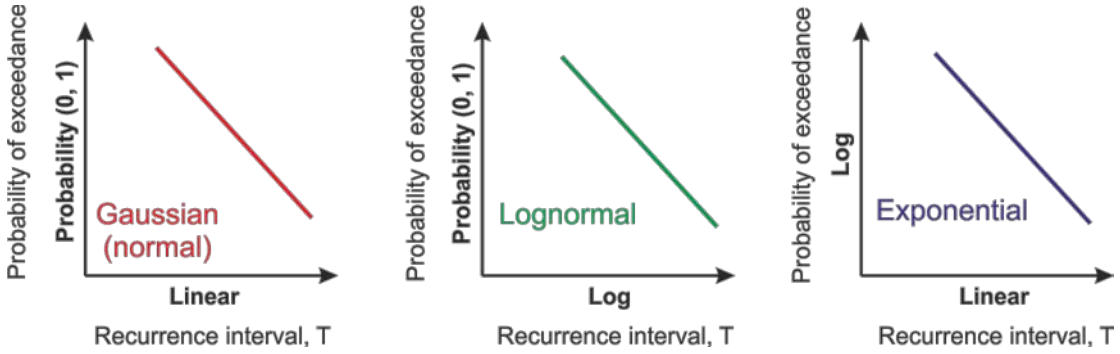

Figure 2.2: Exceedance plots showing straight lines indicating a Gaussian (normal) distribution on a linear-probability plot, a lognormal distribution on a log-probability plot, and an exponential distribution on a log-linear plot (Adapted from Clare, 2015).

2.7.1.2 Rescaled range analysis

Rescaled range analysis was developed as a test for temporal clustering or 'memory' in time series data (Hurst, 1951). It is defined as the range of cumulative deviations from the mean, divided by the standard deviation, obtained for multiple subsets of the recurrence data (Bassingthwaighte and Raymond, 1994). This test has the advantage of being independent of frequency distribution form (Kristoufek, 2012). The test produces a modified Hurst exponent (K) or 'self-similarity parameter', which measures the intensity of long range dependence in a time series (Weron, 2001). In simple terms, when $K \cong 1$ or $K \cong 0$ the data show persistence or anti-persistence respectively, indicative of time-dependent behaviour. Values of $K \cong 0.5$ are considered to be random or time-independent.

2.7.1.3 Mann-Whitney and Kolgomorov-Smirnov tests

In order to provide additional confidence in the outcome of distribution tests using small sample sizes, we can compare data of unknown distribution with data that have a known distribution. The Mann-Whitney (M-W) and Kolgomorov-Smirnov (K-S) tests are non-parametric formal normality tests that can be used to determine the probability that these prior data, and data of unknown distribution come from populations with the same distribution. Turbidite recurrence datasets from different basins and settings likely have significantly different medians. This makes applying distribution tests of normality like the Mann-Whitney and Kolmogorov-Smirnoff tests difficult. In order to overcome this, the data are normalised to the mean prior to analysis (Clare et al., 2014).

The Mann-Whitney test computes a U statistic that is the difference between the two rank totals of the different datasets (Lehmann and D'Abrera, 2006). Generally, the smaller the U statistic the less likely it is to have originated by chance. The test also generates a p-value of the significance. If the p-value is small, the idea that the difference is due to random sampling can be rejected, and it can be concluded that the populations have different medians. In contrast, the Kolmogorov-Smirnov test computes a D value, which is a measure of the difference between the cumulative distributions of the two datasets. Typically lower (>0.1) D values indicate no significant difference between two datasets. As with the Mann-Whitney test, the Kolmogorov-Smirnoff test produces a p-value that can be viewed as the probability that the result is due to random chance.

2.7.2 Testing explanatory variables on turbidite recurrence

In order to better understand the processes that might control the timing and recurrence rate of large, potentially damaging landslides and turbidity currents, we employ both regression and goodness-of-fit statistical methods. In statistical modelling regression is commonly used to test the relationship between a response variable of interest such as turbidite recurrence, and an explanatory variable. One major problem in the testing of explanatory variables on turbidite recurrence records is finding explanatory datasets with enough length and temporal resolution. The statistical analysis of a long-term (> 1 Ma) record of turbidite recurrence is limited by a lack of records of other environmental variables with similar length.

Several factors may exert control on landslide and turbidity current recurrence, including earthquakes, sedimentation, slope stability and sea level. The regional records of large earthquakes capable of triggering large submarine landslides are generally poor. These earthquake records often have too few observations and do not extend far back enough in time to be statistically useful. Sedimentation as an explanatory variable is problematic as rates of accumulation at any one point are dependent on other processes such as sea level and the location of the sediment depocentre. Slope stability and associated stress changes are in turn dependent on sedimentation rate and are also problematic to reconstruct over long time periods. Given the role of sea level in controlling sedimentation and slope stability by shifting the location of sediment depocentres closer to the continental slope during lowstand, it is a useful explanatory variable to test (Stow and Piper, 1984;

Posamentier et al., 1991; Covault and Graham, 2010). In this thesis three distinct regression-based methods are used to test sea level as an explanatory variable; linear modelling, generalised linear modelling, and Cox proportional hazard modelling.

2.7.2.1 Linear models

Linear and generalised linear models are widely used statistical tools in the analysis of a variety of different data types. While they are both types of regression analysis the key difference is how they model the change in response variable as a function of the explanatory variable (McCullagh and Nelder, 1989). Linear models assume that the response variable (e.g. recurrence) changes linearly with changes in the explanatory variable (e.g. sea level). Thus, for a sea level increase of 1 m, a linear model might predict a 50 year decrease in the recurrence of turbidites. However, beginning with a turbidite that has a 200 year recurrence, a subsequent 120 m drop in sea level would indicate a turbidite recurrence of 100 - (120*50) = -5900 years. However, linear models are useful for gaining some initial insights into the relationships between variables. Linear models are appropriate when the response variable has a normal or exponential distribution. The linear model framework is expressed in equation 2.1:

$$Y_i = \beta_0 + \beta_1 X + \epsilon_i \text{ (Equation 2.1)}$$

where Y_i is the predicted value of the response variable, β_0 is the intercept of the regression line, $\beta_1 X$ is the regression coefficient, and ϵ_i is the normally distributed error term for the ith sample with a mean of 0. The parameters β_0 and $\beta_1 X$ are estimated using a least squares method expressed below:

$$\beta_1 = \frac{\sum_{i=1}^{n}(x_i - \bar{x})(y_i - \bar{y})}{(x_i - \bar{x})^2} \text{ (Equation 2.2)}$$

$$\beta_0 = \bar{y} - \beta_1 \bar{x} \text{ (Equation 2.3)}$$

where $\sum_{i=1}^{n}$ is the sum of n successive samples, x_i and y_i are the ith sample of the explanatory and response variables respectively, and $\bar{x}$ and $\bar{y}$ are the sample means of the explanatory and response variables respectively.

Linear models produce a p-value; a value that is often used as a measure of the significance of an explanatory variable within the model framework. Importantly, the p-value cannot be universally used to evaluate the strength of a regression model, as p-values vary increasingly with decreasing statistical power. In the case of smaller sample sizes (N = <100) we might expect statistical power to be lower, and thus the p-value will be less reliable (Halsey et al., 2015). P-values may indicate the significance of an explanatory variable, but do not provide a quantitative measure of the effect. Hence, there are several other characteristics of regression models that we can use to evaluate the strength of a statistical relationship.

Linear models also produce a regression coefficient, which is a measure of the change in a response variable (e.g. recurrence) with a 1 unit change in the explanatory variable (e.g. sea level). They also produce a correlation coefficient (R^2), which is a measure of the variance in the data that is accounted for by the explanatory variable (Schemper and Stare, 1996). Another method of analysing the strength of a regression model is viewing the model residuals. Residuals are defined as the difference between the observed and predicted response data values within the linear model. An ideal linear model fit would have a purely random and non-systematic distribution of residual values (Lin et al., 2002). General rules of thumb exist for determining the minimum sample size for regression analysis. Prior statistical studies indicate that testing for statistical power and effect size in regression will require between N = 23 and N = 106 events to detect a large effect of an explanatory variable (Green, 1991; Tabachnik and Fidell, 2007). Smaller effects thus require considerably larger datasets.

2.7.2.2 Generalised linear models

In contrast, generalised linear models allow for response variables that have non-normal distributions. They require an *a priori* definition of the distribution form, which can be any distribution from the exponential family (e.g. normal, gamma, Poisson). This type of analysis is particularly useful where data are non-normally distributed due to truncation and censoring; a common occurrence in natural systems (Limpert et al., 2001). The generalised linear model consists of three components: a variance function for the response variable defined by its

prescribed distribution form, a link function that transforms the response variable onto a linear scale, and a linear predictor similar to ordinary regression (McCullagh and Nelder, 1989).

$$g(\mu_i) = \beta_0 + \beta_1 X \text{ (Equation 2.4)}$$

$$var(Y_i) = \emptyset V(\mu) \text{ (Equation 2.5)}$$

where $g(\mu_i)$ is the link function transform of the response variables (Y) to a linear scale, $\beta_0 + \beta_1 X$ is the intercept and the regression coefficient as in ordinary regression, and $var(Y_i) = \emptyset V(\mu)$ for simplicity represents the prescribed distribution form of response variables from the exponential family. In this way, generalised linear models can be used to predict a linear change if the distribution of the response data is considered to be normal, or they can be used to predict a rate of change if the data considered to be exponential. This gives them considerably more flexibility than other, simpler types of regression. As with linear regression, the generalised linear model gives a p-value, a regression coefficient, and a plot of residuals; all of which can be used to assess the strength of a regression model.

2.7.2.3 Cox Proportional Hazards models

Linear and generalised linear regressions are parametric models that evaluate the role of explanatory variable respective to time. In our case we are evaluating how the recurrence interval of turbidites changes in response to sea level. Instead we might want to understand how changes in explanatory variables like sea level affect turbidity current hazard function. The hazard function $[h(t)]$ describes the risk of an event during an interval after time t given that an event occurred at $t = 0$ (Smith et al., 2003).

$$h(t) = \frac{F'(t)}{P(T>t)} \text{ (Equation 2.6)}$$

where $F'(t)$ is the rate of events per unit time, and $P(T > t)$ is the probability (P) of an event (T) occurring later than some time (t) (Kleinbaum and Klein, 2005; Clare, 2016). For example, (T) might be a given turbidite recurrence interval and (t) a specified time. In order to test the effect of some assumed explanatory variable (covariate) on the hazard rate the Cox Proportional Hazards Model (PHM) is used (Cox, 1972).

$$h_i(t) = h_0(t) * \exp(\beta_1 X_{i1}) \text{ (Equation 2.7)}$$

where $h_0(t)$ is an unspecified baseline hazard function and $\beta_1 X_{i1}$ is a regression vector (β_1) for a given event (X_{i1}). The baseline hazard function and regression vector are equivalent to the intercept and regression slope in standard regression. $\beta_1 X_{i1}$ is estimated using a complex maximum likelihood method not described in this thesis. This model is widely applicable because it does not require a specification of the baseline hazard function $[h_0(t)]$, and so no assumption is made about the time between events. Instead, the model produces a proportional hazard ratio, calculated by comparing the regression vectors of two events in relation to the explanatory variable.

$$\frac{\cancel{h_i(t)}}{\cancel{h_j(t)}} = \frac{\cancel{h_0(t)} * \exp(\beta_1 X_{i1})}{\cancel{h_0(t)} * \exp(\beta_1 X_{j1})} \text{ (Equation 2.8)}$$

$$= \exp\{\beta_1 (X_{i1} - X_{j1})\} \text{ (Equation 2.9)}$$

In equations 2.8. and 2.9 we can see that the hazard ratio has no dependence on time and events are proportional to one another (Collett, 2003). If the resulting ratio is 1 then there is no effect of the explanatory variable on survival, and thus the hazard rate. A ratio of > 1 or < 1 indicates either an increasing or decreasing hazard rate with respect to changes in the explanatory variable. For continuous variables, a hazard ratio of 1.01 would indicate that with every unit of change in the explanatory variable the risk of an event increases by 1% (Walters, 2009). This estimated increase in risk is accompanied by 95% confidence intervals and a p-value, which also aid in the interpretation of a Cox PHM model. The cox model has previously been applied to turbidite recurrence data (Hunt et al., 2013b; Clare et al., 2015; Allin et al., 2016) and it serves as a useful tool requiring no prior information about the distribution of recurrence times. Three statistical tests produced in the model (Likelihood, Logrank, and Wald) aid in evaluating the strength of a statistical relationship between actual and hypothesised values.

Chapter 3: Different frequencies and triggers of canyon filling and flushing events in Nazaré Canyon, offshore Portugal

Summary:

Long (>50 kyr) records of turbidity current frequency are relatively rare in the scientific literature. This limits our understanding of their timing, triggers and preconditioning factors. Several papers have demonstrated that climate change and sea level have an impact on the frequency of canyon filling turbidity currents through changes in sedimentation rate and availability. Other papers have suggested that these turbidites canyon flushing are temporally random, and not affected by changes in sea level or climate. This study presents one of the most spatially complete records of turbidity current frequency from any submarine canyon system. The data allow the first comparison of recurrence interval distributions recorded in both a submarine canyon and its recipient deep water basin. This chapter aims to:

1. Determine the frequency of turbidity currents within the Nazaré Canyon.
2. Establish whether or not sea level has an effect on on turbidity currents frequency.
3. Determine the frequency of much larger, poorly documented canyon-flushing events that reach the Iberian Abyssal plain.
4. Better understand the processes that might trigger canyon-flushing, and determine any relationship with sea level.

The results indicate that sea level has a significant effect on the recurrent intervals of turbidity currents that fill the Nazaré submarine canyon. In contrast to this, there is no comparable sea level control on the recurrence intervals of large flushing turbidity currents. Turbidity currents that fill and flush submarine canyons appear to have different frequency distributions and relationships to sea level, and thus potentially different triggers.

This chapter has been published in its entirety as: **Allin**, J.R., Hunt, J.E., Talling, P.J., Clare, M.E., Pope, E., Masson, D.G., 2016. Different frequencies and triggers of canyon filling and flushing events in Nazaré Canyon, offshore Portugal. Marine Geology 371, 89-105.

Abstract

Submarine canyons are one of the most important pathways for sediment transport into ocean basins. For this reason, understanding canyon architecture and sedimentary processes has importance for sediment budgets, carbon cycling, and geohazard assessment. Despite increasing knowledge of turbidity current triggers, the down-canyon variability in turbidity current frequency within most canyon systems is not well constrained. New AMS radiocarbon chronologies from canyon sediment cores illustrate significant variability in turbidity current frequency within Nazaré Canyon through time. Generalised linear models and Cox proportional hazards models indicate a strong influence of global sea level on the frequency of turbidity currents within the canyon. Radiocarbon chronologies from basin sediment cores indicate that larger, canyon-flushing turbidity currents reaching the Iberian Abyssal Plain have a significantly longer average recurrence interval than turbidity currents that fill the canyon. The recurrence intervals of these larger canyon-flushing turbidity currents also appear to be unaffected by long-term changes in global sea level. This indicates that the factors triggering, and thus controlling, the frequency of canyon-flushing and canyon-filling events are very different. Canyon-filling appears to be predominantly controlled by sediment instability during sea level lowstand and by storm and nepheloid transport during the present day highstand. Canyon-flushing exhibits time-independent behaviour. This indicates that a temporally random process, or summation of non-random processes that cannot be discerned from a random signal, are triggering canyon flushing events.

3.1 Introduction

Understanding variability in turbidity current frequency and magnitude is important for several reasons. First, turbidity currents are one of the most voluminous sediment transport mechanisms, and they create some of the largest sediment accumulations on our planet (Ingersoll et al., 2003). Second, understanding the frequency and scale of large turbidity currents informs risk assessment for undersea installations that are at risk of damage by turbidity currents, such as oil and gas infrastructure, pipelines, and telecommunications cables (Bruschi et al., 2006; Carter et al., 2012a; Carter et al., 2014).

Submarine canyon systems are recessed topographic features on continental margin slopes that act as conduits for sediment transport into the deep sea (Stow et al., 1985; Normark and Piper, 1991; van Weering et al., 2002). Turbidity currents are the main transport processes within submarine canyon systems, and can be triggered by a wide variety of mechanisms. Potential triggers include storm activity, tidal resuspension, sediment failures (triggered in some cases by earthquakes), and river discharges (Marshall, 1978; Masson et al., 2006; Piper and Normark, 2009; Masson et al., 2011a; Talling et al., 2012; Talling, 2014).

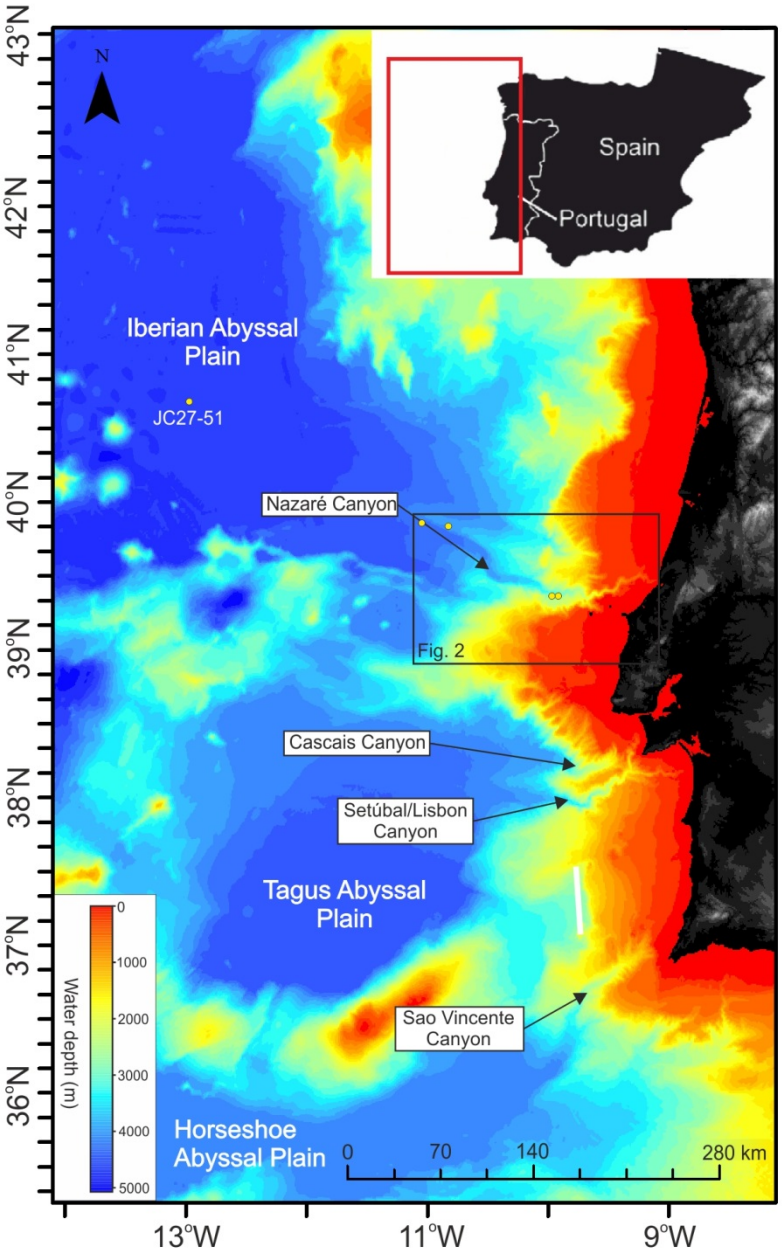

Figure 3.1: Map of the Portuguese Margin, showing the location of the main sedimentary basins and their feeder canyons. Core JC27-51, located in the distal Iberian Abyssal Plain is also shown. Bathymetry data are from the GEBCO database (IOC, IHO, BODC, 2003).

Turbidity currents in submarine canyons are proposed to be one of two broad end-member types: filling and flushing (Parker, 1982; Piper and Savoye, 1993; Canals et al., 2006; Piper and Normark, 2009; Talling et al., 2012). Canyon-filling turbidity currents are hypothesised to slowly deposit sediment within canyons over hundreds or even thousands of years (Paull et al., 2005; Canals et al., 2006; Arzola et al., 2008; Puig, et al., 2014). Canyon-filling turbidity currents are considered to be the result of localised sediment failures, hyperpycnal flows, or storm resuspension (Marshall, 1978; Arzola *et* al., 2008; Khripounoff et al., 2009; Masson et al., 2011a; Talling et al., 2013; Talling, 2014). Canyon-flushing turbidity currents are erosive flows that remobilise and transport large volumes of this canyon-filling sediment out onto canyon-mouth fans or distal basin floors (Parker, 1982; Piper and Savoye, 1993; Xu et al., 2004; Paull et al., 2005; Piper and Normark, 2009; Kriphounoff et al., 2012; Talling et al., 2012; Puig et al., 2014). Canyon-flushing turbidity currents have yet to be directly monitored, and are suggested to operate on much longer timescales than those that fill the canyon (Piper and Savoye, 1993; de Stigter et al., 2007; Arzola et al., 2008; Talling et al., 2013). The causes of canyon-flushing events are not clear, although they likely result from large sediment failures (Normark and Piper, 1991; Masson et al., 2006; Goldfinger et al., 2007; Piper and Normark, 2009; Hunt et al., 2013a; Talling, 2014).

3.1.1 Observations of canyon-filling

Previous work on the Nazaré Canyon has focussed on the factors controlling sedimentation within the upper and middle reaches of the canyon (van Weering et al., 2002; de Stitger et al., 2007; Oliveira et al., 2007; Arzola et al., 2008; Martin et al. 2011). As many as four turbidity currents have been observed in the upper canyon per year (de Stigter et al., 2007; Martin et al., 2011; Masson et al., 2011a). These frequent turbidity currents are typically the result of winter storms that re-suspend canyon sediments, but may also be the result of small intra-canyon failures (de Stigter et al., 2007; Martin et al., 2011; Masson et al., 2011a). Direct monitoring from below 4,000 m water depth indicates that turbidity currents annually reach the lower canyon. However, these flows are

generally dilute, restricted to the incised thalweg, and are not considered to be erosive (de Stigter et al., 2007).

Canyon terraces at 3500 m water depth and 40 m elevation above the thalweg) record multiple thicker (>25cm) turbidites deposited over the last 1,000 years. Turbidites recorded on terraces are interpreted as the result of large flushing events by Arzola et al. (2008) and Masson et al. (2011a). Given the presence of erosive scours within the lower reaches of the canyon, it is possible that these frequent turbidity currents are erosive and flush sediment onto the canyon-mouth fan (Arzola et al., 2008). To date, no deep water (>5000 m) core descriptions have been published from Nazaré Canyon, and so our understanding of the recurrence rates of both canyon-filling and canyon-flushing turbidity currents is limited to the upper and middle canyon, above 4,000 m water depth.

3.1.2 Aims of the study

Recent statistical analyses of long-term (>0.15 Ma) records indicates that large volume turbidites in distal basin plains can have a temporally random distribution, and are not strongly influenced by non-random glacio-eustatic sea level variability (Hunt et al., 2013b; Clare et al., 2014). Other studies suggest that sea level is a dominant control; however, they do not consider a sufficient number of events for statistical analysis (Maslin et al., 2004; Owen et al., 2007; Lee, 2009; Smith et al., 2013). It has also been proposed that climate-driven sea level change can affect the frequency of canyon-filling turbidity currents by influencing slope stability (Vail et al., 1977; Shanmugam and Moiola, 1982; Lebreiro et al., 1997; Piper and Normark, 2001; Lebreiro et al., 2009; Brothers et al., 2013). Therefore, the first aim is to determine whether the frequency of canyon-filling shows a significant correlation with glacio-eustatic sea level change.

This present study is novel because few papers provide a complete overview of the frequency of turbidity currents from the upper to lower reaches of submarine canyons and out into deep water basins. No studies to date have statistically assessed both a basin and canyon record from a single system to test for any overarching control on the recurrences of canyon-filling and canyon-flushing. Therefore, this work also aims to assess whether or not canyon-flushing events have similar recurrence intervals to canyon filling events, and whether their recurrence intervals have similar

statistical distributions. This will help determine whether they are likely to have similar (or different) triggers (Urlaub et al., 2013; Clare et al., 2014; 2015).

3.2 Regional Setting

The study area is located on the Western Iberian Margin between 36^{o} and 43^{o} N (Fig. 3.1). The shelf and continental slope is incised by several large submarine canyons, including the Setúbal-Lisbon, Cascais, Sao Vincente and Nazaré canyons. These canyons feed into 3 deep sedimentary basins; the Iberian, Tagus and Horseshoe Abyssal Plains (Fig. 3.1).

3.2.1 Nazaré Canyon

Nazaré Canyon occurs in the central-west Iberian Margin, and extends from ~1 km offshore from the coastline and into the Iberian Abyssal Plain (Fig. 3.1). The canyon incision into the continental shelf and slope coincides with the presence of the Nazaré Fault, which runs ENE-WSW and extends across the margin. The Nazaré Canyon system is not directly fed by major rivers, as is the case with the Setúbal and Cascais Canyons to the south. Instead, Nazaré Canyon is fed largely by littoral drift sediment from smaller river systems to the north, and nepheloid transport of material to deeper sections of the canyon (van Weering et al., 2002; Oliveira et al., 2007; de Stigter et al., 2007).

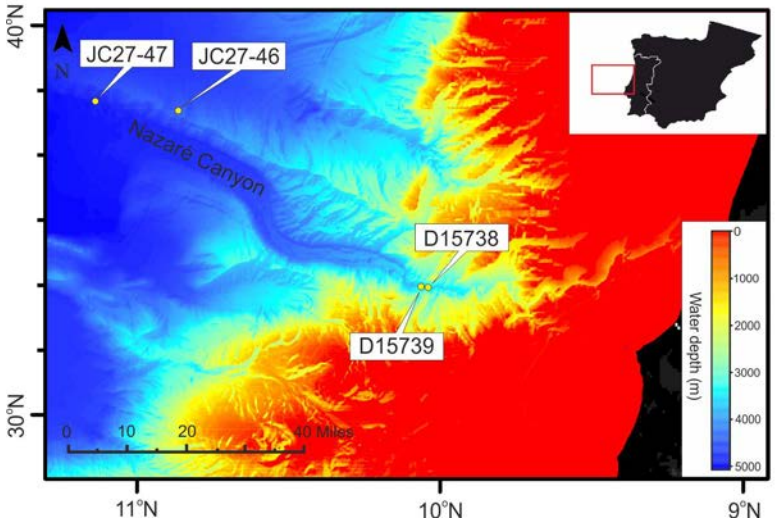

Figure 3.2: Location map of the Nazaré Canyon and the locations of canyon cores used in this Chapter.

The canyon itself can be divided into three sections; the upper section that extends from the canyon head to 2,000 m water depth; the middle section that spans between 2,000 and 4,000 m; and the lower section that lies below 4,000 m (Figs. 3.1 and 3.2) (Vanney and Mougenot, 1990; van Weering et al., 2002). The upper and middle sections have a steep v-shaped profile and are incised deeply into the continental shelf (200 - 2,500 m water depth), with a channel thalweg that is <100 m wide. Below 4,000 m water depth the canyon broadens to a width of 8 – 10 km and is markedly less incised into the substrate. Below 4,500 m water depth the canyon is less incised, and large levee structures have developed to the north and south of the canyon axis. These levees are between 100 and 200 m in height and taper distally into the Iberian Abyssal Plain, where they terminate at 5,300 m water depth (Arzola et al., 2008; Lastras et al., 2009).

3.2.2 Iberian Abyssal Plain

The Iberian Abyssal Plain is located 200 km off the western coast of Portugal between 40^{o} N and 43^{o} N and extends approximately 700 km to the northwest. The abyssal plain has an average water depth of ~5,300 m but can be as deep as 5,400 m. The basin is bounded by the Galicia Bank to the northeast, the Estremadura Spur to the south, and by a series of seamounts along its western margin. The total area of the basin covers approximately 107,000 km^{2}. Previous work from ODP leg 149 has detailed the long-term basin infill record extending back to the Lower Cretaceous (140 Ma) (Milkert et al., 1996a; 1996b). This work demonstrated an onset of, terrestrial-derived turbidite deposition in the Iberian Abyssal Plain between 2.2 and 2.6 Ma, which continued into the late Pleistocene. Despite the extensive record from ODP drilling legs in the Iberian Abyssal Plain, very little of the recent (<100 ka) sedimentary architecture has been evaluated in detail. As a result, little is currently known about the frequency of large volume turbidity currents in the basin through the late Pleistocene.

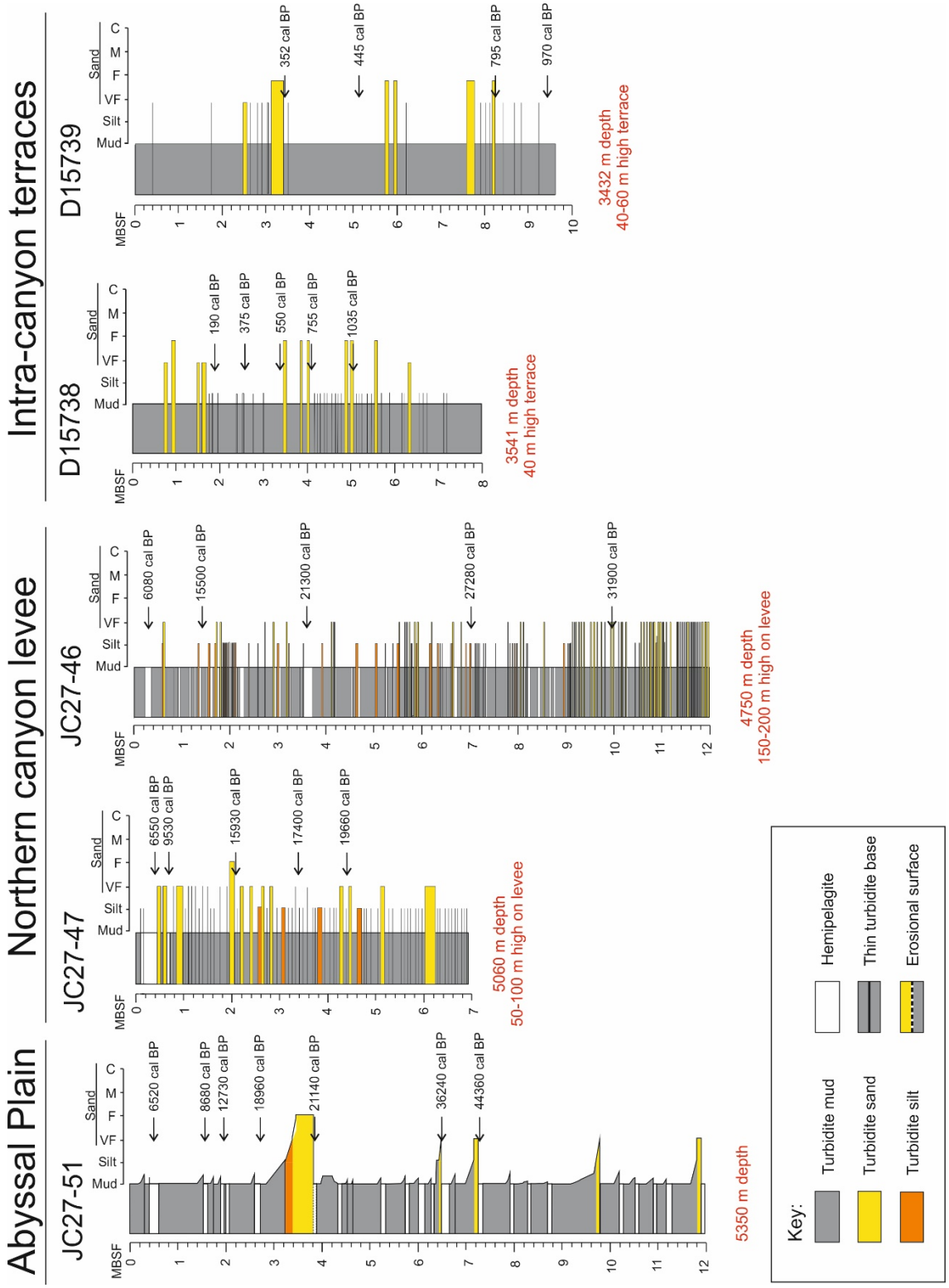

Figure 3.3: Lithological description of the cores used in this chapter. Dark grey represents turbidite mud, orange represent silt and yellow represents sand. Radiocarbon dates and their core positions are indicated with black arrows.

3.3 Methods

3.3.1 Piston coring

The cores used in this study have been collected during two different scientific campaigns. Piston cores JC27-51, JC27-47 and JC27-46 come from the abyssal plain and levee sections, and were recovered during cruise JC027 (Wynn et al., 2009). Core JC27-51 was retrieved from the Iberian Abyssal Plain, and cores JC27-46 and JC27-47 were retrieved from the northern external and internal levees respectively (Fig. 3.3). The piston cores from the middle section of Nazaré Canyon were retrieved during cruise CD157 (Weaver et al., 2004). Cores were sited using bathymetric and geophysical data. Cores D15738 and D15739 were both collected from terraces 40 - 60 m above the canyon axis and have existing radiocarbon dates (Figs. 3.2 and 3.3). There are no sediment cores from the upper canyon above 2,000 m water depth from which AMS radiocarbon ages could be determined. The coarse-grained nature of the sediment in the upper canyon, the rapid rate of accumulation, and the tidally-driven re-working of material prevent any long-term record of turbidity currents being obtained through piston or gravity coring techniques (de Stigter et al., 2007).

3.3.2 Identification of turbidites and hemipelagite

In order to develop age models and determine recurrence intervals for turbidity currents, differentiating their deposits from background hemipelagic sediment is vital. Hemipelagic sediments typically contain randomly dispersed foraminifera giving a pitted surface texture. They also lack primary sedimentary structures and are often bioturbated (Stow and Piper, 1984). In contrast, turbidity current deposits are often well sorted, have normal grading, and have observable internal structure. The fine-grained mud cap of turbidity currents is commonly homogenous and often devoid of foraminiferal material, while the basal contact of turbidites is often sharp and sometimes erosional (Bouma, 1962: Stow and Piper, 1984).

3.3.3 Age model development

Age control for this study is provided by AMS radiocarbon dating. AMS radiocarbon dates were obtained for cores JC27-51, JC27-47 and JC27-46 in order to develop age models and calculate turbidity current recurrence intervals. Nine AMS radiocarbon dates were previously determined for terrace cores D15738 and D15739 (Masson et al., 2010) (Table 1). Samples were taken from hemipelagic mud units, with care being taken to avoid sampling any turbidite mud or coarse turbidite bases. In cores JC27-51, JC27-47 and JC27-46, 2 - 10 cm^3 of sediment was sampled to pick the 8 - 10 mg of foraminifera required for accurate AMS 14C dates. No one foraminiferal species was abundant enough to collect monospecific samples in all cases, so most samples consist of mixed species assemblages. The dominant species were *Orbulina universa, Globigerina bulloides, Neogloboquadrina pachyderma, Globorotalia truncatulinoides, Globigerinoides ruber* and *Globorotalia hirsute*. Where monospecific samples were possible, *Orbulina universa* was selected. The conventional radiocarbon ages returned from analysis were converted to calibrated ages (Cal years BP) using the MARINE13 database (Reimer et al., 2013) (Table 1).

Lab code	Core #	Core depth (cm)	Conventional age (BP)	Max. probabilty (Cal BP)	1σ Cal age ranges (Cal BP)	2σ Cal age ranges (Cal BP)	Source
BETA-385402	JC27-46	32-33	5,940 ± 30	6,078	5,995-6,165	5,918-6,233	This study
BETA_385403	JC27-46	158-159	13,639 ± 50	15,494	15,334-15,629	15,234-15,768	This study
BETA_385404	JC27-46	349-350	18,290 ± 60	21,303	21,143-21,465	20,994-21,599	This study
BETA_385405	JC27-46	701-702	23,600 ± 100	27,280	27,163-27,406	27,020-27,514	This study
BETA_385406	JC27-46	996-997	28,790 ± 140	31,750	31,568-32,146	31,449-32,521	This study
SUERC-31798	JC27-47	53-54	6,120 ± 35	6,270	6,197-6,341	6,117-6,422	This study
BETA-401321	JC27-47	70.5-71.5	8,510 ± 30	8,760	8,652-8,889	8,584-8,972	This study
SUERC-31799	JC27-47	212-214	13,530 ± 47	15,300	15,201-15,479	15,117-15,638	This study
BETA-401322	JC27-47	340-341.5	14,910 ± 50	14,700	17,211-17,469	17,089-17,576	This study
SUERC-31802	JC27-47	445-448	16,910 ± 55	19,580	19,484-19,725	19,360-19,894	This study
	JC27-51	48.5-49.5	6,355 ± 37	6,520	6,433-6,604	6,342-6,680	This study
BETA-382057	JC27-51	155-156	8,470 ± 30	8,680	8,604-8,769	8,567-8,893	This study
	JC27-51	196.5-197.5	11,535 ± 39	12,730	12,661-12,810	12,613-12,904	This study
	JC27-51	264-265	16,415 ± 53	18,960	18,883-19,083	18,808-19,206	This study
	JC27-51	381-382	18,196 ± 62	21,140	21,019-21,322	20,886-21,469	This study
BETA-382053	JC27-51	649-650	33,010 ± 200	36,240	36,000-36,454	35,722-36,719	This study
BETA-382054	JC27-51	726-727	41,500 ± 550	44,360	43,825-44,875	43,310-45,314	This study
SUERC-18143	D15738	178.5	573 ± 37	190		90-290	Masson et al, 2011a
SUERC_18146	D15738	250.5	738 ± 37	375		290-460	Masson et al, 2011a
SUERC_18147	D15738	335	934 ± 37	550		480-620	Masson et al, 2011a
SUERC_18148	D15738	405	1,204 ± 37	755		660-850	Masson et al, 2011a
SUERC_18149	D15738	509.5	1,482 ± 35	1,035		940-1,130	Masson et al, 2011a
SUERC-18150	D15739	334.5	703 ± 37	352		270-435	Masson et al, 2011a
SUERC-18151	D15739	489.5	821 ± 37	445		370-520	Masson et al, 2011a
SUERC-18153	D15739	829.5	1,245 ± 37	795		700-890	Masson et al, 2011a
SUERC-18156	D15739	959.5	1,411 ± 37	970		890-1,050	Masson et al, 2011a

Table 3.1: List of radiocarbon samples used in this study. Note: cal BP ages from D15738 and D15739 (Masson et al., 2011a) are median values, and not determined using maximum probability.

In order to account for local reservoir offsets, an average of five reservoir correction (ΔR) values was used from nearby locations. These ΔR values are from samples collected along the Iberian shelf; the main pathway for ocean currents and sediment transport to the head of Nazaré Canyon (Monges Soares, 1993; van Weering et al., 2002; Oliveira et al., 2007; de Stigter et al., 2007). This yields a ΔR correction value of +267 years, which is consistent with reconstructed past reservoir offsets along the Iberian Margin (Bronk Ramsey et al., 2012).

Using the radiocarbon ages, and the thicknesses of hemipelagic sediment between them, sedimentation rates were calculated. The thicknesses of hemipelagic sediment were then divided by the sedimentation rates to convert them into time intervals (Wynn et al., 2002; Grácia et al., 2010; Clare et al., 2014). From these time intervals the ages of individual turbidites can be estimated

(Table 2). This method relies on the assumption that there is minimal fluctuation in the rate of hemipelagic sediment accumulation through time (Lebreiro et al., 2009; Grácia *et al*, 2010; Clare et al., 2015). It also relies on the assumption that subsequent turbidity currents are not significantly erosive (Weaver and Thomson, 1993; Thomson and Weaver, 1994; Weaver, 1994; Wynn et al., 2002; Gutiérrez-Pastor et al., 2009; Grácia et al., 2010).

Turbidite no	Turbidite base depth (cm)	Turbidite thickness (cm)	Approx age (cal BP)	Recurrence interval (years)
1	25	25	4,850	0
2	45	20	4,850	4,430
3	155	103	8,680	1,700
4	172	13	10,300	0
5	187	15	10,300	1,200
6	194	4	11,505	3,200
7	254	53	14,700	5,550
8	378	110	20,250	1,350
9	428	46	21,600	1,500
10	454	22	23,100	0
11	468	14	23,100	0
12	503	35	23,100	1,600
13	523	16	24,700	2,550
14	570	40.5	27,250	1,950
15	597	24	29,200	4,300
16	618	10	33,500	1,200
17	645	24	34,700	9,000
18	671	12.5	43,700	0
19	725	54	43,700	3,600
20	790.5	57.5	47,300	5,850
21	837	36	53,150	1,250
22	870	30.5	54,400	8,800
23	978	102	63,200	3,350
24	1016	38	66,550	3,350
25	1050	26	69,900	6,300
26	1091	36	76,200	2,500
27	1119	20	78,700	3,350
28	1187	60	82,050	

Table 3.2: Core JC27-51 turbidites, their projected ages, and recurrence interval determined using a linear age model.

3.3.4 Calculation of turbidite recurrence intervals and frequency

Using the age model to estimate the emplacement age of each turbidite allows for the calculation of individual recurrence intervals. Here the recurrence interval of a turbidite is defined as the length of time since the turbidite that preceded it (Clare et al., 2014; 2015; Pope et al., 2015). Where hemipelagic age models cannot be constructed, recurrence interval was calculated by dividing the length of time by the number of turbidites to get an 'average recurrence interval'. The determination of recurrence intervals requires that individual turbidites be distinguished from

multiple upward-fining units deposited during the same turbidity current. These multiples of upward-fining sediment can result from differential sorting due to changing bed-shear stresses, or from multi-staged failures (Piper and Bowen, 1978; Stow and Shanmugam, 1980; Hunt et al., 2013a). Interpreting multiple upward-fining units within a single turbidite as multiple individual turbidites has the potential to bias any analysis by the incorrect counting of turbidites; and hence, incorrectly estimating their recurrence intervals (Lebreiro et al., 2009).

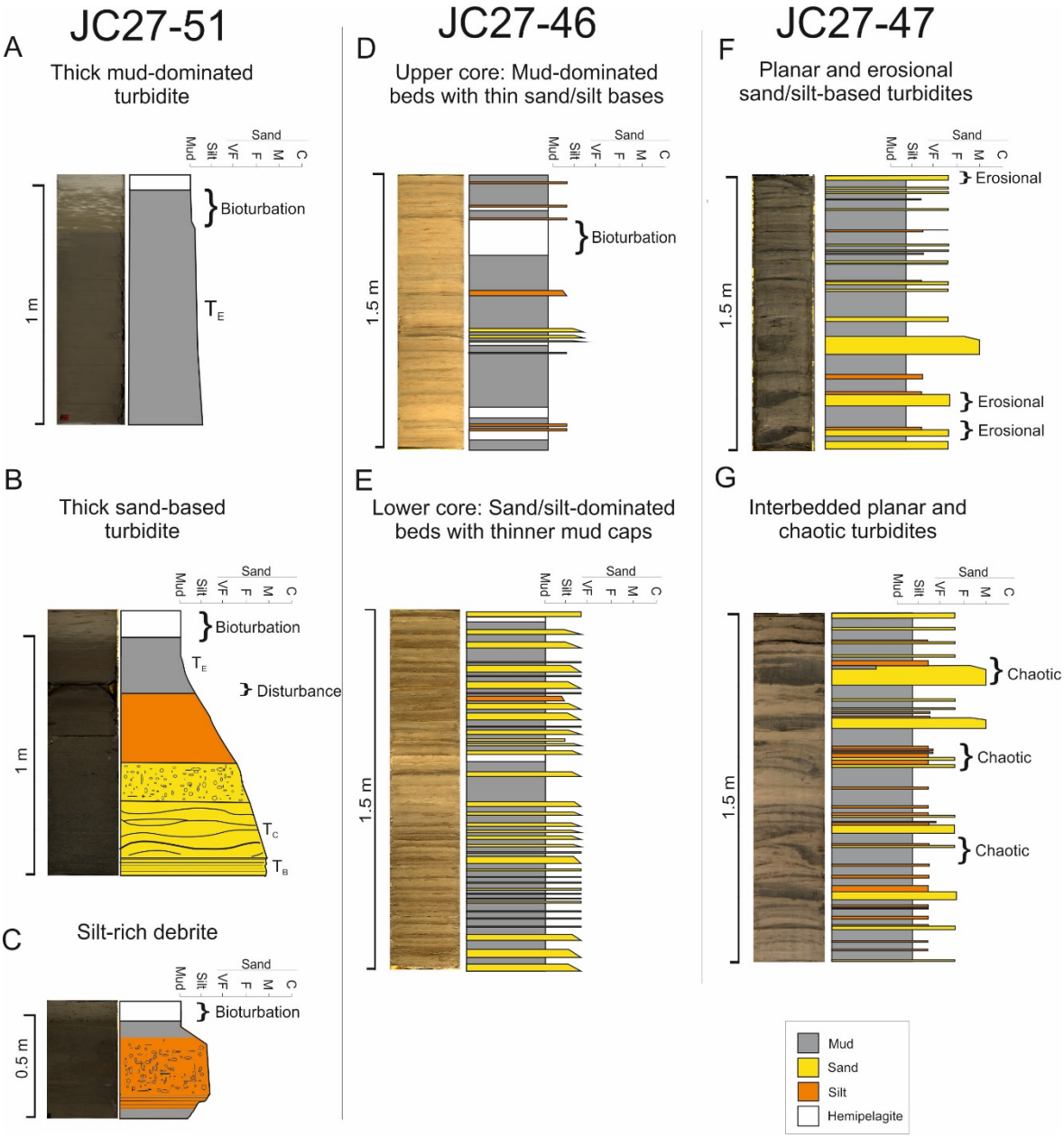

Figure 3.4: Bed types present in JC27 sediment cores. JC27-51: (A) Thick mud-dominated turbidites wich bioturbated mud caps, (B) thick sand rich turbidites with discernible Bouma (T) divisions , and (C) a debrite with mud and silt clasts. JC27-46: (D) The upper 6 m of the core is composed of thin sand or silt-based turbidite with a dominant mud unit and hemipelagic sediment intervals. (E) The lower 6m is mainly composed of thin-bedded sand rich turbidites with a thinner

mud cap and sparse hemipelgic sediment. JC27-47: Turbidites are typically (F) planar and often erosive, or (G) chaotically structured, with reverse grading, overturned layers and evidence of scouring.

3.3.5 Statistical analysis of turbidite recurrence and frequency

Statistical analysis can be a powerful tool for the analysis of time series data, such as turbidite recurrence (e.g. Hunt et al., 2014; Moernaut et al., 2015; Ratzov et al., 2015); however, it is important to understand how recurrence is measured before specific tests are selected. Recurrence is here inferred from intervals of hemipelagic fallout between turbidity currents, and the average accumulation rate of hemipelagic mud between dated horizons. This method is most appropriate in distal basin settings such as basin core JC27-51, where past work has shown there is little or no erosion by successive turbidity current, and the hemipelagic mud is not removed (Weaver and Thomson, 1993; Thomson and Weaver, 1994; Weaver, 1994; Wynn et al., 2002; Gutiérrez-Pastor et al., 2009; Grácia et al., 2010; Clare et al., 2014). In more proximal, slope and confined settings, the effects of erosion may be greater, but it is difficult to discern this from core samples due to their relatively narrow diameter (typically 10 cm). The recurrence data is therefore binned at the more proximal levee core site JC27-46, by counting the number of turbidites within prescribed time intervals to account for this uncertainty in the precise measurement of individual recurrence intervals. As bin dimensions can potentially affect the statistical outcome (Urlaub et al., 2013; Pope et al., 2015) three different bin widths (250, 500 and 1000 years) are considered in our analysis. The influence of sea level on binned turbidite recurrence is investigated at levee site JC27-46, where sufficient turbidites were sampled (N = 201) to permit regression and survival analysis. In addition to different data bin sizes, three different sea level curves are used as the explanatory variable. The sea level reconstructions of Lambeck et al. (2014), Rohling et al. (2010), and Peltier and Fairbanks (2006) are widely used and have suitable resolution over the late Pleistocene. Less sophisticated frequency analysis is used for individual turbidite recurrence intervals at basin site JC27-51, as fewer turbidites were sampled (N = 26) thus limiting the power of statistical tests (Pope et al., 2015).

3.3.5.1 Assessing the significance of sea level on turbidite recurrence at JC27-46

Two different statistical analyses were used to investigate the significance of sea level in relation to turbidite recurrence at JC27-46. The first is a parametric Generalised Linear Model, which tests for the significance of sea level as an explanatory variable on the recurrence of turbidites (McCullagh and Nelder, 1989; Clare et al., 2016). As it is a parametric test, the Generalised Linear Model requires *a priori* definition of the distribution form of the relationship between the two variables. We apply variants of the model using Gamma, Gaussian and Poisson distribution forms, and assess the most appropriate model using quantile-quantile (Q-Q) plots. While Q-Q plots do not provide a quantitative measure of the goodness-of-fit, they can be qualitatively interpreted to understand how much a given data set deviates from the specified distribution (Salkind and Rasmussen, 2007).

General rules of thumb exist for determining the minimum sample size for regression analysis. Tabachnick and Fidell (2007) indicate that testing for the effect of one individual variable will require N = 106 events. Green (1991) performed a more detailed analysis, which incorporated an assessment of statistical power and effect size, suggesting that at least N = 23 is required to detect large effects and N = 53 for detecting medium effects of one explanatory variable. We also apply a non-parametric Cox Proportional Hazards (PH) Model (Cox, 1972) as a comparative test because it requires no *a priori* specification of frequency distribution form. The Cox PH model is typically used to determine a hazard rate in medical studies (e.g. rate of patient fatality) but has also been applied to turbidite frequency analysis (Hunt et al., 2014; Clare et al., 2015). The hazard rate is the ratio between the change in the explanatory variable (e.g. sea level) and the response variable – in this case turbidite recurrence. Previous work has shown that the Cox PH model requires at least a minimum sample size of N = 20 (Vittinghoff and McCuloch, 2007). The Cox PH model performs survival analysis and three separate tests (likelihood, Wald and log-rank), for which a p-value is derived. For both Generalised linear and Cox PH models, where the resultant p-value is small (<0.05) sea level is found to be a significant variable to explain turbidite recurrence. Where the p-value is large ($p > 0.05$), sea level cannot be implicated as a statistically significant control on turbidite recurrence. Levee core site JC27-46 features N = 201 turbidites, which is well above the minimum sample size threshold for both regression and survival analysis. Distal basin core JC27-

51 only features N = 28 turbidites, which is close to the minimum sample size limit, and therefore would yield only low statistical power. Therefore, only the frequency distribution form of turbidite recurrence at JC27-51 is analysed to provide insights into triggering and possible controls, instead of performing more sophisticated survival or regression analysis.

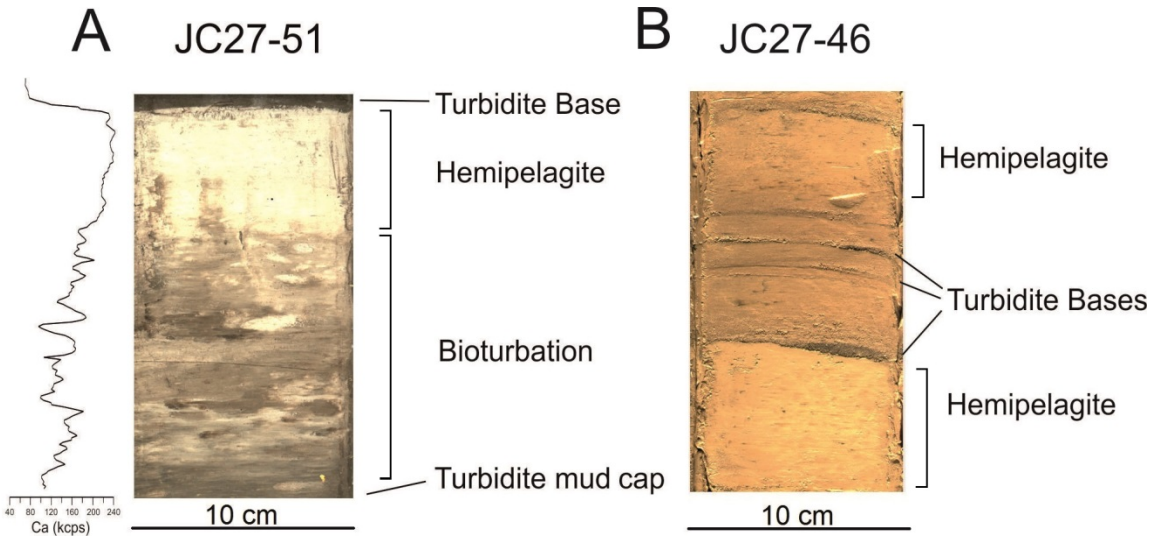

Figure 3.5: Hemipelagic material and turbidites present within cores JC27-51 and JC27-46. ITRAX Calcium records assist in defining the boundaries between pure hemipelagite and bioturbated turbidite mud cap in JC27-51. There are no ITRAX data for JC27-46, but hemipelagite can still be defined by the presence of a colour change and dark mottling.

3.3.5.2 What is the frequency distribution form of turbidite recurrence at JC27-51?

A Poisson distribution implies time-independence and a lack of memory in a system (Parzen, 1962). Thus, recurrence intervals that fit a Poisson (exponential) distribution form can be viewed as occurring randomly in time, with no dependence on when the previous event occurred, or when the next will happen. This memoryless, time-independent behaviour is in contrast to non-random processes such as sea level change. Therefore, where recurrence intervals conform to a Poisson distribution, non-random processes cannot be directly attributed to a singular or dominant control on recurrence (Urlaub et al., 2013; Clare et al., 2014). In contrast, time-dependent distributions may indicate that a single process (e.g. Normal) or series of processes (e.g. log-normal) are exerting significant control on a system (van Rooij et al., 2013; Clare et al., 2016). Therefore, frequency distribution form of turbidite recurrence intervals at JC27-51 was determined to provide some insights into possible triggering and controlling mechanisms for canyon flushing events. This work

also aims to determine whether the frequency distribution form of turbidite recurrence in the abyssal plain is distinctly different to that observed at the more proximal levee location.

Here parametric and non-parametric goodness-of-fit methods were employed to test recurrence interval distribution. The Anderson-Darling test is a parametric test that gives the probabilities that the data come from different populations with specific distributions, including Poisson, normal, log-normal and Weibull (Stephens, 1974). To further test the distribution of canyon flushing events, non-parametric (Mann-Whitney and Kolmogorov-Smirnov) tests were used to determine if the frequency distribution form of Iberian Basin turbidite recurrence is significantly different to that of other distal abyssal plains. For this the published datasets of Clare et al. (2014 and 2015) were considered, which demonstrates that multiple basin turbidite records conform to a Poisson distribution. The Mann-Whitney test is based on the null hypothesis that the datasets are sampled from populations with identical distributions (Lehmann and D'Abrera, 2006). The Kolmogorov-Smirnov test compares the cumulative distributions of two data sets and poses the null hypothesis that they were randomly sampled from populations with identical frequency distributions (Lehmann and D'Abrera, 2006). The result gives the probability that the two cumulative frequency distributions would be as far apart as observed in our data. These three tests were used to provide confidence in the results.

3.4 Results

3.4.1 Core sedimentary characteristics

Core JC27-51 shows a depositional sequence comprised of pale grey mud units with abundant foraminifera interbedded with well sorted and normally-graded sedimentary units (Fig. 3.3). The graded units are often greater than 50 cm thick and many are mud-dominated (Fig. 3.4A). Some of these mud-dominated deposits exhibit thin silt or fine sand bases. Three deposits within the core have sandy bases, with one of these (core depth 320 - 390 cm) having a much thicker medium- to coarse-grained sand base with planar and ripple laminations (Fig. 3.4B). We interpret these graded units as turbidite deposits after Bouma (1962), and Stow and Piper (1984). A silt unit with interspersed mud clasts occurs at 395 - 420 cm depth in the core, and has a subtle reverse-to-

normally graded sequence (Fig. 3.4C), which we interpret as a debrite, in the sense of Naylor (1980).

The pale sediment in core JC27-51 exhibits different colour, grain size, and lightness characteristics than turbidite deposits (Fig. 3.5A). Unlike the more homogenous olive-green turbidites, the pale grey sediment is noticeably rich in foraminiferal sand and exhibits bioturbation structures. This foraminiferal sand gives the sediment a pitted surface texture. From the photospectrometer data the pale grey sediment in JC27-51 exhibits an L* value typically within a range of 50 - 65, while turbidites are typically within 35 - 50. From the ITRAX XRF Calcium counts (kcps) data, the pale grey sediment typically exhibits values greater than 160 kcps (Fig. 3.5A). In contrast, turbidite deposits have values ranging from 40 to 120 kcps. These differences in the geochemical and geophysical properties are likely due to the high amounts of calcareous foraminiferal shells within the sediment. We interpret this pale grey sediment as background hemipelagic accumulation, after Stow and Piper (1984) and Hoogakker et al. (2004). Typically, the boundaries between the upper turbidite mud cap and the following hemipelagic sediment are gradational (Fig. 3.5A). This is due largely to bioturbation, but also likely due to the slow settling of turbidite mud suspension clouds and incorporation of carbonate material from background hemipelagic sediment. The boundaries between the bases of the turbidite deposits are flat and sharp (Fig. 3.5A; Appendix A).

Core JC27-46 consists largely of interbedded silt and fine sand units that are normally graded and typically have thin mud caps (Fig 3.4; Appendix A). These graded deposits can be broadly classified into two different types. Type 1 deposits are normally graded, with 1 - 4 cm thick silt or fine sand bases, and thicker 10 - 20 cm upper mud units. Type 2 deposits are thinly-bedded and have 0.5 - 4 cm thick, faintly gradational fine- to medium-grained sand bases. The thin sand bases typically grade sharply into a thin (0.5 - 3 cm) fine-grained mud (Fig. 3.4D and E). Type 1 deposits are dominant in the upper 6 m of the core, while type 2 are dominant in the lower 4 m. We interpret these deposits to be the result of turbidity currents in the sense of Stow and Shanmugam (1980). Within the core there are lighter, pale grey units that are rich in foraminiferal sand, have a pitted

surface, and show evidence of bioturbation. Based on the similarity with hemipelagic deposits from core JC27-51 we also interpret these to have a hemipelagic origin.

Core JC27-47 is dominated by thicker sand-rich, normally-graded deposits with medium- to coarse-grained sand bases (Fig. 3.4F and G). Sand units vary between 0.5 and 20 cm thick and grade sharply into fine-grained mud. Several of these deposits have clear erosional bases, with several units presenting a chaotic texture and uneven or folded bedding (Fig. 3.4G). We interpret deposits with normal grading and erosional bases to be turbidites (Fig. 3.4F). Deposits with folded bedding or chaotic texture are interpreted to be the result of small-scale slumping or debris flows after Shanmugam et al. (1995). The upper 60 cm of the core contains of the same pale grey, bioturbated and foraminiferal-rich sediment present in cores JC27-46 and JC27-51. As with the two previous cores, we interpret this to be hemipelagic sediment. Hemipelagic sediment is not present below 60 cm depth in the core, possibly due to erosion from subsequent turbidites over-spilling the internal canyon levee (Fig. 3.3; Appendix A).

Middle canyon cores are located on terraces at 40 - 60 m elevation above the canyon thalweg (Fig. 3.3). Cores D15738 and D15739 are composed largely of clay with interspersed faintly-graded fine sand or silt beds (Fig. 3.3). These are interpreted by Arzola et al. (2008) as turbidite deposits resulting from turbidity currents that overspill onto canyon terraces. Basal contacts between the sand and the underlying mud are typically erosional, and previous work indicates there is no discernible hemipelagic material between turbidite units due to the high level of shelf-derived terrigenous material transported in nepheloid layers to deeper in the canyon (de Stigter et al., 2007; Arzola et al., 2008).

3.4.2 Age model and sedimentation rate

Seven AMS radiocarbon dates were collected from JC27-51, five from JC27-46 and five from JC27-47 (Fig. 3.3). Using these dates and the known thickness of hemipelagic sedimentation, age models place the base of core JC27-51 at ca 83,000 Cal years BP and the base of core JC27-46 at ca 33,500 Cal years BP (Fig. 3.6). Linear regressions on the age models yielded R^2 values of 0.9934 and 0.9975 in cores JC27-51 and JC27-46 respectively (Fig. 3.6). These values give us a high level

of certainty in a stable hemipelagic sedimentation rate over long periods at both core sites (Swan and Sandilands, 1995). Average hemipelagic sedimentation rates for cores JC27-51 and JC27-46 are 2.3 and 7.8 cm/ka respectively (Fig. 3.6).

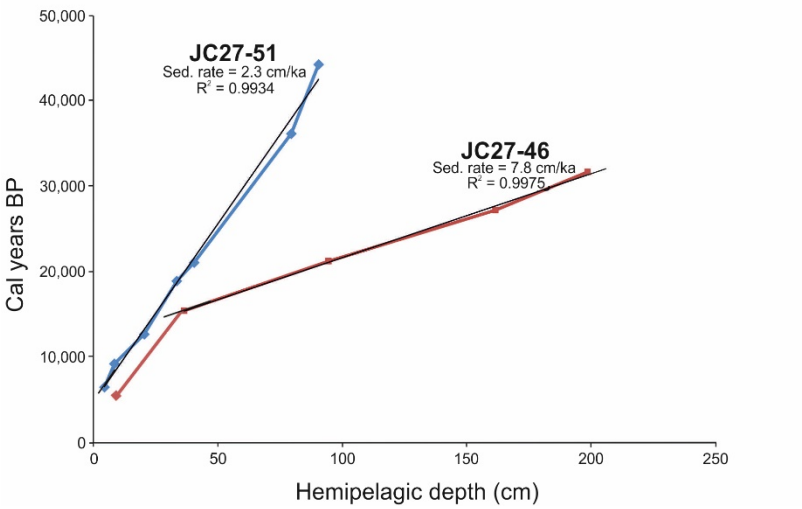

Figure 3.6: Hemipelagic age models for cores JC27-51 and JC27-46. R^2 values indicate minimal deviation from the line and thus a relatively stable hemipelagic sedimentation rate in both cores. This serves as a reasonable basis for using a stable sedimentation rate to interpolate between radiocarbon dates and further back in the record beyond radiocarbon age.

Individual turbidite ages derived from the two age models can be seen in Table 3.2, and in Appendix B. Due to the presence of multiple erosive sandy turbidites in core JC27-47, hemipelagic material is only discernible in the upper 60 cm (Fig. 3.3). Below 60 cm core depth, hemipelagic sediment is sparse and indistinguishable from fine-grained turbidite deposits. Similarly in cores D15738 and D15739, hemipelagic deposits contain a high percentage of terrigenous mud with sparse foraminifera, and are therefore indistinguishable from turbidite muds (Arzola et al., 2008; Masson et al., 2011a). AMS radiocarbon dates from cores JC27-47, D15738 and D15739 originate from foraminifera collected out of bulk sediment samples. Because of the uncertainty in correctly defining hemipelagic thicknesses, recurrence intervals for each deposit cannot be calculated using a hemipelagic age model. Instead, an average turbidity current recurrence interval is calculated by dividing the number of turbidites by the time between radiocarbon dates (Fig. 3.3).

3.4.3 Regular filling events in the middle canyon

Previously collected AMS radiocarbon ages from middle canyon terrace cores place the bases of cores D15738 and D15739 at ca 1,500 BP and ca 1,000 BP respectively. Core D15738 contains 25 identifiable sandy turbidite bases above the oldest AMS radiocarbon date, while core D15739 has 21 turbidites above the oldest radiocarbon date (Fig. 3.3). By dividing the time interval by the number of turbidites we are able to calculate an average recurrence for turbidites. This gives us give an average turbidity current recurrence of 43 years on terraces that are 40 - 60 m above the canyon floor.

3.4.4 Sea level control on canyon-filling in JC27-46

For visual comparison of sea level and turbidite frequency, we use the 500 year binned turbidite data from core JC27-46 (Fig. 3.7A). This 500 year interval is considered to be an appropriate resolution for the length of the record (Lebreiro et al., 2009). Turbidite frequency in core JC27-46 on the external levee crest is highly variable during the sea level lowstand from 33.5 to 23.5 ka; the 10,000 year period prior to North Atlantic warming and associated sea level rise (Clark et al., 2004; Carlson and Windsor, 2012) (Fig. 3.7A). From the modelled ages for turbidites, an average of the estimated recurrence intervals during lowstand conditions is 68 years, lower than at any point during the 33,500 year record.

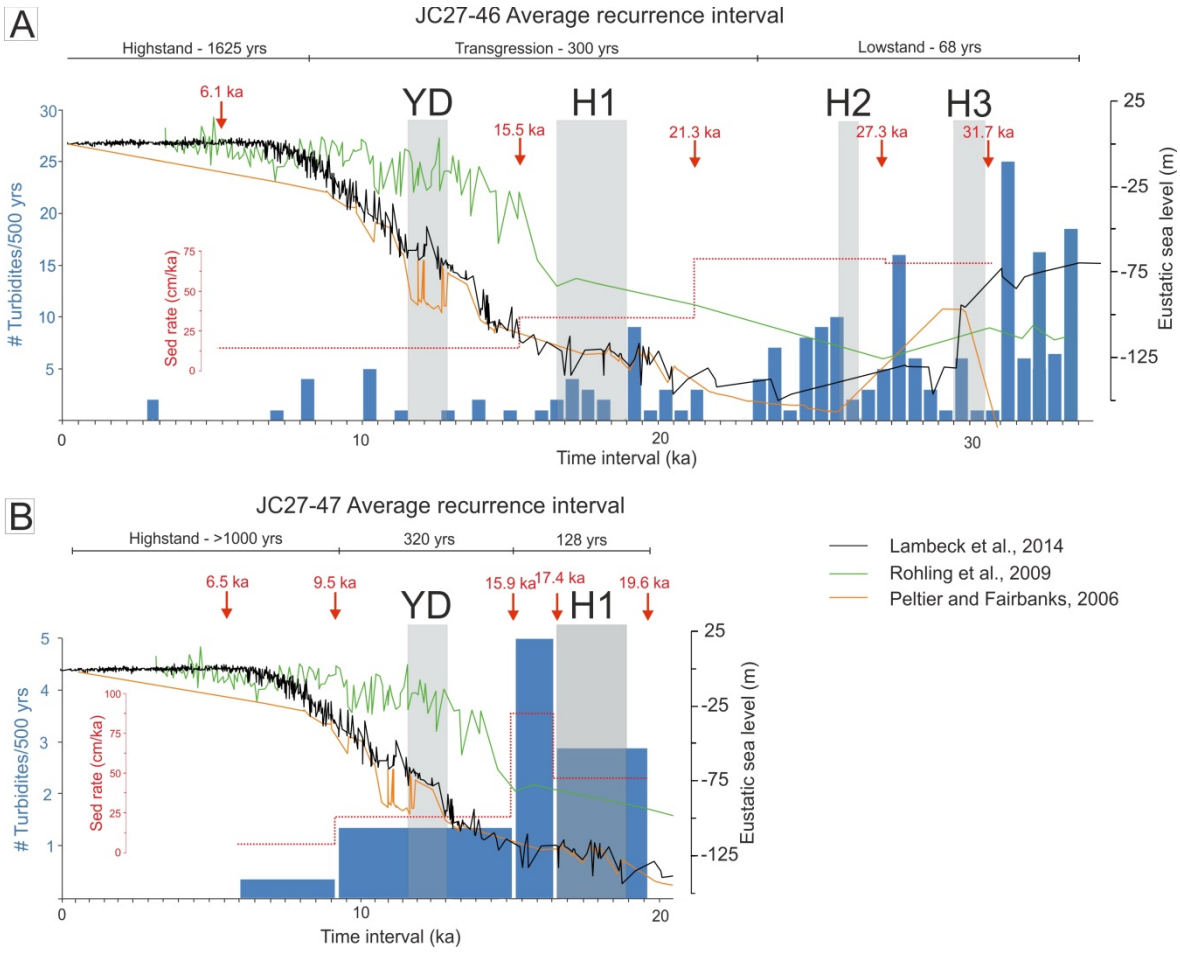

Figure 3.7: A: Frequency of turbidites contained within core external levee JC27-46. Turbidites are binned into 500 year intervals and plotted against global eustatic sea level curves. Trend suggests near shutdown of large canyon-filling turbidites recorded in the levee following the onset of sea level highstand at 7 ka. B: Frequency of turbidites from internal levee core JC27-47. It illustrates a similar pattern of decline through sea level transgression and into the present-day highstand. H1-3 = Heinrich events. YD = Younger Dryas.

Turbidite frequency decreased to 0 – 3 events per 500 years during the period from 23 and 19.5 ka, the onset of sea level transgression (Fig. 3.7A). This initial decline of turbidite frequency starting at 23 ka occurred considerably before the rapid global eustatic sea level rise at 20 ka (Chappelle, 2002; Peltier and Fairbanks, 2006; Clark et al., 2009; Rohling et al., 2009; Lambeck et al., 2014). Following the onset of rapid sea level rise at 17 - 19 ka (Clark et al., 2004; 2009), there is an increase in frequency (4 turbidites/500 years) that lasts until 15.5 ka. Turbidite frequency decreased significantly after 15 ka towards the Younger Dryas. An average of recurrence intervals for the global sea level transgression is 300 years. Following the onset of the present-day sea level highstand at ~7 ka there is an average of recurrence intervals of 1625 years (Fig. 3.7A).

A similar pattern of increasing recurrence intervals through the period of deglaciation can be seen in JC27-47 (Fig. 3.7B). The recurrence interval values for turbidites are also broadly comparable to those recorded in JC27-46 on the external levee for the same time period. In JC27-47, recurrence intervals are approximately 120 years at the beginning of sea level transgression at 20 ka. During the end of the sea level transgression the average recurrence interval increases to 320 years, similar to the 300 year recurrence rate found in JC27-46 (Fig. 3.7A and B). As in core JC27-46, following the onset of the present-day highstand at 7 ka, recurrence intervals have increased to >1000 years (Fig. 3.7B).

The results of generalised linear models indicate that sea level is a significant explanatory variable ($p<0.05$; Appendix C) in relation to the frequency of late Pleistocene canyon-filling turbidity currents at JC27-46. As observed visually, periods of lowered sea level correspond to more frequent turbidity currents. This correlation holds for individual and binned (250, 500 and 1000 year) recurrence intervals, against all of the sea level curves that are considered by this study (i.e. Rohling et al., 2010; Peltier and Fairbanks, 2006; Lambeck et al., 2014; Appendix C). A Gaussian distribution appears to best parameterise the relationship. Cox Proportional Hazard Models also indicate a significant influence of sea level on the turbidite recurrence for all but two model runs; a significant relationship was not observed when the Lambeck et al. (2014) sea level curve is analysed against 250 year-bins and individual turbidite recurrence (Appendix C).

3.4.5 Time-independent canyon-flushing in JC27-51

The most recent turbidite present in core JC27-51 from the Iberian Abyssal Plain dates to ca 4,850 Cal years BP, while the oldest dates to ca 82,000 Cal years BP (Table 3.2). Based on a hemipelagic sedimentation rate of 2.3 cm/ka (Fig. 3.6) a lack of hemipelagite between two turbidites indicates a short recurrence interval. Turbidity currents in the basin are assumed to be non-erosive, and so two or more turbidites with no intervening hemipelagite are assumed to be near-synchronous, and are assigned a recurrence interval of 0 years (Table 3.2). This gives a 2,880 year average of recurrence intervals for flushing turbidity currents that reach the Iberian Abyssal Plain.

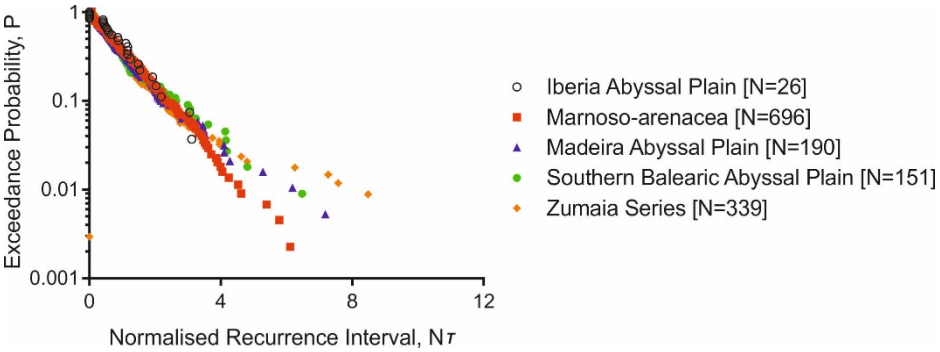

Figure 3.8: Comparison of Iberian Abyssal Plain recurrence intervals with published recurrence intervals from several long-term basin records in Clare et al. (2014). The vertical axis plots the probability (P) that a given turbidite recurrence interval value (time since last event, T) will exceed the average recurrence interval for its respective dataset. The horizontal axis plots normalised recurrence interval data. The recurrence intervals are normalized by subdividing each recurrence interval (T) by the mean recurrence interval (λ) for each of the data sets to plot a dimensionless variable, R_T. N = number of events in each basin data series.

We compare the recurrence intervals for JC27-51 with data from four other distal abyssal plains (Clare et al., 2014; 2015). When recurrence intervals are normalised to the mean value for each dataset, they all approximate a straight line on an exceedance plot (Fig. 3.8), which is indicative of an exponential distribution. Non-parametric Mann-Whitney and Kolmogorov-Smirnov tests demonstrate statistically that the distribution form of turbidite recurrence at JC27-51 shows no significant difference to the four other exponentially-distributed basin plain records (Appendix D). Given the relatively small sample size (i.e. N = 26), it is possible that we do not have sufficient turbidites to make a fully conclusive statement, but we can state that it is not possible to differentiate the recurrence record from other time-independent records. The Mann-Whitney and Kolmogorov-Smirnov tests also allow us to demonstrate that the frequency distribution form of turbidite recurrence in the abyssal plain (JC27-51) is significantly different ($p<0.0001$) to the time-dependent recurrence at levee location JC27-46. Thus, recurrence intervals for canyon-flushing turbidites in the Iberian Abyssal Plain may be considered time-independent and occurring at a significantly different tempo and to that of canyon-filling flows.

3.5 Discussion

In this section we first discuss the triggers and controls on canyon-filling turbidity currents in Nazaré Canyon, and how external factors such as sea level affect recurrence rates. Second, we discuss the possible triggering mechanisms for large canyon-flushing turbidity currents. Finally, we evaluate the implications of these findings for geohazard assessment and in light of future climate change predictions.

3.5.1 Canyon-filling in the present day highstand

The process of canyon-filling occurs on a variety of different temporal and spatial scales within Nazaré Canyon. Previous monitoring in Nazaré Canyon has documented as many as four turbidity currents may occur in the upper canyon per year (de Stigter et al., 2007; Martin et al., 2011; Masson et al., 2011a). These small and frequent turbidity currents do not appear to deposit on canyon levees, or the abyssal plain, as there is a general absence of turbidites deposited more recently than 3 ka (Figs 3.3, and 3.7A and B). These sub-annual turbidity currents are confined primarily to the incised canyon thalweg and typically dissipate before reaching depths greater than 4,000 m water depth (Fig. 3.9A). One turbidity current recorded by de Stigter et al. (2007) below 4,000 m water depth also did not appear to deposit on canyon levees or on the abyssal plain. These flows may erode previously emplaced sediment, but are not considered to flush large volumes of material (Fig. 3.9A).

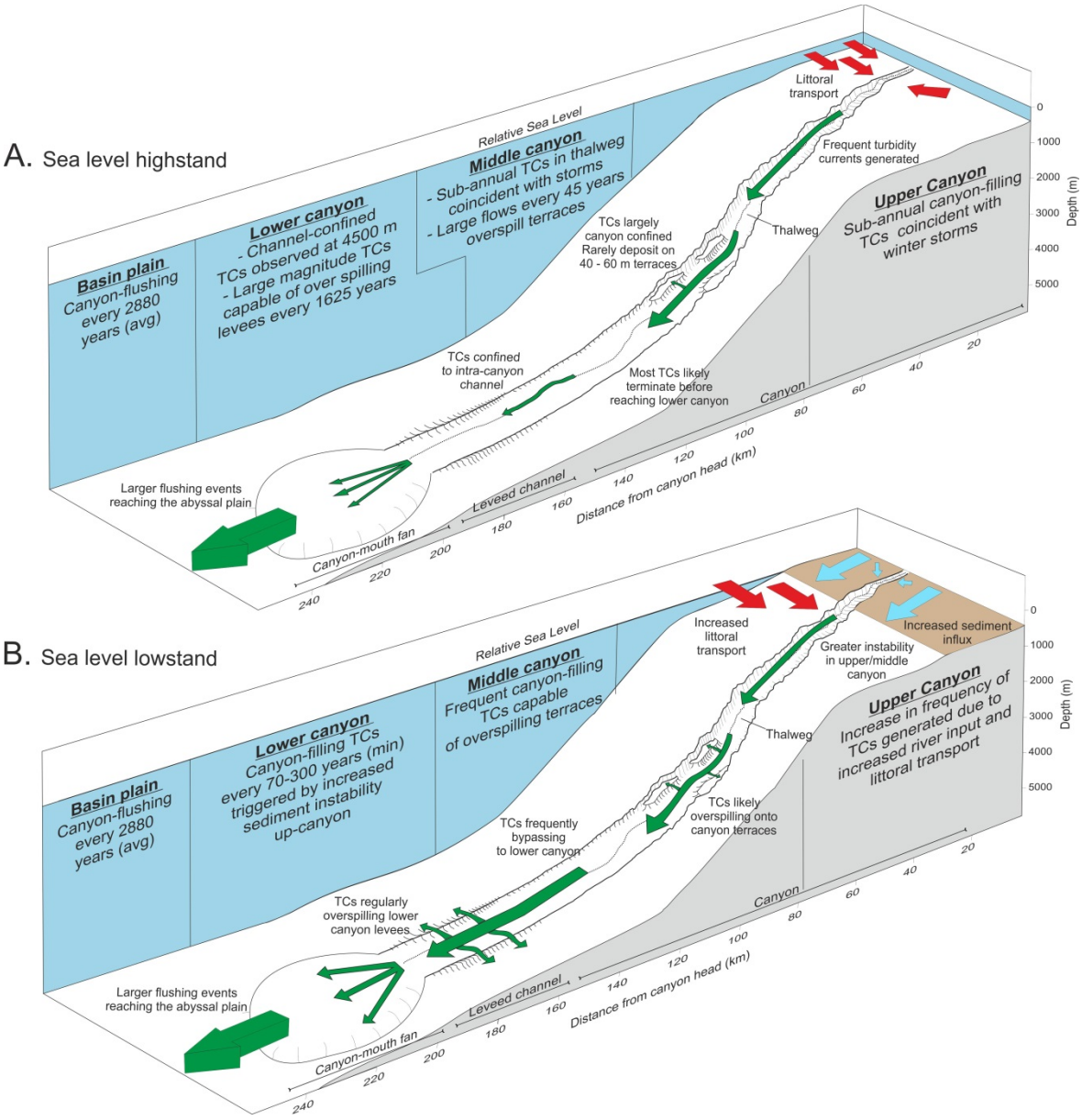

Figure 3.9: Schematic displaying the spatial and temporal variability in turbidity current frequency in Nazaré Canyon during periods of sea level lowstand and highstand. A: During the present day highstand canyon-filling turbidity currents (TCs) are frequent in the upper canyon, but only small thalweg-confined turbidity currents reach to greater than 4,000 m water depth. B: During lowstand conditions canyon-filling turbidity currents were much larger, were able to reach the lower canyon, and regularly over-spilled canyon levees. Infrequent canyon-flushing turbidity currents were not affected by changes in sea level and continued into the present-day highstand.

Terrace cores at 3,500 m water depth and 40 m elevation above the thalweg reveal a mean recurrence of 43 years for larger turbidity currents over the last 1,000 years. These distal turbidite deposits are interpreted as the result of large flushing turbidity currents by Arzola *et al.* (2008), although there is no evidence of post 1 ka deposits in the Iberian Abyssal Plain that would indicate canyon-flushing has occurred (Fig. 3.4, and 3.7A and B). Given the presence of erosive scours

within the lower reaches of the canyon, it is possible that these frequent turbidity currents are erosive and do flush sediment from for the upper to the lower canyon, but are too small to overtop levees or reach the abyssal plain (Fig. 3.9A) (de Stigter et al., 2002; Arzola et al., 2008). However, no age-models exist for lower canyon cores making this difficult to support.

3.5.2 Canyon-filling during sea level lowstand

The role of sea level lowstand in exposing continental shelves and resulting in more terrigenous sediment delivery to many continental slope and deep-sea fans is widely documented; as is the role of canyons as conduits for sediment delivery into the deep sea (Vail et al., 1977; Shanmugam and Moiola, 1982; Posamentier et al., 1991; Piper and Savoye, 1993; Lebreiro et al., 1997; Clark and Mix, 2000; Ducassou et al., 2009; Lebreiro et al., 2009; Covault and Graham, 2010). Our hemipelagic age model reveals that the frequency of canyon-filling turbidity currents was highest during sea level lowstand (Fig. 3.7A and B). Lowstand-dominated canyons typically occur when the canyon does not incise the entire continental shelf (Covault and Graham, 2010). During highstand conditions such canyons are not in direct contact with the shoreline or fluvial sources, limiting sediment delivery. During sea level lowstand, sequence stratigraphic models predict direct connection between rivers and canyon heads. This results in a higher frequency of turbidity currents due to increased sediment supply and associated instability (Shanmugam and Moiola, 1982; Stow et al., 1984; Posamentier et al., 1991; Piper and Savoye, 1993; Lebreiro et al., 2009; Covault and Graham, 2010).

Nazaré Canyon extends across the continental shelf to within 50 m of the present day shoreline, making it distinct from many submarine canyons worldwide (Harris and Whiteway, 2011). The processes of canyon filling during sea level lowstand may have therefore been different. During sea level lowstand approximately a third of the Iberian continental shelf would have been subaerially exposed (Fig. 3.9B). The larger area of exposed continental shelf likely resulted in considerable erosion and seaward transport of unconsolidated shelf sediments. These sediments may have been entrained into ongoing littoral currents and transported into deeper and more unstable areas of the

Nazaré Canyon, thereby accounting for the increase in turbidity current frequency during sea level lowstands (Fig. 3.9B; Posamentier et al., 1991; Sommerfield and Lee, 2004; Durán et al., 2013).

Despite the lack of a direct fluvial sediment supply into Nazaré Canyon, there are a number of small river systems to the north which feed onto the continental shelf (Fig. 3.9B). Increased sediment supply to the shelf from these river systems during glacial conditions may also have led to increased littoral sediment transport, and contributed to the higher frequency of turbidity currents being generated (Fig. 3.9B). It is also possible that these river systems were routed across the shelf and into the canyon head during sea level lowstand, although there is no geomorphic evidence available to support this.

Lebreiro et al. (2009) have suggested that slope instability in the Setúbal/Lisbon and Cascais Canyons (Fig. 3.1) is highest during sea level transgression. This implies that large turbidity currents that fill the Setúbal/Lisbon and Cascais Canyons switch-off at 15.5 ka. Work by Masson et al. (2011b) instead demonstrates that the Setúbal/Lisbon and Cascais Canyons experienced an almost complete switch-off in large canyon-filling turbidity current activity at 6.6 ka. The switch-off of canyon-filling activity in the Setúbal/Lisbon and Cascais Canyons proposed by Lebreiro et al. (2009) at 15.5 ka could more easily be explained by the 200 m elevation of their core site. This elevation above the canyon would bias the record towards the largest turbidity currents (de Stigter et al., 2011). Our age models and statistical analyses from Nazaré Canyon also indicate that large canyon-filling turbidity currents switch-off at ~7 ka (Fig. 3.9B). This is suggestive of a margin-wide sea level control on large-scale canyon-filling in Portuguese Margin canyons.

3.5.2.1 Uncertainties of the statistical analyses

The results of the generalised linear models and Cox proportional hazards models indicate that sea level is well correlated with turbidite frequency recorded on the external canyon levee (Appendix C). While sea level is generally accepted as having a dominant control on sedimentation in many other deep sea fan settings, our results should be treated with some caution. Our data set contains 201 turbidites, and while this is a sufficient number for regression-based analyses (Green, 1991; VanVoorhis and Morgan, 2007), it is smaller than many other datasets used in statistical analyses

of recurrence (Clare et al., 2014; 2015). The height of the JC27-46 core site above the canyon floor may also bias the turbidite record towards those turbidity currents large enough to over-spill the outer levee. There may also be turbidite deposits that are not visually detectable because they are sub-millimetre in scale. Moreover, the sea level curves used in this study are all global (eustatic) reconstructions, and may not be suitable for local analysis where the effect of eustatic sea level changes may be outweighed or convoluted by localised isostatic and tectonic influences (Shanmugam and Moiola, 1982; Stow et al., 1984; Covault and Graham, 2010; Romans et al., 2015). Importantly, binning the data appears to have an effect on the significance of sea level. 500 year and 1000 year bin sizes appear to be less significant or not significant when tested against sea level (Appendix C). This has also been observed in other statistical analyses of turbidite recurrence (Urlaub et al., 2013; Pope et al., 2015)

In addition to uncertainties in the use of numerical datasets and statistical analyses, the exact position of the boundaries between turbidites and hemipelagic sediment can also be unclear. The age model used in this work relies on accurately identifying the boundary between the two sediment types in order to estimate the amount of hemipelagic accumulation between age datums, as well as the age of turbidites through interpolation. Bioturbation by infaunal organisms can mix sediment types and make defining this boundary difficult. In order to account for this any bioturbated boundaries between turbidites and hemipelagite are taken to be where both sediment ocurrs in equal proportions. The mixing of sediment by bioturbation can also skew the ages of radiocarbon dates by incorporating either older or younger carbon into a sampling zone; although this is impossible to quantify. Bioturbation can therefore result in additional uncertainty in the age of turbidites and in the statistical analyses.

3.5.3 Potential triggers of canyon-flushing

The frequency distribution of canyon flushing flows in Nazaré Canyon is indicative of temporally random, time-independent behaviour. A temporally random distribution can result from *a)* a single temporally random or pseudo-random process, *b)* numerous non-random processes affecting a single source overprinting and resulting in a random distribution, *c)* several different sources

feeding into the same basin, or *d)* shredding of environmental (triggering) signal due to the long recurrence intervals (Urlaub et al., 2013; van Rooij et al., 2013; Clare et al., 2014; 2015; Pope et al., 2015; Romans et al., 2015). Here we will evaluate different processes that could trigger canyon-flushing events.

3.5.3.1 Are large storms a trigger?

It has been stated that storms have the potential to trigger turbidity currents that transport sand into deep water (TsuTsui et al., 1987; Shanmugam, 2008). Within Nazaré Canyon, storm-triggered turbidity currents play a significant role in small-scale canyon-filling during the present day (Fig. 3.9A) (van Weering et al., 2002; de Stigter et al., 2007; Martin et al., 2011; Masson et al., 2011a). One of the limiting factors in assessing the role of storms in canyon-flushing events is the length of the observational record. Meteorological data available for the last 63 years indicates that there have been over 150 storms (wave height >1.6 m) recorded since 1952 (Lozano et al., 2004; Almeida et al., 2011). Despite the number of storm events, we see no recent turbidite deposits in the levee or abyssal plain cores; however, the cores may not contain the most recent sediments due to sampling loss. If storms had been a trigger of canyon-flushing through the Holocene, we would expect to see turbidites throughout Holocene sedimentary sequences. It may be possible that some extremely rare storms are large enough to generate turbidity currents that are erosive and capable of flushing the canyon. The lack of turbidites observed in the Iberian Abyssal Plain during last 2,000 years, combined with the likely number of storm events, makes it improbable that storms are a trigger of canyon-flushing (Fig. 3.3 and Table 3.2).

3.5.3.2 Is sea level control undetectable due to 'signal shredding'?

Certain sedimentary environments serve as ideal long-term archives of climatic or environmental signals. This is particularly true in the case of deep-water fan and continental slope settings. In these deep-water settings, one of the principal expressions of sea level variability is changes in down-system sediment transport (Stow and Piper, 1984; Posamentier et al., 1991; Covault and Graham, 2010; Covault et al., 2010).

Signal shredding can be defined here as the filtration of environmental signals through a system by a non-linear process; in this case sediment transport (Jerolmack and Paola, 2010; Romans et al., 2015). Environmental signals like sea level may be considered a linear input into a system. However, the recording of this signal in sedimentary archives by sediment transport and deposition is typically non-linear. This is because sediment transport and deposition is highly variable and dependent on several initial and transport conditions. For turbidity currents these can include the triggering mechanism, sediment volume, run-out distance, and whether or not these currents bypass or deposit (Piper and Normark, 2009; Talling et al., 2013, Talling, 2014). These preconditions impart non-linearity that can ultimately filter or 'shred' the signal of environmental change. In the case of Nazaré canyon-filling turbidity currents, the sea level signal is preserved in the levee due to the number of events recorded, the proximity to source, and the regularity with which they were deposited. The height of the levee above the canyon also likely prevents smaller, more frequent events triggered by storm or wave activity from depositing at the core site. Storm and wave activity could be considered a separate environmental signal and may mask the longer-term sea level signal (Romans et al., 2015).

In contrast to this, canyon-flushing events are typically less frequent, often having recurrence intervals of >2000 years (Fig. 3.9 and Table 3.2). They involve the remobilisation of sediment stored within the canyon over many thousands of years (Paull et al., 2005; Talling et al., 2007a; Piper and Normark, 2009; Talling, 2014). This implies that if canyon-flushing events are the result of climatic variability or change, their rarity (non-linearity) in the depositional record could have shredded any signal of this climatic control (Covault and Fildani, 2014; Clare et al., 2015; Romans et al., 2015). Such signal-shredding could explain the temporally random distribution of canyon-flushing events in the Iberian Abyssal Plain.

3.5.3.3 Are regional earthquakes a trigger?

Turbidite paleoseismology involves the use of marine or lacustrine turbidite recurrence rates as a proxy for earthquake recurrence. This method has been applied to numerous settings to develop estimates of long-term earthquake hazard rate (Adams, 1990; Monecke et al., 2004; Goldfinger et

al., 2007; Polonia et al., 2013; Moernaut et al., 2014, 2015). Sumner et al. (2013) outline four independent criteria for identifying an earthquake trigger for turbidites: 1) synchronous turbidites in multiple basins; 2) observing an identical number of turbidites above and below the confluence of submarine channels; 3) identifying a larger relative volume for turbidites compared with others deposited in the same setting; 4) a historical or observational record of an earthquake that is coeval with the turbidite.

Nazaré canyon has three branching channels, with confluences at 500 and 3,000 m water depth (Fig. 3.2; Lastras et al., 2009). There are no sediment cores positioned directly below or above these confluences, making the confluence test of Adams (1990) unsuitable in this study area. Due to a lack of core coverage in the basin it is also impossible to estimate turbidite volumes and invoke a seismic trigger. Turbidite paleoseismology has been previously applied to the Iberian Margin and a catalogue of Late Quaternary seismo-turbidites exists for the Tagus and Horseshoe Basins (Fig. 3.10A) (Garcia-Orellana et al., 2006; Gràcia et al., 2010; Masson et al., 2011b). This serves as a basis to test for earthquake triggering of turbidites in the Iberian Abyssal Plain.

Comparison with published Iberian turbidite records reveals that only three turbidites correlate well into the adjacent Tagus Abyssal Plain (TAP), and only one turbidite is well correlated in all three basins (Fig. 3.10A). Other large turbidites from the Iberian Abyssal Plain (IAP) are not synchronous with proposed seismo-turbidites from the Tagus or Horseshoe Abyssal Plain. The Iberian Margin contains multiple faults as a result of the compressional rotation associated with the Azores-Gibraltar fracture zone to the south (Fig. 3.10B) (Buforn et al., 1988; Borges et al., 2001; Zitellini et al., 2004; Custódio et al., 2015). The Nazaré Fault (NF) and the Lower Tagus Valley Fault (LTVF) are quite proximal, suggesting that large earthquakes originating from the LTVF might be capable of triggering sediment failures which ignite and flush Nazaré Canyon (Fig. 3.10B) (Johnston, 1996). This could explain why several turbidites are synchronous in both the Tagus and Iberian Abyssal Plains (Fig. 3.10A).

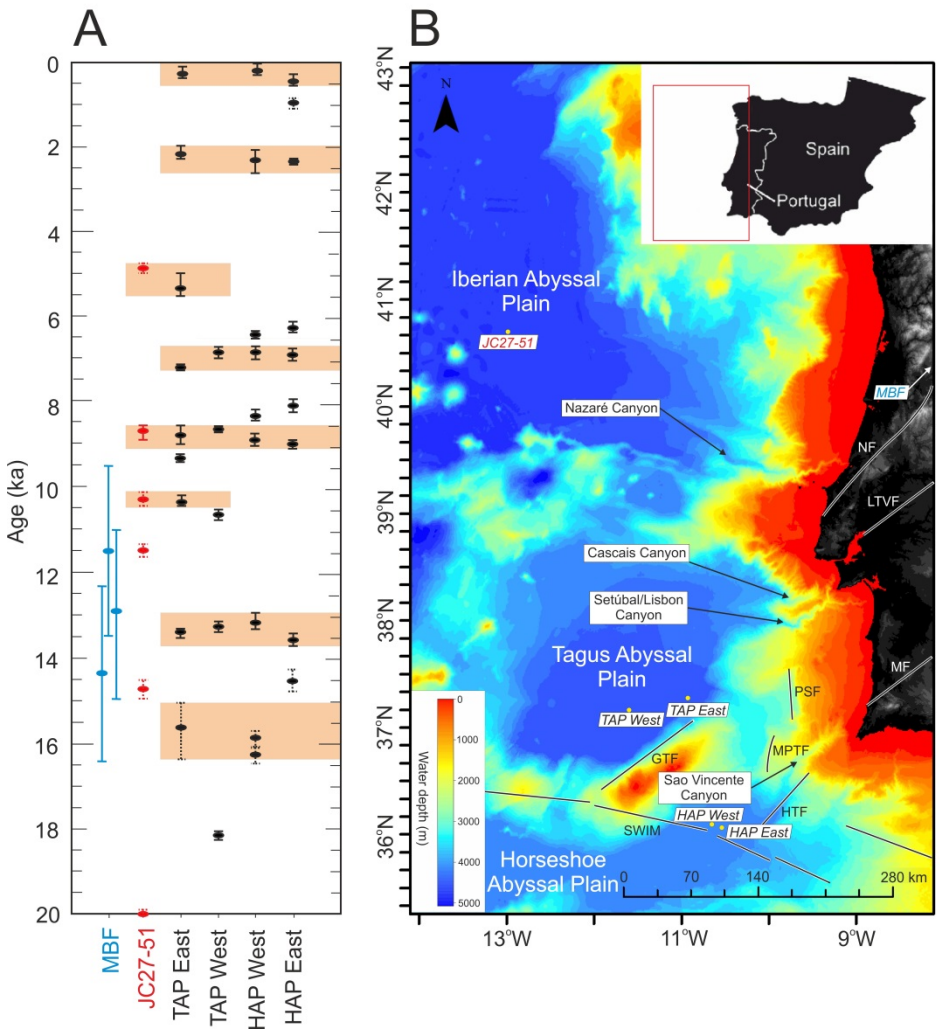

Figure 3.10: A: Proposed seismoturbidites from the Tagus and Horseshoe Abyssal Plains from Grácia et al. (2010) and Masson et al. (2011b) (shown as black dots). Turbidites from the Iberian Abyssal Plain are shown in red, and paleoearthquakes from the Manteigas-Braçanga Fault are shown in blue. Orange bars represent event which can be correlated based on their age uncertainties. Dashed error bars on ages represent ages that are determined through linear interpolation. B: Map of the Portuguese Margin showing primary structural faults. MTB = Manteigas-Braçanga Fault, NF = Nazaré Fault, LTVF = Lower Tagus Valley Fault, MF = Messejana Fault, PSF = Pereira de Sousa Fault, MPTF - Marquês de Pombal Thrust Fault, HTF = Horseshoe Thrust Fault, GTF = Gorringe Thrust Fault, SWIM = South-western Iberian Margin lineaments. Labels in italics indicate locations of paleoseismic reconstructions in Fig. 3.10A.

The tectonic regime along the south-western section of the Iberian Margin is more complicated, with several extensive offshore faults capable of generating large earthquakes (Fig. 3.10B) (Pro et al., 2013; Custódio et al., 2015). There is 300 km distance from the south-west margin to Nazaré Canyon, and there is no continuous fault system between the areas. Paleoseismic intensity reconstructions and seismic propagation models indicate large earthquakes along the south-western

section of the margin are unlikely to trigger canyon-flushing in Nazaré Canyon (Dobrovolsky et al., 1979; Buforn et al., 1988; Fukushima and Tanaka, 1990; Johnston, 1996; Zitellini et al., 2004). This could explain why several turbidites present in the Tagus and Horseshoe Abyssal Plain are not present in the Iberian Abyssal Plain (Fig 3.10A).

The synchronous deposition test does not strongly support regional earthquakes as a trigger for canyon-flushing turbidites in the Iberian Abyssal Plain. The historical record of large Portuguese earthquakes extends back to the Portugal and Galicia Earthquake at 60 BC (Galbis, 1932; Baptista and Miranda, 2009). Several earthquakes dating further back to 7,000 Cal years BP have been inferred from onshore paleo-tsunami records (Ruiz et al., 2008). Importantly, these records place the epicentres of many of these past earthquakes along the South-western Iberian Margin, and not proximal to Nazaré Canyon. This also makes them unsuitable as an independent earthquake archive with which to compare Iberian Abyssal Plain turbidite ages.

The Nazaré Fault (NF) forms part of a larger NNE-SSW-trending Variscan fault system which extends across the peninsula (Fig. 3.10B) (Buforn et al., 1988; Zitellini et al., 2004). Paleoseismic reconstructions on these NNE-SSW trending fault zones in Central and Northern Portugal are sparse, and no such record exists for the Nazaré Fault. This makes identifying possible earthquake triggering of canyon-flushing from nearby faults problematic. Optically Stimulated Luminescence (OSL) dates from fault surfaces along the Manteigas-Bragança Fault (MBF) north-east of the Nazaré Fault reveal three large (Mw 7.3) earthquakes between 11.5 and 14.5 ± 2 ka, (Fig. 3.10A). These ages do not correspond well with turbidites in the Iberian Abyssal Plain, although the wide margins of error do encompass 2 turbidites at 11.7 ka and 14.9 ka (Fig. 3.10A). It has been proposed that these NNE-SSW-trending Variscan faults primarily accommodate reverse faulting and not strike-slip faulting. In contrast, WNW–ESE-trending faults on the South-western Iberian Margin exhibit strike-slip behaviour (Borges et al., 2001; Custódio et al., 2015). This would imply that unlike the southwestern margin, earthquakes along the Central Portuguese Margin do translate down-fault, limiting seismic propagation (Sylvester, 1988).

A small number of turbidites from the Iberian Abyssal Plain can be correlated with seismo-turbidites previously identified in the Tagus and Horseshoe Abyssal Plains (Fig. 3.10A). Turbidites which do not correlate in the Tagus or Horseshoe Basins could be the result of earthquakes originating from further north along the ENE-SSW Fault zone. However, given the wide uncertainties on earthquake ages, and the structure of the fault system, any correlation with canyon-flushing events would be largely speculative. There are multiple other intraplate faults that may trigger canyon-flushing, but without accurate paleoseismic records it is impossible to imply causation (Buforn et al., 1988; Zitellini et al., 2004; Villamor et al., 2012; Custódio et al., 2015). The lack of convincing evidence for earthquake triggered canyon-flushing along this margin highlights the problems of applying turbidite paleoseismology methods to structurally complex margins.

3.5.4 Climate change and geohazard implications

As previously outlined, many authors have suggested that large continental margin failures are associated with times of significant climatic and sea level change (Maslin et al., 2004; Owen et al., 2007; Lee, 2009; Smith et al., 2013; Brothers et al., 2013). One implication of this is that future climate and sea level change might increase the frequency of large continental margin failures. Our findings contribute to a growing body of literature that suggests large sediment failures in multiple settings are temporally random and are not significantly influenced by climate or sea change (Beattie and Dade, 1999; Urlaub et al., 2013, 2014; Clare et al., 2014; Hunt et al., 2014; Moernaut et al., 2014; Talling et al., 2014). It might be reasonable to conclude that the recurrence intervals of large sediment failures and canyon-flushing along the Central Iberian Margin will not be significantly influenced by any future sea level rise. Canyon-flushing in other deep-sea canyons is currently poorly understood and few estimates of recurrence rates exist. Additional work into other canyon systems would help to determine if temporal randomness is a wide-spread characteristic of canyon-flushing.

Our statistical analysis demonstrates that sea level is a significant control on canyon-filling. However, the current sea level highstand features limited canyon-filling events. These are typically

small, channel-confined turbidity currents that die before reaching the lower canyon (Fig 3.9A). Intuitively, we might expect future sea level rise to further limit canyon-filling turbidity currents, as past sea level rise did. However, future sea level rise has been predicted to increase rates of coastal erosion (Gornitz, 1991; Bray and Hooke, 1997; Leatherman et al., 2000). This increase in sediment delivery to the Iberian Shelf could lead to an increase in littoral transport into the head of Nazaré Canyon, thereby promoting greater instability. These smaller turbidity currents may not have large geohazard implications, but are important for assessing risk to seafloor structures such as pipelines and telecommunication cables.

3.6 Conclusions

Canyon-flushing turbidity currents have been predicted to occur much less frequently than those that fill canyons (Paull et al., 2005; Canals et al., 2006; Arzola et al., 2008; Puig, et al., 2014). Here we demonstrate that canyon-flushing turbidity currents in this system have recurrence rates of several thousands of years on average. This recurrence rate is an order of magnitude longer than those filling the canyon during sea level lowstand, and more than two orders of magnitude longer than those that fill the canyon in the present day. The recurrence intervals for canyon-filling and canyon-flushing appear to have distinctly different statistical distributions. Moreover, unlike canyon filling, the recurrence rate of canyon-flushing events does not appear to be affected by long-term changes in sea level. This suggests that they may have different triggers, or that the signal of triggering mechanisms is shredded due to the long recurrence intervals. From a geohazard assessment perspective, this implies that the frequency of potentially hazardous canyon-flushing events may not be influenced by future sea level predictions. The tectonic complexity of the margin, uncertainties in age-control, and the time-independent behaviour of canyon-flushing make determining a trigger for canyon-flushing problematic; although earthquakes may trigger some events.

Chapter 4: Does eustatic sea level variability affect the flushing of submarine canyons?

Summary:

The flushing of submarine canyons by sediment gravity flow processes transports enormous volumes of sediment into the deep sea, and is one of the main processes creating and maintaining submarine canyons over geological timescales. The previous chapter revealed a strong statistical relationship between sea level and the frequency of canyon-filling turbidity currents. However, no relationship between sea level and the largest canyon flushing turbidity currents was identified. The record of canyon flushing only covered the last 80,000 years, and did not extend over a full glacial cycle. In this chapter a much longer 1.8 Ma record of canyon flushing is used to identify any control of sea level on the recurrence rates of canyon flushing in Nazaré Canyon. This chapter aims to:

1. Determine the long-term recurrence rate of turbidity currents that flush Nazaré Canyon and deposit in the Iberian Abyssal Plain.
2. Establish whether or not eustatic sea level is a preconditioning factor for canyon flushing.
3. Determine the distribution form of canyon flushing recurrences to help in identifying possible triggers.

The results indicate that there is no detectable statistical relationship between eustatic sea level and the recurrence rate of canyon flushing events in the Nazaré Canyon. Instead, changes in the amplitude and periodicity of eustatic sea level variability are associated with an increase in the size and frequency of canyon flushing. The recurrence intervals of canyon flushing conform to a lognormal distribution, which is fundamentally different to several other distal basin records. This suggests that the controls and triggers of canyon flushing events reaching the Iberian Abyssal Plain are different than in other distal basin settings.

This chapter in its entirety has been submitted to the Geological Society of America Bulletin. as: Allin, J.R., Hunt, J.E., Clare, M.A., Talling, P.J.. Does eustatic sea level control the flushing of submarine canyons?

Abstract

Turbidity currents are the principal processes responsible for creating submarine canyons and maintaining them over geological timescales. The turbidity currents that maintain or 'flush' submarine canyons are some of the most voluminous sediment transport events on Earth. Long-term controls on the frequency and triggers of canyon flushing events are poorly understood in most canyon systems due to a paucity of long sedimentary records. Here we analyse a 160 m long ODP core to determine the recurrence intervals of canyon flushing events in the Nazaré Canyon over the last 1.8 million years. We then investigate the role of eustatic sea level in controlling the frequency and magnitude of these canyon flushing events. Canyon-flushing turbidity currents that reach the Iberian Abyssal Plain have an average recurrence interval of 2,770 years over the last 1.8 million years. Eustatic sea level has minimal effect on the recurrence rate of canyon flushing, despite being a dominant control on the frequency of canyon filling events. However, sharp increases in the amplitude and periodicity of global eustatic sea level variability during the mid-Pleistocene transition between 0.9 - 1.2 Ma were associated with more frequent canyon flushing events. This change into high-amplitude, long-periodicity sea level variability may have remobilised large volumes of shelf sediment not previously exposed to sub-aerial weathering, and increased the frequency and magnitude of canyon-flushing turbidity currents. Canyon flushing is therefore largely independent of eustatic sea level variability, but may sometimes be affected by changes in its amplitude and periodicity. Turbidite recurrence intervals in the Iberian Abyssal Plain have a lognormal distribution, which is fundamentally different to the exponential distribution of recurrence intervals observed previously in other basin turbidite records. The lognormal distribution of turbidite recurrence intervals seen in the Iberian Abyssal Plain is inferred to result from the variable run-out distance of turbidity currents, such that distal records are less complete, combined with the multiplicative effects of diverse sources or triggering mechanisms. The changing form of turbidite recurrence intervals at different locations within the Iberian Abyssal Plain is important because it ultimately determines the probability of turbidity current-related geohazards.

4.1 Introduction

Turbidity currents are volumetrically some of the most important sediment transport mechanisms operating on our planet. An individual turbidity current can be capable of transporting as much sediment as all the world's rivers in one year combined (Talling et al., 2007a; Korup, 2012). The most voluminous turbidity currents are triggered by large (> 1 km^3) submarine landslides originating from continental margins and volcanic islands. These large landslides and their resultant turbidity currents pose considerable geohazard risk, and have the potential to generate tsunamis that can damage coastal settlements and cause considerable loss of life (Bondevik et al., 1997a; Piper et al., 1999; Tappin et al., 2001; Harbitz et al., 2006). Landslides and turbidity currents may also damage submarine infrastructure such as pipelines and telecommunication cables (Bruschi et al., 2006; Carter et al., 2012a; Carter et al., 2014; Pope et al., 2016). For these reasons, understanding the triggering mechanisms and frequencies of volumetrically large submarine landslides and turbidity currents is important for geohazard assessment.

Turbidity currents in submarine canyons are proposed to be one of two broad end-member types: those that are restricted to and fill the canyon, and those that flush the canyon and continue into deeper water (Parker, 1982; Piper and Savoye, 1993; Canals et al., 2006; Piper and Normark, 2009; Talling et al., 2012; Allin et al., 2016). 'Filling' turbidity currents triggered by localised failures, hyperpycnal river discharge, or storms accumulate sediment within canyons over hundreds or even thousands of years (Marshall, 1978; Paull et al., 2005; Canals et al., 2006; Arzola et al., 2008; Khripounoff et al., 2009; Masson et al., 2011; Talling et al., 2013; Talling, 2014). 'Flushing' turbidity currents are infrequent (>100 yr) events that erode considerable volumes (>0.2 km^3) of this unconsolidated sediment from the canyon floor and transport it to distal abyssal plains (Parker, 1982; Piper and Savoye, 1993; Paull et al., 2005; Piper and Normark, 2009; Talling et al., 2012; Puig et al., 2014). Given sufficient coarse-grained material, a high energy canyon-flushing turbidity current may also erode the canyon bedrock, which is the main mechanism through which large submarine canyons are created and maintained over geological timescales (Parker, 1982; Pratson et al., 1994; Piper and Normark, 2009). Canyon flushing is therefore important for sediment transport as well as geohazard assessment.

It has been previously proposed that non-random processes like climate-driven sea level change are an important control on the recurrence rates of large volume landslides and turbidity currents (Milkert et al., 1996a; Maslin et al., 2004; Owen et al., 2007; Lebreiro et al., 2009; Lee, 2009; Brothers et al., 2013; Smith et al., 2013). Subsequently, climate-driven sea level change is also a dominant control on submarine fan and canyon development by altering sediment volumes and the location of deposition relative to the continental shelf-edge (Vail et al., 1977; Shanmugam and Moiola, 1982; Posamentier et al., 1991; Piper and Savoye, 1993; Lebreiro et al., 1997; Ducassou et al., 2009; Covault and Graham, 2010; Allin et al., 2016). Conversely, large volume canyon-flushing turbidity currents that reached the Iberian Abyssal Plain are temporally random and are not affected by sea level changes that control canyon-filling turbidity currents (Hunt et al., 2013b; Urlaub et al., 2013; Clare et al., 2014; Allin et al., 2016). Due to the limited direct observations of canyon-flushing events, it is unclear whether sea level controls the timing of flushing events or whether other factors such as earthquakes are dominant (de Stigter et al., 2011; Masson et al., 2011a).

4.1.1 Aims

This contribution has three principal aims. The first aim is to build a long-term (1.8 Ma) record of the frequency of canyon-flushing events originating from Nazaré Canyon. In order to do this a long and complete turbidite record is used from an Ocean Drilling Program (ODP) borehole in the Iberian Abyssal Plain, which contains over 600 individual turbidites. This represents one of the longest ever complete records of canyon-flushing turbidity currents and extends over multiple glacial cycles. The second aim is to test whether eustatic sea level change during the Pleistocene affects the frequency of these large volume canyon-flushing events. To test this we will use a global eustatic sea level curve from the Pleistocene along with regression-based statistical methods. Establishing whether or not glacio-eustatic sea level change affects the recurrence rates of large-volume canyon flushing is important for geohazard assessment in light of future sea level change projections. The third aim is to identify the distribution form of turbidite recurrence intervals. The distribution form, or shape, of turbidite recurrence intervals may yield information about possible preconditioning or triggering mechanisms of canyon-flushing events in the Nazaré Canyon.

4.2 Regional setting

The Iberian Abyssal Plain is located 200 km off the western coast of Portugal between 40^{o} N and 43^{o} N. It extends approximately 700 km to the northwest at an average water depth of 5,300 m (Fig. 4.1). The basin is bounded by the Galicia Bank to the northeast, the Estremadura Spur to the south, and by a series of seamounts along its western margin. The total area of the basin covers approximately 107,000 km^{2} (Weaver et al., 1987). ODP leg 149 initial reports have detailed the long-term basin infill record extending back to the Lower Cretaceous (140 Ma) (Milkert et al., 1996a; 1996b). This work demonstrated an onset of terrestrial-derived turbidite deposition in the Iberian Abyssal Plain between 2.2 and 2.6 Ma, which continued into the late Pleistocene.

The Iberian Abyssal Plain is fed by the Nazaré Canyon, which begins 500 m from the Portuguese coastline and extends for 200 km down to a water depth of 5,200 m (Fig. 4.1) (Lastras et al., 2009). The Oporto and Aveiro Canyons are two smaller canyon systems that enter the Iberian Abyssal Plain north of Nazaré Canyon (Guerreiro et al., 2007). These canyons are not considered to be active in the present day, but may have acted as sources of turbidity currents reaching the Iberian Abyssal Plain during times of sea level lowstand (Posamentier et al., 1991; Guerreiro et al., 2007; 2009).

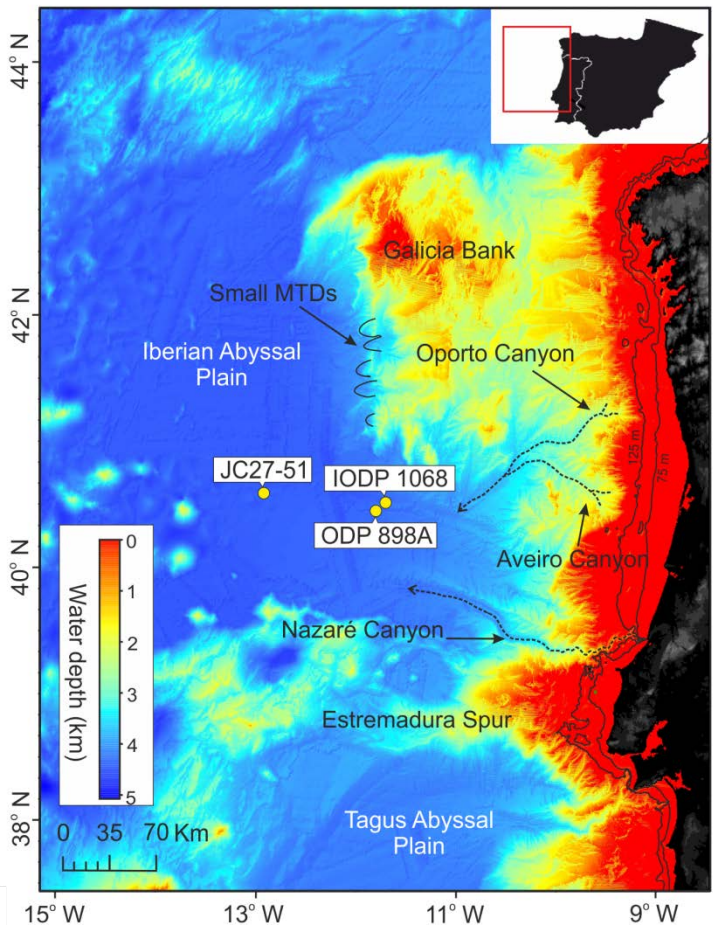

Figure 4.1: Bathymetry map of the Iberian Abyssal Plain showing the locations of core site ODP Hole 898A. Also shown are small mass transport deposits (MTDs) originating from the Galicia Bank, and the three canyons that feed into the Iberian Abyssal Plain; the Nazaré, Aveiro, and Oporto Canyons. Sites IODP 1068 and JC27-51 are shown and are discussed later. Bathymetry data are from the GEBCO database (IOC, IHO, BODC, 2003).

4.3 Methods

4.3.1 Identification of hemipelagic sediments

Age models are developed to determine the recurrence intervals for the deposits of turbidity currents, known as turbidites. These turbidites must be differentiated from 'background' hemipelagic sediment that is continuously deposited out of the water column. Turbidites are often well sorted, have normal grading, and have observable internal structure (sometimes representing bedforms) developed from traction beneath the flow. The fine-grained mud cap of turbidites is commonly homogenous and often devoid of foraminiferal material, while the basal contact of the turbidite is often sharp and erosional (Bouma, 1962: Stow and Piper, 1984). In contrast,

hemipelagite sediments typically consist of bioturbated detrital clay that contains randomly dispersed foraminifera and lacks sedimentary structures (Stow and Tabrez, 1998; Hoogakker et al., 2004).

4.3.2 Age model development and recurrence estimation

Age control for core ODP Hole 898A is provided by coccolith biostratigraphy. The thirteen biostratigraphic datum horizons for Pleistocene deposits were identified using coccolith assemblages and standard zonal boundaries (Fig. 4.2; Liu et al., 1996; Milkert et al., 1996a). Using these datums, and the thicknesses of hemipelagic sediment between them, sedimentation rates were calculated. The thicknesses of hemipelagic sediment were then divided by the sedimentation rates to convert them into time intervals (Thompson and Weaver, 1994; Wynn et al., 2002; Grácia et al., 2010; Clare et al., 2014). From these time intervals the ages of individual turbidites can be estimated. Using the age model to estimate the emplacement age of each turbidite allows us to calculate individual recurrence intervals. Here we define the recurrence interval of a turbidite as the length of time since the turbidite that preceded it (Clare et al., 2014, 2015; Pope et al., 2015). The use of hemipelagic age models in determining the age of turbidites relies on two assumptions: firstly that there is minimal fluctuation in the rate of hemipelagic sediment accumulation through time (Milkert et al., 1996a; Lebreiro et al., 2009; Allin et al., 2015; Clare et al., 2015), and secondly that turbidity currents do not erode the sea floor (Weaver and Thomson, 1993; Thomson and Weaver, 1994; Weaver, 1994; Wynn et al., 2002; Gutiérrez-Pastor et al., 2009; Grácia et al., 2010).

4.3.3 Statistical analysis of turbidite recurrence

4.3.3.1 Testing the statistical distribution form of recurrence intervals in core ODP Hole 898A

The shapes of recurrence interval distribution forms can yield information about the dynamics governing the system that gave rise to them (van Rooij et al., 2013). It has been demonstrated that certain statistical distributions of recurrence intervals indicate time-dependent behaviour. These statistical distributions may indicate that additive process (e.g. for a normal distribution) or a multiplicative interaction of processes (e.g. for a lognormal distribution) are exerting control on a

system (van Rooij et al., 2013; Clare et al., 2016). Equally, distributions may indicate (pseudo)randomness or a lack of memory (e.g. for an exponential distribution). We aim to determine the frequency distribution form of turbidite recurrence intervals at ODP Hole 898A over the last 1.8 Ma to understand possible triggers and controls for canyon-flushing turbidity currents. We use exceedance plots to determine the distribution form of turbidite recurrence intervals from the Iberian Abyssal Plain. Exceedance plots have been used as a visual test of data distribution over different scales, and plot the likelihood that a given recurrence interval will exceed the longest recurrence interval in the dataset (Talling, 2001; Sylvester, 2007; Hunt et al.,2013b; Clare et al., 2014; 2016). In addition to exceedance plots, we compare the distribution form of turbidite recurrence in ODP Hole 898A with the lognormally-distributed turbidite recurrence dataset of Clare et al. (2015). This turbidite recurrence dataset originates from IODP borehole 1068 in the Iberian Abyssal Plain and extends from 48 - 65 Ma (Fig. 4.1).

4.3.3.2 Testing for a persistent trend over shorter time periods

Given the long 1.8 Ma time span of the ODP Hole 898A core record and the large number of turbidites (N = 666), it is possible that a given distribution is not uniform across all of the data. In order to determine whether or not a distribution is persistent over shorter subsets of the data, we divide the data into subgroups (A through K) based on changes in the gradient of the cumulative recurrence curve. The subgroups are shown on exceedance plots to determine whether they have similar or different distributions. Lack of a common distribution form may indicate that processes governing turbidite recurrence intervals are not consistent through time.

4.3.3.3 Testing for time-dependence

Rescaled range analysis was developed as a test for temporal clustering or ‘memory’ in time series data (Hurst, 1951). It is defined as the range of cumulative deviations from the mean, divided by the standard deviation, obtained for multiple subsets of the recurrence data (Bassingthwaighte and Raymond, 1994). This test has the advantage of being independent of frequency distribution form (Kristoufek, 2012). The test produces a modified Hurst exponent (K) or ‘self-similarity parameter’, which measures the intensity of long range dependence in a time series (Weron, 2001). In simple

terms, when K ≅ 1 or K ≅ 0 the data show persistence or anti-persistence respectively, indicative of time-dependent behaviour. Values of K ≅ 0.5 are considered to be random or time-independent.

4.3.3.4 Testing for sea level control on recurrence at site ODP Hole 898A

Statistical analyses are widely used to understand geohazard frequency and triggering, and are most informative where large (N = >100) datasets are available (Green, 1991; Tabachnick and Fidell, 2007; Clare et al., 2016). As ODP Hole 898A contains over 600 individual turbidites, covering 1.8 million years, it is an ideal location to test for the influence of climatic variability on the recurrence rate of canyon-flushing events. The first statistical analysis is a linear model, which tests for the significance of sea level as an explanatory variable on the recurrence of turbidites (McCullagh and Nelder, 1989; Allin et al., 2015; Clare et al., 2016). Linear models produce a regression coefficient, which is a measure of the change in a response variable (recurrence interval) with a 1 unit (meter) change in the explanatory variable (sea level). They also produce a correlation coefficient (R^2), which is a measure of the variability in the data that is accounted for by the explanatory variable (Schemper and Stare, 1996).

To further test the effect of sea level change on turbidite recurrence, a non-parametric Cox Proportional Hazards (PH) Model is applied (Cox, 1972). The Cox PH model requires no *a priori* specification of frequency distribution form and is independent of time. The Cox PH model is typically used to determine a hazard rate (regression coefficient) in medical studies (e.g. rate of patient fatality) but has also been applied to turbidite frequency analysis (Hunt et al., 2014; Allin et al., 2016; Clare et al., 2016). The hazard coefficient is analogous to a regression coefficient, and is the ratio between the change in the explanatory variable (e.g. sea level) and the response variable – in this case turbidite recurrence. Previous work has shown that the Cox PH model requires at least a minimum sample size of N = 20 (Vittinghoff and McCuloch, 2007). In addition to a hazard coefficient, the Cox PH model performs survival analysis using three separate tests (likelihood, Wald and log-rank), for which p-values are derived. For both linear and Cox PH models, where the resultant p-value is small (<0.05) we can reject the null hypothesis and sea level can be considered a significant variable to explain turbidite recurrence. Where the p-value is large (p >0.05), we

cannot reject the null hypothesis and sea level cannot be implicated as a statistically significant control on turbidite recurrence.

For both the linear model and Cox proportional hazards model we test the turbidite recurrence data against the global eustatic sea level curve of Miller et al. (2005). This sea level curve is constructed from borehole $\delta^{18}O$ measurements and has a 5 ka resolution. Although this resolution is much lower than sea level curves used in some other statistical analyses of turbidite recurrence (Urlaub et al., 2013; Allin et al., 2016), major sea level transitions associated with Pleistocene glacial cycles are well recorded. This suggests that the sea level curve is appropriate for the analysis of turbidite records through the Pleistocene.

4.4 Results

4.4.1 Core sedimentology

ODP hole 898A contains multiple dark, normally graded upward-fining sequences with silty/sandy bases interspersed with pale microfossil-rich clays (Fig. 4.2). The upwards fining sequences are interpreted to be turbidites in the sense of Stow and Piper (1984). The pale, nanofossil-rich clay is interpreted to be hemipelagite after Stow and Tabrez (1998). 666 individual turbidites can be identified within ODP Hole 898A (Fig. 4.2; Appendix E). Turbidites range from 0.5 to 400 cm in thickness. The boundaries between the upper turbidite units and the hemipelagic clays are sometimes obscured by mixing due to bioturbation. In these cases we consider the boundary between the two facies to be where the ratio is approximately 50:50.

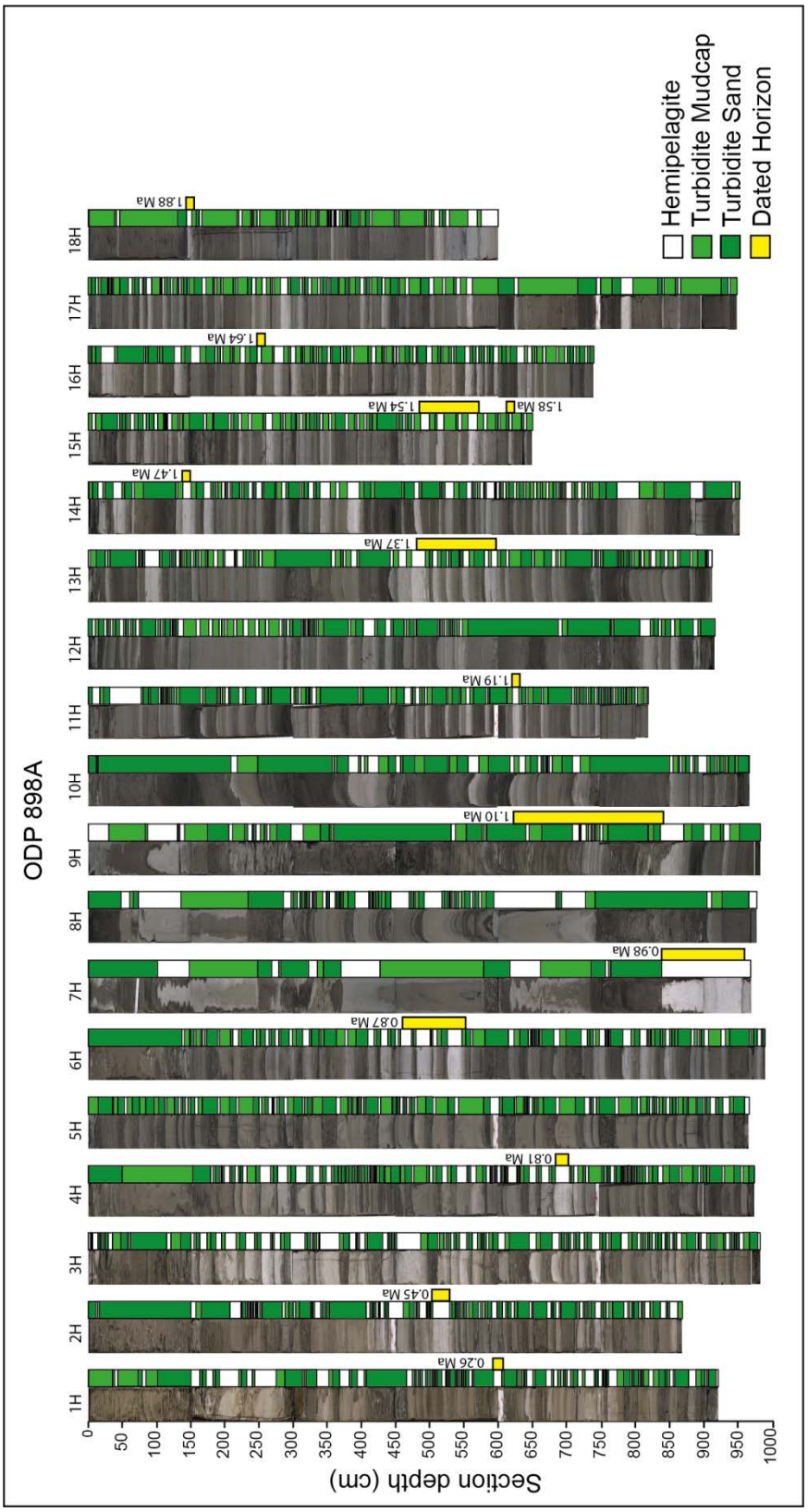

Figure 4.2: Photographs of cores recovered from ODP Hole 898A and the chronostratigraphic datums (yellow) used in the age model. The thickness of the biostratigraphic datums shows their depth uncertainty within the core. Beside the photos are interpretations of the core section, with green being turbidites and white being hemipelagic sediment.

4.4.2 Age model and sedimentation rate

The biostratigraphic datum horizons and age model for ODP hole 898A can be seen in Fig. 4.3 (Milkert et al., 1996a). Uncertainties associated with these datums are difficult to constrain, as they are rarely reported in the literature. Conservative estimates of uncertainty surrounding the use of coccolith biostratigraphy are ± 10 ka (Hunt et al., 2013a). The age model shows a relatively linear hemipelagic sedimentation rate since 1.8 Ma (R^2 = 0.97) (Fig. 4.3). The average sedimentation rate for the entire record is 2.01 cm/ka, although the sedimentation rate between each datum has been used for calculating individual turbidite recurrences. The minimum resolvable hemipelagic interval within core ODP Hole 898A is 0.5 cm thick.

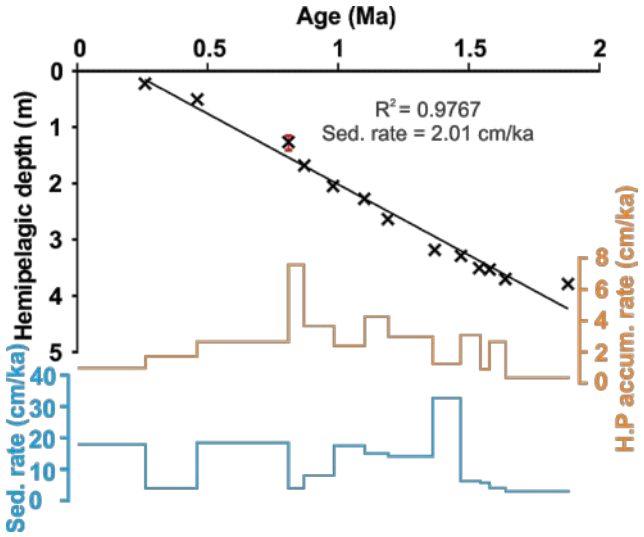

Figure 4.3: Age model for core ODP Hole 898A from biostratigraphic and magnetostratigraphic datums outlined in Milkert et al., 1996b (Fig. 4.2). The R^2 correlation coefficient indicates a relatively constant sedimentation rate through time. The graph in orange shows the hemipelagic accumulation rate, while the graph in blue shows the total sedimentation rate. Red bars on age tie points show depth uncertainty.

4.4.3 Distribution form of turbidite recurrence intervals at ODP Hole 898A

Exceedance plots also show a strong similarity between the lognormally distributed recurrence data of Clare et al. (2015) spanning 48 - 68 Ma and the distribution form of turbidite recurrences from the last 1.8 Ma (Fig. 4.4). Both datasets from the Iberian Abyssal Plain show a similar distribution on a log-probability plot, a log-linear plot, and a log-log plot (Fig. 4.4 A-C). When analysed using a Mann-Whitney U-test, the ODP Hole 898A turbidite recurrence data are not significantly different

from a synthetic recurrence dataset with a lognormal distribution (P >0.05). When the ODP Hole 898A dataset is subdivided based on changes in the slope of cumulative recurrence (Fig. 4.5A) a persistent lognormal trend within the majority of the data can be seen on exceedance plots (Fig. 4.5B and C). All but subgroups A and G exhibit this trend, indicating the bulk of the data conform to a lognormal distribution.

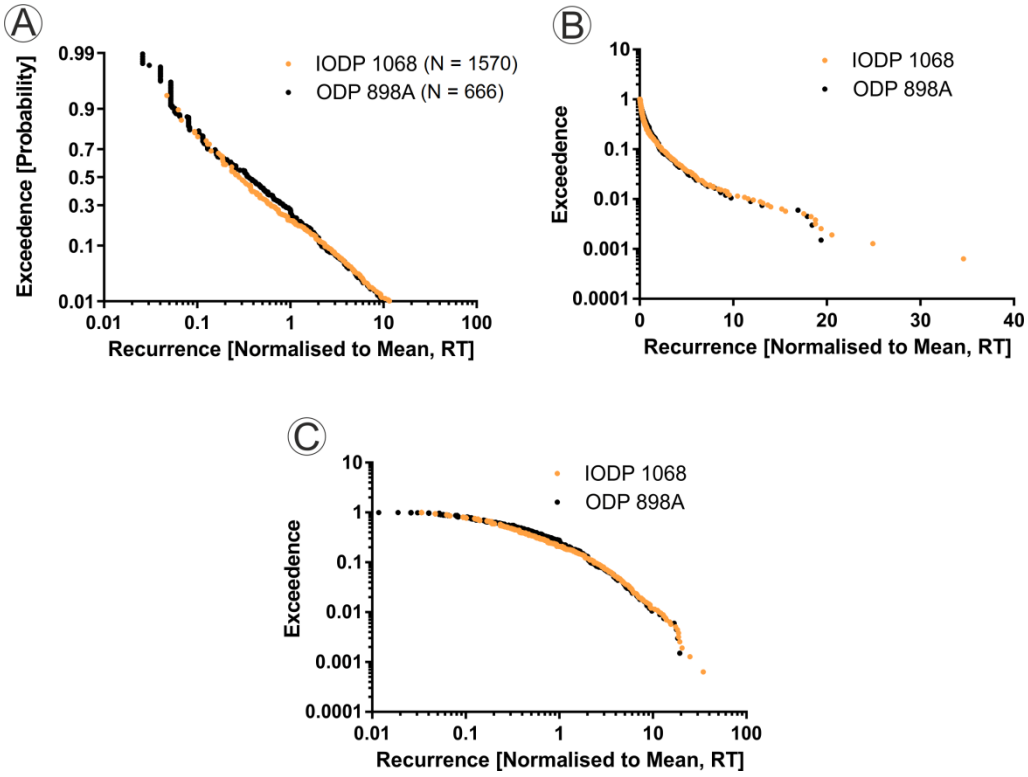

Figure 4.4: Exceedance plots of the ODP Hole 898A dataset compared with the lognormally distributed recurrence dataset from IODP 1068 (Clare, 2015; Clare et al., 2015). Normalised recurrence data is plotted on a log-probability plot (A), a linear-log plot (B), and a log-log plot (C). The ODP Hole 898A data distribution shows considerable agreement with the IODP 1068 distribution, indicating a similar form.

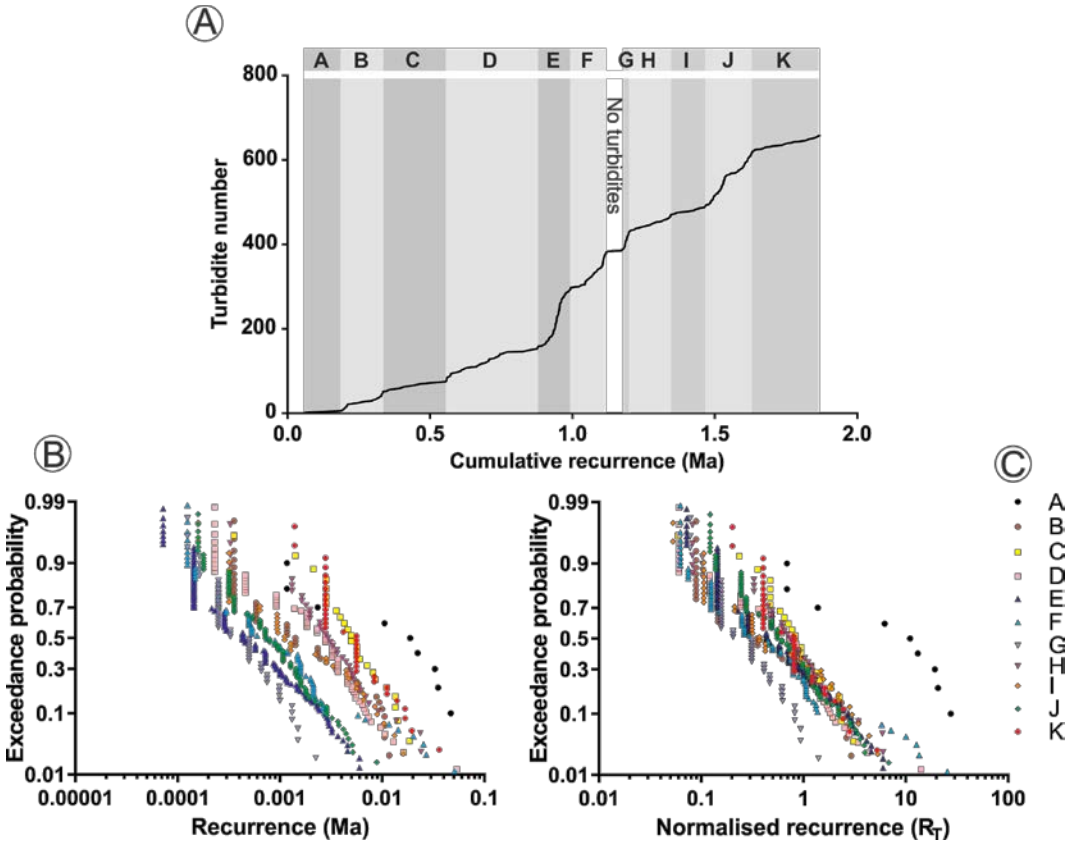

Figure 4.5: A: subdivisions of the ODP Hole 898A data based on changes in the slope of cumulative recurrence. B and C: Log-probability plots of recurrence and normalised recurrence data respectively. Both show a consistent trend for all data subdivisions except A and G.

4.4.4 The influence of sea level on turbidite recurrence and thickness at ODP Hole 898A

Due to the temporal resolution of the sea level curve it is difficult to visually identify any correlation between individual cycles of sea level change and turbidite recurrence. Plotting the curves of cumulative turbidite age and cumulative turbidite thickness against a global eustatic sea level curve shows a change in both trends between 0.9 - 1.1 Ma (Fig. 4.6). This change coincides with the mid-Pleistocene transition between 0.9 - 1.2 Ma; when long-periodicity (>0.1 Ma), high-amplitude glacial variability began to emerge (Mudelsee and Schultz, 1997; Clark et al., 2006). Prior to the mid-Pleistocene transition the average recurrence rate of canyon-flushing was 3,007 years, and the average turbidite thickness was 17.9 cm (Fig. 4.6). The coefficients of variability for turbidite recurrence and thickness before the mid-Pleistocene transition are 149 and 92 respectively (Fig. 4.7). The coefficient of variation is a dimensionless ratio of the standard deviation to the mean, and is a measure of the variability in a data set.

During the mid-Pleistocene transition between 0.9 - 1.2 Ma the average turbidite recurrence decreased to 2,188 years while the thickness increased to 33.7 cm. There is a considerable fall in sea level to -100 m towards the end of the mid-Pleistocene transition that is associated with the lowest turbidite recurrence intervals contained within the ODP Hole 898A record (Fig. 4.6). The coefficients of variability for turbidite recurrence and thickness during the mid-Pleistocene transition are 322 and 155 respectively, indicating higher variability than the period before the onset of the transition.

After the mid-Pleistocene transition, between 0 - 0.9 Ma, turbidite recurrence re-stabilised at an average duration of 2,857 years; slightly shorter than before the mid-Pleistocene transition. The average turbidite thickness for this period is 13.7 cm; although turbidite thickness remained consistently higher than before the mid-Pleistocene transition until ~0.5 Ma (Fig. 4.6). Box and whisker plots of turbidite recurrence and thickness illustrate increased variability in both relative to the pre-transition values (Fig. 4.7). The coefficients of variability for turbidite recurrence and thickness during the mid-Pleistocene transition are 191 and 106 respectively, indicating higher variability than the pre-transition period (Fig. 4.7). Kolmogorov-Smirnov and Mann-Whitney tests indicate the populations of both turbidite recurrence and thicknesses are significantly different before and after the mid-Pleistocene transition (P = <0.05).

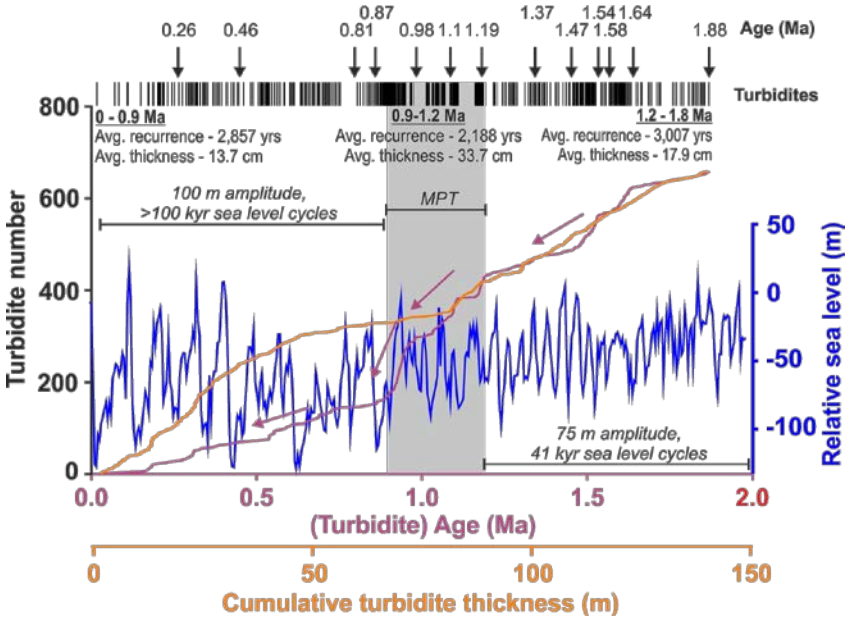

Figure 4.6: Turbidite ages and thicknesses from ODP Hole 898A (N = 666) plotted against the sea level curve (blue) of Miller et al., 2005. The purple line is the cumulative age of turbidites, and the orange line is the cumulative turbidite thickness. There is a significant decrease in the average turbidite recurrence and an increase in the average thickness during the mid-Pleistocene transition. Following the onset of >0.1 Ma glacial cycles at 0.9 Ma the average turbidite recurrence increased and the average thickness decreased relative to the pre-transition values.

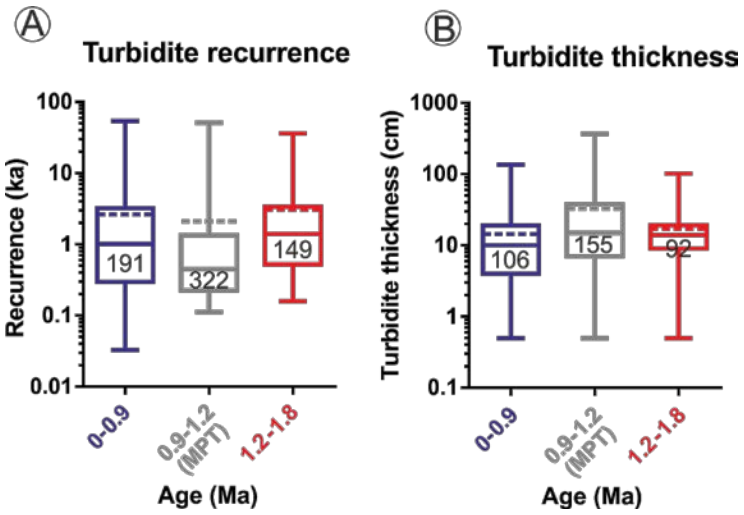

Figure 4.7: A box and whisker plot illustrating the differences in turbidite recurrence (A) and turbidite thickness (B) before (red) and after (blue) the onset of 100 ka sea level cycles following the mid-Pleistocene transition. Boxes show the upper and lower quartiles, whiskers show maximum and minimum values, the solid line in the box shows the median value, and the dashed line shows the average recurrence. Recurrence decreases following the mid-Pleistocene transition, with the median, mean and upper/lower quartile values lower than values observed before the mid-Pleistocene transition. The same decreases in the median, mean and upper/lower quartile values are observed in the turbidite thickness data following the mid-Pleistocene transition. Values inset in quartile boxes are coefficients of variation.

Given the log-normal distribution form of the turbidite recurrence data (Fig. 4.4), a log transform of the data is required to test the influence of eustatic sea level using linear regression (Manning, 1998; Limpert et al., 2001; Gustavsson et al., 2014). The p-value (<0.05) of the log-linear model indicates that we can reject the null hypothesis that sea level does not influence turbidite recurrence (Fig. 4.8A). Another method of analysing the strength of a regression model is viewing the model residuals. Residuals are defined as the difference between the observed and fitted response data values within the log-linear model. An ideal model fit would have a purely random and non-systematic distribution of residual values (Lin et al., 2002). A quantile-quantile (Q-Q) plot of residuals is a visual check to test whether the data satisfy the distributional assumption in a regression model. While the spread of residuals (Fig. 4.8B) and the good fit on a Q-Q plot (Fig.

4.8C) in this model might indicate a good fit to the data, the low correlation coefficient (R^2 = 1.9%) reveals that the majority of the variance in recurrence intervals cannot be explained by eustatic sea level.

The low p-values from the Cox proportional hazards model indicate that we cannot reject the null hypothesis that turbidite recurrence does not correlate with sea level (Table 4.1). However, the hazard coefficient indicates only a small (< 1%) change in the recurrence of turbidity currents in response to a 1 m change in sea level (Table 4.1). Both the rate of sea level change (first derivative) and sea level combined with its first derivative are not significant in either the linear or the Cox proportional hazards models (Table 4.1). The Hurst exponent for the turbidite record ODP Hole 898A calculated from rescaled range analysis of recurrence is 0.55. This value indicates the data display little to no serial time dependence, and are non-systematic.

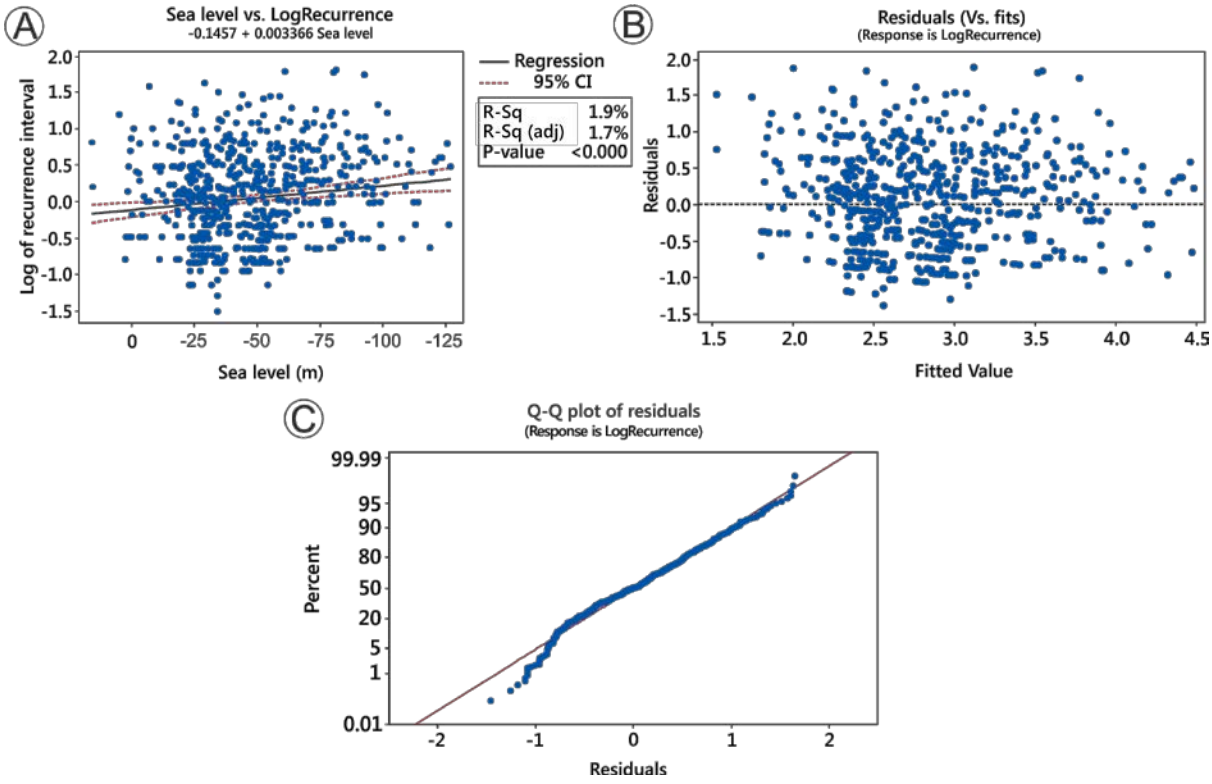

Figure 4.8: Results of the linear model of log-transformed turbidite recurrence with sea level as the explanatory variable. The fitted line plot (A) shows a large amount of variance within the data, indicating sea level is a poor explanatory variable. The residual plot (B) and Q-Q plot (C) show that the model provides a good fit for the data. However, the model has poor explanatory power due to the low R^2 value, and sea level cannot be implicated as a significant control on turbidite recurrence.

Loglinear model			
Explanatory variable	P-value	Regression coefficient	Correlation coefficient (R-sq)
Sea level	<0.005	0.003	1.9
First derivative of sea level	0.42	0.0002	*
Sea level + First derivative	0.939	-3.518 x 10-7	*

Cox Proportional Hazards Model				
Explanatory variable	Likelihood [p]	Wald [p]	Logrank [p]	Hazard coefficient
Sea level	0.0085	0.0088	0.0087	1.004
First derivative of sea level	0.1472	0.1453	0.1453	1
Sea level + First derivative		0.3645		1

Table 4.1: Summary table of the results of the linear model and Cox proportional hazards models (PHM). Sea level appears to be significant in the linear model (p = <0.000), but the regression and correlation (R^2) coefficients are low. Similarly with the Cox PHM the p-value is significant, but the hazard coefficient only indicates a <1% change in the hazard. This indicates minimal change in recurrence in response to sea level. Neither the change in sea level (first derivative), nor the combination of sea level and its derivative (rate) are significant in either linear or proportional hazards models. * = *Testing the rate (first derivative) of sea level against turbidite recurrence was done using a generalised linear model. This method is similar to the log-linear model except no correlation coefficients are generated.*

4.5 Discussion

The next section will discuss the influence of climatically-driven sea level changes on canyon-flushing within Nazaré Canyon. We will also discuss the significance of a lognormal distribution of turbidite recurrence for determining the triggers of canyon-flushing events.

4.5.1 Are all turbidites the result of canyon-flushing?

Before discussing eustatic sea level control on canyon-flushing it is important to determine whether all of the turbidites present in core ODP Hole 898A are the result of canyon-flushing. Canyon-flushing events can be described as the erosion of unconsolidated sediments within a submarine channel by turbulent or cohesive sediment gravity flows, often triggered by sediment failures or ignitive density flows, which then deposit material on slope fans and distal basin plains (Piper and Normark, 2009). The flushing of submarine canyons generally requires that large volumes of

unconsolidated sediment are available for remobilisation by density currents, or turbulent or cohesive sediment gravity flows. The sediment within the Nazaré Canyon must be recharged over time by littoral, nepheloid, hemipelagic, and density and gravity flow processes (de Stigter et al., 2002; Oliveira et al., 2007; Masson et al., 2011a). The rate of this sediment recharge is likely an important factor in canyon flushing. However, decreases in the frequency of turbidity currents that fill the Nazaré canyon do not appear to affect the recurrence of canyon flushing, suggesting the relationship between flushing and recharge is not linear (Allin et al., 2016).

Precise criteria for identifying canyon-flushing events in the depositional record vary, but sediment volumes of >0.2 km^3, the presence of erosional hiatuses within canyons and channels, and lateral continuity within a canyon-fed basin have been suggested (Paull et al., 2005; Talling et al., 2007a; Piper and Normark, 2009; Masson et al., 2011b; Talling, 2014). Using only a single core (ODP Hole 898A) in the Iberian Abyssal Plain makes determining turbidite volume or lateral extent impossible. The ODP Hole 898A core is from a similar water depth (5270 m) and a comparable distance (>50 km) from the Nazaré Canyon mouth as the JC27-51 site described in Allin et al. (2016; Fig. 4.1). The recurrence intervals and thicknesses of turbidites in ODP Hole 898A are also similar to those observed in distal Iberian Abyssal Plain core JC27-51, shown by Allin et al. (2016) to be canyon flushing events. Thus, we infer that the majority of turbidites in the ODP Hole 898A record are the result of canyon-flushing turbidity currents.

4.5.2 Does eustatic sea level affect canyon-flushing?

The role of sea level as an important control on the development of many deep-sea sedimentary systems is well documented (Vail et al., 1977; Shanmugam and Moiola, 1982; Posamentier et al., 1991; Piper and Savoye, 1993; Lebreiro et al., 1997; Ducassou et al., 2009). This includes turbidity currents that fill submarine canyons (Lebreiro et al., 2009; Covault and Graham, 2010). However, the role of eustatic sea level changes in controlling canyon-flushing events in the Nazaré Canyon is less clear (Allin et al., 2016). Here, the statistical analyses reveal little correlation between sea level and the recurrence of turbidites in the Iberian Abyssal Plain (Fig. 4.8 and Table 4.1). However, the onset of the mid-Pleistocene transition at ~1.2 Ma is associated with a change in both the recurrence rate and thickness of turbidites.

The mid-Pleistocene transition is a globally recognised climatic shift from short-periodicity, low-amplitude glacial cycles into long-periodicity, high-amplitude glacial cycles that occurred between 0.9 - 1.2 Ma (Mudelsee and Schultz, 1997; Clark et al., 2006). Prior to 1.2 Ma turbidite recurrence is relatively stable, as is the thickness of turbidites (Fig. 4.6). Sea level before 1.2 Ma fluctuated with a 41 ka periodicity, had <75 m amplitude, and had lowstands that persisted for only 5,000 - 15,000 years. Following the mid-Pleistocene transition the periodicity in sea level cycles increased to >100,000 years, while the amplitude increased to >100 m and lowstands persisted for over 20,000 years (Fig. 4.6; Shackleton et al., 1990; Mudelsee and Schultz, 1997; Paillard, 1998; Head and Gibbard, 2005;Miller et al., 2005; Clark et al., 2006). Sequence stratigraphic models predict that sea level lowstands shift sediment deposition towards the shelf-edge and promote increased deep-sea fan development (Posamentier et al., 1991). The mid-Pleistocene shift from <75 to >100 m sea level amplitudes is recognised in seismic surveys on the Iberian, Mediterranean, and Moroccan Margins, where it corresponds to the onset of thick, notably cyclic sediment deposition (Ercilla et al., 1994; Llave et al., 2001; Hernández-Molina et al., 2002; Le Roy et al., 2014). There would have been an increase in sediment availability on the continental shelf after the increase in the amplitude of sea level variability associated with the mid-Pleistocene transition. Therefore it might be expected that large-scale canyon-flushing events in Nazaré Canyon would increase after the mid-Pleistocene transition.

Despite the increased periodicity and amplitude of sea level variability after the mid-Pleistocene transition, the 2,857 year average recurrence interval of turbidites was similar to the pre-transition average of 3,007 years; albeit with more variability in recurrence values (Figs. 4.6 and 4.7A). Furthermore, turbidites in the Iberian Abyssal Plain are on average thinner after the mid-Pleistocene transition in spite of the predicted increase in sediment delivery due to greater continental shelf exposure (Fig. 4.7B). This suggests that the recurrence rates and sediment volumes of canyon-flushing events are largely independent of consistent eustatic sea level amplitude and periodicity, but are associated with changes in sea level amplitude and periodicity.

The most dramatic increase in the recurrence rate of canyon flushing broadly coincides with the lowest sea level in the last 10 million years, beginning at 0.9 Ma (Fig. 4.6; Miller et al., 2005). This

initial sea level fall would have exposed a large portion of the Iberian continental shelf not previously subjected to sub-aerial weathering, resulting in a considerable basin-ward flux of sediment (Fig. 4.1). Following the onset of >100 ka sea level cycles the system reached a new equilibrium state in which canyon flushing frequency and sediment volume are only slightly lower than the pre-1.2 Ma values (Figs. 4.6 and 4.7).

4.5.2.1 Sources of uncertainty in age-depth modelling and statistical analyses

The age model used to estimate the recurrence interval of turbidites is based on two main assumptions: 1) continuous hemipelagic accumulation between age datums and 2) largely non-eroding turbidity currents. While there is evidence that hemipelagic sedimentation in the Iberian Abyssal Plain is relatively consistent over glacial-interglacial timescales, there is likely to be some variability in hemipelagic sedimentation rate that is not captured due to the limited number of age datums (Lebreiro et al., 2009; Gràcia et al., 2010; Clare et al., 2015; Allin et al., 2016). The age datums that underpin the model are subject to depth uncertainty in the ODP Hole 898A core, with some having hemipelagic depth uncertainty of up to ±50 cm (Fig. 4.2). This is due to uncertainty in the precise position of first and last occurrences of key coccolith species. The age uncertainties of the datums are much more variable (Milkert et al., 1995a). Error on biostratigraphic datums within the late-Quaternary are conservatively taken to be ±10,000 years (Hunt et al., 2013a), although this error is most likely greater beyond 100 ka.

Turbidity currents within abyssal basins can be non-erosional, but some may contain higher concentrations of sediment and subsequently erode the seafloor (Weaver and Thomson, 1993; Thomson and Weaver 1994; Weaver, 1994; Wynn et al., 2002; Gutiérrez-Pastor et al., 2009; Gràcia et al., 2010; Allin et al., 2016). Basal erosion has the potential to bias the age model by removing hemipelagic sediment as well as older turbidites; although Clare et al. (2015) demonstrated that error due to erosion does not affect the distribution form of recurrence intervals. In addition to uncertainties in the hemipelagic accumulation rate, the exact position of the boundaries between turbidites and hemipelagic sediment can also be unclear. The hemipelagic age model relies on accurately identifying the boundary between the two sediment types in order to estimate the amount of hemipelagic accumulation between age datums, as well as the age of turbidites through

interpolation. Bioturbation by infaunal organisms can mix sediment types and make defining this boundary difficult. In order to account for this any bioturbated boundaries between turbidites and hemipelagite are taken to be where both sediment occurs in equal proportions. Bioturbation can therefore result in additional uncertainty in the age of turbidites and in the statistical analyses.

The results of the log-linear model and Cox proportional hazards model indicate that neither sea level nor the rate of sea level change is a dominant control on the recurrence intervals of canyon-flushing turbidity currents (Table 4.1). However, the sea level curve of Miller et al. (2005) has a 5,000 year resolution, which is sufficient to capture broad glacial-interglacial variability, but may be too coarse to capture any statistical correlation with recurrence intervals (Fig. 4.6). Furthermore, the Miller et al. (2005) sea level curve is a global eustatic sea level curve, and may not capture local variability associated with isostatic and tectonic influences (Shanmugam and Moiola, 1982; Stow et al., 1984; Covault and Graham, 2010). Other sea level curves covering the Pleistocene exist, but are either too short to cover the full length of the ODP 898A record (Rohling et al., 2009), or too coarse to provide any meaningful comparison (Haq and Schutter, 2008). The uncertainties associated with age datums have potentially imparted error onto the recurrence intervals of turbidites, masking the influence of sea level change. However, positions of the age datums within the core do not seem to effect the clustering of turbidites, implying the clusters are real rather than an artefact of the age-modelling (Fig. 4.6). Thus the effect of the mid-Pleistocene transition on turbidite recurrence can also be considered real.

4.5.3 Were earthquakes responsible for increased canyon flushing during the mid-Pleistocene transition?

The south-western Iberian Margin is tectonically active as a result of the compressional rotation associated with the Azores–Gibraltar fracture zone (Buforn et al., 1988; Borges et al., 2001; Zitellini et al., 2004; Custódio et al., 2015). Several turbidites observed in the Tagus and Horseshoe basins to the south of the Iberian Abyssal Plain are proposed to have been caused by regional earthquakes (Gràcia et al., 2010; Masson et al., 2011). However, it is not clear whether earthquakes trigger canyon-flushing events in Nazaré Canyon (Allin et al., 2016). It has been proposed that eustatic sea level cycles affect the flexural stress of faults proximal to the coastline and thus can

increase earthquake generation (Brothers et al., 2013). It is therefore possible that the greater sea level variability associated with the mid-Pleistocene transition increased the frequency of earthquakes, and thus increased the frequency of canyon flushing during this period.

Flexural stress modelling in several settings worldwide has suggested that offshore fault activity is inhibited during times of sea level lowstand, while onshore fault activity is promoted (Luttrell and Sandwell, 2010). Offshore fault activity responsible for triggering large flushing turbidity currents in the adjacent Tagus and Horseshoe basins is unlikely to be a trigger of canyon flushing in Nazaré Canyon (Allin et al., 2016). Earthquakes originating from onshore faults are proposed to be more likely triggers of canyon flushing in Nazaré Canyon (Rockwell et al., 2009). However, these onshore faults have a low likelihood of reactivation as a result of sea level change (Neves et al., 2015). Therefore it is difficult to implicate seismicity as a cause of increased canyon flushing during the mid-Pleistocene transition.

4.5.4 Significance of a lognormal distribution

Lognormal distributions are typically observed where the mean value is low and where large variance is observed in the data (Limpert et al., 2001). A lognormal distribution of data can result from a lognormally distributed random variable, but more likely results from multiplication of the probabilities of two or more independent random variables (Limpert et al., 2001; Grönholm and Annila, 2007; van Rooij et al., 2013). A theoretical example of lognormal multiplicative interactions between independent probabilities after Clare et al. (2015) can be seen in equation 1:

$$P_{(\text{TC at ODP Hole 898A site})} = P_{(\text{trigger generates LS})} \times P_{(\text{LS disintegrates to TC})} \times P_{(\text{TC reaches ODP Hole 898A})} \quad (1)$$

where P is probability, LS represents landslide, and TC represent turbidity current. Previous work on the distribution form of basin turbidite recurrence intervals has revealed exponential distributions in basin records in 5 locations (Clare et al., 2014; Allin et al., 2016). This exponential distribution is indicative of temporally random behaviour resulting from an exponential trigger, multiple input sources, or as a result of multiplicative processes.

The lognormal distribution of turbidite recurrence intervals observed in ODP Hole 898A is fundamentally different from the exponential distribution observed in these basins, including more distally in the Iberian Abyssal Plain (Fig. 4.9). The lognormal distribution of turbidite recurrence intervals observed in core IODP 1068 between 48 - 65 Ma suggests that the distribution form of turbidite recurrence has remained consistent in this part of the Iberian Abyssal Plain through geological time (Fig. 4.4; Clare et al., 2015). A lognormal distribution of turbidite recurrence likely results from at least one temporally-ordered process; although time-dependence is not a fundamental characteristic of a lognormal distribution. However, the ODP Hole 898A recurrence data during the last 1.8 Ma cannot be correlated confidently with sea level using linear or Cox regression methods. Rescaled range analysis also shows no temporal ordering within the data. The absence of any statistically significant sea level control on turbidite recurrence implies that a lognormal distribution is not a direct result of sea level influence and may not be indicative of temporal ordering.

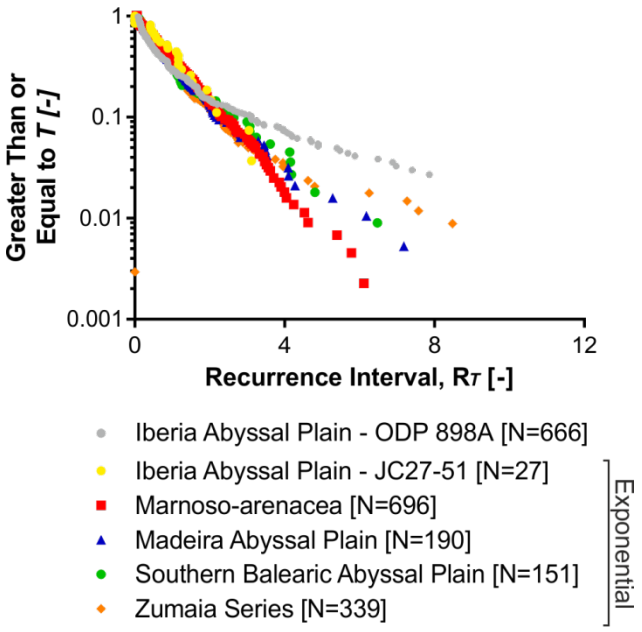

Figure 4.9: Comparison of exceedance plots showing recurrence data from several basin turbidite records worldwide. The lognormal distribution of recurrence data from ODP Hole 898A is fundamentally different from the exponential form observed in many other distal basin records. Recurrence data are from Clare et al. (2014) and Allin et al. (2016).

4.5.5 Origin of a lognormal distribution

We propose three hypotheses to explain the lognormal distribution of turbidites at site ODP Hole 898A: **1)** variable turbidity current run-out distance is biasing the depositional record. This variable run-out distance has resulted in a different distribution at site ODP Hole 898A than the exponential form observed at the more distal JC27-51 site. **2)** The distribution may have resulted from a combination of turbidity currents with different triggering mechanisms originating from Nazaré Canyon, leading to an overprinting of records. **3)** The Oporto and Aveiro Canyons may have been sources of turbidity currents during times of sea level lowstand, resulting in the record at ODP Hole 898A representing turbidity currents sourced from three different areas on the continental margin. Here we will discuss the three hypotheses.

4.5.5.1 Variable turbidity current run-out distance is biasing the depositional record

Long-term sedimentary archives, like those found in abyssal plain settings, can store records (signals) of climatic or environmental variability through time. One of the ways in which the signal of sea level variability is recorded in the deep sea stratigraphic record is through the deposition of sediment via mass transport processes (Romans and Graham, 2013; Romans et al., 2016). This is because sea level change can limit, or otherwise increase sediment supply to the shelf-edge where mass transport processes dominate (Stow and Piper, 1984; Posamentier et al., 1991; Covault and Graham, 2010; Covault et al., 2010). However, the fidelity of such a record is dependent of the ability of sediment transport processes to reach and deposit at core sampling locations.

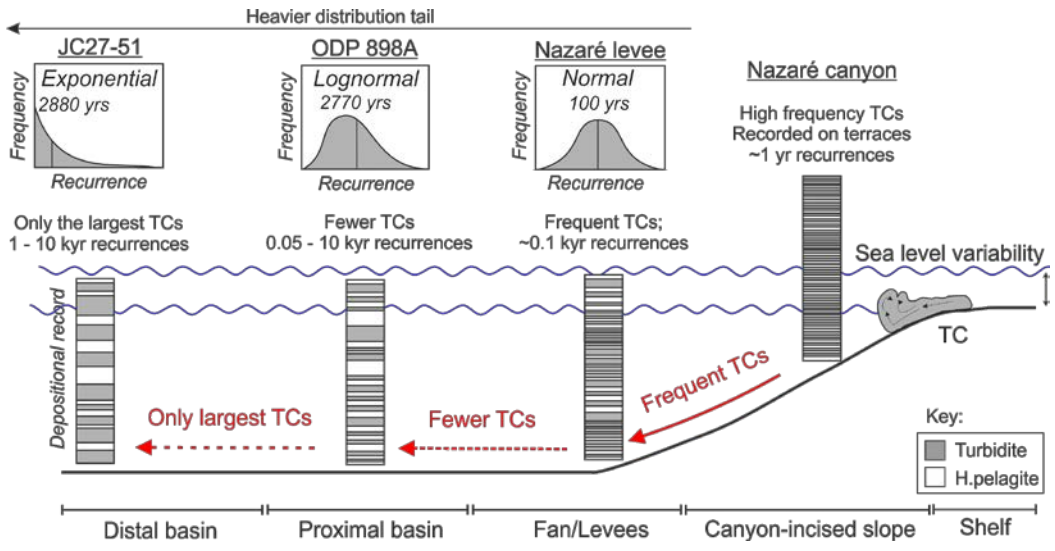

Figure 4.10: Model illustrating how the distribution form of turbidite recurrence may change with increasing distance from sediment source in the Iberian Abyssal Plain. At the mouth of the canyon the distribution is normal reflecting the influence sea level (Allin et al., 2016). In the proximal basin at site ODP Hole 898A fewer of the small, frequent turbidity currents are able to reach this site, biasing the depositional record towards turbidites with longer recurrences. None but the largest turbidity currents are able to reach the distal basin resulting in an exponential distribution. Values above probability distributions are the average recurrence interval; Nazaré levee and JC27-51 data from Allin et al. (2016). TC = turbidity current.

Turbidite recurrence intervals within the Nazaré Canyon have been suggested to conform to a normal distribution resulting from the dominant control of eustatic sea level (Allin et al., 2016). However, turbidite recurrence intervals in the distal Iberian Abyssal Plain site JC27-51 conform to an exponential or time-independent distribution (Fig. 4.1; Allin et al., 2016). This basic difference in the distribution form of recurrence intervals is likely due to more distal locations in the Iberian Abyssal Plain receiving fewer turbidity currents. This is because only a small number of turbidity currents have the sediment volumes to achieve long run-out distances (Fig. 4.10). Additionally, debris flow deposits in core JC27-51 (Allin et al., 2016) suggest that the transformation and collapse of erosive flows due to choking by sediment entrainment may also act to limit the run-out distance of canyon flushing events (Amy et al., 2006; Talling et al., 2007a; Talling et al., 2012). Core site ODP Hole 898A with a lognormal distribution is more proximal to the mouth of Nazaré Canyon than the most distal JC27-51 site (Fig. 4.1) that displays an exponential distribution of turbidite recurrences. It is possible that the skewed lognormal distribution in ODP Hole 898A results from more turbidity currents reaching this site than the more distal JC27-51 site (Fig. 4.10).

We might assume that turbidites with small recurrences (<500 yrs) or thicknesses (<10 cm) within the ODP Hole 898A record do not extend to the distal JC27-51 site due to limited sediment availability, thus accounting for the exponential distribution observed. Manipulation of the lognormal ODP Hole 898A turbidite recurrence data indicates that the distribution form can be altered by filtering out turbidites randomly, or removing those with the smallest recurrences and thicknesses (Cohen, 1991). However, an exponential distribution cannot be accurately recreated using this method, suggesting that run-out distance may not be the only factor affecting the distribution form of turbidite recurrences across the Iberian Abyssal Plain.

4.5.5.2 Combination of turbidity currents with distinct triggers

The Iberian Margin is prone to large-magnitude (Mw >7) earthquakes due to the presence of the Azores-Gibraltar fracture zone and its associated faults (Custódio et al., 2015). These large-magnitude earthquakes (~2,000 year recurrence) have been invoked as triggers of canyon-flushing turbidity currents that deposit large-volume turbidites in the Tagus and Horseshoe Abyssal Plains, south of the Iberian Abyssal Plain (Fig. 4.1) (Gràcia et al., 2010, Masson et al., 2011). The role of earthquakes in triggering large canyon-flushing turbidity currents in the Nazaré Canyon is less clear. Only 3 out of the 6 turbidites in the distal Iberian Abyssal Plain during the last 20,000 years can be correlated with seismoturbidites in adjacent basins (Grácia et al., 2010; Masson et al., 2011; Allin et al., 2016). This makes it difficult to infer a seismic trigger for turbidites in the Iberian Abyssal Plain. If we assume that a limited number of turbidites in ODP Hole 898A are earthquake-triggered, then there is a separate environmental signal that may overprint any signal of sea level. The recurrence intervals of turbidites within Nazaré Canyon appear to be normally distributed (Allin et al., 2016). Large magnitude (Mw >7) earthquakes capable of triggering large (>1 km^3) slope failures can approximate several different distribution forms of recurrence depending on the location and magnitude of earthquakes that are considered (Hagiwara, 1974; Gardner and Knopoff, 1974; Kagan and Jackson, 1991; 2000). The combinative effect of normally distributed turbidite recurrences, and turbidites that are earthquake-triggered could result in a distinct, possibly lognormal distribution form (Fig. 4.11A). However, this assertion is difficult to test as it is impossible to discriminate between seismically and non-seismically triggered turbidites in core ODP Hole 898A (Sumner et al., 2013).

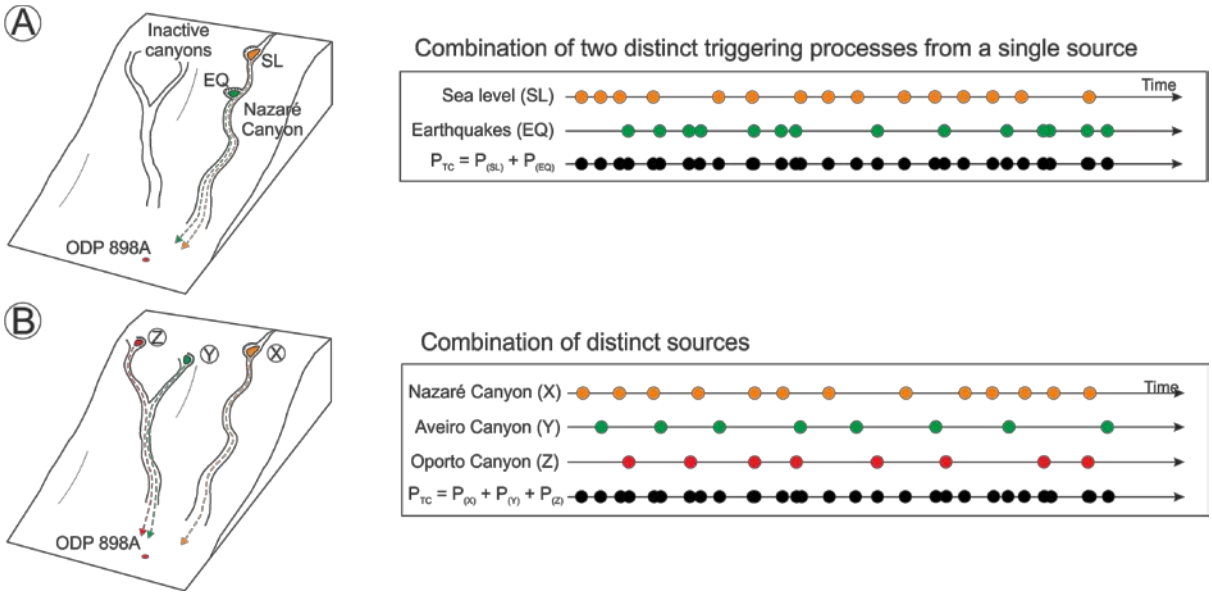

Figure 4.11: Schematic cartoons and abacus plots illustrating two of the different scenarios that might result in a lognormal distribution of turbidite recurrence. A: different triggering mechanisms operating within the Nazaré Canyon. B: a combination of different sources of turbidites along the Portuguese Margin. P is probability and TC is turbidity current.

4.5.5.3 Multiple sources of turbidity currents

In addition to the Nazaré Canyon, there are two smaller canyons that feed into the Iberian Abyssal Plain; the Oporto and Aveiro Canyons. Core site ODP Hole 898A is located 70 km away from where the Oporto and Aveiro Canyons reach the Iberian Abyssal Plain (Fig. 4.1). These canyons do not have heads that connect to the present-day shoreline, and are considered to be largely inactive in the present day due to restricted sediment supply (Guerreiro et al., 2007; 2009). However, littoral transport may have fed the heads of these canyons during lowstand conditions, similar to the Nazaré Canyon today. This renewed littoral sediment supply would have resulted in increased instability and turbidity current generation, similar to other such stranded canyons (Stow and Piper, 1984, Posamentier et al., 1991; Covault and Graham, 2010; Paull et al., 2014). Therefore, it is possible that the lognormal ODP Hole 898A record represents a mixing of turbidites with more than one source area (Fig. 4.11B). However, it has been observed that multiple, distinct sources of turbidity currents that feed into basin plains typically result in exponential distributions of turbidite recurrence, making this scenario less likely (Clare et al., 2014).

The western slopes of Galicia Bank feature mass transport deposits (MTDs) and submarine channel systems (Fig. 4.1), indicating that some turbidites in core ODP Hole 898A may not have originated from the Nazaré Canyon (Hernández-Molina et al., 2009). However, sediment supply to the Galicia Bank area is largely pelagic, and turbidites derived from this pelagic sediment are calcareous-rich and readily distinguishable from those of terrigenous origin (Milkert et al., 1996b; Alonso et al., 2008). In core ODP Hole 898A less than 5% of turbidites are calcareous and so Galicia Bank can be ruled out as a significant source of turbidites (Milkert et al., 1996b).

4.5.6 Climate change and geohazard implications

Previous statistical work has suggested that global eustatic sea level change does not affect the recurrence rates of large landslide-triggered turbidity currents (Urlaub et al., Clare et al., 2014). This study demonstrates little to no association between eustatic sea level variability and canyon flushing in Nazaré Canyon. While these canyon-flushing events do not pose the same tsunami risk as open slope failures, they have the potential to break submarine telecommunication cables and damage hydrocarbon infrastructure (Carter et al., 2012a; 2014). Canyon flushing should therefore be incorporated into risk models for infrastructure development. The lognormal distribution provides a probability density function from which hazard models can be derived. However, given the lack of any apparent eustatic sea level control on these canyon-flushing events, their recurrence rate may not change significantly due to future projected sea level rise.

4.6 Conclusions

Here we demonstrate that the recurrence rates and of canyon-flushing events within the Nazaré Canyon, as well as the thickness of their deposits, cannot be confidently correlated with eustatic sea level, and may be unaffected by it. Canyon-flushing recurrences and turbidite thicknesses are instead associated with changes in the periodicity and amplitude of eustatic sea level variability, such as during the mid-Pleistocene transition between 1.2 - 0.9 Ma. The increase in frequency and thickness of turbidites during the mid-Pleistocene transition is likely the result of increased subaerial exposure of the continental shelf and increased basin-ward sediment transport; although tectonic factors cannot be ruled out.

Chapter 4: Does eustatic sea level variability affect the flushing of submarine canyons?

Large volume turbidites in the Iberian Abyssal Plain conform to a lognormal distribution of recurrence over the last 1.8 Ma. A lognormal distribution of recurrence is thought to result from at least one time-dependent process. However, common statistical methods applied to the ODP Hole 898A record reveal no obvious influence of sea level change on turbidite recurrences. A persistent lognormal trend through time is potentially due to truncation of the depositional records because of distance from source; although multiple sources or turbidites and distinct triggering mechanisms (e.g. earthquakes) are also likely to be a factor. Statistical distributions of geohazard recurrences and their associated probability density functions are important for designing predictive hazard models. This work indicates that the distribution form of turbidite recurrence intervals can vary with sampling location. This presents considerable uncertainty when attempting to understand turbidity current triggers using statistical distributions that only allow us to make broad inferences about the governing dynamics of a sediment routing system.

Chapter 5: Tsunamigenic potential of large (>400 km^3), 'top-down' submarine landslides that fail in closely spaced stages

Summary:

The previous two chapters of the thesis have focussed on turbidity current frequency in the Nazaré Canyon and Iberian Abyssal Plain and the associated geohazards. This chapter shifts the focus onto very large (>100 km^3) submarine landslides on the Norwegian Margin. The Trænadjupet Slide is a >400 km^3 submarine landslide that originated from a glacial trough mouth fan approximately 4,000 years ago; although the available radiocarbon ages from the landslide scar deposits range from ~1,500 to ~4,000 calendar years BP. Recent research has demonstrated that the Trænadjupet Slide did not trigger a tsunami. Determining why such large landslides do not generate widespread tsunamis is important for regional geohazard assessment. This is also important because another large slide, the Nyk Slide, has originated from this section of the margin since the last glacial maximum. This chapter aims to:

1. Refine the age of the Trænadjupet Slide and identify possible triggers.
2. Determine how many slides have originated from the Trænadjupet area to estimate recurrence.
3. Understand whether the Trænadjupet Slide was bottom-up (retrogressive) or top-down (progressive).
4. Quantify the time gaps between the different stages of the Trænadjupet Slide. Both time gaps and top-down or bottom-up nature of submarine slides affects their tsunamigenic potential.

The age of the Trænadjupet Slide is refined here to between ~2,600 and ~3,400 cal BP. At least three slides have occurred on this section of margin. The absence of a widespread tsunami associated with the Trænadjupet Slide may be explained by its emplacement dynamics (e.g. speed, acceleration, or time gaps between stages of failure). Sediment cores 26, 29, 31, and 57 described in this chapter and the radiocarbon dates collected from them (Fig. 5.10) have contributed to a

Chapter 5: Tsunamigenic potential of large, top-down submarine landslides

manuscript submitted as: Mozzato, A., Allin, J.R., et al. Do large (>400 km^3) submarine landslides always trigger tsunamis, and what is their relationship to glacial cycles? Earth and Planetary Science Letters. The interpretation of the Trænadjupet landslide area used in this thesis (Fig. 5.1) originated from this manuscript, and is referenced accordingly. The remainder of this chapter is solely my own and has not formed part of or the basis for any other scholarly work or publication.

Abstract

Submarine landslides can be orders of magnitude larger than terrestrial landslides and are important because they sometimes generate exceptionally damaging and widespread tsunami. The 400 - 700 km^3 Trænadjupet Slide is the most recent very large (> 400 km^3) submarine landslide, and is one of the largest landslides yet mapped on Earth. It is located further along from the Norwegian Margin from the 3,000 km^3 Storegga Slide that produced a major tsunami, but no tsunami deposits are observed for the Trænadjupet Slide even along adjacent coastlines. Here, we employ newly acquired sediment cores, bathymetric, and radiocarbon datasets to refine the ages and better understand the timing and emplacement dynamics of the Trænadjupet Slide, and the older and underlying Nyk Slide. Understanding submarine landslide emplacement is important because it determines the magnitude of associated tsunami, whilst the timing helps to understand triggers and frequency. First, a more precise age for the Trænadjupet Slide is provided (2,600 - 3,400 cal BP) that coincides with a cluster of smaller landslides in Norwegian fjords, perhaps suggesting a common earthquake trigger. The Nyk Slide occurred between 18,600 and 20,900 cal B.P., whilst a third large failure older than 43,500 cal B.P is proposed. Second, it's demonstrated that the Trænadjupet Slide failed progressively from the top-down in at least three main stages. This is important because previous models for large submarine landslides have assumed that they failed from the bottom-up in a retrogressive fashion. Third, the Trænadjupet Slide failed in a series of stages that appear to be closely spaced in time (~few minutes). Multiple stages of failure are recorded by three headwalls and deposit lobes, but they produced only one graded turbidity current deposit in distal basins. This suggests that closely spaced failures generated turbidity currents that coalesced. This study therefore provides a new (top down) model for large submarine landslides that occur in multiple closely-spaced stages and are only weakly tsunamigenic.

5.1 Introduction

Large volume (>100 km^3) submarine landslides are some of the most important sediment transport mechanisms on Earth, and one slide can transport up to 300 times more sediment than all the world's rivers do in a year (Talling et al., 2007a; Korup, 2012). Submarine landslides with such prodigious volume have the potential to generate very damaging tsunamis for populated coastlines (Piper et al., 1988; Bondevik et al., 1997a; 1997b; Tappin et al., 2001; Bondevik et al., 2003). These slides also pose considerable risk to expensive subsea infrastructure such as pipelines and telecommunication cables (Piper et al., 1988; Carter et al, 2014; Pope et al., 2016). Several such large-volume submarine landslides have originated from the Norwegian Margin in the last 20,000 years. This includes the tsunamigenic Storegga Slide at approximately 8,000 years before present (BP), with a volume of 3,000 km^3 (Bugge et al., 1988; Bondevik et al., 1997a; Haflidason et al., 2004; Bryn et al., 2005).

Previous models for large, slope-parallel submarine landslides have proposed that they occur retrogressively from the bottom-up (Haflidason et al., 2004; Bryn et al., 2005; Masson et al., 2006; Masson et al., 2010). This retrogressive model posits that slides initially fail in deeper water, which accommodates multiple subsequent failures that propagate upslope and produce a staircase-like morphology. Importantly, the length of time between the stages of retrogression appears to have a marked effect on the generation of tsunamis, with shorter (< ~few minutes) time-spans between sub-stages of failure increasing tsunami wave amplitude (Haughen et al., 2005; Harbitz et al., 2006 Løvholt et al., 2015). The water depth and speed of the slope failures are also important because deep-water and slower landslides tend to produce smaller tsunamis than rapid landslides in shallow water (Haughen et al., 2005; Harbitz et al., 2014; Løvholt et al., 2015). Therefore, understanding the emplacement dynamics of large submarine slides is critically important for estimating their tsunami hazard.

The Trænadjupet and Nyk Slides are large-volume, lobate submarine landslides 700 km north of the Storegga Slide along the Norwegian Margin (Fig. 5.1; Kenyon, 1987; Dowdeswell et al., 1996; Laberg and Vorren, 2000a, Laberg et al., 2002a). Both these slides occurred on a glacigenic trough-

mouth fan that was active during Plio-/Pleistocene glaciations (Henriksen and Vorren, 1996; Laberg et al., 2002a; Dowdeswell et al., 2006). The more recent Trænadjupet Slide was previously dated at ~4,000 years BP and had a volume of between 400 - 700 km^3. This makes it one of the most recent large landslides yet mapped on Earth (Korup et al., 2010; Urlaub et al., 2013). The Trænadjupet Slide comprises 3 headwalls and 3 deposit lobes, which are inferred to indicate multiple retrogressive stages; although the time gaps between these retrogressive stages were previously unknown (Fig. 5.1; Laberg and Vorren, 2000a; Laberg et al., 2006; Mozzato et al., in review). Although the Trænadjupet Slide volume is ~20% of the Storegga Slide and is also inferred to be retrogressive, investigation has not revealed coeval tsunami deposits on adjacent coastlines in Norway or Scotland (Bondevik, 2002; Bondevik et al., 2003; 2005a; Mozzato et al., in review). To accurately determine the geohazard risk posed by large-volume submarine landslides it is important to understand why some generate damaging tsunamis while others do not.

AMS radiocarbon ages dating the Trænadjupet slide scar range from 1,111 - 4,056 cal BP (Fig. 5.1), while existing AMS radiocarbon ages of a turbidite in the Lofoten Basin place the slide between 3,200 - 5,200 cal BP (Laberg et al., 2002b; Haflidason et al., 2007; Mozzato et al., in review). Tsunami deposits have been observed in low-lying (<5 m) lakes on the Norwegian and Shetland Island coastlines that date to between 5,310 - 5,550 cal BP (Bondevik et al., 2005a). It is possible that these ~5,500 cal BP tsunami deposits on the Shetland Islands are the result of a tsunami caused by the Trænadjupet Slide. Alternatively, the Trænadjupet Slide may coincide with a widespread occurrence of fjord landslides on the Norwegian coastline between 2,800 - 3,200 cal BP, supporting an earthquake trigger (Bøe et al., 2012). Accurately determining the age, and thus the frequency of large submarine landslides is important for understanding their triggers and their widespread geohazard.

5.1.1 Aims

In this study we set out four principal aims: The first aim is to reduce the uncertainties on the age of the Trænadjupet Slide, and therefore test whether it coincides with ~5,500 cal BP tsunami deposits or fjord-landslides seen elsewhere between 2,800 - 3,200 cal BP. This will help determine whether the Trænadjupet Slide was tsunamigenic, and help identify possible triggers of the slide. The

second aim is to determine how many slides have occurred in this area. Two slides are known to have occurred during the last 20,000 years: the Trænadjupet and Nyk Slides, but here we aim to identify whether another older slide may have occurred. Determining the age and frequency of large submarine slides will inform hazard assessment. The third aim is to understand whether the Trænadjupet Slide was bottom-up (retrogressive) or top-down (progressive). Most previous models for large submarine landslides have assumed that they fail retrogressively, from the bottom up. This will contribute to the understanding of how the slide was triggered. The fourth aim is to ascertain whether distal turbidites in the Lofoten Basin record substantial time gaps between different stages of failure. The length of these time gaps is a crucial parameter in whether or not large submarine landslides are capable of generating tsunamis. This aim will help understand why no coeval tsunami deposits are observed on adjacent coastlines. Understanding the failure and emplacement dynamics of these large slides will provide important information for tsunami generation and propagation modelling, and thus the risk such prodigious landslides pose to North Atlantic coastlines.

5.2 Regional setting and previous work

The Trænadjupet Slide is located on the north-east side of the Vøring Plateau on the Norwegian continental margin. The headwall of the slide complex is located at the mouth of the Traenadjupet Cross-shelf Trough (Fig. 5.1). During Plio-/Pleistocene glaciations this trough was repeatedly filled by ice streams from continental ice sheets (Henriksen and Vorren, 1996; Laberg et al., 2002a; Dowdeswell et al., 2006). Sediment deposition from these ice streams during glacial periods resulted in very thick and rapid accumulations of glacigenic debris and stratified glacimarine sediments within the Trænadjupet Trough and on the Norwegian continental slope (Dahlgren and Vorren, 2003; Dowdeswell et al., 2006).

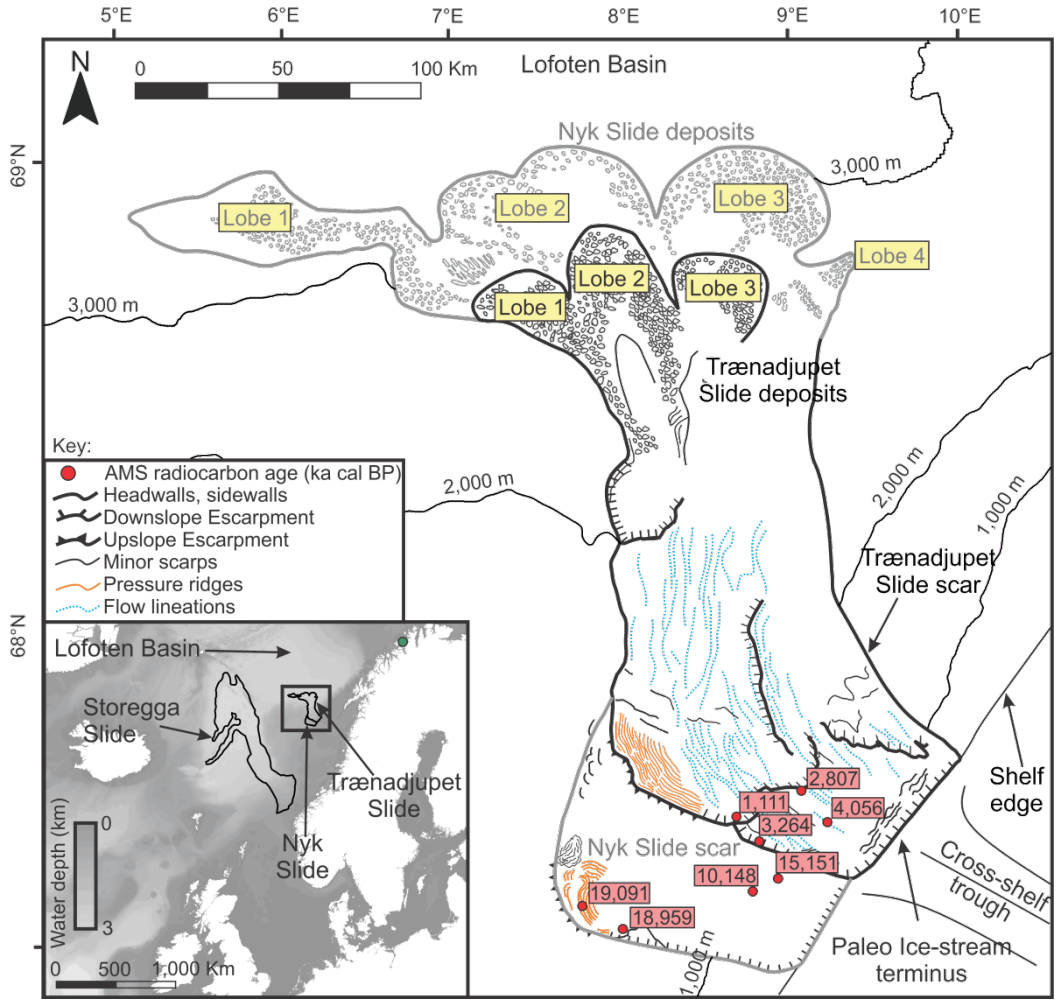

Figure 5.1: Map detailing the primary morphology of the Trænadjupet Slide Complex determined from bathymetry data from Mozzato et al. (in review) and TOBI data (Laberg and Vorren, 2000a; Laberg et al., 2002a). The Trænadjupet Slide is outlined in black, while the Nyk Slide is outlined in grey. Inset: location map showing the Trænadjupet Slide, and its position and scale relative to the Storegga Slide. The morphology of the Trænadjupet and Nyk Slides is adapted from Mozzato et al. (in review). Contours and inset bathymetry data from IBCAO Ver. 3 (Jakobsson et al., 2012). Red dots and labels are the locations of previously collected AMS radiocarbon ages (cal BP) of the oldest hemipelagic sediment draping the Nyk and Trænadjupet Slide scars (Laberg et al., 2002a; 2002b; Lindberg et al., 2004).

The total area affected by landsliding is approximately 14,000 km^2, including slide scars and associated deposits (Laberg and Vorren, 2000a). There are two primary slide scars documented within the slide area (Fig. 5.1). The younger of these is the Trænadjupet Slide scar that extends from 400 m down to 2200 m water depth (Laberg and Vorren, 2000a; Laberg et al., 2002a; Mozzato et al., in review). This Trænadjupet Slide scar covers an area of between 4,000 - 5,000 km^2 and has a headwall height of 100 - 120 m (Laberg and Vorren, 2000a). The trigger of the Trænadjupet Slide is not known, but seismicity due to isostatic rebound has been proposed (Laberg

et al., 2002a). Southwest of the Trænadjupet Slide is the slide scar of an older slide known as the Nyk Slide (Fig. 5.1). The Nyk slide scar extends from 400 m down to 1500 m water depth but is largely truncated by the presence of the more recent Trænadjupet scar, making its area and full depth range difficult to estimate (Lindberg et al., 2004). As with the Trænadjupet Slide, the trigger of the Nyk Slide is not well known, although high glacial sedimentation rates and the presence of weak, contouritic sediments are thought to have played a role (Lindberg et al., 2004).

The distal ends of both the Nyk and Trænadjupet Slides lie in the Lofoten Basin, and form a set of two lobate, stacked debris flow deposits (Fig. 5.1; Kenyon, 1987; Laberg and Vorren, 2000a, Laberg et al., 2002a; 2006; Mozzato et al., in review). Both stacked slide deposits consist primarily of large remobilised sediment blocks, some of which are over 300 m wide and 40 m high (Laberg and Vorren, 2000a; Mozzato et al., in review). The lower and more extensive of these debris flows is interpreted to be related to the Nyk Slide at approximately 19,000 cal BP (Fig. 5.1; Lindberg et al., 2004; Mozzato et al., in review). The Nyk Slide deposit comprises 4 distinct lobes and covers an area of approximately 8,000 km^2 (Fig. 5.1; Laberg and Vorren, 2000a; Laberg et al., 2002a). The upper and smaller of the two lobate debris deposits is interpreted as the result of the Trænadjupet Slide, which was previously thought to have been emplaced between 3,200 and 5,200 cal BP (Laberg et al., 2002a; 2006; Mozzato et al., 2016). We further refine this date in this contribution. The Trænadjupet Slide deposit is made up of 3 lobes that cover approximately 3,500 km^2; less than half the area of the underlying Nyk deposits (Fig. 5.1: Mozzato et al., in review). Downslope of the Trænadjupet Slide lobes, turbidites and debris flow deposits dated to Trænadjupet age have been described draping the older Nyk Slide deposits, and are also found more distally within the Lofoten Basin (Haflidason et al., 2007; Mozzato et al., in review).

5.3 Materials and methods

5.3.1 Bathymetric data

The swath bathymetry data were acquired on RV Pelagia cruise 64PE391 using a hull-mounted Kongsberg EM302 multibeam echo-sounder at 30 kHz. The area covered by this dataset is about 8000 km^2. This bathymetry data set is complemented with bathymetry data on the Norwegian

continental margin provided by the MAREANO Programme (www.mareano.no), and from cruise JR51.

5.3.2 Sedimentology

Sediment cores used in this study were collected aboard cruise 64PE391 using piston and multi-coring techniques. 12 Piston and multi cores were collected from both Trænadjupet and Nyk Slide deposits, and the Lofoten Basin (Fig. 5.2; Appendix F). Several pairs of piston and multi-cores have coincident locations. This is because the multi-cores capture the most recent sediments that are often lost during piston coring. Cores were visually logged for sedimentary grain size, lithology and sedimentary structures. MSCL-XYZ, MSCL-CIS, and MSCL-S core loggers were used to acquire magnetic susceptibility and gamma bulk density data, as well as core photographs. X-radiographs of the cores were acquired using an ITRAX-µXRF core scanner. Quantitative grain size data were obtained using a Malvern Mastersizer laser particle size analyser.

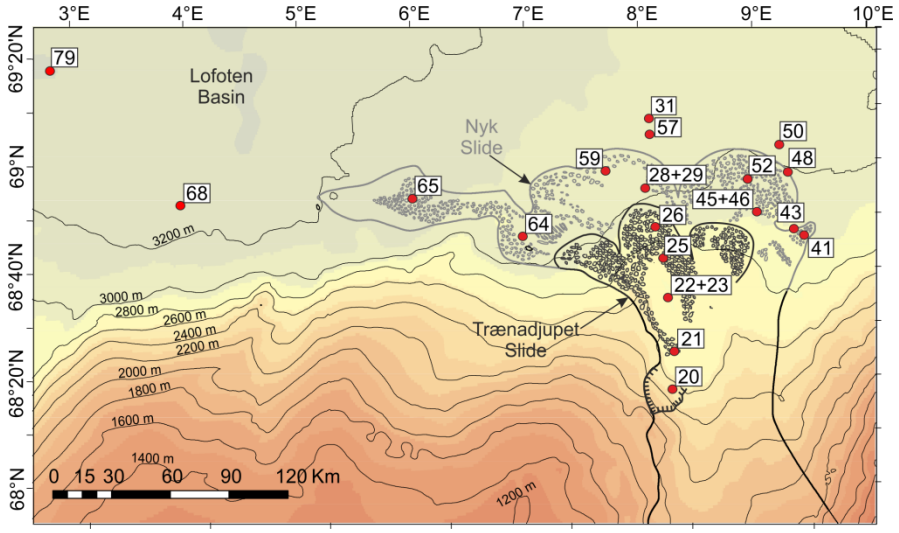

Figure 5.2: Map showing the locations of sediment cores used in this chapter (red dots). Black deposits are the Trænadjupet Slide, grey deposits are the Nyk Slide. Bathymetry data from IBCAO Ver. 3 (Jakobsson et al., 2012).

5.3.3 AMS radiocarbon dating of landslide events

Accelerator mass spectrometry (AMS) radiocarbon dating was carried out on 38 samples of foraminiferal carbonate from hemipelagic sediments to constrain the ages of turbidite emplacement, as well as the background sedimentation rate. Where possible the samples were monospecific using *Neogloboquadrina pachyderma (sin)*. Otherwise mixed assemblage samples

were used that also included *Globigerna bulloides, Globorotalia truncatulinoides and Orbulina universa*. Conventional radiocarbon ages were calibrated using the Marine13 curve with a ΔR reservoir correction value of 5 ± 25 years (Laberg et al., 2002b; Reimer et al., 2013). Conventional AMS ages are reported as 2-sigma ranges and as a median age (Table 5.1).

AMS radiocarbon samples were taken immediately above and below turbidites to get minimum and maximum ages of emplacement respectively. The upper boundaries of some turbidites were more difficult to determine, as bioturbation can mix turbidite mud with the overlying hemipelagic sediment. For dating turbidites with an unclear upper boundary AMS radiocarbon samples were collected where hemipelagic and turbidite sediments are in equal proportions. Where samples could not be collected at upper or basal turbidite boundaries, ages were interpolated or extrapolated using Oxcal p-sequence modelling (Bronk Ramsey, 2008). The use of extrapolation and interpolation in determining the ages of turbidites relies on the assumption that there is minimal fluctuation in the rate of hemipelagic sediment accumulation through time (Lebreiro et al., 2009; Grácia *et al*, 2010; Clare et al., 2015). The use of radiocarbon ages from the base of turbidites also relies on the assumption that turbidity currents are not significantly erosive (Weaver and Thomson, 1993; Thomson and Weaver, 1994; Weaver, 1994; Wynn et al., 2002; Grácia et al., 2010). For this reason, radiocarbon ages from the upper boundaries turbidites are favoured; although bioturbation can introduce uncertainty into the dating of turbidites (Urlaub et al., 2013).

Lab code	Core no.	Core depth (cm)	Conventional age (yrs BP)	2σ age ranges (Cal BP)	Median age (Cal BP)	Source
SUERC-64868	64PE391_23	4-5	1375 ± 37	795-1026	916	This study
SUERC-64869	64PE391_23	15-16	2765 ± 37	2345-2657	2489	This study
UCIAMS-170242	64PE391_23	21-22	3425 ± 15	3199-3375	3289	This study
SUERC-64871	64PE391_29	13-14	1898 ± 35	1331-1541	1440	This study
BETA 405508	64PE391_29	23-24	3450 ± 30	3201-3382	3297	Mozzato et al., 2016
BETA 405510	64PE391_29	129.5-130.5	11150 ± 40	12559-12729	12639	Mozzato et al., 2016
BETA 405511	64PE391_29	132.5-133.5	11650 ± 40	12965-13249	13120	Mozzato et al., 2016
BETA 405512	64PE391_29	156.5-157.5	12910 ± 40	14299-15005	14678	Mozzato et al., 2016
BETA 405513	64PE391_31	62.5-63.5	5040 ± 30	5290-5449	5368	Mozzato et al., 2016
BETA 406174	64PE391_31	99-100	8800 ± 30	9389-9511	9450	Mozzato et al., 2016
SUERC-64874	64PE391_31	175-176	15929 ± 49	18643-18902	18778	Mozzato et al., 2016
SUERC-64878	64PE391_31	204-205	17635 ± 59	20567-20898	20772	Mozzato et al., 2016
BETA 405516	64PE391_31	224.5-225.5	18990 ± 80	22261-22626	22433	Mozzato et al., 2016
SUERC-64880	64PE391_43	4-5	1068 ± 37	539-700	629	This study
SUERC-64881	64PE391_43	9-10	2325 ± 36	1818-2060	1936	This study
SUERC-64882	64PE391_43	15.5-16.5	3116 ± 37	2761-3015	2885	This study
UCIAMS-170243	64PE391_45	2-3	3705 ± 15	3521-3711	3616	This study
SUERC-64884	64PE391_45	9-10	2137 ± 37	1591-1842	1719	This study
SUERC-64888	64PE391_45	14-15	3071 ± 37	2739-2948	2832	This study
BETA 418454	64PE391_46	241.5-242.5	10240 ± 40	11114-11350	11221	This study
SUERC-64889	64PE391_46	258-259	1177 ± 36	641-821	716	This study
BETA 418455	64PE391_46	283-284	13260 ± 40	15153-15561	15333	This study
SUERC-64890	64PE391_56	13-14	2958 ± 36	2646-2843	2732	This study
UCIAMS-170244	64PE391_57	21-22	3060 ±15	2745-2905	2819	This study
BETA 405523	64PE391_57	89-90	5220 ± 30	5469-5621	5559	Mozzato et al., 2016
BETA 418456	64PE391_57	181.5-182.5	10570 ±40	11461-12012	11806	Mozzato et al., 2016
BETA 418457	64PE391_57	250.5-251.5	16570 ± 50	19274-19648	19484	Mozzato et al., 2016
SUERC-64892	64PE391_64	22-23	22248 ± 96	25855-26295	26051	This study
SUERC-64893	64PE391_64	63.5-64	4714 ± 36	4820-5075	4935	This study
SUERC-64894	64PE391_64	178-179	18821 ± 68	22017-22468	22301	This study
BETA 405521	64PE391_65	15-16	8090 ± 40	8412-8676	8542	This study
BETA 406175	64PE391_65	65-66	16140 ± 60	18820-19165	18979	This study
SUERC-64898	64PE391_65	114-115	25773 ± 129	29030-29815	29431	This study
BETA 405522	64PE391_65	303-304	Infinite	N/A	N/A	This study
SUERC-64899	64PE391_65	367-368	Infinite	N/A	N/A	This study
BETA 406178	64PE391_68	18-19	2920 ± 30	2545-2775	2702	This study
BETA 405935	64PE391_68	224.5-225.5	3650 ± 30	3440-3666	3546	Mozzato et al., 2016
BETA 406187	64PE391_79	341-342	17190 ± 60	20029-20463	20240	This study
BETA-194767	GS134-01		4600 -/+ 40	(4881-4637)	4793	Haflidason et al. 2007
BETA-194768	GS134-02		4130 -/+ 40	(4295-4000)	4157	Haflidason et al. 2007
KIA6016	23545-1		9325 -/+ 40	10230-9995	10148	Laberg et al. 2002b
TUa-1757	JM96-42/1		4060 -/+ 60	4237-3875	4056	Laberg et al. 2002b
TUa-1760	JM96-45/1		16125 -/+ 130	19289-18678	18954	Laberg et al. 2002b
TUa-1767	JM96-47/1		13150 -/+ 70	15371-14821	15151	Laberg et al. 2002b
TUa-2289	JM98-632/1		16250 -/+ 120	19431-18825	19091	Lindberg et al 2004
TUa-2353	JM98-637/1		1580 -/+ 75	1263-950	1111	Laberg et al. 2002a
TUa-2934	JM00-543/1		3055 -/+ 65	2965-2691	2807	Laberg et al. 2002a
TUa-2935	JM00-545/1		3425 -/+ 65	3429-3080	3264	Laberg et al. 2002a

Table 5.1: Table of all the radiocarbon ages used in this study. Conventional ages are reported, along with 2-sigma (2σ) calibrated range and median age.

5.4 Results

5.4.1 Sedimentary facies

The sedimentary deposits of the Trænadjupet Slide are complex, and represent a range of different transport processes related to the movement and disintegration of a large volume submarine landslide. Within the piston and multi-cores used in this study seven facies (*a* - *g*) were identified and described using photographs, lithology, magnetic susceptibility, and gamma bulk density. These facies classifications will be used to distinguish mass transport deposits from hemipelagic sediments, as well as understand their emplacement dynamics.

Facies a: Hemipelagite

These sediments are characterised as structure-less clay with foraminifera present throughout in varying abundance. The colour of the sediment varies from light brown to light grey (Fig. 5.3a). Bioturbation structures are sometimes evident within the sediment. The facies is typically characterised by low (<50 SI) magnetic susceptibility and a stable density profile of between 2.5 - 2.7 g/cc on MSCL data (Fig. 5.3a). Based on the lack of sedimentary structures, and the presence of calcareous microfossils and bioturbation structures, we interpret these sediments to be hemipelagic, resulting from the slow settling of biogenic material along with fine-grained suspension of terrigenous and oceanic origin (Stow and Tabrez, 1998). Importantly, these characteristics of hemipelagite allow us to distinguish it from mass transport deposits, and thus sample for AMS radiocarbon and develop sedimentary age models.

Facies b: Structureless clay/silt

Structure-less clay/silt is found primarily in sediment cores from the Lofoten Basin, below 3,000 m water depth. The deposits are dark brown/grey in colour, devoid of any microfossils, do not have any coarse bases or obvious grading, and have very stable magnetic susceptibility and density profiles on MSCL data (Fig. 5.3b). The basal contacts of these deposits are typically sharp, which along with the lack of microfossils suggests more rapid deposition. The upper contacts are

gradational and exhibit bioturbation structures. We interpret these clays/silts as the deposits of fine-grained, distal turbidity currents after Stow and Piper (1984).

Facies c: Graded sand/silt

Graded sand deposits are largely found in cores from the Lofoten Basin floor. Most of the deposits have a basal unit of laminated or massive sands. This is overlain by fine sand grading into silt and clay, although this is often very thin. The facies is characterised by a high (>200 SI) and variable magnetic susceptibility, and low bulk density than hemipelagic sediments (Fig. 5.3c). Based on the normal grading, internal structures such as cross bedding, erosional basal contact, and small proportion of fine-grained sediment, we characterise this facies as the deposits of low-density turbidity currents in the sense of Bouma et al., (1962) and Middleton and Hampton (1973)..

Facies d: Pebble conglomerate

This facies is composed of 0.5 - 5 mm sub-rounded clasts of indurated clay with 30-50% medium to coarse sand and microfossils. The facies is normally graded, with some larger (> 5 cm) sandy mud clasts interspersed. The facies has an irregular magnetic susceptibility signature, and the density increases towards the top of the deposits, both of which are likely due to increasing sand content (Fig. 5.3d). This facies is likely a type of debris flow, although there is little mud matrix (Mulder and Cochonat, 1996; Mulder and Alexander, 2001).

Facies e: Pebble-cobble conglomerate

Facies *e* is a mixture of pebble- to cobble-sized, indurated, sub-rounded mud clasts ranging from 5 to 50 mm in size with 20 - 40% muddy-sand matrix. The facies shows no obvious grading and is poorly sorted. The magnetic susceptibility and density profiles for this facies are very irregular due to the different grain/clast sizes and compositions (Fig. 5.3e). This facies is interpreted to be the result of cohesive debris flows (Mulder and Alexander, 2001; Talling et al., 2013).

Facies f: Cobble-boulder conglomerate

Facies *f* is a mixture of cobble-sized, indurated clay clasts with larger (>50 mm) clasts or rafts of sediment whose pre-failure internal bedding is often still partly visible (Fig. 5.3f). The matrix is

typically less than 20% and consists of sandy-silt. Unlike facies *d* and *e*, the magnetic and density profiles for this facies are much more stable, likely due to larger clast sizes and a lower concentration of sand matrix. As with facies *e*, this facies is interpreted to be the result of cohesive debris flows (Mulder and Alexander, 2001; Talling et al., 2013).

Facies g: Boulder breccia

Facies *g* consists of large (>25 cm), angular blocks of indurated clay that have internal sedimentary structures and are visibly deformed and sheared. Clast contacts are often clean with little to no matrix material. Magnetic and density profiles for the blocky sediment are very stable, likely due to the absence of a sand or silt matrix (Fig. 5.3g). This facies is interpreted as the result of debris flows containing rafted blocks of sediment that have experienced internal faulting and deformation, but have not disaggregated into clast-rich debris flows.

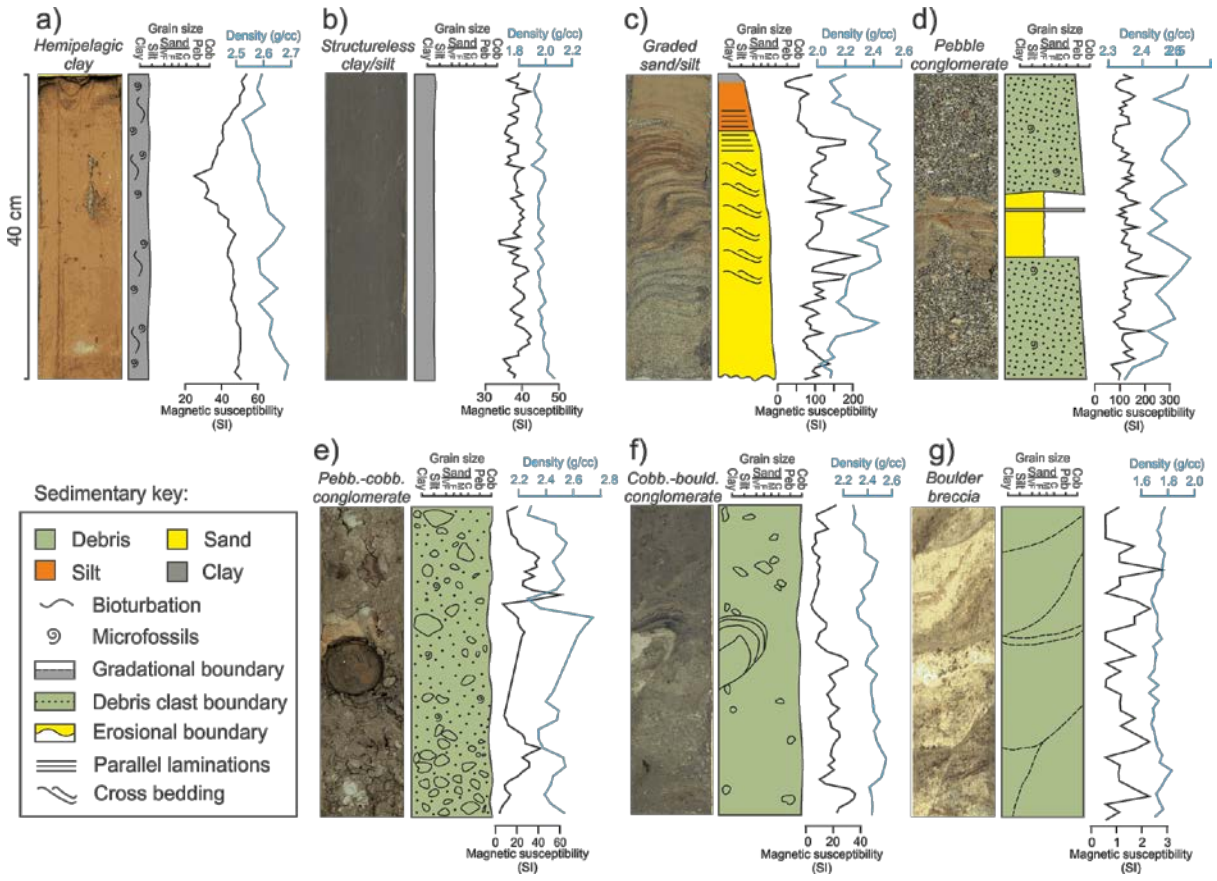

Figure 5.3: Facies classification for sediments across the Trænadjupet and Nyk Slides. The facies are hemipelagic clay (a), structure-less clay/silt (b), graded sand/silt (c), pebble conglomerate (d), pebble-cobble conglomerate (e), cobble-boulder conglomerate (f), and boulder breccia (g). Density and magnetic susceptibility data are from a Geotek MSCL.

5.4.2 Distribution of facies within the Nyk and Trænadjupet Slides

The slide scars and deposits of the Trænadjupet and Nyk Slides have been mapped previously using TOBI side-scan sonar and multi-beam bathymetry, with their morphology described in some detail (Laberg and Vorren, 2002a; Laberg et al., 2002a; 2002b; 2006; Lindberg et al., 2004; Mozzato et al., in review). However, the sedimentary characteristics of these deposits are largely unknown, with only a small number of sediment cores previously collected and described. The new cores are grouped here in relation to the geomorphology of the Nyk and Trænadjupet Slides (Fig. 5.1), and are described from proximal to distal settings.

5.4.2.1 Trænadjupet Slide

Core 20 recovered from the upper extent of the slide deposits consists primarily of cobble-boulder conglomerate facies (*f*) (Fig. 5.4). Core 21 downslope of the uppermost Trænadjupet Slide deposits consists almost entirely of boulder breccia facies (*g*), with 20 cm of cobble-boulder conglomerate (*f*) grading into a sandy unit (*c*) above. These mass transport deposits are draped by a 20 cm thick unit of hemipelagic sediment (*a*). Core 22, from the centre of the Trænadjupet Slide deposits contains 2 m of boulder breccia and cobble-boulder conglomerate at the base. These debris flow deposits are overlain by an 8 m thick, graded turbidite, and finally by a 10 cm hemipelagic drape. Core 25 from Lobe 2 of the Trænadjupet Slide contains a mixture of boulder breccia and cobble-boulder conglomerate (Fig. 5.4). This is again draped by a thin (<10 cm) hemipelagic unit. Core 26 from the more distal end of Lobe 2 contains a mixture of pebble-cobble (*e*) and cobble-boulder conglomerates, as well as some boulder breccia (Fig. 5.4).

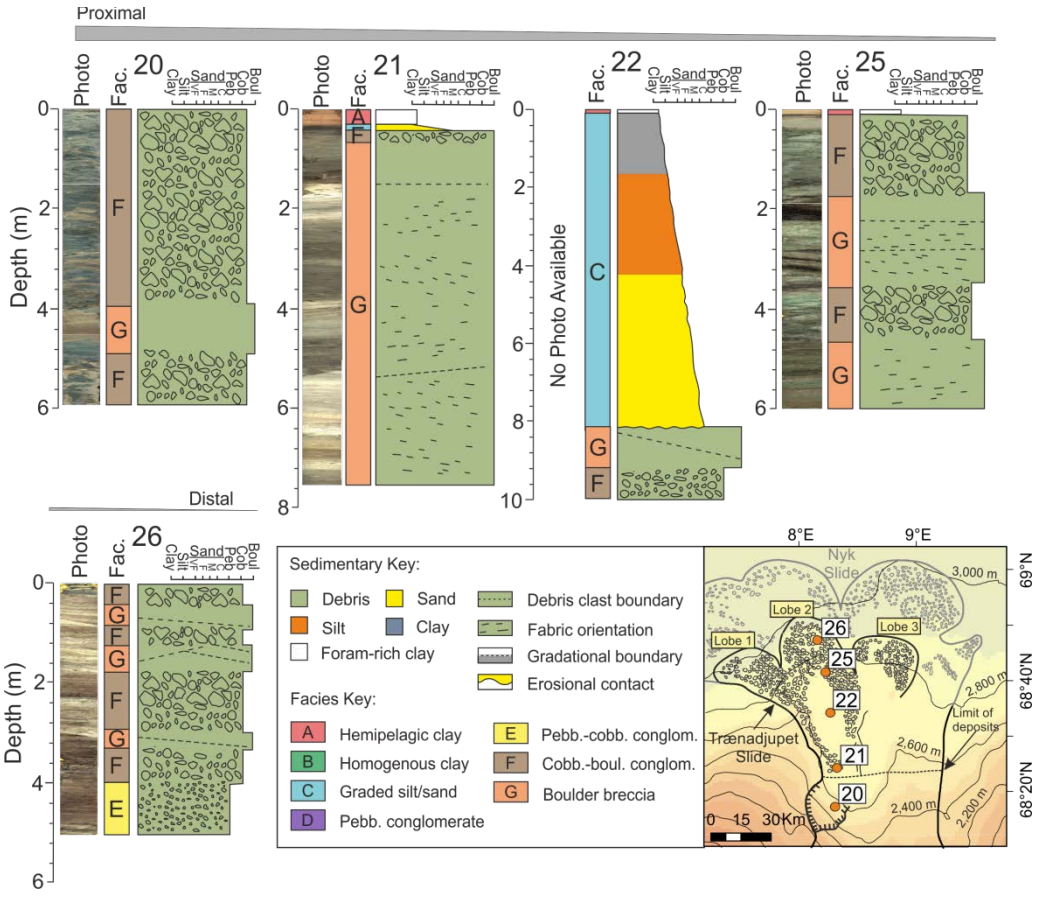

Figure 5.4: Sediment cores collected from the blocky deposits of the Trænadjupet Slide. Inset map shows core locations and morphology of the Trænadjupet Slide deposits.

5.4.2.2 Nyk Slide

Core 64 was recovered proximally from Lobe 1 of the Nyk Slide, and consists largely of hemipelagic sediment (Fig. 5.5). Between 20 - 60 cm core depth there is a flay-lying, sandy debrite with interspersed mud clasts. Core 65 collected more distally on Lobe 1 of the Nyk Slide also consists largely of hemipelagic sediment, with some flat-lying, structureless clay/silt layers towards the base of the core (Fig. 5.5).

Core 29 recovered from Lobe 2 of the Nyk Slide contains two mass transport deposits (Fig. 5.5). The basal mass transport deposit consists of a >2 m thick unit of boulder breccia overlain by 2 m of cobble-boulder conglomerate and a small (<15 cm) graded sand unit. Between the upper and lower deposits, between 1.5 - 2.2 m depth, there is a hemipelagic clay interval. The upper mass transport deposit has an 80 cm thick pebble-cobble conglomerate layer overlain by a graded sandy turbidite. This is draped by a further 25 cm of hemipelagic clay. Core 59 recovered more distally from Lobe

2 of the Nyk Slide contains 2 m of boulder breccia, overlain by 1.8 m of cobble-boulder conglomerate with an upper 20 cm of graded sand (Fig. 5.5).

Core 46 was recovered from the proximal Lobe 3 of the Nyk Slide, and contains a 15 cm silty turbidite at its base (Fig. 5.5). This silty turbidite is draped by a 60 cm thick hemipelagic interval, which is overlain by a 2.4 m thick pebble-conglomerate debris flow with a cobble conglomerate base. Core 48, recovered from the distal end of Lobe 3 of the Nyk Slide contains 50 cm of boulder breccia overlain by 1.3 m of graded sand-silt and is draped by 20 cm of foraminifera-rich clay (Fig. 5.5). Core 52, from 2,970 m water depth on Lobe 3 of the Nyk Slide consists of a basal cobble-boulder conglomerate overlain by a 70 cm thick graded sand-silt turbidite and a 10 cm thick hemipelagic drape. Core 50, from 3,200 m water depth at the edge of Lobe 3 of the Nyk Slide, contains a 3 m thick boulder breccia, overlain by 60 cm of foraminifera-rich clay (Fig. 5.5). The upper section of core 50 contains a 50 cm thick graded sand/silt unit with a pebble conglomerate (*d*) base and a thin hemipelagic drape.

Core 41, retrieved from Lobe 4 of the Nyk Slide consists of an upper sand unit that is 3 m thick and contains some coarser debris and grading (Fig. 5.5). The lower 1 m of the core consists of boulder breccia. Core 41 is the only piston core retrieved from Lobe 4 of the Nyk Slide.

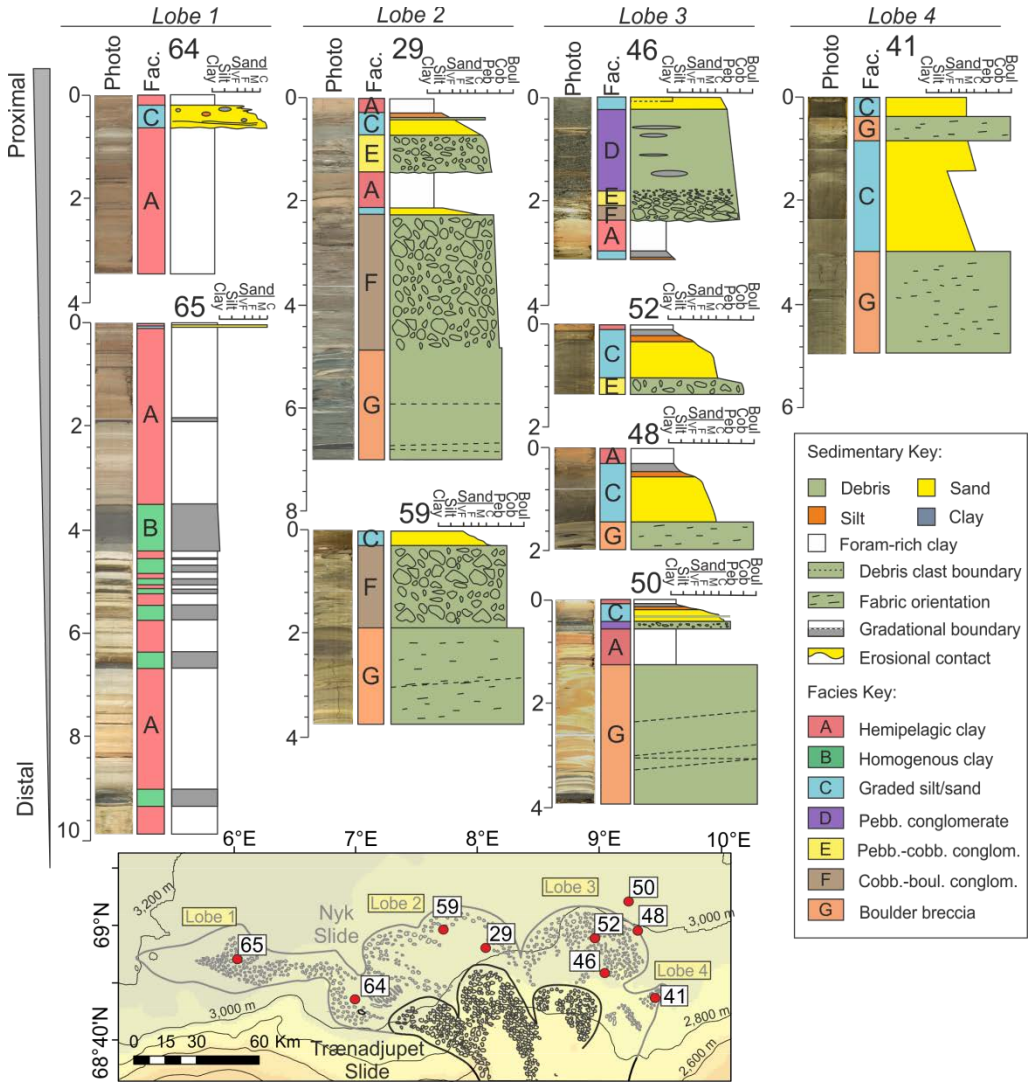

Figure 5.5: Sediment cores collected from the deposits of the Nyk Slide, beyond the limit of the Trænadjupet Slide lobes.

5.4.2.3 Lofoten Basin

Core 57 was collected from the most proximal part of the Lofoten Basin, beyond Lobe 2 of the Nyk Slide, and contains two mass transport deposits separated by a 1.8 m thick unit of hemipelagite (Fig. 5.6). The lower deposit in the core is composed of boulder breccia overlain by pebble-cobble conglomerate and graded sand. The upper deposit is a graded turbidite unit with a basal layer of pebble conglomerate, and is draped by 20 cm of hemipelagite (Fig. 5.6). Core 31 also from the proximal Lofoten Basin is composed largely of hemipelagic clay, with two ~40 cm, normally-graded turbidite deposits in the upper 2 m of the core (Fig. 5.6). There are some smaller mass transport deposits below 4 m core depth, but these are typically less than 15 cm thick. Core 68 in the southern Lofoten Basin consists largely of structureless clay/silt turbidites (*b*) that are 10 - 160

cm thick. These clay/silt turbidites are intercalated with intervals of hemipelagic sediments (Fig. 5.6). Core 79 in the central Lofoten Basin also records several thick structureless clay/silt turbidites intercalated with hemipelagic sediment, as well as two thicker graded sand/silt deposits (Fig. 5.6).

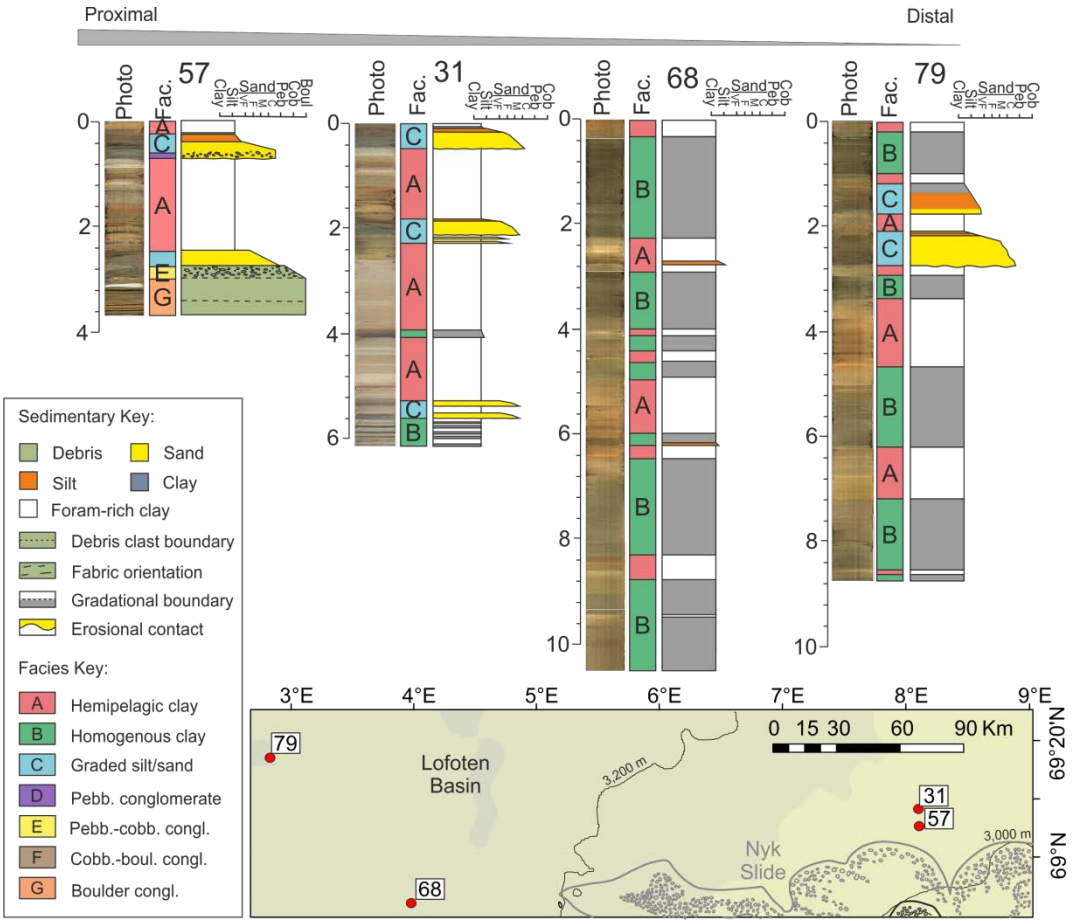

Figure 5.6: Sediment cores collected from the Lofoten Basin, beyond the extent of the Nyk and Trænadjupet Slide lobes.

5.4.3 Morphology of headwalls within the Trænadjupet slide scar

Three distinct headwalls (H1 - 3) have been identified within the Trænadjupet slide scar (Fig. 5.7A; Laberg and Vorren, 2000a; Laberg et al., 2002a; Mozzato et al., in review). However, the ages and relative timing of these headwalls are not well known. Here we aim to use the new bathymetric dataset from the Trænadjupet slide scar to determine the relative timing of these headwalls. Determining the relative timing of failure associated with these headwalls is important for determining the emplacement dynamics of the Trænadjupet Slide.

The shallowest headwall (headwall 1) runs parallel to the shelf edge between 270 and 350 m water depth and has a height of between 100 and 120 m (Fig. 5.7B). Downslope of headwall 1 there are

detached sediment blocks and flow lineations perpendicular to the shelf edge. There are also some small-scale debris flow lobes originating from the headwall that extend for approximately 2 - 5 km (Fig. 5.7B).

The second headwall (headwall 2) extends from 1,450 down to 1,650 m water depth, is more irregular in shape, and has a height of between 50 and 100 m (Fig. 5.7C). Downslope of headwall 2 there are more detached sediment blocks and a greater number of flow lineations visible. These individual flow lineations do not crosscut headwall 2. Furthermore, no blocky sedimentary drape observed in some retrogressive slides can be seen extending down over the headwall (Fig. 5.7C; Masson et al., 2010). The northern end of headwall 2 is difficult to define due to the large number of smaller scarps present along the northern edge of the slide scar area (Baeten et al., 2014). At least two possible continuations of headwall 2 can be identified from this bathymetry data (Fig 5.7A and C).

The third headwall extends from 2,200 down to 2,500 m, has an amphitheatre-like shape, and has a height of between 80 and 120 m (Fig. 5.7D). Below headwall 3 there are large clusters of remobilised sediment blocks, but flow lineations are generally absent. Above headwall 3 there are flow lineations, but these are not traceable to below the headwall (Fig. 5.7D). As with headwall 2, no blocky sediment drape observed in some retrogressive slides can be seen extending down over the headwall. It should however be noted that some areas of headwall 3 are not covered by this bathymetric dataset.

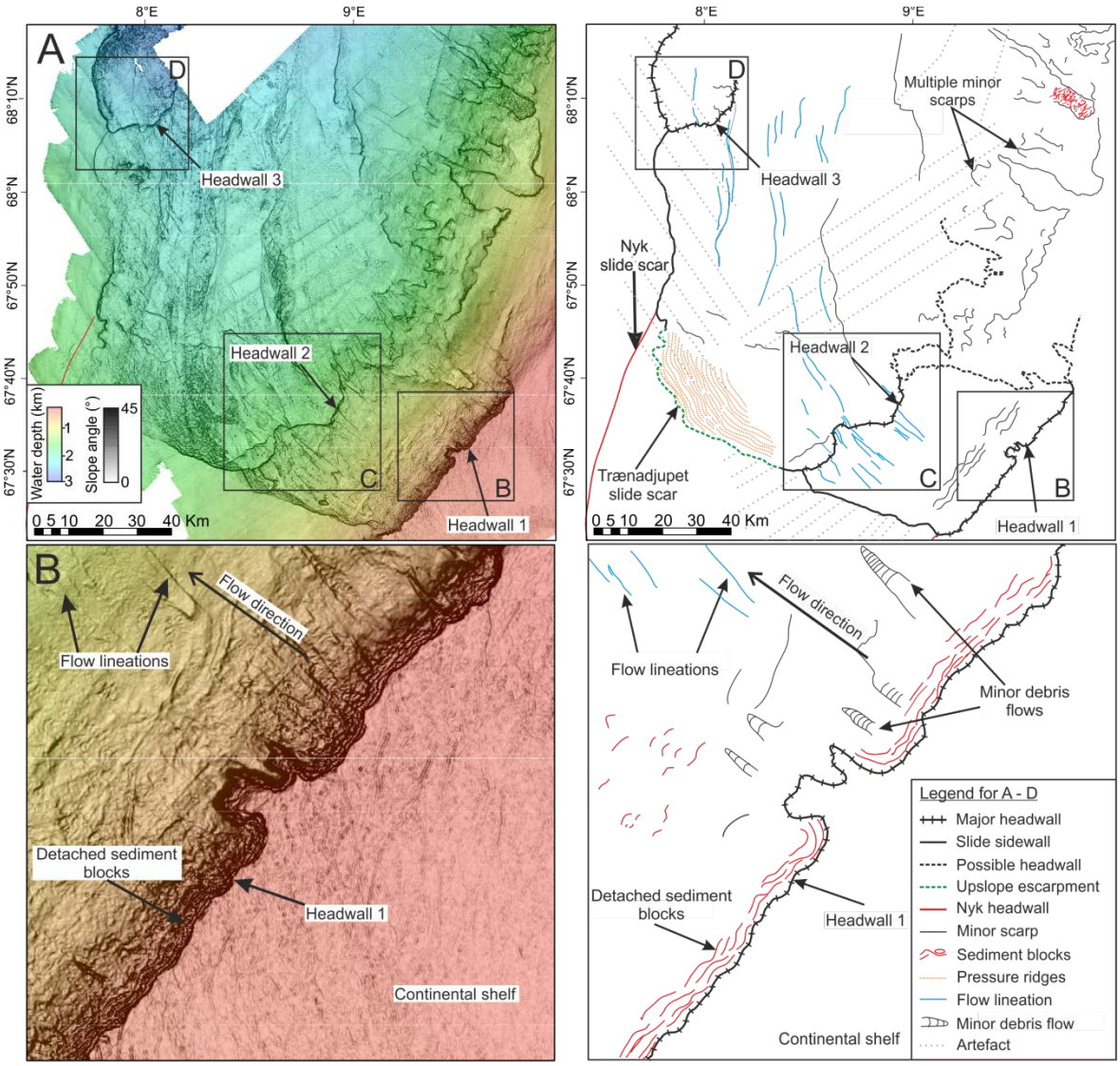
A
B
C
D
8°E
9°E
68°10'N
68°N
67°50'N
67°40'N
67°30'N
Headwall 3
Headwall 2
Headwall 1
Water depth (km)
Slope angle (°)
0 5 10 20 30 40 Km
Flow direction
Flow lineations
Detached sediment blocks
Continental shelf
Multiple minor scarps
Nyk slide scar
Trænadjupet slide scar
Minor debris flows
Legend for A - D
Major headwall
Slide sidewall
Possible headwall
Upslope escarpment
Nyk headwall
Minor scarp
Sediment blocks
Pressure ridges
Flow lineation
Minor debris flow
Artefact

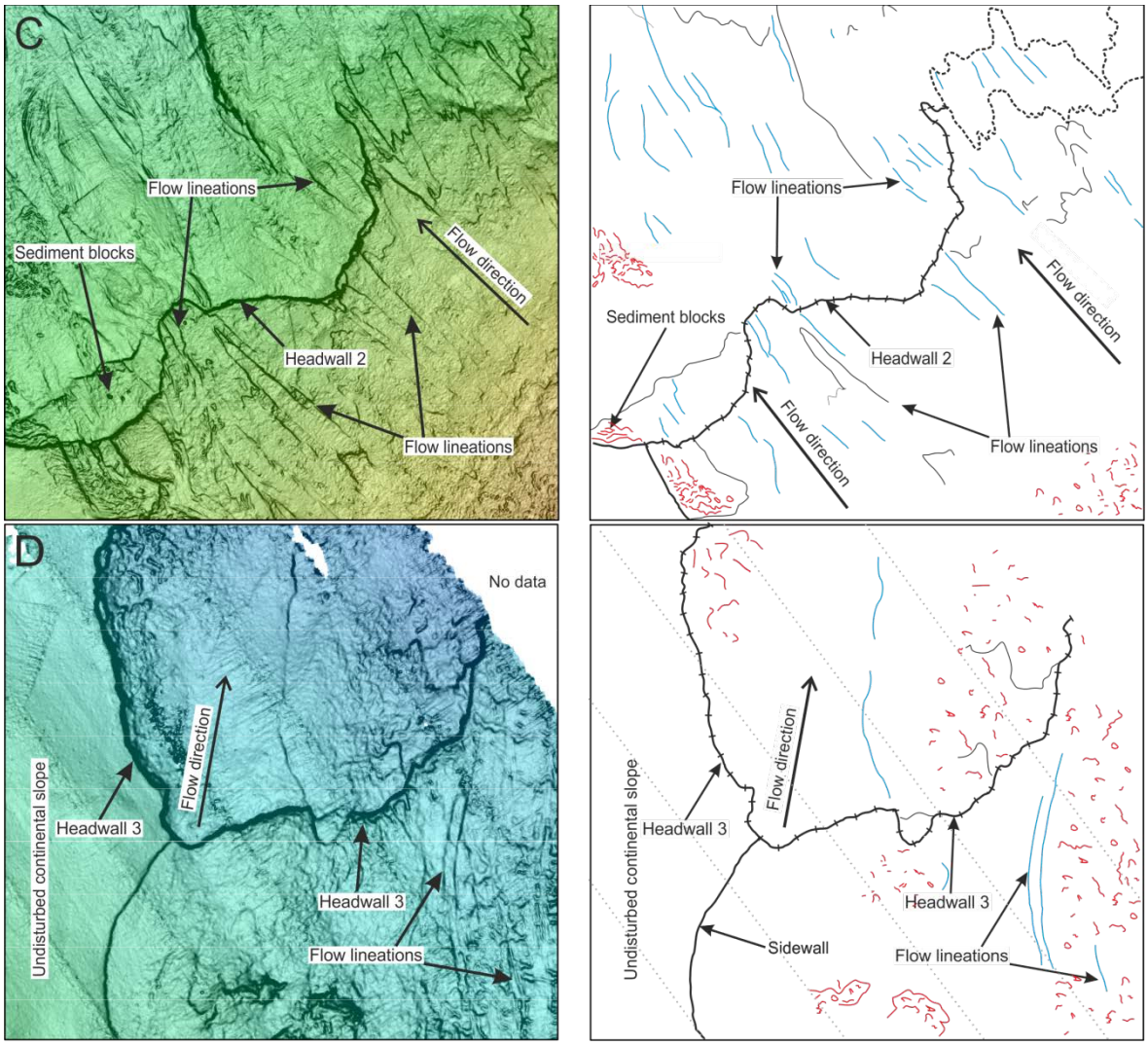

Figure 5.7: Bathymetric data and shaded slope angle (left) from the Trænadjupet Slide scar, and the interpretation (right). A Bathymetric data from the Trænadjupet slide scar shows 3 principal headwalls: headwall 1 (B), headwall 2 (C), and headwall 3 (D). Flow lineations are not continuous from above to below headwall 2, suggesting headwall 2 cut previous flow features. Headwall 3 truncates the upslope sidewall of the slide associated with H2, indicating it was the last stage of failure. Greyscale indicates slope angle (º). Coloured bathymetry data are from IBCAO Ver. 3 (Jakobsson et al., 2012).

5.4.4 Ages of individual lobes of the Trænadjupet Slide

In order to determine the emplacement age of each lobe of the Trænadjupet Slide, the most recent mass transport deposits contained in piston and multi-cores from sites beyond the lobe edges, and atop the slide were dated using AMS radiocarbon (Table 5.1). The emplacement of the Trænadjupet Slide has produced at least one event bed traceable into the Lofoten Basin (Haflidason et al., 2007; Mozzato et al., in review). If there are large disparities (i.e. greater than the uncertainties of ~300 years in radiocarbon dating) between the ages of emplacement of Lobes 1 - 3

of the Trænadjupet Slide, this should be recognisable by differences in the age of the most recent turbidites proximal to each lobe.

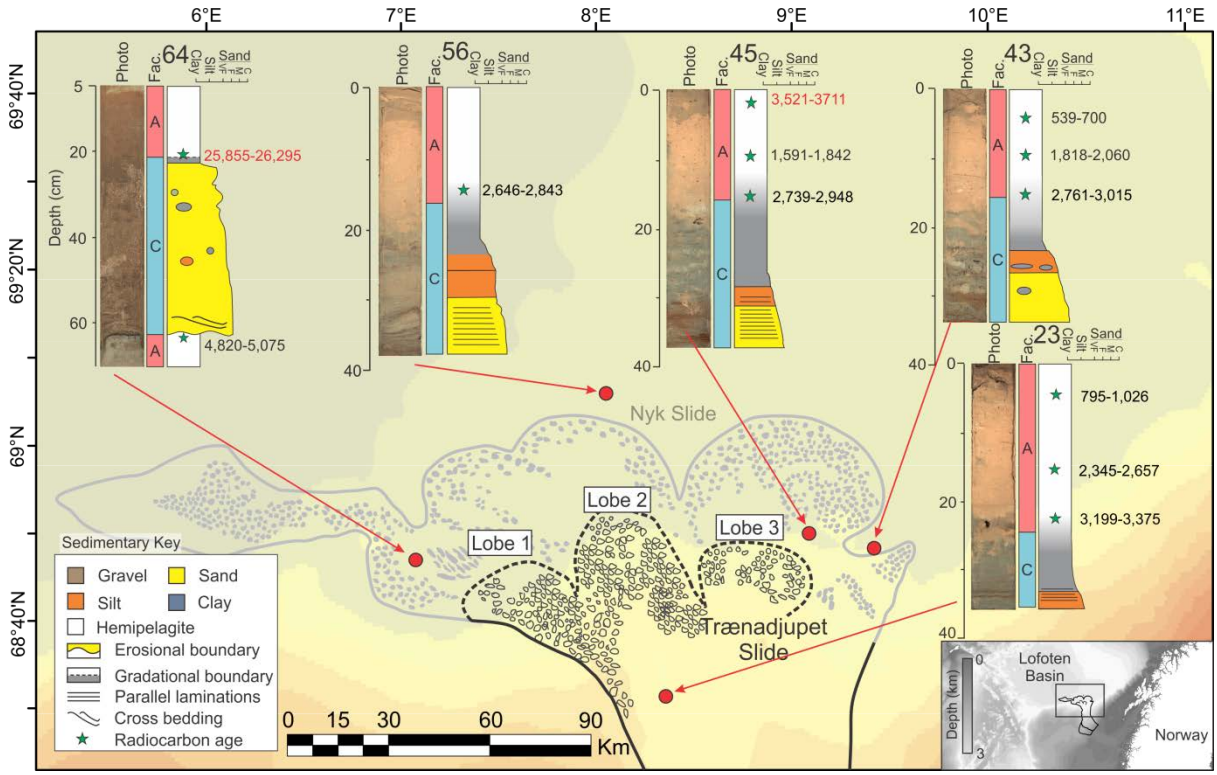

Figure 5.8: Locations, lithological logs, and AMS radiocarbon dates of cores containing deposits of Trænadjupet Slide age. Core 64 is a piston core, while all other cores are multicores. All AMS radiocarbon ages are in calibrated years before present (cal BP). Facies A - D are described in Fig. 5.3. Minimum ages for the Trænadjupet Slide are consistent between cores 43, 45, and 56. The minimum age in core 23 is slightly older, at 3199 - 3375 cal BP, while in core 64 the age is likely erroneous.

Piston core 64 from the western side of the slide complex, beyond Lobe 1 contains a sandy debrite with a basal age of 4,820 - 5,057 cal BP (Fig. 5.8). The age recorded directly above the turbidite is 25,855 - 26,295 cal BP (Fig. 5.8). Multi-core 56 from the Lofoten Basin, downslope from Lobe 2, records a turbidite with a minimum age of 2,646 - 2,848 cal BP. Multi-cores 43 and 45, both of which are proximal to Lobe 3, record turbidites with ages of 2,761 - 3,015 and 2,739 - 2,948 cal BP respectively (Fig. 5.3). Multi-core 23 collected from the central body of the Trænadjupet Slide records a turbidite with a minimum age of 3,199 - 3,375 cal BP (Fig. 5.8).

5.4.5 Character of turbidites associated with the Trænadjupet Slide

Multi-staged submarine and subaerial landslides have been inferred from multiple stacked, fining-upward turbidite sequences that are deposited in distal abyssal plains (Wynn and Masson, 2003; Hunt et al., 2013a). If there was a substantial time gap between emplacement of the lobes of the Trænadjupet Slide, this may result in the deposition of similarly stacked turbidites in the Lofoten Basin. Longer piston cores collected from the Lofoten Basin that recovered Trænadjupet-age deposits have therefore been analysed for grain size changes within turbidites.

Core 31 is located in the proximal Lofoten Basin and contains two >20 cm thick turbidites, the most recent of which has a basal age 5,290 - 5,445 cal BP and is most likely the result of the Trænadjupet Slide (Mozzato et al., in review; Fig. 5.9A). The grain size data show a relatively consistent upward fining pattern within the deposit, albeit with minor variations on the order of a few %. Magnetic susceptibility data through the turbidite deposit are irregular, with several sharp spikes throughout. Gamma bulk density data are also irregular but generally increases towards the top of the deposit (Fig. 5.9A).

Core 50 located in the proximal Lofoten Basin, beyond Lobe 3 of the Trænadjupet Slide, contains a 50 cm thick turbidite in its upper section (Fig. 5.9B). Although no radiocarbon dates exist for this core, the 10 cm depth below seafloor of this turbidite and its proximity to Lobe 3 suggest that it originated from the Trænadjupet Slide. The deposit consists of four 1 - 3 cm thick alternating layers of pebble conglomerate and sand (*d*) at the base, which are overlain by sand grading normally into silt (Fig. 5.9B). Grain size is only represented semi-quantitatively on the lithological log due to the granular mud content. Magnetic susceptibility is highly variable through the deposit, although peaks in susceptibility do not broadly correspond with apparent changes in grain size. Similarly, changes in density do not correspond well with lithological unit observed in the core (Fig. 5.9B).

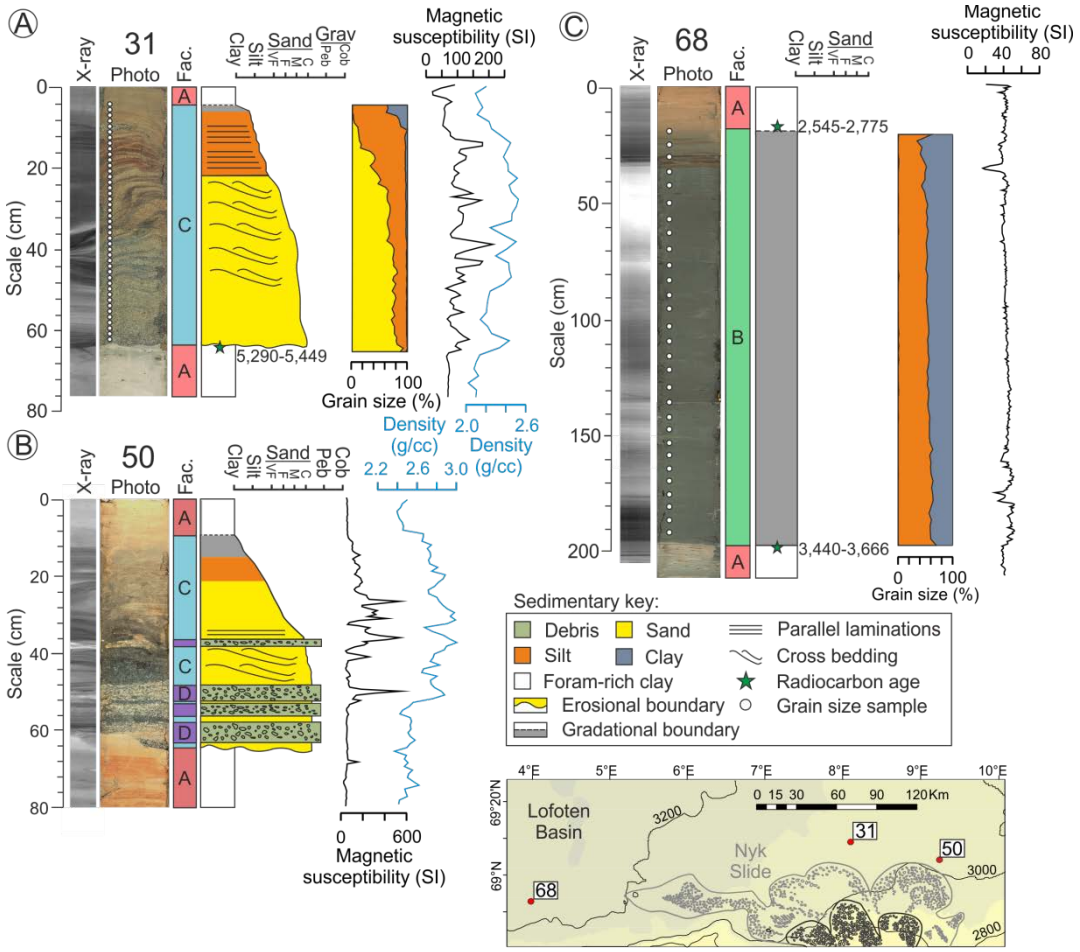

Figure 5.9: Grain size and geophysical data from turbidites of Trænadjupet Slide age in the Lofoten Basin. A: core 31 proximal to the slide complex. B: the most recent deposit from core 50, beyond Lobe 3 of the Nyk Slide, contains repeating bands of pebble conglomerate within coarse sand. C: core 68 in the southern Lofoten Basin contains a thick, clay/silt-dominated turbidite with consistent grain-size and mag-sus profiles. All radiocarbon ages are in calibrated years before present (cal BP).

Piston core 68, located in the southern Lofoten Basin, is in a more distal setting and may contain more well-defined fining-upward deposits indicative of multi-staged failure (Fig. 5.9C). This is because fining upward deposits can be eroded by subsequent flows in proximal settings. The most recent turbidite in core 68 has a maximum age of 3,440 - 3,666 cal BP, The grain size data through this turbidite is very consistent, with a very subtly upward-fining profile. The magnetic susceptibility is also consistent throughout the 2 m deposit, with little variation around 40 SI (Fig. 5.9C). No gamma bulk density data is available for this core.

5.4.6 Emplacement age of the Nyk Slide

Sediment cores containing deposits of Nyk-age are scarcer within this core dataset. Core 29 contains 3 AMS radiocarbon dates below the most recent deposit, that when extrapolated down give an age of between 14,877 - 18,658 cal BP for the Nyk deposit (Fig. 5.10). The lowermost deposit in core 57 has a minimum age of 19,274 - 19,648 cal BP. Core 31 contains a turbidite between 1.75 - 1.95 m depth that has a minimum age of 18,643 - 18,902 cal BP and a maximum age of 20,567 - 20,898 cal BP (Fig. 5.10). These cores are proximal to only Lobe 2 of the Nyk Slide, but are consistent with the previously determined ~19,000 cal BP age for the slide (Fig. 5.1; Lindberg et al., 2004). Few cores from other areas were able to penetrate deep enough to reach deposits of Nyk age. Core 46 located on Lobe 3 of the Nyk Slide contains a thick pebbly-conglomerate deposit with a basal date of 11,114-11,350 cal BP, similar to the basal age of the Trænadjupet deposit in core 29 (Fig. 5.10). A small turbidite can be seen at the base of core 46 with a minimum of age of 15,153 - 15,561 cal BP; although only the upper 20 cm of this deposit has been recovered. These ~11,000 and ~15,000 cal BP turbidites in core 46 have similar ages to radiocarbon ages dating the oldest sediments in the Nyk Slide scar (Fig. 5.1; Lindberg et al., 2004).

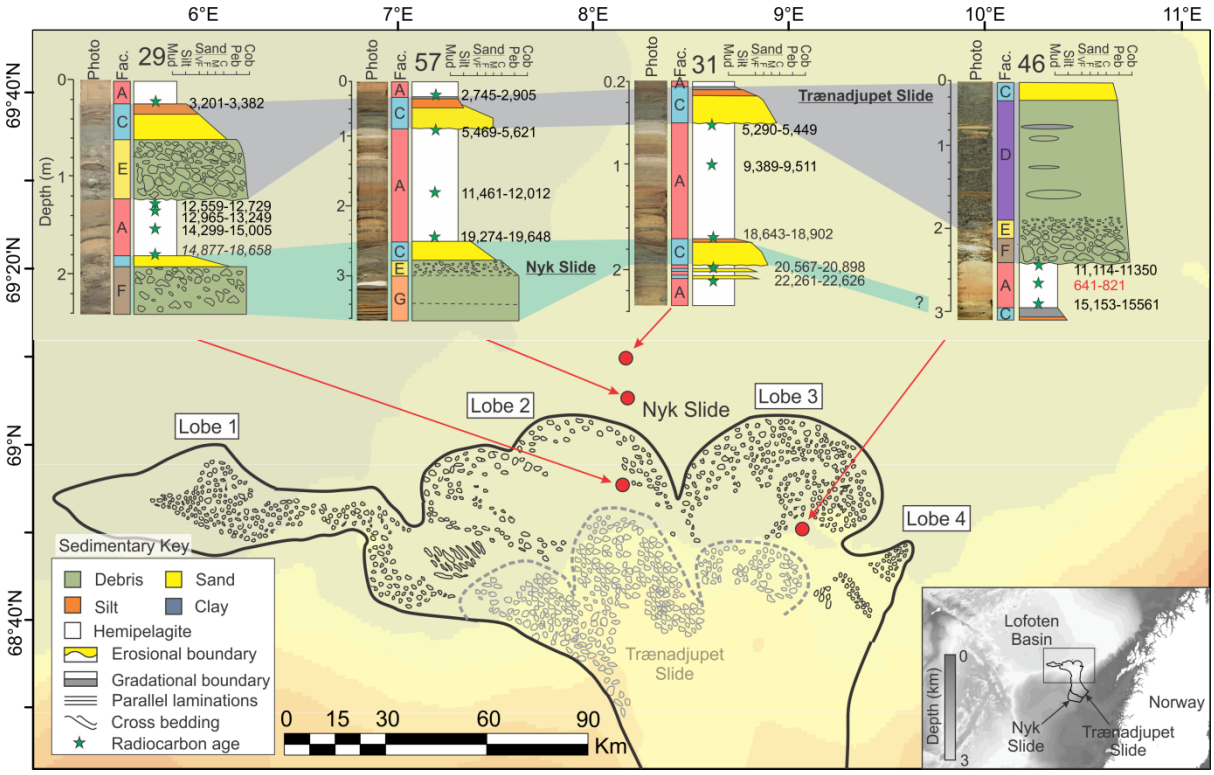

Figure 5.10: Locations, lithological logs, and AMS radiocarbon dates of cores containing deposits of Nyk Slide age. All AMS radiocarbon ages are in calibrated years before present (cal BP). Ages in italics are extrapolated using Oxcal P-sequence modelling and ages in red are considered to be erroneous. The upper deposit in all cores is determined to be the Trænadjupet Slide, while the lower deposit is interpreted to be the Nyk Slide.

5.4.7 Emplacement of Lobe 1 - A third major slide event?

Lobe 1 has a distinct morphology to Lobes 2 and 3 of the Nyk Slide, and its direction of flow is perpendicular to the largely northward direction of slide movement (Figs. 5.1 and 5.10). AMS radiocarbon dates have been collected to determine whether this Lobe 1 is related to the Nyk Slide or is the result of another slide event. Core 65 was retrieved from the centre of Lobe 1 but contains no deformed mass transport deposits within the last ~43,000 years, and is largely composed of hemipelagic sediment (Fig. 5.11A and B). The core has evidence of shearing towards the base (Fig. 5.11C). Core 64 collected from the proximal end of lobe 1, close to the edge of Nyk Lobe 2, also has a largely hemipelagic composition (Fig. 5.11A and D). Within core 64 there is a coarse, graded sand deposit with a basal age of 4,820 - 5,075 cal BP from 20 - 60 cm core depth. However, as with core 65 there is no evidence of mass transports deposits that are coeval with the Nyk Slide at ~19,000 cal BP (Fig. 5.11D).

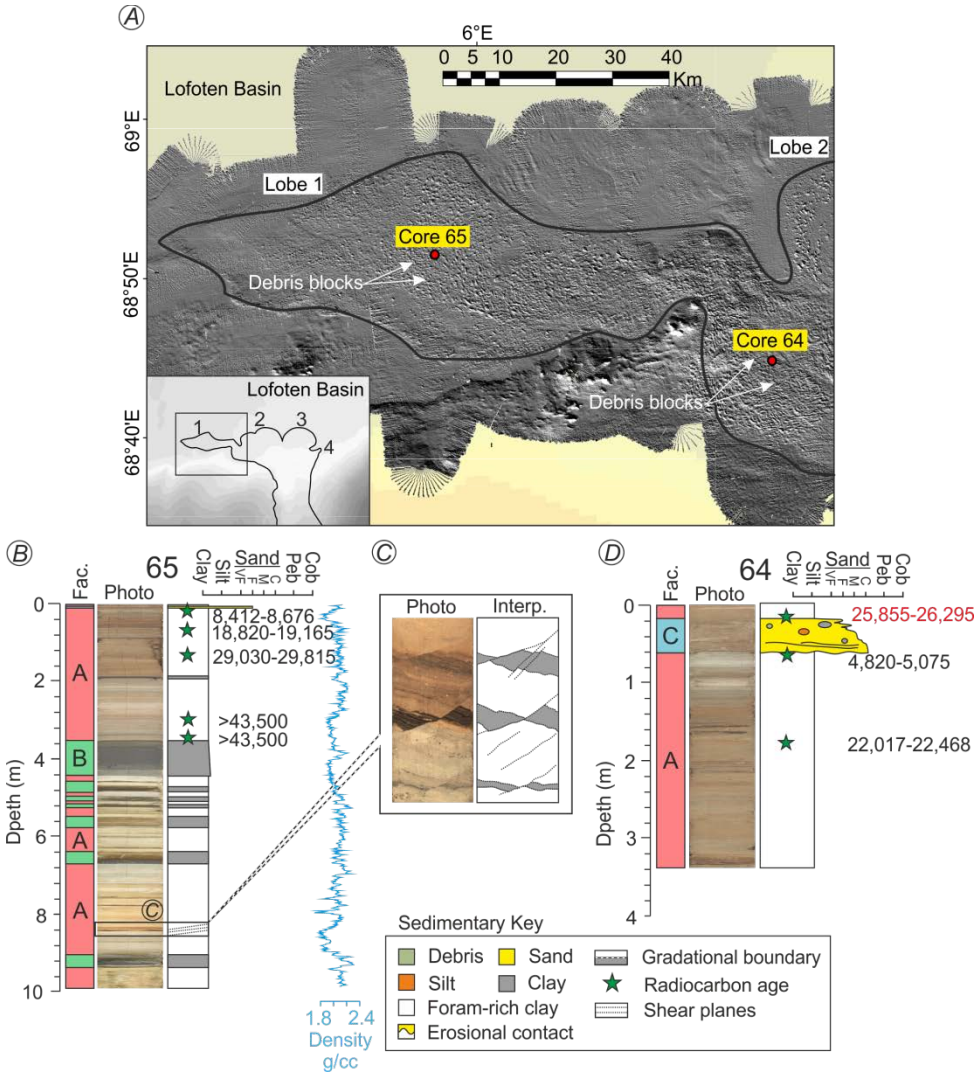

Figure 5.11: *A*: Shaded relief image from Lobe 1 of the Nyk Slide and location of cores 64 and 65. *B*: Core 65, which contains a flat-lying hemipelagic stratigraphy with no mass transport deposits like those observed in other lobes of the Nyk Slide. *C*: shear planes at the base of core 65 imply that this sediment could have undergone remobilisation. Core is 10 cm in width. *D*: core 64 from a more proximal site contains a Trænadjupet-age deposit, but no deposits of Nyk age. For facies classifications A - C see Fig. 5.3.

5.4.8 What do distal turbidites tell us about the emplacement of the Nyk Slide?

Grain size trends in the distal turbidites of the Nyk Slide were documented to determine whether these turbidites contain multiple fining-up sequences linked elsewhere to multistage failure. Core 31 from the proximal Lofoten Basin contains a turbidite deposit with a maximum age of 20,567 - 20,898 cal BP, consistent with previously observed ages of the Nyk Slide (Fig. 5.12A; Lindberg et al., 2004; Mozzato et al., in review). The grain size data from this turbidite show a somewhat irregular up-ward fining profile, but there is no compelling evidence of repeated fining-up

units. The magnetic susceptibility data is also irregular and shows several sharp spikes in intensity towards the base, although these are not related to any notable change in grain size. Gamma bulk density increases from 2.2 g/cc at the base to 2.6 g/cc towards the top of the deposit (Fig. 5.12).

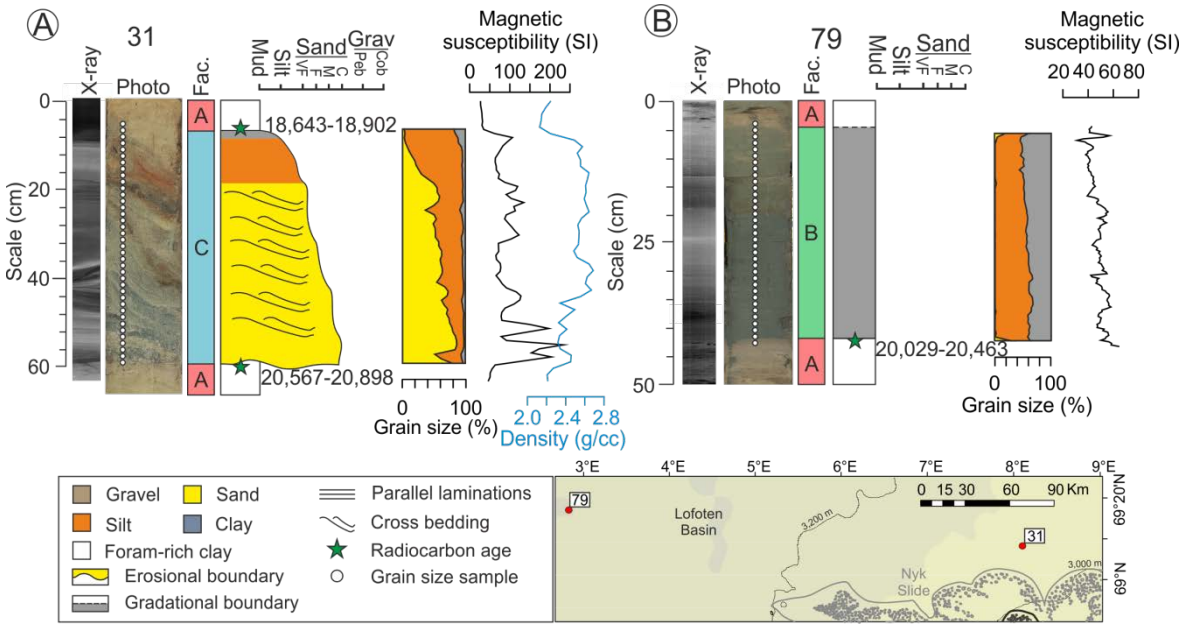

Figure 5.12: Lithology, grain size, and geophysical data from turbidites of Nyk Slide age in the Lofoten Basin. A: core 31 proximal to the slide complex. B: core 79 in the southern Lofoten Basin. Inset map shows core locations. All radiocarbon ages are in calibrated years before present (cal BP).

Core 79 from the central Lofoten Basin contains a 35 cm thick turbidite deposit with a basal age of 20,029 - 20,463 cal BP, interpreted here to be related to the Nyk Slide (Fig. 5.12B). The grain size data through this turbidite shows a consistent, gently upward-fining profile. The magnetic susceptibility data is somewhat more irregular, and has some sharp increases; although SI values only vary from 40 - 60 (Fig. 5.12B). No Gamma bulk density data is available for core 79.

5.5 Discussion

Implications of the newly refined emplacement ages of the Trænadjupet and Nyk Slides are discussed initially, including their implications for landslide frequency and triggers. Whether or not the Trænadjupet Slide was emplaced progressively from the top down, or retrogressively from the bottom up, is then addressed. The implications of slide emplacement, turbidite morphology, and the

absence of tsunami deposits on nearby coastlines are discussed. Finally, the wider implications of this work for submarine landslide tsunami hazard will then be considered.

5.5.1 Landslide emplacement ages and possible triggers

Accurately determining the age of large submarine landslides and the frequency with which they occur is critical for hazard assessment. Here the new ages of the Trænadjupet Slide from AMS radiocarbon dating of distal turbidites will be discussed. Possible triggers of the slide, as well as potentially coeval onshore tsunami deposits will also be considered. We will also discuss the age of the Nyk Slide, as well as the newly documented slide older than 43,500 cal BP.

Before discussing the landslide emplacement ages it is important to mention some key sources of uncertainty in dating submarine landslides, Determining the age of landslide and turbidity current deposits relies on identifying the exact boundary between turbidites and hemipelagic sediment, which can be unclear. This is often due to bioturbation by infaunal organisms, which can mix sediment types and make defining this boundary difficult. This mixing of sediment by bioturbation can skew the ages of radiocarbon dates by incorporating either older or younger carbon into a sampling zone; although this is impossible to quantify. In order to account for this any bioturbated boundaries between turbidites and hemipelagite are taken to be where both sediment ocurrs in equal proportions.

5.5.1.1 The Trænadjupet Slide

AMS radiocarbon dates from above and below turbidites in the Lofoten Basin give a reasonable age range of 2,750 to 5,600 cal BP for the Trænadjupet Slide. However, the maximum ages of ~5,600 cal BP found in cores 31 and 57 are likely skewed by the incorporation of older carbon due to basal erosion at more proximal sites (Fig. 5.10). Basal erosion is also seen below the upper deposit in core 29, giving a considerably older maximum age of 12,559 - 12,729 cal BP (Fig. 5.10). It is possible that this upper deposit in core 29 is older than the Trænadjupet Slide. However, the absence of any younger deposits in core 29, and the upper radiocarbon age of 3,201 - 3,382 cal BP make this unlikely (Fig. 5.10). Using the radiocarbon ages from above deposits of the Trænadjupet

Slide in cores 23, 43, 45, 56 (Fig. 5.7), 29, and 57 (Fig. 5.10) gives an emplacement age range of 2,600 to 3,400 cal BP.

An earthquake or series of earthquakes has been proposed as the trigger of the Trænadjupet Slide (Laberg and Vorren, 2000a). However, independent evidence to support this earthquake trigger is not extensive, and there is considerable uncertainty over how the slide was triggered (Laberg and Vorren, 2000a; Laberg et al., 2002a). The Trænadjupet Slide postdates the most rapid periods of glacial rebound that may have triggered particularly large and frequent earthquakes (Bungum et al., 2010). Multiple small mass transport deposits were emplaced between 2,800 and 3,200 cal BP in fjords and lakes along the Norwegian coastline (Bøe et al., 2012). This age range broadly coincides with the 2,600 to 3,400 cal BP age range of the Trænadjupet Slide emplacement. It is possible that these mass transport deposits in fjord and lakes were also triggered by the regional earthquake or series of earthquakes that is proposed to have triggered the Trænadjupet Slide. However, the occurrence of these small-scale mass movements has been attributed to climatic 'irregularities' on the basis of the ~400 year range of radiocarbon ages; although their triggers are uncertain.

It has been proposed that large submarine landslides tend to coincide with rapid sea level rise (Smith et al., 2010; Brothers et al., 2013), although this is not shown by the most recent global compilations of landslide ages (Urlaub et al., 2013). Furthermore, the Trænadjupet Slide does not coincide with rapid global eustatic or local sea level rise (Lambeck et al., 2014; Barnett et al., 2015), and was not likely triggered in this way. The late Holocene timing of the Trænadjupet Slide, as well as smaller and more recent slides originating from the headwall (Laberg et al., 2002a), may support the view that landslide recurrence is close to temporally random (Clare et al., 2014; Pope et al., 2015). The randon or near-random occurrence of such slides on both passive and active margins, as well as during all sea level states makes them difficult to predict (Urlaub et al., 2013; Baeten et al., 2014; Li et al., in press). However, the risk they pose to offshore infrastructure requires that they be fully considered in geohazard assessment.

5.5.1.2 The Nyk Slide

AMS radiocarbon ages for the Nyk Slide from cores 31, 57, and 79 give a maximum age of 20,898 cal BP and a minimum age of 18,643 cal BP for lobe 2 of the Nyk Slide (Figs. 5.10 and 5.12). This age range is relatively consistent with the previously reported age of ~19,000 cal BP for the Nyk Slide (Lindberg et al., 2004). Core 46 contains the fine-grained mud cap of a deposit at its base, with a minimum age of 15,153 - 15,561 cal BP (Fig. 5.10). It is unclear whether this deposit is related to the Nyk Slide, or to smaller landslides that are observed on the adjacent Norwegian Margin to the east (Baeten et al., 2014). If this deposit relates to the emplacement of Lobe 3 of the Nyk Slide, it suggests that there is approximately 3,000 - 4,000 year age difference between the two largest lobes. The age ranges of 2 event deposits found in core 46 (11,114 - 11,350 and 15,153 - 15,561 cal BP; Fig. 5.12) broadly correspond to radiocarbon ages of the oldest hemipelagic drape in the western areas of the Nyk Slide scar (10,148 and 15,151 cal BP; Fig 5.1). This further supports the Nyk Slide as having multiple stages of failure; although no other deposits in the Lofoten Basin have been dated to these same ages (Fig. 5.12)

Drawing conclusions about the dynamics of the Nyk Slide is more problematic than for the Trænadjupet Slide. The number of cores that contain Nyk-aged deposits is substantially smaller than those containing Trænadjupet deposits, making determining the ages of the individual lobes difficult. Of those radiocarbon ages that do exist for the Nyk Slide, most are minimum ages given that the majority of cores have not penetrated through the thick deposits. The lack of bathymetry data, core coverage, and AMS radiocarbon ages mean we cannot say with any certainty whether the Nyk Slide was multi-staged, nor whether it was top-down or bottom-up. Here we can estimate the age of the Nyk Slide to 18,600 - 20,900 cal BP, consistent with previous age information (Fig. 5.1; Lindberg et al., 2004). The refined age of the Nyk Slide gives us little additional information on possible triggers.

5.5.1.3 Lobe 1 - A third major slide event

The age of Lobe 1 is less clear, as two hypotheses are plausible. The first hypothesis is lobe 1 is relatively old. This assumes that the blocky top of Lobe 1 lies beneath >10 m of flat lying and in-

situ hemipelagic sediment evident in cores 64 and 65 (Fig. 5.11). This hypothesis implies that the age of lobe 1 is considerably older than 43,500 cal BP. This is surprising because it implies that lobe 1 originates from an even earlier failure than the main Nyk Slide. The second hypothesis is that cores 64 and 65 contain flat lying sediment because they penetrated into flat lying blocks comprising failed material within Lobe 1. However, the only evidence for deformation within cores 64 and 65 lies at 8.25m in core 64. Given the blocky nature of lobe 1 (Fig. 5.11A) it is surprising that two cores both penetrated flat areas in such a blocky lobe. Such flat lying deposits also contrast with the clast rich and more extensively deformed deposits that comprise lobes 2 and 3 (Fig. 5.10). From available evidence we favour the initial hypothesis that lobe 1 is much older than both Nyk and Trænadjupet Slides; and thus represents at least a third major episode of slope failure.

5.5.2 Was the Trænadjupet Slide retrogressive (bottom-up) or progressive (top-down)?

There are two proposed emplacement models for multi-staged submarine landslides. The first model is retrogression whereby initial failure occurs in deeper water, and is followed by multiple additional failures that advance upslope creating a step-like morphology (Bryn et al., 2005; Masson et al., 2010). The second is progression, whereby failure is initiated in shallower water near the shelf edge, and is followed by additional landslides that propagate downslope (Gee et al., 1999; Masson et al., 2010). This second progressive model has largely been discounted for most mapped landslides in favour of retrogression based on the stepped morphology of many large slides and blocky debris flows that drape headwalls (Canals et al., 2004; Masson et al., 2006; Masson et al., 2010)

The lobate structure of the Trænadjupet Slide is proposed to be the result of multiple landsliding stages (Laberg et al., 2006). However, the time between the stages of landsliding is unknown, as is the relationship between Lobes 1 - 3 and the 3 observed headwalls. Here we will use the newly acquired bathymetric dataset to address which landslide emplacement model best describes the failure of the Trænadjupet Slide.

5.5.2.1 Slide morphology and relative timing of headwalls 1 - 3

Previously published sidescan sonar and bathymetric data from the Trænadjupet Slide have revealed 3 distinct headwalls (Fig. 5.7A; Laberg and Vorren, 2000a; Mozzato et al., in review). These headwalls are associated with linear features that most likely represent erosional lineations or debris flow lobes (c.f. Masson et al., 2006; Fig. 5.7). More detailed imaging of the data from these headwalls indicates that these linear features are not continuous from above to below these headwalls (Fig. 5.7B - D). There is also no convincing evidence of blocky sediment drape that originated upslope extending over headwalls; a feature that has been observed in some large, retrogressive submarine landslides (Haflidason et al., 2004; Masson et al., 2010). Assuming that such features are not below the resolution of the bathymetric data (~0.5% water depth or < 50 m across), this suggests that the headwalls cut all previous erosional lineations or debris flow lobes generated by failure further upslope. Importantly, headwall 3 clearly truncates the side wall of the Trænadjupet Slide that is linked to headwalls 1 and 2 (Fig. 5.7D). Thus, failure of headwall 3 appears to represent the final stage of the Trænadjupet Slide. The truncation by H3 into the previous H2 side wall and the presence of blocky debris orientated parallel to the western edge of the H3 scar (Fig. 5.7D) suggests that this final stage also involved failure of the side wall.

It is proposed here that headwall 1 (H1) failed initially, followed by headwall 2 (H2) and finally by headwall 3 (H3), indicating a top-down or progressive failure. Headwalls 1 and 2 accounted for ~500 km^3 of material, whilst headwall 3 represents around ~100 km^3 (Mozzato et al., in review). This is a notable conclusion, as many previous studies have inferred that large submarine landslides are retrogressive, and fail from the bottom up (Canals et al., 2004; Bryn et al., 2005; Masson et al., 2006; 2010). In this instance, it appears that failure began initially near the top of the slope (headwalls 1 and 2), and the final stage of failure (headwall 3) was in deep water. However, the bathymetric data cannot provide an indication of the time between these different stages of failure.

5.5.2.2 Relationship between the Trænadjupet Slide and other small slides on the margin

The exact position of the northern end of headwall 2 is unclear due to the large number of smaller landslides described along the continental slope north of the Trænadjupet Slide (Fig. 5.7A and C).

The precise relationship between the Trænadjupet Slide and these smaller slides is still unknown, although they are inferred to have been contemporaneous with the Trænadjupet Slide, further supporting an earthquake trigger (Baeten et al., 2014). The failure of the Trænadjupet Slide may have facilitated these smaller slides by destabilising sediment upslope; possibly along the same failure surface. If these smaller slides post-date the Trænadjupet Slide, they may have obscured or removed the northern sidewall of the slide, as well as the northern end of headwall 2. This could account for the difficulty in identifying features on the northern edge of the Trænadjupet Slide using the bathymetric data (Fig. 7.5A). Alternatively, these small slides may be unrelated to the Trænadjupet Slide. Thinning of the Trænadjupet Slide towards its northern edge could explain the absence of clearly defined side- and headwalls (Haflidason et al., 2003).

5.5.3 How closely spaced were the stages of the Trænadjupet Slide?

Numerical simulations of retrogressive submarine landslides have demonstrated that the time between individual stages of failure is important for determining tsunami wave amplitude (Haughen et al., 2005; Harbitz et al., 2006; Løvholt et al., 2015). Therefore determining any time between the deposition of individual turbidites, or in the emplacement age of the lobes associated with the Trænadjupet Slide is important for building numerical simulations of the slide and the associated tsunami generation.

5.5.3.1 Lobe emplacement ages

The ages of lobes 2 and 3 in the Trænadjupet Slide appear to be broadly comparable (Fig. 5.7). Lobe 2 has an age range of ~2,750 - 2,900 cal BP from dates above the most recent deposit in core 57 (Fig. 5.10). Lobe 3 generated turbidites in cores 43 and 45 with an age ranges of ~2,750 - 3000 and ~2,750 - 2,950 cal BP respectively (Fig. 5.7). However, the uncertainties involved in dating marine sediments make it unlikely that differences in emplacement age of less 100 - 300 years would be resolvable (Urlaub et al., 2013).

5.5.3.2 Distal turbidites

As the Trænadjupet Slide occurred as a series stages the time gaps may be recorded by hemipelagic sediments between stacked turbidites in the Lofoten Basin (Wynn and Masson, 2003; Hunt et al.,

2013a). Deposits from cores 31 and 68 in the Lofoten Basin show no evidence of repeated upward fining sequences that might result from disparate landslide events (Figs. 5.9A and C). The only notable exception to this is core 50, which contains a debris flow deposit with a repeating pattern of pebble conglomerate overlain by coarse sand (Fig. 5.9B). It is possible that this alternating pattern is representative of debris flows from multiple landslide stages reaching this core site. However, given the absence of similar deposits in any other cores, it is more likely that this repeating pattern is the result of pulsing or surging within a single debris flow (Syvitski and Haim, 1991; Major, 1997). Therefore, data collected from the deposits of the Trænadjupet Slide appear to support a single block failure, or a multi-staged failure with closely spaced stages that prevented stacked deposits from accumulating.

It is difficult to say with any certainty how much time separated the different stages of the Trænadjupet Slide. Basal erosion by turbidites can cannibalise deposits from previous landslides and hemipelagite, stripping any record of multi-staged failure and affecting the ability to accurately date slide sediments (Masson et al., 2011). Turbidity currents have the potential to bypass areas of seafloor, leaving little or no depositional record of the landslides that generated them (Piper and Normark, 2009; Stevenson et al., 2013). Turbidity currents may also fail to reach core locations due to their distance from source or the local topography (Arzola et al., 2008; Lebreiro et al., 2009; Allin et al., 2016). However, the absence of any stacked turbidite deposits implies that the slide more likely occurred as a series of closely spaced (~hours) stages (Bryn et al., 2005; Haughen et al., 2005; Løvholt et al., 2015).

5.5.4 Do Trænadjupet-aged tsunami deposits exist?

Lake records on the Norwegian Margin and Shetland Islands have revealed some of the largest Storegga tsunami run-up heights observed; in some cases greater than 20 m (Bondevik et al., 1997b; 2005a; b). Investigation has revealed no similar tsunami deposits that are coeval with the Trænadjupet Slide (Bondevik, 2002; Mozzato et al., in review). Garth Loch on the Shetland Island coastline contains a tsunami deposit date at ~5,500 cal BP that may have resulted from the Trænadjupet Slide (Fig. 5.13; Bondevik et al., 2005a). Another potential Trænadjupet tsunami deposit has been identified in Skjolnesmyra isolation basin on the southern Norwegian coastline

dated to between 5,310 - 5,470 cal BP, consistent with the deposits observed on the Shetland Islands (Romundset et al., 2015).

The newly defined 2,600 - 3,400 cal BP age range of the Trænadjupet Slide places it younger than the ~5,500 cal BP tsunami deposits found on the Shetland Island and southern Norwegian coastlines. Thus the ~5,500 cal BP tsunamite observed at sites on the Shetland Islands is the result of a more localised tsunami event that may have deposited at isolated sites on the Norwegian Margin, or vice versa.

5.5.5 Why did the Trænadjupet Slide not produce a large tsunami?

The absence of any coeval tsunami deposits doesn't fully prove that the Trænadjupet Slide was not tsunamigenic. However, it does suggest that if a tsunami was generated it was small enough not to be widely preserved on coastlines close to the slide headwall. There are a number of explanations for the absence of a widespread tsunami deposit associated with the Trænadjupet Slide. Here we will discuss these possible explanations in light of the new information on the behaviour of the Trænadjupet Slide.

5.5.5.1 Incomplete tsunami records

Tsunami records used by Mozzato et al. (in review) were obtained from lakes that were between 0 - 5 m above sea level at the proposed time of the Trænadjupet Slide (Fig. 5.13; Bondevik, 2002). Given the number of lakes studied, their typically low elevations above sea level, and the proximity of some lakes to the Trænadjupet headwall, it seems unlikely that these lakes would not have recorded a tsunami if one had occurred. One possibility is that the presence of winter ice along the Norwegian coastline hindered the deposition of characteristic tsunami sediments within these lakes (Romundset and Bondevik, 2011).

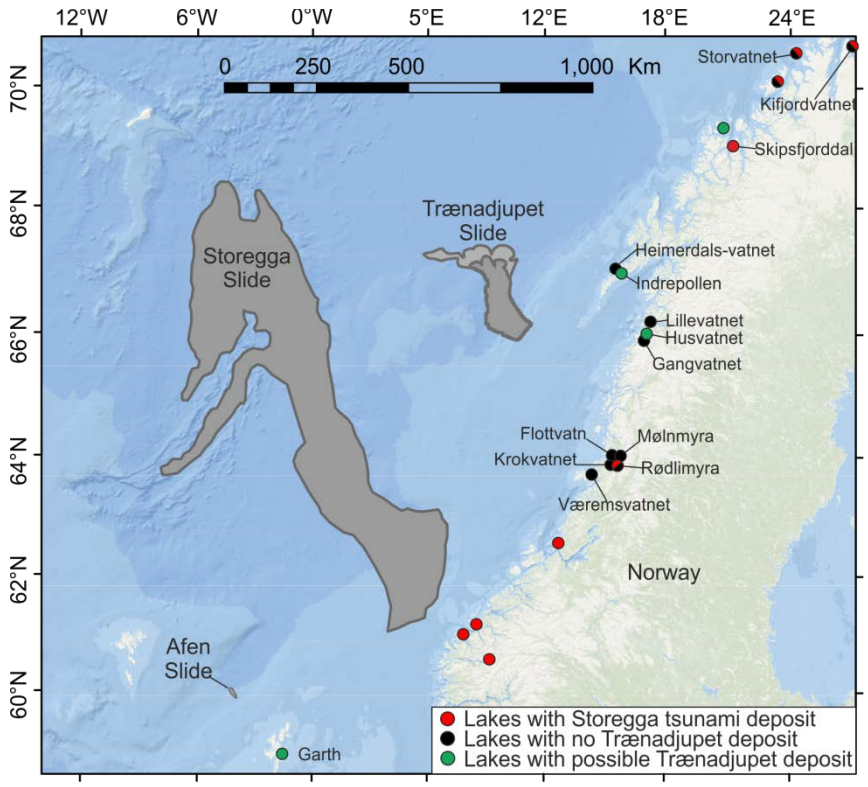

Figure 5.13: Map showing the locations of lake cores with Storegga tsunami deposits, without Trænadjupet tsunami deposits, and those with potential Trænadjupet tsunami deposits such as 5,500 cal BP Garth on the Shetland Islands. Also shown is the location of the Afen Slide at <5800 cal BP, which may also have generated a tsunami capable of depositing the Garth tsunamite on Shetland Islands (adapted from Mozzato et al., in review).

5.5.5.2 Multi-staged behaviour

While large strides in our understanding of submarine landslides have been made through numerical simulations, only a limited number of such studies have considered the influence of multi-staged failure in tsunami generation (e.g. Bondevik et al., 2005b; Haughen et al., 2005; Løvholt et al., 2015). The majority of these numerical experiments have assumed retrogressive slide behaviour for large slides (Bondevik et al., 2005b). A top-down emplacement, such as observed for the Trænadjupet Slide, has largely been neglected in numerical experiments.

One of the key factors affecting the generation of tsunamis by multi-staged landslides is the timescale of the individual failures. Numerical modelling has shown that time lags >60 seconds between stages of landsliding can substantially reduce the amplitude of the resulting tsunami wave. Conversely, time lags ~20 seconds between stages may act to positively reinforce the tsunami wave, resulting in greater amplitudes (Haughen et al., 2005; Løvholt et al., 2015). Time lags on the

order of 60 seconds between stages of the Trænadjupet Slide may explain why no large tsunami was generated. However, the absence of clear cross-cutting lineations and debris flows suggests that failure originating at H1 traveled downslope beyond the location of H2 before the second stage of failure occurred. Given the 40 Km downslope distance between H1 and H2, and assuming a speed of ~20 m/s, time lags of ~hours between stages of failure seem more likely. These ~hour time gaps might explain why no stacked turbidite deposits are observed in the Lofoten Basin, as these likely require days or weeks between failure stages to form (Wynn and Masson, 2003; Hunt et al., 2013a). The apparent lack of a tsunami generated by the Trænadjupet Slide may therefore be due to a slow initial acceleration of the slide (Haughen et al., 2005). The blocky nature of the Trænadjupet Slide deposits might suggest a slower movement than more rapid, disintegrative landslides such as the Storegga Slide (Bryn et al., 2005). Steeper slopes are associated with larger tsunamis, so the low (~1°) slope angle of the Trænadjupet area may have prevented the generation of a tsunami (McAdoo and Watts, 2004). However, the slope angles for the Storegga and Trænadjupet areas are broadly similar (~1°), suggesting slope angle was not a key limiting factor (Laberg and Vorren, 2002a; Bryn et al., 2005).

5.5.6 Implications for landslide geohazards

Submarine landslide-triggered tsunamis have been recognised since at least the 1950s (Heezen and Ewing, 1952), and historical events have resulted in considerable damage and loss of life (Tappin et al., 2008). What has been less clear is whether or not all large (>1 km^3) submarine landslides are capable of generating tsunamis. Answering this question has proven problematic due to the >50,000 year (i.e. pre radiocarbon) age of many such landslides, as well as uncertainty surrounding their characteristics (i.e. volume, velocity, acceleration, and emplacement style). Furthermore, the preservation potential of paleo-tsunami deposits that can be correlated with landslides is in many instances very poor, particularly in arid regions prone to flooding, or in regions affected by repeated glaciation (Weiss and Bahlburg, 2006; Spiske et al., 2013); although progress has been made on certain slides (e.g. Iglesias et al., 2012; Løvholt et al., 2014).

The Trænadjupet Slide did not produce a tsunami, or produced a tsunami that was not large enough to leave any deposits in isolated basins at or near sea level (Bondevik, 2002; Mozzato et al., in

review). The similarities between the Nyk and Trænadjupet Slides in terms of deposit types and morphology implies that their failure dynamics may have been similar. Thus, the tsunamigenic potential for both may have been minimal, despite their considerable volumes. However, this would need to be further substantiated with numerical modelling experiments.

While considerable strides have been made in our understanding of large submarine landslides, their tsunami hazard is a function of their failure dynamics; something that is difficult to reconstruct precisely. Other than a few exceptions like the Storegga Slide, the Big ’95 Slide, and now perhaps the Trænadjupet Slide, the dynamics and tsunamigenic potential of many large submarine landslides remain poorly understood. The tsunami risk from large submarine landslides is limited to those slides that have sufficient volume, dimensions, initial acceleration, velocity, and fail as a single or closely spaced (~mins to hours) stages (Bondevik et al., 2005b; Haughen et al., 2005; Løvholt et al., 2014; Løvholt et al., 2015). Slides that conform to these criteria and can generate damaging tsunamis may be infrequent on the North Atlantic Margin and elsewhere, which would have implications for global geohazard assessment. More detailed investigations of the age and emplacement dynamics of large submarine slides is needed if the hazards they pose are to be fully realised.

5.6 Conclusions

The deposits of the Trænadjupet Slide are largely comprised of coarse debris flow sediments, fining distally to debrites/coarse turbidites, and eventually into fine silt/mud in the Lofoten Basin. Based on radiocarbon dates from distal and proximal deposits the age of the Trænadjupet Slide can be refined to between ~2,600 and ~3,400 cal BP. The Trænadjupet Slide is not coeval with ~5,500 cal BP tsunami deposits discovered in Garth Loch on the Shetland Islands. Instead, the Garth tsunamite is likely the result of a localised event on the Shetland or Norwegian Margins. The Trænadjupet Slide is broadly coeval with a widespread occurrence of submarine landslides in fjords and lakes on the Norwegian Margin between 2,800 and 3,200 cal BP. This coincident timing supports a seismic trigger of the Trænadjupet Slide; although climatic factors may also have been responsible.

The Trænadjupet Slide was a top-down progressive failure, with headwall 1 (H1) failing initially, followed by H2 and H3 respectively. This is an important conclusion, as most models for large-volume landslide emplacement propose retrogressive behaviour. The distal deposits of the Trænadjupet Slide show no evidence of stacked turbidites, and so do not record multiple stages of failure. It is likely that turbidites from the individual stages of failure coalesced downslope, indicating a rapid (~several hours) landslide progression. These times between stages of failure could also account for the absence of any tsunami deposits on adjacent coastlines.

A new age of between 18,600 and 20,900 cal BP is proposed for the Nyk Slide based on widespread turbidites in the Lofoten Basin. An additional slide has also been identified that is older than 43,500 cal BP, meaning at least three large slides have originated from this section of margin. The youngest of these, the Trænadjupet Slide, did not occur during phases of sea level change, high sedimentation rate, or rapid isostatic adjustment associated with glacial retreat. This lends support to the view that large submarine landslides are temporally random in time.

Chapter 6: Conclusions and Future Work

6.1 Conclusions

This thesis concludes that long turbidite records from deep sea canyons and abyssal plains can be used to understand both the controlling mechanisms and emplacement dynamics of submarine landslides and turbidity currents. Statistical analysis of long term turbidite records can reveal information about the long-term controls on turbidity current frequency. This is important for hazard assessment of strategic infrastructure in light of projected environmental change such as sea level rise. Submarine landslides may also be less tsunamigenic than their volume suggests, requiring a more in depth analysis of submarine landslide timing and emplacement dynamics before their tsunamigenic hazards are considered. The key findings of this thesis are summarised as follows:

1. Turbidity current frequency within the Nazaré Canyon decreases downslope and with increasing elevation above the canyon floor. The correct positioning of sediment cores within submarine canyons is essential to recovering accurate records of turbidity current frequency. Terraces can provide shorter-term records of sediment transport on the order of ~1,000 years. However, distal canyon levees are likely the best setting for recovering long (> 10 kyr) turbidite records that can be analysed using statistical methods.
2. The frequency of turbidity currents that fill Nazaré Canyon over geological timescales is strongly controlled by eustatic sea level. Periods of sea level highstand are characterised by a low frequency of turbidity currents reaching the lower canyon and over spilling the levees. Periods of sea level lowstand are accompanied by an increase in turbidity currents reaching the lower canyon. The frequency of turbidites over the last 30,000 years can also be correlated statistically with 3 different eustatic sea level reconstructions, indicating it is a dominant factor.
3. The frequency of turbidity currents that flush large volumes of sediment out of the Nazaré Canyon and into the Iberian Abyssal Plain are largely unaffected by eustatic sea level

variability. The recurrences of canyon flushing events in the Iberian Abyssal Plain are not statistically correlated with eustatic sea level variability. However, the recurrence intervals of canyon flushing are associated with changes in the amplitude and periodicity of eustatic sea level. This is likely due to the increased exposure of Portuguese continental shelf to subaerial erosion and a subsequent increase in basin-ward sediment transport. Some of these canyon flushing events may be triggered by earthquakes, although a seismic trigger is difficult to invoke for all turbidites.

4. Two different distribution forms of canyon-flushing recurrences are observed in the Iberian Abyssal Plain. An exponential distribution form is observed more distally, indicating a lack of time-dependence. In contrast, recurrence intervals of turbidites in the proximal Iberian Abyssal Plain conform to a lognormal distribution form and also cannot be linked to sea level change. This change in distribution form across may be explained by variable turbidity current run-out distance, although different sources and triggers of turbidity currents may also be responsible. The differing distribution forms further suggests that the location of core sampling sites can affect the record of turbidity currents, and thus affect the estimates of frequency and recurrence that underpin hazard prediction.
5. Based on newly acquired AMS radiocarbon dates, the emplacement age of the Trænadjupet Slide can be refined to between ~2,600 and ~3,400 cal BP.
6. The Trænadjupet Slide was likely a progressive failure with ~hourlags between stages. These time lags may have been short enough to prevent a tsunami from being generated, while also resulting in the coalescing of individual turbidites. Alternatively, the lack of a tsunami could be explained by a slow initial acceleration of the slide; although this hypothesis is impossible to test using the data available here.
7. The emplacement age of the Nyk Slide can be better refined to between 18,600 and 20,900 cal BP.
8. Lobe 1 of the Nyk Slide represents a much older (>43,500 cal BP) landslide event, meaning that at least three slides have occurred on this section of margin.
9. The absence of a tsunami generated by the Trænadjupet Slide, suggest that other very large (>100km^3) submarine landslides may have a lower geohazard potential than other well

documented slides such as the Storegga Slide. More detailed assessments of the age and emplacement dynamics of large submarine landslides are needed before their hazard potential is fully realised.

6.2 Future Work

The following are proposals for future work on submarine landslide frequency and triggers. The two key geographical areas will focussed on: The Iberian Abyssal Plain and the Trænadjupet Slide.

6.2.1 Iberian Abyssal Plain

While this thesis has documented the presence of large-volume turbidity currents reaching the Iberian Abyssal Plain, the exact volumes and extent of these turbidites are unknown. There is a suite of cores from across the Iberian Abyssal Plain in various states of description that could provide estimates of sediment volumes, run-out distance, and sediment transport mechanism of turbidity currents that flush submarine canyons.

One aspect of sediment transport not addressed in this thesis would follow previous work evaluating the organic carbon storage and burial in the Nazaré Canyon. Many turbidites in the Iberian Abyssal Plain have volumes that are likely greater than 10 km^3, implying that significant amounts of carbon are transported into the deep ocean by canyon flushing turbidity currents. This research would have importance for understanding global carbon budgets and sequestration.

One final aspect that was not fully addressed in Chapter 3 was the role of earthquakes in triggering turbidites in the Iberian Abyssal Plain. Turbidites in the Tagus and Horseshoe Abyssal Plains are proposed to be the result of regional earthquakes. However, only 3 turbidites in the Iberian Abyssal Plain can be confidently correlated into these two basins (Fig. 5.10). The comparison with the Tagus and Horseshoe Abyssal Plain is limited by the short 25 kyr length of their existing turbidite records, as opposed to the 80 kyr record in the Iberian Abyssal Plain (Grácia et al., 2010; Masson et al., 2011b). New AMS radiocarbon dates have been collected from existing Tagus and Horseshoe Abyssal Plain cores that extend the records of turbidites back to ~35 kyr. This extension of the turbidite record in the Tagus and Horseshoe Abyssal Plains will provide a better insight into the

role of earthquakes in triggering sediment gravity flows along the Iberian Margin. This longer record may also provide more insight into the role of earthquakes in triggering canyon flushing in the Nazaré Canyon.

6.2.2 Trænadjupet Slide

This thesis has provided additional insight into the failure and emplacement dynamics of the Trænadjupet Slide. However, whether or not the proposed short time lags (~60s) between stages of failure can fully account for the absence of a tsunami is still unclear. Furthermore, no estimates of slide acceleration or velocity can be made using only the sedimentary and AMS radiocarbon data. These gaps in understanding limit the ability to model the Trænadjupet Slide and its geohazard potential. Previous work on the Storegga Slide used landslide-tsunami modelling with different landslide velocities and accelerations. The values for these parameters that best recreated the observed run-up heights of the Storegga tsunami on nearby coastlines were deemed to be good approximations of the slide's characteristics. One approach to determining the failure characteristics of the Trænadjupet Slide might be to test what values for parameters such as velocity, acceleration, and lags between stages of failure can generate little or no tsunami in numerical simulations. This type of modelling (a reverse inference) may provide additional information about the dynamics of the Trænadjupet Slide and corroborate the conclusions drawn in this thesis.

Appendices

Appendix A	Core photographs from cores used in Chapter 3.
Appendix B	Hemipelagic thicknesses, age model, and turbidite ages from core JC27-46.
Appendix C	Results of the Linear and Cox PHM from core JC27-46.
Appendix D	Results of the Mann Whitney and Kolmogorov-Smirnoff tests of Iberian Abyssal Plain turbidites from core JC27-51 against other distal basin records.
Appendix E	Hemipelagic thicknesses, age model and turbidite ages from ODP Hole 898A.
Appendix F	Photographs of cores used in Chapter 5.

References

Abdel Aal, A., Barkooky, A. El., Gerrits, M., Meyer, H., Schwander, M., Zaki, H., 2000. Tectonic evolution of the Eastern Mediterranean Basin and its significance for hydrocarbon prospectivity in the ultradeepwater of the Nile Delta. The Leading Edge 19 (10), 1086-1102.

Abraimov, S.G., Turcotte, D.L., Shcherbakov, R., Rundle, J.B., Yakovlev, G., Goltz, C., Newman, W.I., 2008. Earthquakes: Recurrence and interoccurrence times. Pure and Applied Geophysics 165, 777-795.

Adams, J., 1990. Paleoseismicity of the Cascadia subduction zone: Evidence from turbidites off the Oregon-Washington margin. Tectonics 9, 569–583.

Allin, J.R., Hunt, J.E., Talling, P.J., Clare, M.E., Pope, E., Masson, D.G., 2016. Different frequencies and triggers of canyon filling and flushing events in Nazaré Canyon, offshore Portugal. Marine Geology 371, 89-105.

Almeida, L.P., Ferreira, Ó., Vousdoukas, M.I., Dodet, G., 2011. Historical variation and trends in storminess along the Portuguese South Coast. Natural Hazards and Earth System Sciences 11, 2407–2417.

Alonso, B., Ercilla, G., Casas, D., Estrada, F., Farrán, M., Garcia, M., Rey, D., Rubio, B., 2008. Late Pleistocene and Holocene sedimentary facies on the SW Galicia Bank (Atlantic NW Iberian Peninsula). Marine Geology 249, 46–63.

Alves, T.M., Gawthorpe, R.L., Hunt, D.W., Monteiro, J.H., 2003. Cenozoic tectono-sedimentary evolution of the western Iberian margin. Marine Geology 195, 75-108.

Amy, L.A., Talling, P.J., Edmonds, V.O., Sumner, E.J., Lesueur, A., 2006. An experimental investigation of sand–mud suspension settling behaviour: implications for bimodal mud contents of submarine flow deposits. Sedimentology 53(6), 1411-1434.

References

Arzola, R.G., Wynn, R.B., Lastras, G., Masson, D.G., Weaver, P.P.E., 2008. Sedimentary features and processes in the Nazaré and Setúbal submarine canyons, west Iberian margin. Marine Geology 250, 64-88.

Atwater, B.F., Carson, R., Griggs, G.B., Johnson, H.P., Salmi, M.S., 2014. Rethinking turbidite paleoseismology along the Cascadia subduction zone. Geology 42, 827-830.

Baeten, N.J., Laberg, J.S., Vanneste, M., Forsberg, C.F., Kvalstad, T.J., Forwick, M., Vorren, T.O., Haflidason, H., 2014. Origin of shallow water submarine mass movements and their glide planes - Sedimentological and geotechnical analyses from the continental slope off northern Norway. Journal of Geophysical Research: Earth Surface 119, 2335-2360.

Bagnold, R.A., 1962. Auto-suspension of transported sediment: turbidity currents, Royal Society of London Proceedings, Series A 265, 315-319.

Balsam, W.L., Deaton, B.C., Damuth, J.E, 1999. Evaluating optical lightness as a proxy for carbonate content in marine sediment cores. Marine Geology 161, 141-153.

Baptista, M.A., Miranda, J.M., 2009. Revision of the Portuguese catalogue of tsunamis. Natural Hazards and Earth System Sciences 9, 25–42.

Barnett, R.L., Gehrels, W.R., Charman, D.J., Saher, M.H., Marshall, W.A., 2015. Late Holocene sea-level change in Arctic Norway. Quaternary Science Reviews 107, 214-230.

Bassingthwaighte, J.B., Raymond, G.M., 1994. Evaluating rescaled range analysis for time series. Annals of Biomedical Engineering 22, 432-444.

Bates, R.L., Jackson, J.A., 1987. Glossary of Geology. Amer. Geol. Inst., Alexandria, USA. 788 pp.

Beattie, P. D., & Dade, W. B. (1996). Is scaling in turbidite deposition consistent with forcing by earthquakes? Journal of Sedimentary Research 66 (5), 909-915.

Bellwald, B., Hjelstuen, B.O., Sejrup, H.P., Haflidason, H., 2016. Postglacial mass failures in the inner Hardangerfjorden system, Western Norway. In: Lamarche, G., Mountjoy, J., Bull, S.,

et al. (eds). Submarine mass movements and their consequences. Advances in Natural and Technological Hazards Research, vol 41. Kluwer, The Netherlands, pp 73-84.

Bøe, R, Longva, O., Lepland, A., Blikra, L.H., Sønstegaard, E., Haflidason, H., Bryn, P., Lien, R., 2012. Postglacial mass movements and their causes in fjords and lakes in western Norway. Norwegian Journal of Geology 84, 35-55.

Bondevik, S., 2002. Records of paleo-tsunamis around the Norwegian Seas. Report, Norsk Hydro, University of Tromsø.

Bondevik, S., Løvholt, F., Harbitz, C., Mangerud, J., Dawson, A., Svendsen, J.I., 2005b. The Storegga Slide tsunami—comparing field observations with numerical simulations. Marine and Petroleum Geology 22, 195-208.

Bondevik, S., Mangerud, J., Dawson, S., Dawson, A., Lohne, Ø., 2005a. Evidence for three North Sea tsunamis at the Shetland Islands between 8000 and 1500 years ago. Quaternary Science Reviews 24, 1757-1775.

Bondevik, S., Mangerud, J., Dawson, S., Dawson, A.G., Lohne, Ø., 2003. Record-breaking Height for 8000-Year-Old Tsunami in the North Atlantic. EOS, Transactions of the American Geophysical Union 84 (31), 289-293.

Bondevik, S., Svendsen, J.I., Johnsen, G., Mangerud, J., Kaland, P.E., 1997a. The Storegga tsunami along the Norwegian coast, its age and run up. Boreas 26 (1), 29-53.

Bondevik, S., Svendsen, J.I., Mangerud, J., 1997b. Tsunami sedimentary facies deposited by the Storegga tsunami in shallow marine basins and coastal lakes, western Norway. Sedimentology 44 (6), 1115-1131.

Borges, J., Fitas, A.J.S., Bezzeghoud, M. & Teves-Costa, P., 2001. Seismotectonics of Portugal and its adjacent Atlantic area, Tectonophysics 331 (4), 373–387.

Bouma, A.H., 1962. Sedimentology of some Flysch Deposits: A Graphic Approach to Facies

References

Bray, M.J., Hooke, J.M., 1997. Prediction of soft-cliff retreat with accelerating sea-level rise. Journal of Coastal Research 13 (2), 453-467.

Bronk Ramsey, C. et al., 2012. A Complete Terrestrial Radiocarbon Record for 11.2 to 52.8 kyr B.P.. Science 338, 370-374.

Bronk Ramsey, C., 2008. Depositional models for chronological records. Quaternary Science Reviews 27, 42-60.

Brothers, D.S., Luttrell, K.M., Chaytor, J.D., 2013. Sea-level-induced seismicity and submarine landslide occurrence. Geology 41 (9), 979–982.

Brushci, R., Bughi, S., Spinazzè, M., Torselletti, E., Vitali, L., 2006. Impact of debris flows and turbidity currents on seafloor structures. Norwegian Journal of Geology 86, 317-337.

Bryn, P., Berg, K., Forsberg, C.F., Solheim, A., Kvalstad, T.J., 2005. Explaining the Storegga Slide. Marine and Petroleum Geology 22, 11-19.

Buforn, E., Udías, A., Colombás, M.A., 1988. Seismicity, source mechanisms and tectonics of the Azores-Gibraltar plate boundary. Tectonophysics 152, 89-118.

Bugge, T., Belderson, R.H., Kenyon, N.H., 1988. The Storegga Slide. Philosophical Transactions of the Royal Society of London A 325, 357-388.

Bungum, H., Olesen, O., Pascal, C., Gibbons, S., Lindholm, C., Vestøl, O., 2010. To what extent is the present seismicity of Norway driven by post-glacial rebound? Journal of the Geological Society 167, 373-384.

Camilli, R., Reddy, C.M., Yoerger, D.R., Van Mooy, B.A.S., Jakuba, M.V., Kinsey J.C., McIntyre, C.P., Sylva, S.P., Maloney, J.V., 2010. Tracking hydrocarbon plume transport and biodegradation at deepwater horizon. Science 330, 201-204.

Canals, M., Lastras, G., Urgeles, R., Casamor, J.L., Mienert, J., Cattaneo, A., Batist, M.D., Haflidason, H., Imbo, Y., Laberg, J.S., Locat, J., Long, D., Longva, O., Masson, D.G., Sultan, N., Trincardi, F., Bryn, P., 2004. Slope failure dynamics and impacts from seafloor

and shallow sub-seafloor geophysical data: case studies from the COSTA project. Marine Geology 213, 9-72.

Canals, M., Puig, P., de Madron, X.D., Heussner, S., Palanques, A., Fabres, J., 2006. Flushing submarine canyons. Nature 444, 354-357.

Carlson, A.E., Winsor, K., 2012. Northern hemisphere ice-sheet response to climate warming. Nature Geoscience 5, 607-613.

Carter, L., Burnett, D., Drew, S., Marle, G., Hagadorn, L., Bartlett-McNeil, D., and Irvine, N., 2009. Submarine Cables and the Oceans—Connecting the World: United Nations Environment Programme, World Conservation Monitoring Center (UNEP-WCMC) Biodiversity Series No. 31: Cambridge, UK, United Nations Environment Programme, World Conservation Monitoring Center: http://www.unepwcmc.org/resources/publications/UNEP_WCMC_bio_series/31.aspx (accessed February 2014).

Carter, L., Gavey, R., Talling, P.J., Liu, J., 2014. Insights into Submarine Geohazards from Breaks in Subsea Telecommunication Cables. Oceanography 27 (2). 58-67.

Carter, L., Milliman, J.D., Talling, P.J., Gavey, R., Wynn, R.B., 2012a. Near-synchronous and delayed initiation of long run-out submarine sediment flows from a record-breaking river flood, offshore Taiwan. Geophysical Research Letters 39 (12), doi:10.1029/2012GL051172.

Carter, L., Milliman, J., Wynn, R.B., Gavey, R., Talling, P.J., Wu, C-Y., Evans, G., Liu, C.-S., Su, C.-C., 2012b. Typhoon flood and earthquakes form long distance sediment flows through the deep ocean off Taiwan. Geophysical Research Letters L12603. http:// dx.doi.org/10.1029/2012GL051172.

Chappelle, J., 2002. Sea level changes forced ice breakouts in the Last Glacial cycle: new results from coral terraces. Quaternary Science Reviews 21, 1229-1240.

Chiocci, F.L., De Alterils, F., 2003. The Ischia debris avalanche: first clear submarine evidence in the Mediterranean of a volcanic island prehistorical collapse. Terra Nova 18, 202-209.

References

Clare, M.A., 2015. Large landslide and turbidity current frequency: implications for hazards and climate change. PhD thesis, University of Southampton.

Clare, M.A., Cartigny, M.J., North, L.J., Talling, P.J., Vardy, M.E., Hizzett, J.L., Sumner, E.J., Hughes Clarke, J.E., Spinewine, B. and Cooper, C., (2015a). Quantification of Nearbed Dense Layers and Implications for Seafloor Structures: New Insights into the Most Hazardous Aspects of Turbidity Currents, Proceedings of the Offshore Technology Conference, May 2015, Houston, TX, USA

Clare, M.A., Talling, P.J., Challenor, P., Malgesini, G., Hunt, J.E., 2014. Distal turbidites reveal a common distribution for large (>0.1 km^3) submarine landslide recurrence. Geology 42 (3), 263-266.

Clare, M.A., Talling, P.J., Challenor, P.G., & Hunt, J.E., 2016. Tempo and Triggering of Large Submarine Landslides: Statistical Analysis for Hazard Assessment. In Submarine Mass Movements and their Consequences. Springer International Publishing, pp. 509-517.

Clare, M.A., Talling, P.J., Hunt, J.E., 2015. Implications of reduced turbidity current and landslide activity for the Initial Eocene Thermal Maximum – evidence from two distal, deep-water sites Earth and Planetary Science Letters 420, 102-115.

Clark, J.D., Pickering, K.T., 1996. Architectural elements and growth patterns of submarine channels: application to hydrocarbon exploration. AAPG bulletin 80, 194-220.

Clark, P.U., Archer, D., Pollard, D., Blum, J.D., Rial, J.A., Brovkin, V., Mix, A.C., Pisias, N. G., Roy, M., 2006. The middle Pleistocene transition: characteristics, mechanisms, and implications for long-term changes in atmospheric pCO2. Quaternary Science Reviews 25, 3150–3184.

Clark, P.U., Dyke, A.S., Shakun, J.D., Carlson, A.E., Clark, J., Wohlfarth, B., Mitrovica, J.X., Hostetler, S.W., McCabe, A.M., 2009. The Last Glacial Maximum. Science 325, 710-714.

Clark, P.U., McCabe, A.M., Mix, A.C., Weaver, A.J., 2004. Rapid rise of sea level 19,000 years ago and its global implications. Science 304, 1141-1144.

Clark, P.U., Mix, A.C., 2000. Ice sheets by volume. Nature 406, 689–690.

Clift, P.D., Shimizu, N., Layne, G.D., Blusztajn, J.S., Gaedicke, C., Schluter, H.U., Clark, M.K., Amjad, S., 2001. Development of the Indus Fan and its significance for the erosional history of the Western Himalaya and Karakoram. Geological Society of America Bulletin 113, 1039-1051.

Cohen, A.C., 1991. Truncated and censored samples: theory and applications. Statistics: textbooks and monographs 119, Marcel Drekker Inc. New York. ISBN: 0824784472.

Coleman, J.M., Suhayda, J.N., Whelan, T., Wright, L.D., 1974. Mass movement of Mississippi River delta sediments. Gulf Coast Association of Geological Societies Transactions 24, 49-68.

Collett, D., 2003. Modelling Survival Data in Medical Research, Second Edition. Texts in Statistical Science, Chapman and Hall/CRC.

Collot, J.Y., Lewis, K., Lamarche, G. and Lallemand, S., 2001. The giant Ruatoria debris avalanche on the northern Hikurangi margin, New Zealand: Result of oblique seamount subduction. Journal of Geophysical Research-Solid Earth, 106(B9): 19271–19297.

Covault, J.A., & Fildani, A., 2014. Continental shelves as sediment capacitors or conveyors: source-to-sink insights from the tectonically active Oceanside shelf, southern California, USA. Geological Society of London Memoirs 41.1, 315–326.

Covault, J.A., Graham, S.A., 2010. Submarine fans at all sea-level stands: Tectono-morphologic and climatic controls on terrigenous sediment delivery to the deep sea. Geology 38, 939-942.

Covault, J.A., Romans, B.W., Fildani, A., McGann, M., Graham, S.A., 2010. Rapid climatic signal propagation from source to sink in a southern California sediment-routing system. Journal of the Geological Society of America 118, 247–259.

Cox, D.R., 1972. Regression models and life-tables. Journal of the Royal Statistical Society, Series B, 187-220.

References

Croudace, I.W., Rindby, A., Rothwell, G., 2006. ITRAX: description and evaluation of a multi-function X-ray core scanner. In: Rothwell, R.G. (Ed.), New techniques in sediment core analysis. Geological Society of London Special Publications 267, pp. 51–63.

Crutchley, G.J., Mountjoy, J.J., Pecher, I.A., Gorman, A.R., Henrys, S.A., 2016. Submarine slope instabilities coincident with shallow gas hydrate systems: insights from New Zealand examples. In: Lamarche, G., et al. (eds.). Submarine Mass Movements and their Consequences, Advances in Natural and Technological Hazards Research 41, pp 401-409.

Custódio, S., Dias, N.A., Carrilho, F., Góngora, E., Rio, I., Marreiros, C., Morais, I., Alves, P., Matias, L., 2015. Earthquakes in western Iberia: improving the understanding of lithospheric deformation in a slowly deforming region. Geophysical Journal International 203, 127-145.

Dahlgren, K.I.T., Vorren, T.O., 2003. Sedimentary environment and glacial history during the last 40 ka of the Vøring continental margin, mid-Norway. Marine Geology 193, 93– 127.

Dasgupta, P., 2003. Sediment gravity flow - the conceptual problems, Earth Science Reviews 62, 265-281.

Dawson, A.G., Long, D., Smith, D.E., Shi, S., and Foster, I.D.L., 1993. Tsunamis in the Norwegian Sea and North Sea caused by the Storegga submarine landslides. In: Tsunamis in the World, edited by S. Tinti, 228 pp., Kluwer Academic Publishers, The Netherlands, 1993.

Dawson, A.G., Shi, S., 2000. Tsunami deposits. Pure and Applied Geophysics 157, 875-897.

de Stigter, H.C., Boer, W., de Jesus Mendes, P.A., César Jesus, C., Thomsen, L., van der Bergh, G.D., van Weering, T.C.E., 2007. Recent sediment transport and deposition in the Nazaré Canyon, Portuguese continental margin. Marine Geology 246, 144-164.

de Stigter, H.C., Jesus, C.C., Boer, W., Richter, O.T., Costa, A., van Weering, T.C.E., 2011. Recent sediment transport and deposition in the Lisbon-Setúbal and Cascais submarine canyons, Portuguese continental margin. Deep Sea Research II 58 (23), 2321–2344.

Dengler, A.T., Wilde, P., Noda, E.K., Normark, W.R., 1984. Turbidity currents generated by Hurricane Iwa. Geo-Marine Letters 4, 5–11.

Dobrovolsky, I.P., Zubkov, S.I., Miachkin, V.I., 1979. Estimation of the size of earthquake preparation zones. Pure and Applied Geophysics 117 (5), 1025-1044.

Dowdeswell, J.A., Kenyon, N.H., Elverhùi, A., Laberg, J.S., Hollender, F.-J., Mienert, J., Siegert, M.J., 1996. Large-scale sedimentation on the glacier-influenced Polar North Atlantic margins: long-range side-scan sonar evidence. Geophysical Research Letters 23, 3535-3538.

Dowdeswell, J.A., Ottesen, D., Rise, L., 2006. Flow switching and large-scale deposition by ice streams draining former ice sheets. Geology 34, 313-316.

Ducassou, E., Migeon, S., Mulder, T., Murat, A., Capotondi, L., Bernasconi, S.M., Mascle, J., 2009. Evolution of the Nile deep-sea turbidite system during the Late Quaternary: influence of climate change on fan sedimentation. Sedimentology 56, 2061–2090.

Durán, R., Canals, M., Lastras, G., Micallef, A., Amblas, D., Pedrosa-Pàmies, R., Sanz, J.S., 2013. Sediment dynamics and post-glacial evolution of the continental shelf around the Blanes submarine canyon head (NW Mediterranean). Progress in Oceanography 118, 28-46.

Elger, J., Berndt, C., Krastel, S., Piper, D.W.J., Gross, F., Spielhagen, R.F., Meyer, S., 2015. The Fram Slide off Svalbard: a submarine landslide on a lowsedimentation-rate glacial continental margin. Journal of the Geological Society 172, 153-156.

Ercilla, G., Alonso, B. & Baraza, J. 1994. Post-Calabrian sequence stratigraphy of the northwestern Alboran Sea (southwestern Mediterranean). Marine Geology, 120, 249–265.

Evans, D., Harrison, Z., Shannon, P.M., Laberg, J.S., Nielsen, T., Ayers, S., Holmes, R., Hoult, R., Lindberg, B., Haflidason, H., Long, D., Kuijpers, A., Andersen, E.S., Bryn, P., 2005. Paleoslides and other mass failures of Pliocene to Pleistocene age along the Atlantic continental margin of NW Europe. Marine and Petroleum Geology 22, 1131-1148.

References

Field, M. E., 1993. Liquefaction of continental shelf sediment: The northern California earthquake of 1980. In: Submarine Landslides: Selected Studies in the U.S. Exclusive Economic Zone, edited by W. C. Schwab, H. J. Lee, and D.C. Twichell. U.S. Geological Survey Bulletin 2002, 143-150.

Fukushima, Y., Parker, G., Pantin, H.M., 1985. Prediction of ignitive turbidity currents in Scripps submarine canyon. Marine Geology 67, 55–81.

Fukushima, Y., Tanaka, T., 1990. A new attenuation relation for peak horizontal acceleration of strong earthquake ground motion in Japan. Bulletin of the Seismological Society of America 80 (4), 757-778.

Galbis, J., 1932. Cata´logo sı´smico de la zona comprendida entre los meridianos 5° E y 20° W de Greenwich y los paralelos 45° y 25° N, Tomo 1. Instituto Geográfico, Catastral y de Estadística, Madrid. 897pp.

Garcia-Orellana, J., et al., 2006. Identifying instrumental and historical earthquake records in the SW Iberian Margin using 210Pb turbidite chronology. Geophysical Research Letters 33, L24601. http://dx.doi.org/10.1029/2006GL028417.

Gardner, J.K., Knopoff, L., 1974. Is the sequence of earthquakes in southern California, with aftershocks removed, poissonian? Bulletin of the Seismological Society of America 64, 1363-1367.

Gee, M.J.R., Masson, D.G., Watts, A.B., Allen, P.A., 1999. The Saharan Debris Flow: an insight into the mechanics of long runout debris flows. Sedimentology 46, 317–335.

Gennesseaux, M., Mauffret, A. & Pautot, G., 1980. Les glissements sous-marins de la pente continentale niqoise et la rupture de clbles en mer Ligure (Méditerraneé occidentale). C. R. Acad. Sci. Paris, 290, 959-963.

Georgiopoulou, A., 2006. Turbidity currents and the giant Sahara Slide, Northwest African margin: triggers, flow processes and deposits. PhD thesis, University of Southampton.

Georgiopoulou, A., Wynn, R.B., Masson, D.G., Frenz, M., 2009. Linked turbidite–debrite resulting from recent Sahara Slide headwall reactivation. Marine and Petroleum Geology 26, 2021-2031.

Georgiopoulou, A., Masson, D.G., Wynn, R.B., Krastel, S., 2010. Sahara Slide: Age, initiation, and processes of a giant submarine slide. Geochemistry Geophysics Geosystems 11, Q07014, doi:10.1029/2010GC003066.

Gibson, R. E., 1958. The progress of consolidation in a clay layer increasing in thickness with time. Geotechnique 8, 171–182.

Goldfinger, C., Morey, A.E., Nelson, C.H., Gutiérrez-Pastor, J., Johnson, J.E., Karabanov, E., Chaytor, J., Eriksson, A., 2007. Rupture lengths and temporal history of significant earthquakes on the offshore and north coast segments of the Northern San Andreas Fault based on turbidite stratigraphy. Earth and Planetary Science Letters 254, 9–27.

Gornitz, V., 1991. Global coastal hazards from future sea level rise. Palaeogeography, Palaeoclimatology, Palaeoecology (Global Planetary Change Section) 89, 379-398.

Gràcia, E., Vizciano, A., Escutia, C., Asioli, A., Rodés, Á., Pallàs, R., Garcia-Orellana, J., Lebreiro, S., Goldfinger, C., 2010. Holocene earthquake record offshore Portugal (SW Iberia): testing turbidite paleoseismology in a slow-convergence margin. Quaternary Science Reviews 29, 1156-1172.

Graziani, L., Maramai, A., Tinti, A., 2006. A revision of the 1783–1784 Calabrian (southern Italy) tsunamis. Natural Hazards and Earth System Science 6, 1053–1060.

Green, D. H., Wang H. F., 1986. Fluid pressure response to undrained compression in saturated sedimentary rock. Geophysics 51, 948–956.

Green, S.B., 1991. How many subjects does it take to do a regression analysis? Multivariate Behavioral Anaylsis 26 (3), 499-510.

Grönholm, T., Annila, A., 2007. Natural distribution. Mathematical Biosciences 210, 659-667.

References

Guerreiro, C., Oliveira, A., Rodrigues, A., 2009. Shelf-break canyons versus "Gouf" canyons: A comparative study based on the silt-clay mineralogy of bottom sediments from Oporto, Aveiro and Nazaré Submarine Canyons. Journal of Coastal Research 56, 722-726.

Guerreiro, C., Rodrigues, A., Duarte, J., Oliveira, A., Taborda, R., 2007. Bottom sediment signature associated with the Oporto, Aveiro and Nazaré submarine canyons (NW off Portugal). Thalassas 23 (1), 9-18.

Gustavsson, S., Fagerberg, B., Sallsten, G., Andersson, E.M., 2014. Regression models for log-normal data: comparing different methods for quantifying the association between abdominal adiposity and biomarkers of inflammation and insulin resistance. International Journal of Environmental Research and Public Health 11 (4), 3521-3539.

Gutiérrez-Pastor, J., Nelson, C.H., Goldfinger, C., Johnson, J.E., Escutia, C., Eriksson, A., Morey, A.E., and the Shipboard Scientific Party, 2009. Earthquake control of Holocene turbidite frequency confirmed by hemipelagic sedimentation chronology on the Cascadia and Northern California active tectonic continental margins. In: Kneller, B., McCaffrey, W., Martinsen, O.J. (Eds.), External Controls on Deepwater Depositional Systems. SEPM Special Publication, v. 92. Society for Sedimentary Geology, Tulsa, OK, p. 179–197.

Haflidason, H., de Alvaro, M.M., Nygard, A., Sejrup, H.P., Laberg, J.S., 2007. Holocene sedimentary processes in the Andøya Canyon system, north Norway. Marine Geology 246, 86-104.

Haflidason, H., Lien, R., Sejrup, H.P., Forsberg, C.F., Bryn, P., 2005. The dating and morphometry of the Storegga Slide. Marine and Petroleum Geology 22, 123–136.

Haflidason, H., Sejrup, H.P., Berstad, I.M., Nygård, A., Richter, T., Bryn, P., Lien, R., Berg, K., 2003. A weak layer feature on the northern Storegga Slide Escarpment. In: Mienert J, Weaver PPE (eds), European Margin Sediment Dynamics. Springer, Berlin, pp. 55–62.

Haflidason, H., Sejrup, H.P., Nygård, A., Mienert, J., Bryn, P., Lien, R., Forsberg, C.F., Berg, K., Masson, D., 2004. The Storegga Slide: architecture, geometry and slide development. Marine Geology 213, 201–234.

Hagiwara, Y., 1974. Probability of earthquake occurrence as obtained from a Weibull distribution analysis of crustal strain. Tectonophysics 23, 313-318.

Halsey, L.G., Curran-Everett, D., Vowler, S.L., Drummond, G.B., 2015. The fickle P value generates irreproducible results. Nature Methods 12 (3), 179-185.

Hampton, M.A., Lee, H.J., Locat, J., 1996. Submarine landslides. Reviews of Geophysics 34, 33-59.

Harbitz C.B., Løvholt, F., Pedersen, G., Masson, D.G., 2006. Mechanisms of tsunami generation by submarine landslides: a short review. Norwegian Journal of Geology 86, 249–258.

Harbitz, C., Parker, G., Elverhøi, A., Marr, J.G., Mohrig, D., Harff, P.A., 2003. Hydroplaning of subaqueous debris flows and glide blocks: analytical solutions and discussion. Journal of Geophysical Research 108 (B7), 23–49.

Harbitz, C.B., 1992. Model simulations of tsunamis generated by the Storegga slides. Marine Geology 105, 1-21.

Harbitz, C.B., Løvholt, F., Bungum, H., 2014. Submarine landslide tsunamis: how extreme and how likely? Natural Hazards 72, 1341–1374. doi: 10.1007/s11069-013-0681-3.

Harris, P.T., Whiteway, T., 2011. Global distribution of large submarine canyons: Geomorphic differences between active and passive continental margins. Marine Geology 285, 69-86.

Haq, B.U., Schutter, S.R., 2008. A chronology of Paleozoic sea-level changes. Science, 322(5898), 64-68.

Haugen, K.B., Løvholt, F., Harbitz, C.B., 2005. Fundamental mechanism s for tsunami generation by submarine mass flows in idealised geometries, Marine and Petroleum Geology 22 (1–2), 209–217.

References

Haughton, P.D.W., Barker, W.D. and McCaffrey, W.D., 2003. 'Linked' debrites in sand-rich turbidite systems – origin and significance. Sedimentology 50, 459–482.

Hay, A.E., Burling, E.W., Murray, J.W., 1982. Remote acoustic detection of a turbidity current surge. Science 217, 833–845.

Heezen, B.C., Ewing, M., 1952; Turbidity currents and submarine slumps, and the 1929 Grand Banks earthquake. American Journal of Science 250, 849-873.

Henriksen, S., Vorren, T.O., 1996. Late Cenozoic sedimentation and uplift history on the mid Norwegian continental shelf. In: Solheim, A., Riis, F., Elverhøi, A., Faleide, J.I., Jensen, L. N., Cloetingh, S. (Eds.), Impact of Glaciations on Basin Evolution: Data and Models from the Norwegian Margin and Adjacent Areas. Global and Planetary Change 12, 171-199.

Hernández-Molina, F.J., Llave, E., Ercilla, G., Maestro, A., Medialdea, T., Ferrin, A., Somoza, L., Gràcia, E., Masson, D.G., García, M., Vizcaino, A., León, R., 2009. Recent sedimentary processes in the Prestige site area (Galicia Bank, NW Iberian Margin) evidenced by high-resolution marine geophysical methods. Marine Geology 249, 21–45.

Hernández-Molina, F.J., Somoza, L., Vázquez, J.T., Lobo, F., Fernández-Puga, M.C., Llave, E., Díaz del Río, V., 2002. Quaternary stratigraphic stacking patterns on the continental shelves of the southern Iberian Peninsula: their relationship with global climate and palaeoceanographic changes. Quaternary International 92, 5-23.

Hjelstuen, B.O., Andreassen, E.V., 2015. North Atlantic Ocean deep-water processes and depositional environments: A study of the Cenozoic Norway Basin. Marine and petroleum Geology 59, 429-441.

Hogan, K.A., Dowdeswell, J.A., Mienert, J., 2013. New insights into slide processes and seafloor geology revealed by side-scan imagery of the massive Hinlopen Slide, Arctic Ocean margin. Geo-Marine Letters 33, 325-343.

Holmes, R., Bulat, J., Gillespie, E.J., Hine, N., Hobbs, P., Jones, S., Riding, J., Sankey, M., Tulloch, G., Wilkinson, I.P., Walker, A., 1997. Geometry, Processes of Formation and

Timing of the Afen Submarine Landslide West of Shetland. British Geological Survey Technical Report WB/97/33C.

Hoogakker, B.A.A., Rothwell, R.G., Rohling, E.J., Paterne, M., Stow, D.A.V., Herrle, J.O., Clayton, J., 2004. Variations in terrigenous dilution in western Mediterranean Sea pelagic sediments in response to climate change during the last glacial cycle. Marine Geology 211, 21-43.

Hornbach, M.J., Lavier, L.L., Ruppel, C.D., 2007. Triggering mechanism and tsunamogenic potential of the Cape Fear Slide complex, U.S. Atlantic margin. Geochem Geophys Geosyst 8. doi:10,1029/2007GC00001722.

Hühnerbach, V., Masson, D.G., 2004. Landslides in the North Atlantic and its adjacent seas: an analysis of their morphology, setting and behaviour. Marine Geology 213, 343–362.

Hunt, J.E., Talling, P.J., Clare, M.A., Jarvis, I., Wynn, R.B., 2014. Long-term (17 Ma) turbidite record of the timing and frequency of large flank collapses of the Canary Islands. Geochemistry, Geophysics, Geosystems 15 (8), 3322-3345.

Hunt, J.E., Wynn, R.B., Masson, D.G., Talling, P.J., Teagle, D.A.H., 2011. Sedimentological and geochemical evidence for multistage failure of volcanic landslides: A case study from Icod landslide on north Tenerife, Canary Islands. Geochemistry, Geophysics, Geosystems 12, Q12007, doi:10.1029/2011GC003740.

Hunt, J.E., Wynn, R.B., Talling, P.J., Masson, D.G., 2013a. Multistage collapse of eight western Canary Island landslides in the last 1.5 Ma: Sedimentological and geochemical evidence from subunits in submarine flow deposits. Geochemistry, Geophysics, Geosystems 14, 2159–2181.

Hunt, J.E., Wynn, R.B., Talling, P.J., Masson, D.G., 2013b. Frequency and timing of landslide-triggered turbidity currents within the Agadir Basin, offshore NW Africa: Are there associations with climate change, sea level change and slope sedimentation rates? Marine Geology 346, 274-291.

References

Hurst, H.E., 1951. Long term storage capacity of reservoir. American Society of Civil Engineers 116, 770–808.

Iglesias, O., Lastras, G., Canals, M., Olabarrieta, M., González, M., Aniel-Quiroga, Í., Otero, L., Durán, R., Amblas, D., Casamor, J.L., Tahchi, E., 2012. The BIG'95 submarine landslide–generated tsunami: a numerical simulation. The Journal of Geology 120, 31-48.

Ingersoll, R. V., Dickinson, W. R., & Graham, S. A., 2003. Remnant-ocean submarine fans: largest sedimentary systems on Earth. Special Papers - Geological Society of America, 191-208.

IOC, IHO, BODC, 2003. Centenary Edition of the GEBCO Digital Atlas. British Oceanographic Data Centre, Liverpool.

Jakobsson, M., Mayer, L., Coakley, B., Dowdeswell, J.A., Forbes, S., Fridman, B., Hodnesdal, H., Noormets, R., Pedersen, R., Rebesco, M., Schenke, H.W., Zarayskaya, Y., Accettella, D., Armstrong, A., Anderson, R.M., Bienhoff, P., Camerlenghi, A., Church, I., Edwards, M., Gardner, J.V., Hall, J.K., Hell, B., Hestvik, O., Kristoffersen, Y., Marcussen, C., Mohammad, R., Mosher, D., Nghiem, S.V., Pedrosa, M.T., Travaglini, P.G., Weatherall, P., 2012. The International Bathymetric Chart of the Arctic Ocean (IBCAO) Version 3.0. Geophysical Research Letters 39, L12609. http://dx.doi.org/10.1029/2012GL052219.

Jerolmack, D.J., Paola, C., 2010. Shredding of environmental signals by sediment transport. Geophysical Research Letters 37, L19401, doi:10.1029/2010GL044638,

Johnston, A.C., 1996. Seismic moment assessment of earthquakes in stable continental regions-111. New Madrid 181 1-1812, Charleston 1886 and Lisbon 1755. Geophysical Journal International 126, 314-344.

Jorry, S.J., Jégou, I., Emmanuel, L., Silva Jacinto, R., Savoye, B., 2011. Turbiditic levee deposition in response to climate changes: The Var Sedimentary Ridge (Ligurian Sea), Marine Geology 279, 148-161.

Kagan, Y.Y., Jackson, D.D., 1991. Long-term earthquake clustering. Geophysical Journal International 104, 117-133.

Kagan, Y.Y., Jackson, D.D., 2000. Probabilistic forecasting of earthquakes. Geophysical Journal International 143, 438-453.

Kenyon, N. H., 1987. Mass-wasting features on the continental slope of northwest Europe. Marine Geology 74, 57-77.

Khripounoff, A., Crassous, P., Lo Bue, N., Dennielou, B., Silva Jacinto, R., 2012. Different types of sediment gravity flows detected in the Var submarine canyon (northwestern Mediterranean Sea). Progress in Oceanography 106, 138–153.

Khripounoff, A., Vangriesheim, A., Crassous, P., Etoubleau, J., 2009. High frequency of sediment gravity flow events in the Var submarine canyon (Mediterranean Sea). Marine Geology 263, 1–6.

Kleinbaum, D.G. and Klein M. (2005) Survival Analysis: A Self-Learning Text. Statistics in the health sciences. Springer Science and Business Media.

Kneller, B., Buckee, C., 2000. The structure and fluid mechanics of turbidity currents: a review of some recent studies and their geological implications. Sedimentology 47 (Suppl 1), 62-94.

Korup, O., 2012. Earth's portfolio of extreme sediment transport events. Earth Science Reviews 112 (3–4), 115–125.

Krastel, S., Wynn, R.B., Hanebuth, T.J.J., Henrich, R., Holz, C., Meggers, H., Kuhlmann, H., Georgiopoulou, A., Schulz, H.D., 2006. Mapping of seabed morphology and shallow sediment structure of the Mauritania continental margin, Northwest Africa: some implications for geohazard potential. Norwegian Journal of Geology 86, 163–176.

Kremer, K., Simpson, G., Girardclos, S., 2012. Giant Lake Geneva tsunami in AD 563. Nature Geoscience 5, 756–757.

Kristoufek, L., 2012. How are rescaled range analyses affected by different memory and distributional properties? A Monte Carlo study. Physica A: Statistical Mechanics and its Applications 391 (17), 4252-4260.

References

Kvalstad, T. J., Andresen, L. Forsberg, C. F. Berg, K. Bryn, P. Wangen, M., 2005b. The Storegga slide: Evaluation of triggering sources and slide mechanics. Marine and Petroleum Geology 22, 245–256.

Kvalstad, T.J., Nadim, F., Kaynia, A.M., Mokkelbost, K.H., Bryn, P., 2005a. Soil conditions and slope stability in the Ormen Lange area. Marine and Petroleum Geology 22, 299–310.

Kvenvolden, K. A., McMenamin, M. A., 1980. Hydrates of natural gas: their geologic occurrence. U. S. Geological Survey Circular 825.

Laberg, J.S, Vorren, T.O., Mienert, J., Evans, D., Lindberg, B., Ottesen, D., Kenyon, N.H., Henriksen, S., 2002a. Late Quaternary paleoenvironment and chronology in the Trænadjupet Slide area offshore Norway. Marine Geology 188, 35-60.

Laberg, J.S., Vorren, T.O., 1993. A Late Pleistocene submarine slide on the Bear Island Trough Mouth Fan. Geo-Marine Letters 13, 227-234.

Laberg, J.S., Vorren, T.O., 2000b. Flow behaviour of the submarine glacigenic debris flows on the Bear Island TroughMouth Fan, western Barents Sea. Sedimentology 47, 1105–1117.

Laberg, J.S., Vorren, T.O., 2000a. The Trænadjupet Slide, offshore Norway — morphology, evacuation and triggering mechanisms. Marine Geology 171, 95-114.

Laberg, J.S., Vorren, T.O., Dowdeswell, J.A., Kenyon, N.H., Taylor, J., 2000. The Andøya Slide and the Andøya Canyon, north-eastern Norwegian–Greenland Sea. Marine Geology 162, 259-275.

Laberg, J.S., Vorren, T.O., Kenyon, N.H., Ivanov, M., 2006. Frequency and triggering mechanisms of submarine landslides of the North Norwegian continental margin. Norwegian Journal of Geology 86, 155-161.

Laberg, J.V., Vorren, T.O., Mienert, J., Bryn, P., Lien, R., 2002b. The Trænadjupet Slide: a large slope failure affecting the continental margin of Norway 4,000 years ago. Geo Marine Letters 22, 19–24.

Lambe, T. W., and Whitman R. V., 1979. Soil Mechanics, SI Version, John Wiley, New York.

Lambeck, K., Rouby, H., Purcell., P., Sun, Y., Sambridge, S., 2014. Sea level and global ice volumes from the Last Glacial Maximum to the Holocene. Proceedings of the National Academy of Sciences 111 (43), 15296-15303.

Lastras, G., Arzola, R.G., Masson, D.G., Wynn, R.B., Huvenne, V.A.I., Hühnerbach, V., Canals, M., 2009. Geomorphology and sedimentary features in the Central Portuguese submarine canyons, Western Iberian margin. Geomorphology 103, 310-329.

Le Friant, A., et al., 2015. Submarine record of volcanic island construction and collapse in the Lesser Antilles Arc: First scientific drilling of submarine volcanic island landslides by IODP Expedition 340, Geochemistry Geophysics Geosystems 16, 420–442.

Le Roy, P., Sahabi, M., Maad, N., Rabineau, M., Gutscher, M.-A., Babonneau, N., Van Vliet, Lanoë B., Ait Brahim, L., M'hammdi, N., Trentesaux, A., Dakki, M., Hssain, M., 2014. 3D architecture of Quaternary sediment along the NW Atlantic Moroccan Rharb continental shelf: a stratal pattern under the dual control of tectonics and climatic variations. Marine and Petroleum Geology 49, 129–142.

Leatherman, S.P., Zhang, K., Douglas, B.C., 2000. Sea level rise shown to drive coastal erosion. Eos Transactions of the American Geophysical Union 81, 55-57.

Lebreiro, S.M., McCave, I.N., Weaver, P.P.E., 1997. Late Quaternary turbidite emplacement on the Horseshoe abyssal plain (Iberian margin). Journal of Sedimentary Research 67, 856–870.

Lebreiro, S.M., Voelker, A.H.L., Vizcaino, A., Abrantes, F.G., Alt-Epping, U., Jung, S., Thouveny, N., Grácia, E., 2009. Sediment instability on the Portuguese continental margin under abrupt glacial climate changes (last 60 kyr). Quaternary Science Reviews 28, 3211–3223.

Lee, H. J., Locat, J., Desgagnés, P., Parsons, J. D., McAdoo, B. G., Orange, D. L., Puig, P., Wong, F. L., Dartnell, P. and Boulanger, E., 2007. Submarine Mass Movements on Continental Margins, in Continental Margin Sedimentation: From Sediment Transport to Sequence Stratigraphy (eds C. A. Nittrouer, J. A. Austin, M. E. Field, J. H. Kravitz, J. P. M. Syvitski

and P. L. Wiberg), Blackwell Publishing Ltd., Oxford, UK. doi: 10.1002/9781444304398.ch5.

Lee, H.J., 2009. Timing of occurrence of large submarine landslides on the Atlantic ocean margin, Marine Geology 264, 56-64.

Lee, H.J., Chough, S.K., Yoon, S.H., 1996. Slope-stability change from late Pleistocene to Holocene in the Ulleung Basin, East Sea (Japan Sea). Sedimentary Geology 104, 39-51.

Lee, H.J., Edwards, B.D., 1986. Regional method to assess offshore slope stability. Journal of Geotechnical Engineering 112, 489–509.

Lee, H.J., Orzech, K., Locat, J., Boulanger, E., Konrad, J.M., 2004. Seismic strengthening, a condition factor influencing submarine landslide development. 57th Canadian Geotechnical Conference, October, 2004, Session. , 7G, pp. 8–14.

Lehmann, E.L., 2006. Nonparametrics: Statistical methods based on ranks, Springer, New York.

Leynaud, D., Mienert, J., Vanneste, M., 2009. Submarine mass movements on glaciated and non-glaciated European continental margins: A review of triggering mechanisms and preconditions to failure. Marine and Petroleum Geology 26, 618-632.

L'Heureux, J.S., Hansen, L., Longva, O., Emdal, A., Grande, L.O., 2010. A multidisciplinary study of submarine landslides at the Nidelva fjord delta, Central Norway - implications for geohazard assessment. Norwegian Journal of Geology 90, 1–20.

Li, W., Alves, T.M., Urlaub, M., Georgiopoulou, A., Klaucke, I., Wynn, R.B., Gross, F., Meyer, M., Repschläger, J., Berndt, C., Krastel, S., in press. Morphology, age and sediment dynamics of the upper headwall of the Sahara Slide Complex, Northwest Africa: Evidence for a large Late Holocene failure. Marine Geology.

Limpert, E., Stahel, W.A., Abbt, M., 2001. Log-normal distributions across the sciences: keys and clues. Bioscience 51 (8), 341-352.

Lin, D.Y., Wei, L.J., Ying, Z., 2002. Model-checking techniques based on cumulative residuals. Biometrics 58, 1-12.

Lindberg, B., Laberg, J.S., Vorren, T.O., 2004: The Nyk Slide – morphology, progression, and age of a partly buried submarine slide offshore northern Norway. Marine Geology 213, 277-289.

Liu, J.T., Wang, Y-H., Yang, R.T., Hsu, R.T., Kao, S.-J., Lin, H.-L., Kuo, F.H., 2012. Cyclone induced hyperpycnal turbidity currents in a submarine canyon. Journal of Geophysical Research 117, C04033. http://dx.doi.org/10.1029/2011JC007630.

Liu, L., Maiorano, P., Zhao, X., 1996. Pliocene-Pleistocene calcareous nanofossil from the Iberian Abyssal Plain. In: Whitmarsh, R.B., Sawyer, D.S., Klaus, A., and Masson, D.G.. Proceedings of the Ocean Drilling Program, Scientific Results 149, 147-164.

Liu, X., Flemings, P.B., 2009. Dynamic response of oceanic hydrates to sea level drop. Geophysical Research Letters 36.

Llave, E., Hernandez-Molina, F.J., Somoza, L., Díaz del Río, V., Stow, D.A.W., Maestro, A., Alveirinho Dias, J.M., 2001. Seismic stacking pattern of the Faro Albufeira contourite system (Gulf of Cadiz): a Quaternary record of paleoceanographic and tectonic influences. Mar. Geophysical Research 22, 487-508.

Locat, J., Leroueil, S., Locat, A., Lee, H., 2014. Weak layers: their definition and classification from a geotechnical perspective. In: Krastel, S., et al (eds)., Submarine Mass Movements and Their Consequences, Advances in Natural and Technological Hazards Research 37, 3-12. Springer International Publishing, Switzerland.

Locat, J., Martin, F., Levesque, C., Locat, P., Lerouei, l.S., Konrad, J.M., Urgeles, R., Canals, M., Duchesne, M.J., 2003. Submarine mass movements in the upper Saguenay Fjord, (Quebec, Canada), triggered by the 1663 earthquake. In: Locat. J., Mienert, J., (eds) Submarine mass movements and their consequences. Advances in Natural and Technological Hazards Research, vol 19. Kluwer, The Netherlands, pp 509–519.

References

Løvholt, F., Harbitz, C.B., Vanneste, M., De Blasio, F.V., Urgeles, R., Iglesias, O., Canals, M., Lastras, G., Pedersen, G., Glimsdal, S., 2014. Modeling potential tsunami generation by the BIG'95 landslide. In: S. Krastel et al. (eds.), Submarine Mass Movements and Their Consequences, Advances in Natural and Technological Hazards Research 37, 507-515.

Løvholt, F., Pedersen, G., Harbitz, C.B., Glimsdal, S., Kim, J., 2015. On the characteristics of landslide tsunamis. Philosophical Transactions of the Royal Society A 373, DOI: 10.1098/rsta.2014.0376.

Lowe, D.R., 1976. Grain flow and grain flow deposits. Journal of Sedimentary Petrology 46, 188–199.

Lowe, D.R., 1982. Sediment gravity flows: II. Depositional models with special reference to the deposits of high-density turbidity currents. Journal of Sedimentary Petrology 52, 279-297.

Lozano, I., Devoy, R.J.N., May, W., Anderson, U., 2004. Storminess and vulnerability along the Atlantic coastlines of Europe: analysis of storm records and of a greenhouse gases induced climate scenario. Marine Geology 210, 205-225.

Luttrell, K., Sandwell, D., 2010. Ocean loading effects on stress at near shore plate boundary fault systems. Journal of Geophysical Research 115, B08411, doi:10.1029/2009JB006541.

Major, J.J., 1997. Depositional processes in large-scale debris-flow experiments. The Journal of Geology 105, 345-366.

Manning, W.G., 1998. The logged dependent variable, heteroscedasticity, and the retransformation problem. Journal of Health Economics 17 (3), 283-295.

Marshall, N.F., 1978. Large storm-induced sediment slump reopens an unknown Scripps submarine canyon tributary. In: Stanley, D.J., Kelling, G. (Eds.), Sedimentation in Submarine Canyons, Fans and Trenches. Dowden, Hutchinson and Ross Inc., Pennsylvania, pp. 73–82.

Martın, J., Palanques, A., Puig, P., 2006. Composition and variability of downward particulate matter fluxes in the Palamos submarine canyon (NW Mediterranean). Journal of Marine Systems 60, 75–97.

Martin, J., Palanques, A., Vitorino, J., Oliveira, A., de Stitger, H.C., 2011. Near-bottom particulate matter dynamics in the Nazaré submarine canyon under calm and stormy conditions. Deep-Sea research II 58, 2388-2400.

Mas, V., Mulder, T., Dennielou, B., Schmidt, S., Khripounoff, A., Savoye, B., 2010. Multiscale spatio-temporal variability of sedimentary deposits in the Var turbidite system (North-Western Mediterranean Sea). Marine Geology 275, 37–52.

Maslin, M., Owen, M., Day, S., Long, D., 2004. Linking continental-slope failures and climate change: testing the clathrate gun hypothesis. Geology 32, 53–56.

Masson, D. G., Watts, A. B., Gee, M. R. J., Irgeles, R., Mitchell, N. C., Le Bas, T. P., Canals, M., 2002. Slope failures on the flanks of the western Canary Islands, Earth Science Reviews 57, 1–35.

Masson, D.G., Arzola, R.G., Wynn, R.B., Hunt, J.E., Weaver, P.P.E., 2011b. Seismic triggering of landslides and turbidity currents offshore Portugal. Geochemistry, Geophysics, Geosystems 12, doi:10.1029/2011GC003839.

Masson, D.G., Harbitz, C.B., Wynn, R. B., Pedersen, G. and Løvholt, F., 2006. Submarine landslides: processes, triggers and hazard prediction. Philosophical Transactions of the Royal Society 364, 2009–2039.

Masson, D.G., Harbitz, C.B., Wynn, R.B., Pedersen, G. and Løvholt, F., 2006. Submarine landslides: processes, triggers and hazard prediction. Philosophical Transactions of the Royal Society 364, 2009–2039.

Masson, D.G., Huvenne, V.A.I., de Stigter, H.C., Arzola, R.G., LeBas, T.P., 2011a. Sedimentary features in the middle Nazaré Canyon. Deep-Sea Research II 58, 2369-2387.

References

Masson, D.G., Watts, A.B., Gee, M.J.R., Urgeles, R., Mitchell, N.C., Le Bas, T.P., Canals, M., 2002. Slope failures on the flanks of the western Canary Islands. Earth-Science Reviews 57, 1 –35.

Masson, D.G., Wynn, R.B., Talling, P.J., 2010. Large Landslides on Passive Continental Margins: Processes, Hypotheses and Outstanding Questions. In: D.C. Mosher et al. (eds.), Submarine Mass Movements and Their Consequences, Advances in Natural and Technological Hazards Research 28, 153-165.

McAdoo, B.G., Watts, P., 2004. Tsunami hazard from submarine landslides on the Oregon continental slope. Marine Geology 203(3), 235-245.

McCullagh, P., Nelder, J.A., 1989. Generalized Linear Models, Second Edition. Chapman and Hall/CRC, London.

Mecklin, C., 2007. Q-Q Plot. In: Salkind, N.J., Rasmussen, K. (Eds.), Encyclopedia of Measurement and Statistics. Thousand Oaks, CA: Sage Publications, Inc., pp. 803-805. doi: http://dx.doi.org/10.4135/9781412952644.n367

Meinert, J., 2004. COSTA—continental slope stability: major aims and topics. Marine Geology 213, 1-7.

Mello, U. T., and Pratson, L.F., 1999. Regional slope stability and slope- failure mechanics from the two-dimensional state of stress in an infinite slope. Marine Geology 154, 339–356.

Middleton, G.V., Hampton, M.A., 1973. Sediment gravity flows: mechanics of flow and deposition. In: Middleton, G.V., Bouma, A.H. (Co-Chairmen), Turbidites and Deep Water Sedimentation. Soc. Econ. Paleontol. Mineral., Pac. Sect., Short Course, pp. 1 – 38.

Mienert, J., Vanneste, M., Haflidason, H., Bünz, S., 2010. Norwegian margin outer shelf cracking: a consequence of climate-induced gas hydrate dissociation? International Journal of Earth Sciences 99 (Suppl 1), S207–S225.

Milia, A., 2000. The Dohrn canyon: a response to the eustatic fall and tectonic uplift of the outer shelf along the eastern Tyrrhenian Sea margin, Italy. Geo-Marine Letters 20, 101-108.

Milkert, D., Alonso, B., Liu, L., Zhao, X., Comas, M., de Kaenel, E., 1996a. Sedimentary facies and depositional history of the Iberia Abyssal Plain. In: Whitmarsh, R.B., Sawyer, D.S., Klaus, A., and Masson, D.G.. Proceedings of the Ocean Drilling Program, Scientific Results 149, Ch. 45, 685-704.

Milkert, D., Weaver, P.P.E., Liu, L., 1996b. Pleistocene and Pliocene turbidites from the Iberia Abyssal Plain. In: Whitmarsh, R.B., Sawyer, D.S., Klaus, A., and Masson, D.G., Proceedings of the Ocean Drilling Program, Scientific Results, 149, Ch. 12, 281-294.

Miller, K.G., Kominz, M.A., Browning, J.V., Wright, J.D., Mountain, G.S., Katz, M.E., Sugarman, P.J., Cramer, B.S., Christie-Blick, N., Pekar, S.F., 2005. The Phanerozoic record of global sea-level change. Science 312, 1293-1298.

Moernaut, J., Van Daele, M., Strasser, M., Clare, M.A., Heirman, K., Viel, M., Cardenas, J., Kilian, R., Ladrón de Guevara, B., Pino, M., Urrutia, R., De Batist, M. (2015) Lacustrine turbidites produced by surficial slope sediment remobilization: a mechanism for continuous and sensitive turbidite paleoseismic records. Marine Geology. doi:10.1016/j.margeo.2015.10.009

Moernaut, J., Van Deale, M., Heirman, K., Fontijn, K., Strasser, M., Pino, M., Urrutia, R., De Batist, M., 2014. Lacustrine turbidites as a tool for quantitative earthquake reconstruction: New evidence for a variable rupture mode in south central Chile. Journal of Geophysical Research: Solid Earth, 119 (3), 1607-1633.

Mohrig, D., Whipple, K.X., Hondzo, M., Ellis, C., Parker, G., 1998. Hydroplaning of subaqueous debris flows. Geological Society of America Bulletin 110, 387-394.

Monecke, K., Anselmetti, F.S., Becker, A., Sturm, M., Giardini, D., 2004. Signature of historic earthquakes in lake sediments in Central Switzerland. Tectonophysics 394, 21–40.

Monges Soares, A.M., 1993. The 14C content of marine shells: Evidence for variability in coastal upwelling off Portugal during the Holocene in Isotope techniques. In: The Study of Past and

Current Environmental Changes in the Hydrosphere and Atmosphere (Proceedings) Vienna. IAEA-SM-329/49. 471-485.

Morgenstern, N.R., 1967. Submarine slumping and the initiation of turbidity currents. In: A.E. Richards (Editor), Marine Geotechnique. Univ. Illinois Press, Chicago, llI., pp. 189-220.

Mozzato, A., Allin, J.R., Bondevik, S., Talling, P.J., Tappin, D.R., Haflidason, H., Hunt, J.E., Baeten, N., Pope, E., Cartigny, M.J.B., Watts, M.J., Long, D., Stanford, J.D., Dowdeswell, J.A., in review. Do large (>400-700 km3) submarine landslides always produce major tsunamis, and what is their relationship to glacial cycles? Earth and Planetary Science Letters.

Mudelsee, M., Schultz, M., 1997. The Mid-Pleistocene climate transition: onset of 100 ka cycle lags ice volume build-up by 280 ka. Earth and Planetary Science Letters 151, 117-123.

Mulder T., Syvitski, J.P.M., Skene, K.I., 1998. Modelling of erosion and deposition by turbidity currents generated at river mouths. Journal of Sedimentary Research, Section A: Sedimentary Petrology and Processes 68, 124-137.

Mulder, T., Alexander, J., 2001. The physical character of subaqueous sedimentary density flows and their deposits. Sedimentology 48, 269-299.

Mulder, T., Cochonat, P., 1996, Classification of offshore mass movements, Journal of Sedimentary Research 66 (1), 43-57.

Mulder, T., Migeon, S., Savoye, B., Jouanneau, J., 2001. Twentieth century floods recorded in the deep Mediterranean sediments. Geology 29, 1011–1024.

Mulder, T., Syvitski, J.P.M., 1995. Turbidity currents generated at mouths of rivers during exceptional discharges to the world oceans. Journal of Geology 103, 285–299.

Naylor, M.A., 1980. Origin of inverse grading in muddy debris flow deposits--a review. Journal of Sedimentary Petrology 50, 1111-6.

Neves, M.C., Cabral, J., Luttrell, K., Figueiredo, P., Rockwell, T., Sandwell, D., 2015. The effect of sea level changes on fault reactivation potential in Portugal. Tectonophysics 658, 206-220.

Normark, W.R., Piper, D.J.W., 1991. Initiation processes and flow evolution of turbidity currents: implications for the depositional record. In: From Shoreline to Abyss, edited by R.H. Osborne, Special Publications SEPM Society for Sedimentary Geology 46, 207 – 230.

Oliveira, A., Santos, A.I., Rodrigues, A., Vitorino, J., 2007. Sedimentary particle distribution and dynamics on the Nazaré canyon system and adjacent shelf (Portugal). Marine Geology 246, 105–122.

Ottesen, D., Dowdeswell, J.A., Rise, L., Bugge, T., 2012. Large-scale development of the mid-Norwegian shelf over the last three million years and potential for hydrocarbon reservoirs in glacial sediments. Geological Society, London, Special Publications 368, 53-73.

Owen, M., Day, S., Maslin, M., 2007. Late Pleistocene submarine mass movements: occurrence and causes. Quaternary Science Reviews 26, 958–978.

Paillard, D., 1998. The timing of Pleistocene glaciations from a simple multiple-state climate model. Nature 391, 378–381.

Palanques, A., Garcıa-Ladona, E., Gomis, D., Martın, J., Marcos, M., et al., 2005. General patterns of circulation, sediment fluxes and ecology of the Palamos (La Fonera) submarine canyon, northwestern Mediterranean. Progress in Oceanography 66, 89–119.

Palanques, A., Puig, P., Latasa, M., Sharek, R., 2009. Deep sediment transport induced by storms and dense shelf water cascading in the northwestern Mediterranean. Deep-Sea Research I 56, 425–434.

Papatheodorou, G., Ferentinos, G., 1997. Submarine and coastal sediment failure triggered by the 1995, M_s = 6.1 R Aegion earthquake, Gulf of Corinth, Greece. Marine Geology 137, 287-304.

References

Parker, G., 1982. Conditions for the ignition of catastrophically erosive turbidity currents. Marine Geology 46, 307-327.

Parsons, J.D., Whipple, K.X., Simoni, A., 2001. Experimental study of the grain-flow, fluid-mud transition in debris flows. Journal of Geology 109, 427–447.

Parzen, E., 1962. On estimation of a probability density function and mode. Annals of Mathematics and Statistics 33 (3), 1065–1076.

Paull, C.K., Brewer, P.G., Ussler, W., III, Peltzer, E.T., Rehder, G., Clague, D., 2003. An experiment demonstrating that marine slumping is a mechanism to transfer methane from seafloor gas-hydrate deposits into the upper ocean and atmosphere. Geo-Marine Letters 22, 198–203.

Paull, C.K., Buelow, W.J., Ussler III, W., Borowski, W.S., 1996. Increased continentalmargin slumping frequency during lowstands above gas hydrate-bearing sediments. Geology 24, 143–146.

Paull, C.K., McGann, M., Sumner, E.J., Barnes, P.M., Lundsten, E.M., Anderson, K., Gwiazda, R., Edwards, B., Caress, D.W., 2014. Sub-decadal turbidite frequency during the early Holocene: Eel Fan, offshore northern California. Geology 42, 858–885.

Paull, C.K., Mitts, P., Ussler III, W., Keaton, R., Greene, H.G., 2005. Trail of sand in upper Monterey Canyon: offshore California. GSA Bulletin 117 (9/10), 1134–1145.

Peltier, W., Fairbanks, R., 2006. Global glacial ice volume and Last Glacial Maximum duration from an extended Barbados sea level record. Quaternary Science Reviews 25, 3322–3337.

Pinder III, J.E., Wiener, J.G., Smith, M.H., 1978. The Weibull distribution: a new method of summarizing survivorship data. Ecology 59 (1), 175-179.

Piper, D.J., and Normark, W.R., 2001, Sandy fans—From Amazon to Hueneme and beyond: American Association of Petroleum Geologists Bulletin 85, 1407–1438.

Piper, D.J.W., 1970. Transport and deposition of Holocene sediment on La Jolla deep sea fan, California. Marine Geology 8, 211–227.

Piper, D.J.W., Cochonat, P., Morrison, M., 1999. The sequence of events around the epicentre of the 1929 Grand Banks earthquake: initiation of debris flows and turbidity currents inferred from sidescan sonar. Sedimentology 46, 79–97.

Piper, D.J.W., Savoye, B., 1993. Processes of late Quaternary .turbidity current flow and deposition on the Var deep-sea fan, north-west Mediterranean Sea. Sedimentology 40, 557-582.

Piper, D.W.J, Bowen, A.J., 1978. Origin of lamination in deep sea, fine-grained sediments. Nature 274, 324-328.

Piper, D.W.J., Normark, W.R., 2009. Processes that initiate turbidity currents and their influence on turbidites: a marine geology perspective. Journal of Sedimentary Research 79, 347–362.

Piper, D.W.J., Shor, A.N., Hughes Clarke, J.E., 1988. The 1929 “Grand Banks” earthquake, slump, and turbidity current. GSA Special Papers 229, 77-92.

Polonia, A., Panieri, G., Gasperini, L., Gasparotto, G., Bellucci, L.G., Torelli, L., 2013a. Turbidite paleoseismology in the Calabrian Arc subduction complex (Ionian Sea). Geochemistry, Geophysics, Geosystems 14, 112–140.

Pope, E., Talling, P.J., Hunt, J.E., Dowdeswell, J.A., Allin, J.R., Cartigny, M.J., Long, D., Mozzato, A., Stanford, J.D., Tappin, D.R., Watts, C.J., 2016. Long-term dynamics of the marine based Barents Sea Ice Sheet from a 140,000 year record. Quaternary Science Reviews 105, 55-66.

Pope, E.L., Talling, P.J., Carter, L., 2016. Which earthquakes trigger damaging submarine mass movements: Insights from a global record of submarine cable breaks? Marine Geology, doi:10.1016/j.margeo.2016.01.009.

Pope, E.L., Talling, P.J., Urlaub, M., Hunt, J.E., Clare, M.A., Challenor, P., 2015. Are large submarine landslides temporally random or do uncertainties in available age constraints make it impossible to tell? Marine Geology 369, 19-33.

Posamentier, H.W., Erskine, R.D., and Mitchum, R.M., Jr., 1991. Submarine fan deposition within a sequence stratigraphic framework. In: Weimer, P., and Link, M.H., eds., Seismic facies and sedimentary processes of submarine fans and turbidite systems. New York, Springer-Verlag, p. 127–136.

Pratson, L. F., Ryan, W. B. F., Mountain, G. S., Twitchell, D. C., 1994. Submarine canyon initiation by downslope-eroding sediment flows: evidence in late Cenozoic strata on the New Jersey continental slope. Geological Society of American Bulletin 106, 395–412.

Pro, C., Buforn, E., Bezzeghoud, M., Udias, A., 2013. Mechanism of 2003, 2007 and 2009 earthquakes (S. Vicente Cape) and implications for the 1755 Lisbon earthquake. Tectonophysics 583, 16–27.

Puig, P., Ogston, A.S., Mullenbach, B.L., Nittrouer, C.A., Sternberg, R.W., 2003. Shelf-to-canyon sediment-transport processes on the Eel continental margin (northern California). Marine Geology 193, 129–149.

Puig, P., Palanques, A., Martin, J., 2014. Contemporary sediment-transport processes in submarine canyons. Annual Review of Marine Science 6, 5.1-5.25.

Puig, P., Palanques, A., Orange, D.L., Lastras, G., Canals, M., 2008. Dense shelf water cascades and sedimentary furrow formation in the Cap de Creus Canyon, northwestern Mediterranean Sea. Continental Shelf Research 28, 2017–2030.

Ratzov, G., Cattaneo, A., Babonneau, N., Déverchère, J., Yelles, K., Bracene, R., & Courboulex, F., 2015. Holocene turbidites record earthquake supercycles at a slow-rate plate boundary. Geology 43 (4), 331-334.

Ratzov, G., Sosson, M., Colloy, J.-Y., Migeon, S., Michaud, F., Lopez, E., Le Gonidec, Y., 2007. Submarine landslides along the North Ecuador – South Colombia Convergent Margin:

possible tectonic control. In: Lykousis et al., (eds.), Submarine Mass Movements and Their Consequences, Advances in Natural and Technological Hazards Research 27, pp 47-55.

Reagan, M.T., Moridis, G.J., 2008. Dynamic response of oceanic hydrate deposits to ocean temperature change. Journal of Geophysical Research 113.

Redin, T., 1991. Oil and gas production from submarine fans of the Los Angeles basin. Active margin basins: AAPG Memoir 52, 239-259.

Reimer, P.J., Bard, E., Bayliss, A., Beck, J.W., Blackwell, P.G., Ramsey, C.B., Buck, C.E., Cheng, H., Edwards, R.L., Friedrich, M., Grootes, P.M., Guilderson, T.P., Haflidison, H., Hajdas, I., Hatté, C., Heaton, T., Hoffmann, D.L., Hogg, A., Hughen, K.A., Kaiser, K., Kromer, B., Manning, S.W., Niu, M., Reimer, R., Richards, D.A., Scott, E.M., Southon, J.R., Staff, R.A., Turney, C., Plicht, J., 2013. IntCal13 AND Marine13 radiocarbon age calibration curves 0–50,000 years cal BP. Radiocarbon 55, 1869–1887.

Riboulot, V., Cattaneo, A., Sultan, N., Garziglia, S., Ker, S., Imbert, P., Voisset, M., 2013. Sea-level change and free gas occurrence influencing a submarine landslide and pockmark formation and distribution in deepwater Nigeria. Earth and Planetary Science Letters 375, 78–91.

Rockwell, T., Fonseca, J., Madden, C., Dawson, T., Owen, L.A., Vilanova, S. & Figueiredo, P., 2009. Palaeoseismology of the Variça Segment of the Manteigas-Bragança Fault in northeastern Portugal, Geological Society, London, Special Publications 316 (1), 237–258.

Romans, B.W., Castelltort, S., Covault, J.A., Fildani, A., Walsh, J.P., 2015. Environmental signal propagation in sedimentary systems across timescales. Earth-Science Reviews 153, 7-29.

Romans, B.W., Graham, S.A., 2013. A Deep-Time Perspective of Land-Ocean Linkages in the Sedimentary Record. Annual Reviews of Marine Science 5, 69-94.

Romundset, A., Bondevik, S., 2011. Propagation of the Storegga tsunami into ice-free lakes along the southern shores of the Barents Sea. Journal of Quaternary Science 26, 457-462.

References

Ross, W.C., Halliwell, B.A., May, J.A., Watts, D.E., Syvitski, J.P.M., 1994. Slope readjustment: a new model for the development of submarine fans and aprons. Geology 22, 511-514.

Rothwell, R.G., Thomson, J. Kahler, G., 1998. Low-sea-level emplacement of a very large Late Pleistocene 'megaturbidite' in the western Mediterranean Sea. Nature 392, 377-380.

Ruiz, F., Abad, M., Vidal, J.R., Ca´ ceres, L.M., Gonza´ lez-Regalado, M.L., Carretero, M.I., Pozo, M., Toscano, F.G., 2008. The geological record of the oldest historical tsunamis in southwestern Spain. Rivista Italiana di Paleontologia e Stratigrafia 114 (1), 145–154.

Schemper, M., Stare, J., 1996. Explained variation in survival analysis. Statistics in Medicine 15, 1999-2012.

Schnellmann, M., Anselmetti, F.S., Giardini, D., McKenzie, J.A., 2005. Mass-movement-induced fold-and-thrust belt structures in unconsolidated sediments in Lake Lucerne (Switzerland), Sedimentology 52, 271–289.

Schwab, W.C., Danforth, W.W., Scanlon, K.M., Masson, D.G., 1991. A giant submarine slope failure on the northern insular slope of Puerto Rico. Marine Geology 96, 237–246.

Shackleton, N.J., Berger, A., Peltier, W.R., 1990. An alternative astronomical calibration on the Lower Pleistocene time scales based on ODP Site 677. Transactions Royal Society Edinburgh, Earth Science 81, 251–261.

Shanmugam, G., 2002. Ten turbidite myths. Earth-Science Reviews 58, 311–341.

Shanmugam, G., 2006. Deep-water Processes and Facies Models: Implications for Sandstone Petroleum Reservoirs, Handbook of Petroleum Exploration and Production, 5, Elsevier, Amsterdam.

Shanmugam, G., Bloch, R.B., Mitchell, S.M., Beamish, G.W.J., Hodgkinson, R.J., Damuth, J.E., Straume, T., Syvertsen, S.E., Shields, K.E., 1995. Basin-Floor Fans in the North Sea: Sequence Stratigraphic Models vs. Sedimentary Facies. AAPG Bulletin 79 (4), 477-512.

Shanmugam, G., Lehtonen, L.R., Straume, T., Syversten, S.E., Hodgkinson, R.J., Skibeli, M., 1994. Slump and debris flow dominated upper slope facies in the Cretaceous of the Norwegian and Northern North Seas (61–67 N): implications for sand distribution. AAPG Bulletin 78, 910-937.

Shanmugam, G., Moiola, R.J., 1982. Eustatic control of turbidites and winnowed turbidites. Geology 10, 231–235.

Siebert, L., 1984. Large volcanic debris avalanches: Characteristics of source areas, deposits, and associated eruptions. Journal of Volcanology and Geothermal Research 22, 163-197.

Skogdalen, J. E., Vinnem, J. E., 2012. Quantitative risk analysis of oil and gas drilling, using Deepwater Horizon as case study. Reliability Engineering and System Safety, 100, 58-66.

Smith, D.E., Harrison, S., Jordan, D.T., 2013. Sea level rise and submarine mass failure on open continental slopes. Quaternary Science Reviews 82, 93-103.

Smith, T., Smith, B, Ryan, M.A.K., 2003. Survival analysis using Cox Proportional Hazards Modelling for single and multiple event time data. Statistics and Data Analysis, SAS Users Group International Proceedings 2003.

Sommerfield, C.K., Lee, H.J., 2004. Across-shelf sediment transport since the Last Glacial Maximum, southern California margin. Geology 32, 345-348.

Spiske, M., Piepenbreier, J., Benavente, C., Bahlburg, H., 2013. Preservation potential of tsunami deposits on arid siliciclastic coasts. Earth Science Reviews 126, 58–73.

Stephens, M.A., 1974. EDF statistics for goodness of fit and some comparisons. Journal of the American Statistical Association 69 (347), 730-737.

Stevenson, C.J., Talling, P.J., Wynn, R.B., Masson, D.G., Hunt, J.E., Frenz, M., Akhmetzhanhov, A., Cronin, B.T., 2013. The flows that left no trace: investigating very large-volume turbidity currents that bypassed sediment through submarine channels without eroding the seafloor. Marine and Petroleum Geology 41, 186-205.

References

Stigall, J., Dugan, B., 2010. Overpressure and earthquake initiated slope failure in the Ursa region, northern Gulf of Mexico. Journal of Geophysical Research 115, b04101, doi:10.1029/2009jb006848,

Stow, D.A.V., Howell, D.G., and Nelson, C.H., 1985. Sedimentary, tectonic, and sea-level controls, in Bouma, A.H., et al., eds., Submarine fans and related turbidite systems. New York, Springer, p. 15–22.

Stow, D.A.V., Howell, D.G., Nelson, C.H., 1984. Sedimentary, Tectonic, and Sea-Level Controls on Submarine Fan and Slope-Apron Turbidite Systems. Geo-Marine Letters 3, 57-64.

Stow, D.A.V., Piper, D.J.W., 1984. Deep-water fine-grained sediments: facies models. In: Stow, D.A.V., Piper, D.J.W. (Eds.), Fine-grained Sediments: Deep-water Processes and Facies. Special Publications, Geological Society of London 14, pp. 611–645.

Stow, D.A.V., Reading, H.G., and Collinson, J.D., 1996. Deep Seas. In: Reading, H.G. (ed), Sedimentary Environments: Processes, Facies and Stratigraphy, 3rd edn., Blackwell Science Ltd., Oxford.

Stow, D.A.V., Shanmugam, G., 1980. Sequence of structures in fine-grained turbidites: comparison of recent deep-sea and ancient flysch sediments. Sedimentary Geology 25, 23–42.

Stow, D.A.V., Tabrez, A.R., 1998. Hemipelagites: processes, facies and model. In: Stoker, M.S., Evans, D., Cramp, A. (eds). Geological Processes on Continental Margins: Sedimentation, Mass Wasting and Stability. Geological Society, London, Special Publications 129, 317-337.

Strasser, M., Moore, G.F., Kimura, G., Kopf, A.J., Underwood, M.B., Guo, J., Screaton, E.J., 2011. lumping and mass transport deposition in the Nankai fore arc: evidence from IODP drilling and 3-D reflection seismic data. Geochemistry Geophysics Geosystems 12.

Strout, J.M., Tjelta, T.I., 2005. In situ pore pressures: What is their significance and how can they be reliably measured? Marine and Petroleum Geology 22, 275-285.

Sultan, N., Cochonat, P., Foucher, J.P., Mienert, J. 2004. Effect of gas hydrates melting on seafloor slope instability. Marine Geology 213, 379–401.

Sumner, E.J., Siti, M.I., McNeill, L.C., Talling, P.J., Henstock, T.J., Wynn, R.B., Djajadihardja, Y.S., Permana, H., 2013. Can turbidites be used to reconstruct a paleoearthquake record for the central Sumatran margin? Geology, doi:10.1130/G34298.1

Swan, A.R.H., Sandilands, M., 1995. Introduction to Geological Data Analysis. Blackwell Science, Oxford; Cambridge, Mass, USA.

Sylvester, A.G., 1988. Strike-slip faults. Geological Society of America Bulletin 100, 1666-1703.

Sylvester, Z., 2007. Turbidite bed thickness distributions: methods and pitfalls of analysis and modelling. Sedimentology 54, 847–870.

Syvitski, J.P.M., Hein, F.J., 1991. Sedimentology of an Artic basin: Itirbilung Fiord, Baffin Island, Northwest Territories. Geological Survey of Canada Paper 91–11, 66 p.

Tabachnick, B.G. and Fidell, L.S., 2007. Using Multvariate Statistics, Fifth Edition, Boston: Pearson Education, Inc.

Talling, P., Clare, M., Urlaub, M., Pope, E., Hunt, J., & Watt, S., 2014. Large Submarine Landslides on Continental Slopes: Geohazards, Methane Release, and Climate Change. Oceanography 27 (2), 32-45.

Talling, P.J., 2001. On the frequency distribution of turbidite thickness. Sedimentology 48, 1297–1329.

Talling, P.J., 2014. On the triggers, resulting flow types and frequencies of subaqueous sediment density flows in different settings. Marine Geology 352, 155–182.

Talling, P.J., Wynn, R.B., Masson, D.G., Frenz, M., Cronin, B.T., Schiebel, R., Akhmetzhanov, A. M., Dallmeier-Tiessen, S., Benetti, S., Weaver, P.P.E., Georgiopoulou, A., Zühlsdorff, C., Amy, L. A., 2007a. Onset of submarine debris flow deposition far from original giant landslide. Nature 450, 541–544.

References

Talling, P.J., Amy, L.A., Wynn, R.B., 2007b. New insights into the evolution of large volume turbidity currents; comparison of turbidite shape and previous modelling results. Sedimentology 54, 737–769.

Talling, P.J., Amy, L.A., Wynn, R.B., Peakall, J., Robinson, M., 2004. Beds comprising debrite sandwiched within co-genetic turbidite: origin and widespread occurrence in distal depositional environments. Sedimentology 51 (1), 163-194.

Talling, P.J., Masson, D.G., Sumner, E.J., Malgesini, G., 2012. Subaqueous sediment density flows: depositional processes and deposit types. Sedimentology 59, 1937–2003.

Talling, P.J., Paull, C.K., Piper, D.J.W. 2013. How are subaqueous sediment density flows triggered, what is their internal structure and how does it evolve? Direct observations from monitoring of active flows. Earth-Science Reviews 125. 244-287.

Tappin, D. R., Watts, P., Grilli, S. T., 2008. The Papua New Guinea tsunami of 17 July 1998: anatomy of a catastrophic event. Natural Hazards and Earth System Science 8, 243-266.

Tappin, D.R., Watts, P., McMurtry, G.M., Lafoy, Y., Matsumoto, T., 2001. The Sissano-Papua New Guinea tsunami of July 1998-offshore evidence on the source mechanism. Marine Geology 175, 1-23.

ten Brink, U.S., Lee, H.J., Geist, E.L., Twichell, D., 2009. Assessment of tsunami hazard to the US East Coast using relationships between submarine landslides and earthquakes. Marine Geology 264, 65-73.

Thomas, S., Bell, L., Ticehurst, K., Dimmock, P. S., 2010. An investigation of past mass movement events in the West Nile Delta. Frontiers in Offshore Geotechnics II, 239.

Thomson, J., and Weaver, P.P.E., 1994. An AMS Radiocarbon method to determine the emplacement time of recent deep-sea turbidites. Sedimentary Geology 89, 1–7.

Traykovski, P., Geyer, W.R., Irish, J.D., Lynch, J.F., 2000. The role of wave-induced density driven fluid mud flows for cross-shelf transport on the Eel River continental shelf. Continental Shelf Research 20, 2113–2140.

Tripsanas, E.K., Bryant, W.R., Phaneuf, B.A., 2004. Slope-instability processes caused by salt movements in a complex deep-water environment, Bryant Canyon area, northwest Gulf of Mexico. AAPG Bulletin 88, 801–823.

Trofimovs, J.; Talling, P. J.; Fisher, J. K.; Hart, M. B.; Sparks, R. S. J.; Watt, S. F. L.; Cassidy, M.; Smart, C. W.; Anne Le Friant; Moreton, S. G.; Leng, M. J., 2013. Timing, origin and emplacement dynamics of mass flows offshore of SE Montserrat in the last 110 ka: Implications for landslide and tsunami hazards, eruption history, and volcanic island evolution. Geochemistry Geophysics Geosystems 14, 385-406.

Tsutsui, B., Campbell, J.F., Coulbourn, W.T., 1987. Storm-generated, episodic sediment movements off Kahe Point, Oahu, Hawaii. Marine Geology 76, 281–299.

Twichell, D.C., Chaytor, J.D., ten Brink, U.S., Buczkowski, B., 2009. Morphology of late Quaternary submarine landslides along the U.S. Atlantic continental margin. Marine Geology 264, 4–15.

Urlaub, M., Talling, P., & Clare, M., 2014. Sea-level-induced seismicity and submarine landslide occurrence: comment. Geology 42, 337.

Urlaub, M., Talling, P.J., Masson, D.G., 2013. Timing and frequency of large submarine landslides: implications for understanding triggers and future geohazard. Quaternary Science Reviews 72, 63–82.

Vail, P.R., Mitchum, R.M.J., Todd, R.G., Widmier, J.M., Thompson, S.I., Sangree, J.B., Bubb, J.N., Hatelid, W.G., 1977. Seismic Stratigraphy and Global Changes of sea Level. In: Payton, C.E. (Ed.), Seismic Stratigraphy — Applications to Hydrocarbon Exploration, AAPG Mem 26. American Association of Petroleum Geologists, Tulsa, Ok, pp. 49–212.

References

Van Daele, M., Moernaut, J., Silversmit, G., Schmidt, S., Fontijn, K., Heirman, K..et al., 2014. The 600 yr eruptive history of Villarrica Volcano (Chile) revealed by annually laminated lake sediments. Geological Society of America Bulletin 126, 481-498.

van Rooij, M.M., Nash, B.A., Rajaraman, S., Holden, J.G., 2013. A fractal approach to dynamic inference and distribution analysis. Frontiers in Physiology 4.

van Weering, T.C.E., de Stigter, H.C., Boer, W., de Haas, H., 2002. Recent sediment transport and accumulation on the NW Iberian margin. Progress in Oceanography 52, 349-371

Vanneste M., Harbitz, C.B., De Blasio, F.V., Glimsdal, S., Mienert, J., Elverhøi, A., 2011. Hinlopen-Yermak Landslide, Arctic Ocean — geomorphology, landslide dynamics, and tsunami simulations. In: R.C. Shipp et al. (eds). Mass-transport deposits in deepwater settings. SEPM Special Publications 96, 509–529.

Vanney, J-R., Mougenot, D., 1990. Un canyon sous-marin du type ’gouf’: le Canhao da Nazare´ (Portugal). Oceanologica Acta 13, 1–14

Vardy, M.E., Pinson, L.J.W., Bull, J.M., Dix, J.K., Henstock, T.J., Davis, J.W., Gutowski, M., 2010. 3D seismic imaging of buried Younger Dryas mass movement flows: Lake Windermere, UK. Geomorphology 118, 176–187.

Villamor, P., Capote, R., Stirling, M.W., Tsige, T., Berryman, K.R., Martinez-Diaz, J.J., Martin-González, F., 2012. Contribution of active faults in the intraplate area of Iberia to seismic hazard: The Alentejo-Plasencia Fault. Journal of Iberian Geology 38 (1), 85-111.

Vittinghoff, E., McCulloch, C.E., 2007. Relaxing the rule of ten events per variable in logistic and Cox regression. American Journal of Epidemiology 165, 710 – 718.

Walters, S.J., 2009. What is a Cox model? What is…? Series, Hayward Medical Communications.

Watt, S.F.L., Talling, P.J., Vardy, M.E., Heller, V., Hühnerbach, V., Urlaub, M., Sarkar, S., Masson, D.G., Henstock, T.J., Minshull, T.A., Paulatto, M., Le Friant, A., Lebas, E., Berndt, C., Crutchley, G.J., Karstens, J., Stinton, A.J., Maeno, F., 2012. Combinations of volcanic-

flank and seafloor-sediment failure offshore Montserrat, and their implications for tsunami generation. Earth and Planetary Science Letters 319–320, 228–240.

Weaver, P.P.E., and scientific shipboard party, 2004. RRS Charles Darwin Cruise CD157, 28 May – 13 June 2004. Sediment transport through the Setubal and Nazaré Canyons. Southampton Oceanography Centre Cruise Report, No. 49, 27pp.

Weaver, P. P. E., 1994. Determination of turbidity current erosional characteristics from reworked coccolith assemblages, Canary Basin, north-east Atlantic. Sedimentology 41, 1025–1038.

Weaver, P.P.E. Thomson, J., Hunter, P., 1987. Introduction. In Weaver, P.P.E., and Thomson, J. (Eds.), Geology and Geochemistry of Abyssal Plains. Geological Society Special Publications, London 31, vii-xii.

Weaver, P.P.E., Thomson, J., 1993. Calculating erosion by deep-sea turbidity currents during initiation and flow. Nature 364, 136–138.

Weiss, R., Bahlburg, H., 2006. A note on the preservation of offshore tsunami deposits. Journal of Sedimentary Research 76, 1267-1273.

Weron, R., 2002. Estimating long range dependence: finite sample properties and confidence intervals. Physica A 312, 285-299.

Whitmarsh, R.B., Sawyer, D.S., 1996. The ocean/continent transition between the Iberian Abyssal Plain and continental rifting to seafloor-spreading processes. In: Whitmarsh, R.B., Sawyer, D.S., Klaus, A.A., Masson, D.G. (Eds.), Proceedings of the Ocean Drilling Program, Scientific Results 149, Ch. 47, pp. 713-736.

Winkelmann, D., Geissler, W., Schneider, J., Stein, R., 2008. Dynamics and timing of the Hinlopen/Yermak Megaslide north of Spitsbergen, Arctic Ocean. Marine Geology 250, 34-50.

References

Winkelmann, D., Stein, R., 2007. Triggering of the Hinlopen/Yermak Megaslide in relation to paleoceanography and climate history of the continental margin north of Spitsbergen. Geochemistry, Geophysics, Geosystems 8, Q06018, doi:10.1029/2006GC001485.

Wright, C.T., Friedrichs, C.T., 2006. Gravity-driven sediment transport on continental shelves: a status report. Continental Shelf Research 26, 2092–2107.

Wynn, R.B., and scientific shipboard party, 2009. Cruise report for JC027: Timing and frequency of landslide and gravity flow geohazards along the eastern North Atlantic continental margin, NERC strategic science programme Oceans 2025. National Oceanography Centre.

Wynn, R. B., Masson, D. G., 2003. Canary island landslides and tsunami generation: can we use turbidite deposits to interpret landslide processes. In: J. Locat & J. Mienert (eds.), Submarine mass movements and their consequences, Advances in Natural and Technological Hazards Research 19, 325–332.

Wynn, R.B., Weaver, P.P.E., Stow, D.A.V., Masson, D.G., 2002. Turbidite depositional architecture across three interconnected deep-water basins on the northwest African margin. Sedimentology 49, 1441–1462.

Xu, J.P., 2011. Measuring currents in submarine canyons: technological and scientific progress in the past 30 years. Geosphere 7, 868–876.

Xu, J.P., Noble, M.A., Rosenfeld, L.K., 2004. In-situ measurements of velocity structure within turbidity currents. Geophysical Research Letters 31, L09311, doi:10.1029/2004GL019718.

Xu, J.P., Sequeiros, O.E., Noble, M.A., 2014. Sediment concentrations, flow conditions, and downstream evolution of two turbidity currents, Monterey Canyon, USA. Deep Sea Research I 89, 11-34.

Zitellini, N., Rovere, M., Terrinha, P., Chierici, F., Matias, L., and Bigsets Team, 2004. Neogene through Quaternary tectonic reactivation of SW Iberian passive margin. Pure and Applied Geophysics 161, 565–587.